Surface composition of cobalt catalysts for steam reforming of ethanol

Sylwia Turczyniak

UNIVERSITÉ DE STRASBOURG

ÉCOLE DOCTORALE DES SCIENCES CHIMIQUES

UMR 7515 – ICPEES

THÈSE

présentée par :

[Sylwia TURCZYNIAK]

soutenue le : **28 Septembre 2016**

pour obtenir le grade de :

Docteur de l'université de Strasbourg

Discipline/ Spécialité : Chimie/ Chimie physique

Surface composition of cobalt catalysts for steam reforming of ethanol

Étude de la composition de la surface des catalyseurs à base de cobalt pour le reformage des vapeurs d'éthanol

THÈSE dirigée par :

[M. ZAFEIRATOS Spyridon]	Chargé de Recherche, ICPEES, Strasbourg, France
[M. MACHOCKI Andrzej]	Professeur, Université Maria Curie-Skłodowska, Lublin

RAPPORTEURS :

[M. HENRY Claude]	Directeur de Recherche, CiNaM, Marseille, France
[M. KOTARBA Andrzej]	Professeur, Université Jagellon, Cracovie, Pologne
[Mme NARKIEWICZ URSZULA]	Professeur, Université de technologie de Poméranie occidentale, Szczecin

---

AUTRES MEMBRES DU JURY :

[M. GOWOREK Jacek]	Professeur, Université Maria Curie-Skłodowska, Lublin
[M. MAJDAN Marek]	Professeur, Université Maria Curie-Skłodowska, Lublin
[M. PIKUS Stanisław]	Professeur, Université Maria Curie-Skłodowska, Lublin

UNIWERSYTET MARII CURIE-SKŁODOWSKIEJ
W LUBLINIE

Wydział Chemii

Sylwia Turczyniak

Surface composition of cobalt catalysts for steam reforming of ethanol

Skład powierzchniowy katalizatorów kobaltowych do reformingu parowego etanolu

Praca doktorska

napisana na Wydziale Chemii

Lublin rok 2016

Table of contents

PART II: EXPERIMENTAL

List of abbreviations

AFM	–	Atomic force microscopy
BE	–	Binding energy
CNF	–	Carbon nanofibers
ESR	–	Ethanol stream reforming
EU	–	European Union
GC	–	Gas chromatography
MS	–	Mass spectrometry
NEXAFS	–	Near edge X-ray absorption fine structure spectroscopy
RWGS	–	Reverse water gas shift
TEM	–	Transmission electron microscopy
TG	–	Thermogravimetry
TPO	–	Temperature programmed oxidation
TPR	–	Temperature programmed reduction
UHV	–	Ultra-high vacuum
WGS	–	Water gas shift
XAS	–	X-ray absorption spectroscopy
XPS	–	X-ray photoelectron spectroscopy
XRD	–	X-ray diffraction
XRF	–	X-ray fluorescense
YSZ	–	Yttria-stabilized zirconia

Acknowledgements

I wish to express my sincere thanks to Prof. Andrzej MACHOCKI and Dr Spyridon ZAFEIRATOS – my dissertation supervisors – for their steady interest, help, guidance during the entire doctoral studies, and for the opportunity to work on this joined Cotutelle research project. I am grateful for the time, that they spend with me on stimulating discussions and explanation of experiments' technical details. Dear supervisors, without your motivation and a great support, in many aspects, I would be not able to fulfil all formal requirements of both Universities.

I acknowledge help of French Government, Campus France, University of Strasbourg, Collège Doctoral Européen – the institutions that supported me financially during my stay in France, and help me very much in everyday life.

This work would be not accomplished without the staff of Maria Curie-Skłodowska University, the surface science group of Institut de Chimie et Procédés pour l'Énergie, l'Environnement et la Santé and the staff from BESSY Synchrotron facility in Berlin.

I want to express my great appreciation first of all to Dr Magdalena Greluk, who cared about my projects during my stay in France, and devoted her time to perform some research. Many thanks to Dr Wojciech Gac, M.Sc. Grzegorz Słowik, M.Sc. Michał Rawski, M.Sc. Bogna Banach, Dr Marek Rotko, M.Sc. Andrzej Sobieszek, and Dr. Leszek Sałamacha for help in data analysis and technical support.

I want to thank also the Authorities of UMCS, the members of my Polish commission, and the staff of administrative department, for their help in many aspects, and understanding.

I am very thankful to Dr Doh Won-hui, Dr Yeuk Ting Law, and Dr Vasiliki Papaefthimiou, who shared with me their experience, knowledge, and who were very supportive. Special thanks to Dr Wen Luo, who beside technical support, helped me with formal issues. Thank also to the others, I appreciate your company, sense of humour, and time that we spend together during breaks.

To all of you, I thank wholeheartedly for your kindness, assistance, and for always staying positive – like a proton.

The Author

The research was carried out with the equipment purchased thanks to the financial support of the European Regional Development Fund in the framework of the Polish Innovation Economy Operational Program(contract no. POIG.02.01.00-06-024/09 Center of Functional Nanomaterials; www.cnf.umcs.lublin.pl).

Executive summary of the doctoral thesis

OUTLINE

Abstract

This part of the PhD thesis consists of a short summary of the entire work written in three languages: English, French and Polish.

Abstract of the doctoral dissertation entitled: "Surface composition of cobalt catalysts for steam reforming of ethanol".

Introduction

The XXIth century brought a lot of changes, which proved that the world is only outwardly economically stable. Experts warn of an impending energy crisis, and point out that there is time to take steps towards planning new investments to ensure energy security. Experts' fears are not completely unfounded. For example in 2003 the severe blackouts that struck Europe and North America showed the importance of development of secure energy sector, which can be achieved by increase of existing network's efficiency and formation of new grids [1, 2]. The member states of European Union are strongly encouraged to use natural resources as hydropower, wind or solar energy. However, recently observed climate changes may cause the sense of dread associated with these investments. Quite recent example could be observed in August 2015 with regard to Poland [3–6]. Recent heat wave, showed that still there are

countries which, in certain situations. are teetering on the brink of a power supply. Moreover, some countries, like Poland and France are lowlands with a relatively low rate of annual rainfall; therefore, constructions of new hydroelectric power plants in most cases might be unprofitable. According to reports from 2015 [7–10], despite some climate inconveniences, the solar and wind sector are experiencing the record popularity globally. Unfortunately, recent [11] report indicates that the profitability of wind power may fall due to a decrease in energy prices, therefore, e.g., the Danish Government abandon the construction of new wind turbines.

Another very promising source of energy which potentially can meet the challenges of sustainable energy system is biomass. The fermentation of sugar- and starch-containing plants leads to obtain bio-ethanol [12–15], which can be used as a clean fuel for combustion engines [16]. However, better energy efficiency can be achieved whereas bio-ethanol is consequently transformed into hydrogen via catalytic steam reforming reaction [17] ($CH_3CH_2OH_{(g)} + 3H_2O_{(g)} \rightarrow 6H_{2(g)} + 2CO_{2(g)}$). Hydrogen obtained in this way may be used for fuel cells-based stationary power generation or in transport [18–20]. Unquestionable advantages of bio-ethanol and hydrogen have been widely discussed in section of this thesis entitled "*Introduction*".

As mentioned, the ethanol steam reforming reaction is a catalytic process; therefore, it requires a catalyst. Among various systems, cobalt-based catalysts were reported to be the promising ones [21–30], thus many research teams focus on examination and development of these systems. In order to stabilize cobalt particles and avoid a catalyst's sintering scientists suggested deposition of cobalt particles on oxide support [24–26], e.g., alumina, ceria, zirconia, zinc oxide, etc. Studies of cobalt supported on listed oxides led to the conclusion that these with redox properties [25, 27, 28], high oxygen mobility and oxygen storage capacity [29] (e.g. ceria), would be the best candidates. From the other side, a good thermal stability of zirconia also made it a potential candidate for catalysts' support, even though it exhibits very low oxygen mobility and almost no reducibility.

Unfortunately it was found that cobalt catalysts even with redox oxides as a support suffer for coking [30, 31]. To minimize coke formation and extend catalyst's lifetime the addition of alkali metals (e.g., Na, or K) was suggested [22, 32–35]. Alkali metal promotion significantly improved catalysts' activity, selectivity and resistance to coke formation [32, 33, 36–38].

In order to further improving catalytic properties it is very important to understand the changes (oxidation state of the catalyst's components, concentration of surface adsorbed species) occurring on a catalyst's surface in the course of the reaction, which may affect catalyst's performance. This may help to suggest the rational strategies of catalysts' improvements and shed a new light into catalysts' development.

The current state-of-art, many important issues and achievements on the catalytic field devoted to the steam reforming of ethanol carried out over cobalt-based catalysts were described in details in literature review part, entitled "*Hydrogen production via catalytic ethanol steam reforming*".

The main goals of the doctoral thesis

The thesis is aimed to understanding the influence of the surface state on catalytic performance of unpromoted and promoted cobalt-catalysts with ceria and zirconia supports with different particles size (nano – HS (high surface area), and micro – LS (low surface area)). The work consists of five chapters of the experimental studies. The first one is devoted to low pressure studies (0.2 (*in-situ*), 4, 10, and 20 mbar) at 420ºC of the high-dispersed Co/CeO_2 catalyst. The next four chapters present results of studies carried out under the total pressure of 1 atm. Two of them concern the influence of the H_2O/EtOH molar ratio (3/1, 9/1, 12/1 mol/mol, 420ºC) on unpromoted low- and high-surface area Co/CeO_2 and Co/ZrO_2 as well as potassium-promoted highly dispersed Co/CeO_2 and Co/ZrO_2 catalysts' surface state and their catalytic properties. The rest are devoted to studies of the potassium-promoted and unpromoted ceria- and zirconia-supported catalysts during long-time (up to 7 hours) ethanol steam reforming reaction (H_2O/EtOH = 12/1 mol/mol, 420ºC).

The main goals of this thesis are listed in the chapter entitled "*Introduction*" and they include:

(i) determination of the state of catalysts surface components on different stages of their life; as activated (pre-reduced) prior to the ESR, in the initial stages of the ESR reaction and how they change under the ESR conditions,

(ii) comparison of the influence of ceria and zirconia supports dispersion on the state of cobalt catalysts surface under the ESR and on the ESR selectivity,

(iii) understanding the influence of the reaction conditions (pressure, the H_2O/EtOH molar ratio) on the surface's state, ethanol conversion selectivity and carbonaceous deposit formation,

(iv) determination which form of cobalt Co(0) or Co(II) dominates under the reaction conditions,

(v) recognition of the influence of potassium promoter on the state of cobalt active phase and its support under the ESR, ethanol conversion selectivity and carbonaceous deposit formation,

(vi) finding the catalyst's surface species and sites that influence the course of the ESR,

(vii) understanding the influence of the reaction time on catalysts' surface state and their ESR catalytic performance,

(viii) detection the catalyst's surface species and sites which influence the course of the ESR,

(ix) providing new data in order to shed a light into the ESR reaction mechanism over ceria- and zirconia-supported cobalt catalysts,

(x) supplementing currently available knowledge.

The role of this part is to briefly summarize the most important findings from this work, in the sequence in which they are presented in the thesis.

Results and discussion of the experimental studies

The cobalt catalyst with nano-ceria (HS) support was prepared by impregnation method [27] and characterized by XRD, XRF, low-temperature nitrogen adsorption and hydrogen chemisorption methods. An average cobalt crystallites size for this catalyst, determined by hydrogen chemisorption, appeared to be very small (3.8 nm). The main technique that was used to characterize the surface's changes under the ESR conditions was X-ray Photoelectron Spectroscopy (XPS). In the course of the reaction, hydrogen and carbon-containing products distribution were analyzed *on-line* by means of mass spectrometer, in order to find the relationships between catalyst's surface chemical state and ESR effects.

The surface state and catalytic performance, of the pre-reduced in hydrogen, HS-Co/CeO_2 catalyst under the ESR (H_2O/EtOH=3/1 mol/mol, 420ºC) was examined in pressure range between 0.2–20 mbar. The results have shown that the pressure

increase influences the catalyst's surface oxidation state (Fig. 1), which consequently affects carbon-containing products distribution (Fig. 1). Under 0.2 mbar, when the surface was strongly reduced, the catalyst was highly selective towards carbon monoxide. The high reduction degree of ceria was in line with a high population of adsorbed hydroxyls species; however, under the low pressure conditions (0.2 mbar), hydroxyls act more as inhibitors rather than promoters of the ESR reaction rate. It was suggested that at very low pressure, chemisorption from the gas phase occurs preferentially on the strong chemisorption centres, which restrain mobility (diffusion) over the surface. The limited mobility of hydroxyls and other adsorbed species hinders possibility of further transformations and inhibits adsorption of reactants due to occupancy of the adsorption sites.

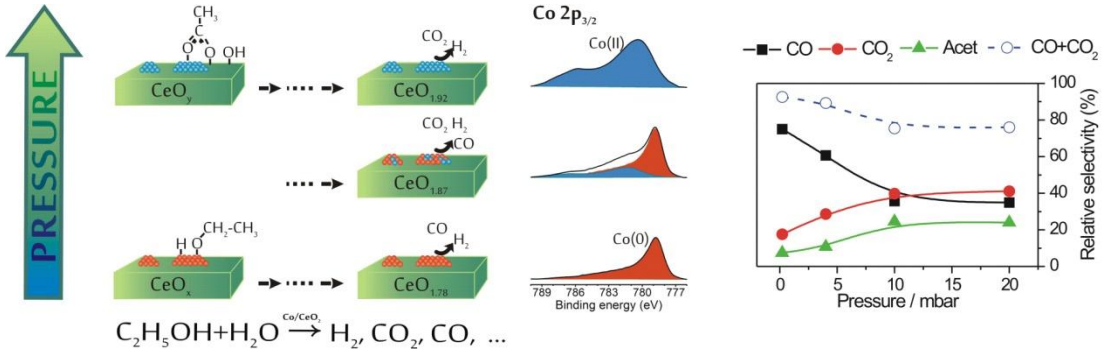

Fig. 1 The influence of the pressure (0.2–20 mbar) on catalyst's surface state and carbon-containing products distribution (HS-Co/CeO_2, H_2O/EtOH=3/1 mol/mol, 420ºC).

The pressure increase (4–20 mbar) resulted in the appearance of CoO_x species (Fig. 1) and higher concentration of Ce(IV) ions and oxygen-containing species, that increased concentration of carbon dioxide among analysed carbon-containing products. Therefore, a higher contribution of carbon dioxide in products might be related to the surface oxidation state; however, it can be also caused by the involvement of weak adsorption centres in the ESR pathways.

Further studies were carried out over the HS-Co/CeO_2 at higher pressure of vapours with various reactants ratio (H_2O/EtOH = 3/1, 9/1, 12/1 mol/mol, $p_{partial}$ = 57 mbar, p_{total} = 1 atm, 420ºC). They showed that cobalt oxidation state in the case of ceria-supported catalysts is not the main factor influencing catalysts' selectivity, whereas the concentration of surface's hydroxyls plays a pivotal role. It is not surprising since it might be expected that depending on the reaction conditions, adsorbed oxygen-containing species can be spectators, inhibitors or they can facilitate some reaction pathways.

Similar studies carried out over a micro-ceria supported counterpart (with cobalt crystallites size of 39.3 nm) led to another important conclusion. Beside surface's concentration of oxygen-containing species, the catalyst's morphology and probably location where oxygen-containing species are chemisorbed may be equally important to their abundance.

It was found that potassium creates another type of selective sites, i.e., $K^{\delta+}$–$O_{surf}^{\delta-}$, concentration of which increases with the water excess in the ESR reaction feed. These species play a promoting role in the steam reforming of ethanol, providing an additional oxygen-containing species reservoir. A coherent relation of both, OH species along with $K^{\delta+}$–$O_{surf}^{\delta-}$ sites, and the selectivity of the ESR to all gaseous products over unpromoted and promoted catalysts was found to correspond with the thermodynamic limit of the hydrogen and carbon dioxide yields.

The catalysts were prone to the formation of carbonaceous deposit, which was especially strongly marked at stoichiometric reactants molar ratio (3/1 mol/mol). The results showed that the form of the carbon deposit depends on the support's morphology and the cobalt particles size. The catalyst with larger cobalt particles favours the growth of carbon nanofibers, whereas on the surface on nano-catalyst, carbon was deposited gradually only onto the outer layers of the catalyst. The amount of deposited coke was significantly lowered after nano-ceria supported catalyst's promotion with potassium.

The importance of both hydroxyls and K–O species was confirmed in long-lasting experiments carried out with the H_2O/EtOH = 12/1 mol/mol. Fig. 2 shows that the concentration of OH and K–O species changes during the ESR, whereas the catalyst's selectivity improves slightly.

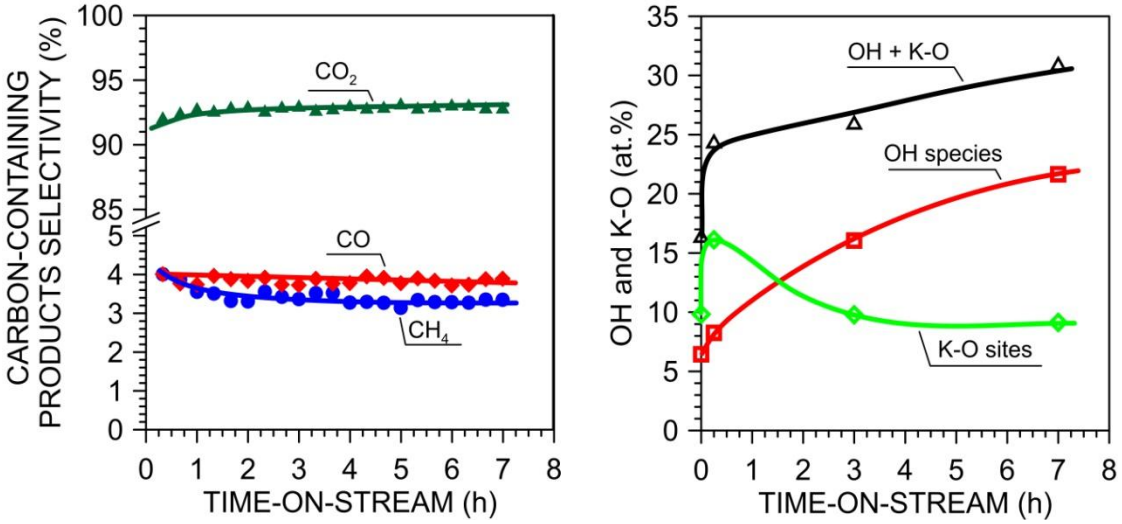

Fig. 2 The influence of time-on-stream on the ESR selectivity to carbon-containing products and changes of oxygen-containg species concentration on the potassium-promoted nano-ceria-supported catalyst's surface during 7 h in the stream (H_2O/EtOH = 12/1 mol/mol, 420ºC, $p_{partial}$ = 57 mbar, p_{total} = 1 atm).

Both OH species and K–O sites were also found to be required for lowering the amount of coke formed, hindering the transformation of CH_x species into fully dehydrogenated carbonaceous form. It was based on the fact, that the similar concentration of hydroxyls does not necessarily result in the catalyst's coking (see Fig. 3). When apart from hydroxyls, the influence of K–O sites is additionally considered, the linear correlation can be found (Fig. 3). Basing on obtained results it can be suggested that in order to maintain the surface carbon free, it should be covered by easy accessible (not too strongly bonded) oxygen-containing species, as hydroxyls and K–O sites.

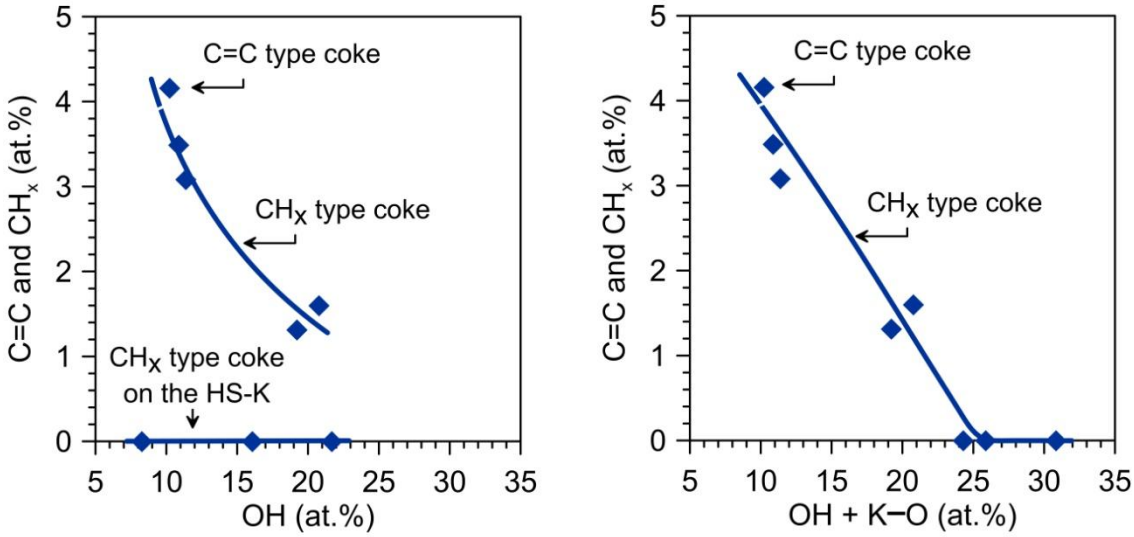

Fig. 3 Correlation of atomic percentage contribution of C=C and CH_x species with hydroxyls concentration, and sum of hydroxyls and K–O sites on the ceria-supported cobalt catalysts' surface.

Similar studies, as those above discussed, were carried out also over cobalt catalysts with nano- (HS) and micro-zirconia (LS) supports. Two catalysts with different cobalt dispersion (22.5 and 42.3 nm, respectively) were obtained by impregnation method [3]. The part of the HS-Co/ZrO_2 was promoted with potassium (2 wt.%).

It should be mentioned, that zirconia in contrast to ceria exhibits no reducibility, very low oxygen mobility and higher acidic nature of its surface; therefore, some slight differences between these two groups of catalysts were expected.

Cobalt particles supported on zirconia exhibited similar behaviour to this observed for ceria-supported ones meaning, that the oxidation state of cobalt increased with the water excess. Similarly to ceria-supported catalysts, the oxidation state of cobalt is not the sole factor influencing catalysts' selectivity. Also similar to ceria-supported catalysts, the concentration of oxygen-containing species, namely OH and K–O, influenced the hydrogen and carbon dioxide yields. Fig. 4 (left panel) shows the correlation of hydrogen and carbon dioxide yield with concentration of oxygen-containing species for both groups of ceria- and zirconia-supported catalysts. This graph (Fig. 4) supports the thesis that the most crucial for selective conversion of ethanol over unpromoted catalysts is concentration of hydroxyl species on the catalysts' surface. The concentration of these species increases with increased water excess in the reaction mixture, in the extent depending on the catalyst dispersion. In the case of potassium-promoted catalysts, the increasing hydroxyls concentration is supplemented by K–O sites. Taking both OH species and K–O sites into consideration, the hydrogen and carbon dioxide yields formed coherent dependences, with limits characteristic for the potassium-promoted catalysts. Those limits are consistent with the thermodynamic limit of hydrogen and carbon dioxide yields in the ethanol steam reforming. Considering equilibrium states of side reactions the equilibrium hydrogen of 5.55 mol/mol_{EtOH} and carbon dioxide 1.85 mol/mol_{EtOH} yield, are obtainable as against the stoichiometric values of 6.0 and 2.0 [39].

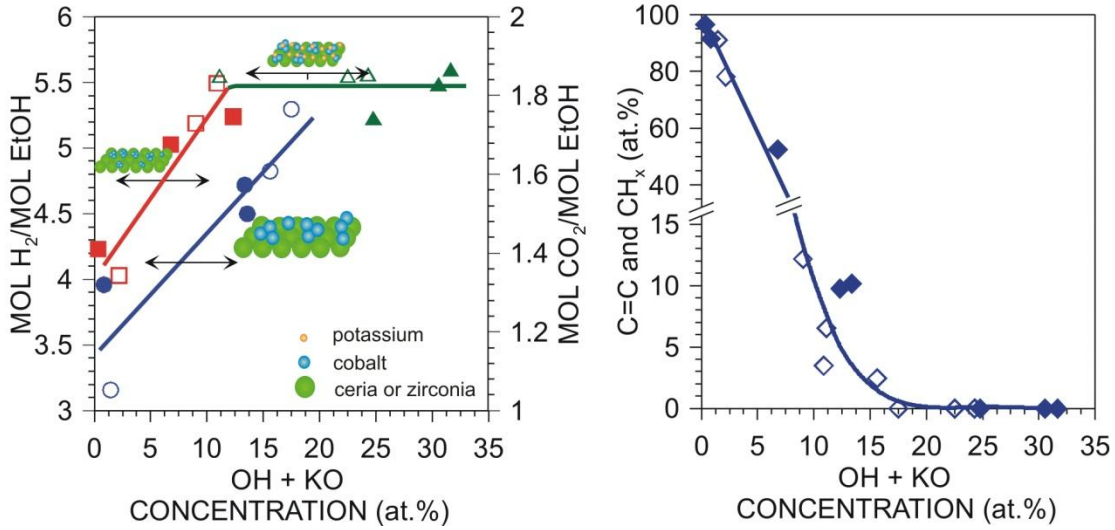

Fig. 4 Correlation of H_2 and CO_2 yields, and the concentration of C=C and CH_x species on the whole catalyst's surface with the concentration of surface oxygen-containing species on the surface of catalysts under the ESR at 420ºC. Each point refers to different H_2O/EtOH molar ratio. Open symbols: ○, □, △ refer to LS-, HS- and HS-K ceria-supported catalysts, whereas filled ones ●, ■, ▲ LS-, HS- and HS-K to zirconia-supported catalysts, respectively. In right figure, open symbols ◇ are related to all ceria-supported catalysts, whereas filled ◆ to zirconia-supported ones.

Beside OH + K–O surface concentration, the size of cobalt crystallites influences the ESR. Fig. 5 depicts that potassium promoter enables selective ESR, even if the cobalt crystallites are very large.

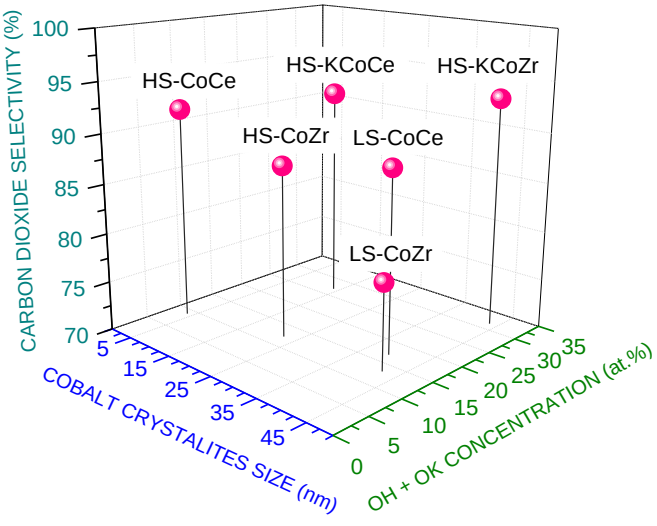

Fig. 5 The influence of cobalt crystallites size and the surface oxygen-containing species atomic concentration on the ceria- and zirconia-supported catalysts' selectivity towards carbon dioxide (H_2O/EtOH = 12/1 mol/mol, 420ºC, t = 1 h).

Another feature that differentiates zirconia-supported catalysts from ceria-supported counterparts is their susceptibility to carbon deposition. The zirconia-supported catalysts appeared to be more prone to coking, which in literature is

ascribed to the poor oxygen mobility, oxygen storage capacity of zirconia [29] and more acidic nature of its surface. The correlation of atomic percentage contribution of deposited coke with concentration of oxygen-containing species (Fig. 3, right panel) showed that the small concentration of OH species and K–O sites leads to dramatic coking of the catalysts, with formation of completely (or almost completely) dehydrogenated C=C type carbonaceous deposit, in a large part as graphitic whiskers and layers (conclusion based on TEM results).

General conclusions

The studies have shown that cobalt and ceria oxidation state depend on the reaction conditions (pressure, reactants molar ratio), while oxidation of cobalt depends also on the support nature. However, it was proved that suggested in literature the special role of oxidation or reduction of catalyst components under reaction conditions is not directly responsible for the ESR selectivity. The greatest significance in this respect was found for surface concentration of oxygen-containing species (OH and O). It is general feature for all catalysts, regardless of the support nature. Beside the surface concentration of these species the dispersion of cobalt active phase is of significant importance. It was found that in the case of catalysts with small cobalt particles, the lower concentration of oxygen-containing species is required in order to achieve good selectivity and the yield of hydrogen and carbon dioxide, as compared to catalysts with large particles. Promotion of catalysts with potassium increases the surface concentration of OH + K–O (and the ESR selectivity) to a high level, independently to the cobalt crystallites size. Therefore, potassium promoter improves zirconia-supported catalysts (with large cobalt crystallites) in a much higher extent than in the case of ceria-supported catalysts (with smaller cobalt crystallites). The concentration of oxygen-containing species influences also the intensity of coke formation. In the case of ceria-supported catalysts the higher concentration of oxygen-containing species changes also the type of coke formed, from fully dehydrogenated C=C type to CH_x type.

Résumé de la thèse intitulée: "Étude de la composition de la surface des catalyseurs à base de cobalt pour le reformage des vapeurs d'éthanol".

Introduction

Le XXI[e] siècle a apporté de nombreux changements qui ont prouvé que la stabilité économique mondiale n'est qu'une illusion. Les experts avertissent de la crise énergétique imminente et signalent qu'il est grand temps d'entreprendre des mesures pour planifier de nouveaux investissements assurant la sécurité énergétique. Les craintes des experts ne sont pas sans fondements. Par exemple, les importantes coupures d'électricité qui ont touché l'Europe et l'Amérique du Nord en 2003 ont révélé la nécessité de développer la sécurité du secteur énergétique, ce qui peut être atteint en augmentant l'efficacité des réseaux déjà existants et la construction de nouvelles infrastructures énergétiques [1, 2]. Les pays membres de l'Union Européenne sont encouragés à utiliser des sources d'énergie naturelles telles que l'énergie de l'eau, du vent ou du soleil. Pourtant, on observe récemment les changements climatiques qui peuvent susciter des inquiétudes justifiées quant à ce type d'investissements. La situation qui a eu lieu en Pologne en août 2015 [3–6] peut servir comme exemple. Les vagues de chaleur ont démontré qu'en Europe il existe toujours des pays qui, dans des situations particulières, sont à deux doigts de la rupture de l'alimentation en énergie.

De plus, certains pays, comme la Pologne ou la France sont des pays de plaines dont le niveau de précipitations annuelles est bas; c'est pourquoi la construction de nouvelles centrales hydroélectriques peut ne pas être rentable. Selon les rapports de 2015 [7–10], l'intérêt pour le secteur de l'énergie solaire et éolienne jouit d'une popularité croissante dans le monde entier, malgré les restrictions climatiques. Malheureusement, les derniers rapports [11] indiquent que la rentabilité des investissements relatifs à l'exploit de l'énergie éolienne peut baisser à cause de la chute des prix de l'énergie. C'est pour cette raison que, par exemple, le Danemark a abandonné la construction de nouvelles turbines éoliennes.

La biomasse est une autre source prometteuse qui peut répondre aux exigences de l'énergie durable. La fermentation de certaines plantes contenant du sucre et de l'amidon permet de produire du bio-éthanol [12–15] que l'on peut utiliser comme un combustible pur dans les moteurs à combustion [16]. Mais on peut atteindre une meilleure efficacité énergétique en transformant le bio-éthanol en hydrogène, suite

à une réaction catalytique du vaporeformage [17] ($CH_3CH_2OH_{(g)} + 3H_2O_{(g)} \rightarrow 6H_{2(g)} + 2CO_{2(g)}$). L'hydrogène ainsi produit peut être utilisé dans des piles à combustibles stationnaires, comme dans le transport [18–20]. Les avantages incontestables du bio-éthanol et de l'hydrogène ont été présentés de manière approfondie dans l'introduction de cette thèse de doctorat.

Comme cela a été dit précédemment, la réaction de vaporeformage de l'éthanol est un procédé de catalyse, d'où la nécessité d'utiliser un catalyseur. Parmi les différents systèmes catalytiques, celui à base de cobalt est considéré comme l'un des plus prometteurs [21–23]. C'est pour cette raison que plusieurs équipes de recherche se concentrent sur l'examen et le développement de ces catalyseurs. Pour stabiliser les particules de cobalt et éviter le frittage du catalyseur, les scientifiques ont suggéré le dépôt du cobalt sur les supports oxydes [24–26] comme l'oxyde d'aluminium, l'oxyde de cérium, l'oxyde de zirconium, l'oxyde de zinc, etc. L'étude du cobalt supporté sur les oxydes énumérés a conduit à la conclusion que les supports avec des propriétés redox [25, 27, 28], une grande mobilité de l'oxygène et la possibilité de le stocker [29] (p.ex. l'oxyde de cérium) se placent parmi les meilleurs candidats. D'un autre côté, une bonne stabilité thermique de l'oxyde de zirconium en fait un candidat potentiel pour les supports des catalyseurs à base de cobalt, bien que la mobilité de l'oxygène au sein de cet oxyde soit réduite et qu'il soit pratiquement irréductible.

Malheureusement, les catalyseurs à base de cobalt, même ceux avec des supports ayant des propriétés redox, ont formé du coke [30, 31]. Il est possible de minimaliser sa quantité et en même temps de prolonger le temps de travail du catalyseur en appliquant les métaux alcalins (p.ex. Na ou K) [22, 32–35]. La promotion avec des métaux alcalins a permis d'améliorer l'activité, la sélectivité et la résistance du catalyseur à la formation du coke [32, 33, 36–38].

Dans le but d'améliorer les propriétés catalytiques, il est particulièrement important de comprendre les changements qui ont lieu à la surface du catalyseur pendant la réaction (le degré d'oxydation des composants du catalyseur, la concentration des groupes adsorbés à la surface) et qui peuvent augmenter la performance du catalyseur. Comprendre ces changements permettra de suggérer des stratégies d'amélioration du catalyseur rationnelles et éclairera d'un jour nouveau le développement des systèmes catalytiques.

L'état actuel des connaissances, les questions importantes et les réussites concernant le vaporeformage de l'éthanol fait sur les catalyseurs à base de cobalt ont

été présentés et décrits dans le chapitre de ce travail intitulé *"La production d'hydrogène par le reformage catalytique de l'éthanol"*.

Les principaux objectifs de la thèse de doctorat

Cette thèse vise à comprendre l'influence de l'état de la surface sur les performances des catalyseurs à base de cobalt promus et non promus, avec les supports d'oxyde de cérium et de zirconium, dont les particules sont de tailles différentes (nano – HS (de grande surface) et micro – LS (de petite surface)). Ce travail est constitué de cinq chapitres consacrés aux études expérimentales. La première partie se rapporte à une étude menée sur le catalyseur Co/CeO_2 de grande surface à basse pression (0.2 (*in-situ*), 4, 10 et 20 mbar) à 420ºC . Les quatre chapitres suivants présentent les résultats des études sous une pression totale de 1 atm. Deux de ces chapitres traitent l'influence du rapport molaire H_2O/EtOH (3/1, 9/1, 12/1 mol/mol, 420ºC) sur l'état de la surface et les propriétés catalytiques des catalyseurs Co/CeO_2 et Co/ZrO_2 non promus à grande et faible surface spécifique, ainsi que des catalyseurs Co/CeO_2 et Co/ZrO_2 à grande surface promus au potassium. Les deux autres chapitres de la partie expérimentale sont consacrés à l'étude de la réaction du vaporeformage de l'éthanol (ESR) (H_2O/EtOH = 12/1 mol/mol, 420ºC) sur les catalyseurs promus au potassium et les non promus, supportés sur oxyde de cérium et oxyde de zirconium, durant sept heures au maximum.

Les objectifs principaux ont été présentés dans l'introduction de cette thèse et contiennent:

(i) détermination du degré d'oxydation des composants du catalyseur après la calcination, immédiatement après la réduction et pendant la réaction d'ESR,

(ii) comparaison de l'influence de la dispersion des supports de cérium et de zirconium sur le degré d'oxydation du cobalt dans les conditions d'ESR et sur la sélectivité du procédé,

(iii) compréhension de l'influence des conditions de la réaction (pression, rapport molaire H_2O/EtOH) sur l'état de la surface, la conversion de l'éthanol, la sélectivité et la formation du dépôt de carbone,

(iv) détermination de la forme dominante de cobalt (entre Co(0) et Co(II)) dans les conditions réactionnelles,

(v) explication de l'influence du promoteur de potassium sur l'oxydation de la phase active et du support pendant la réaction d'ESR, ainsi que l'explication de son influence sur la conversion de l'éthanol, la sélectivité et la formation du dépôt de carbone,

(vi) détection des groupes et des sites présents sur la surface du catalyseur, capables d'influencer le déroulement de la réaction d'ESR,

(vii) compréhension de l'influence du temps de la réaction sur l'état de la surface des catalyseurs et leurs performances catalytiques lors de la réaction d'ESR

(viii) apport des nouvelles informations qui peuvent aider à expliquer le mécanisme de la réaction d'ESR sur les catalyseurs à base de cobalt supportés sur des oxydes de cérium et zirconium,

(ix) développement des connaissances scientifiques actuelles.

La fonction de cette partie est de résumer brièvement les résultats de recherches les plus importants selon l'ordre dans lequel ils ont été présentés dans cette thèse.

Les résultats et la discussion des études expérimentales.

Le catalyseur à base de cobalt supporté sur les nanoparticules de l'oxyde de cérium (HS) a été obtenu à travers la méthode d'imprégnation [27] et caractérisé en utilisant les analyseurs XRD, XRF, l'adsorption de l'azote à basse température et la chimisorption de l'hydrogène. La taille moyenne des cristallites de cobalt pour ce catalyseur, déterminée par la chimisorption de l'hydrogène a été très petite (3.8 nm). La spectrométrie photoélectronique X (XPS) a été la technique principale utilisée dans le but de caractériser les changements de la surface dans les conditions d'ERS. Pendant la réaction, la distribution des produits gazeux, comme l'hydrogène et les cristallogènes, a été analysée par spéctrometrie de masse afin de trouver une corrélation entre l'état chimique de la surface et les effets d'ESR.

L'état de la surface et les propriétés catalytiques du catalyseur pré-réduit sous l'hydrogène HS-Co/CeO_2 lors de la réaction d'ESR (EtOH/H_2O = 1/3 mol/mol, 420ºC) ont été examinés sous des pressions entre 0.2 et 20 mbar. L'étude a démontré que l'augmentation de la pression influence le degré d'oxydation de la surface du catalyseur (Fig. 1), ce qui, en conséquence, exerce une influence sur la distribution des produits de carbone (Fig. 1). Sous la pression de 0.2 mbar, pendant que la surface du catalyseur était fortement réduite, dominait l'oxyde de carbone. Probablement, la prédominance

des ions de Ce(III) était due à une grande quantité des groupes hydroxyles adsorbés à la surface. Dans les conditions de pression basse (0.2 mbar), ils agissaient plutôt comme inhibiteurs que comme promoteurs de la réaction d'ESR. Cela peut suggérer que dans les conditions de pression basse la chimisorption de la phase gazeuse est privilégiée sur les centres de chimisorption forts qui restreignent la mobilité (la diffusion) sur la surface. La mobilité limitée des groupes hydroxyles et d'autres espèces adsorbées entrave la possibilité des transformations suivantes et freine l'adsorption des réactifs à cause des sites d'adsorption occupés. L'augmentation de la pression (4–20 mbar) a provoqué l'apparition de la phase oxydée de cobalt CoO_x (Fig. 1), l'augmentation de la quantité d'ions de Ce(IV) dans la structure du support et dans les groupes de l'oxygène adsorbés sur la surface. Ces changements ont contribué à l'augmentation de la concentration de dioxyde de carbone dans les produits de carbone analysés. Il est donc possible qu'une plus grande contribution du dioxyde de carbone dans les produits après réaction soit liée à l'état d'oxydation de la surface ou qu'elle soit provoquée par l'engagement supplémentaire des centres d'adsorption faibles dans les transformations d'ESR.

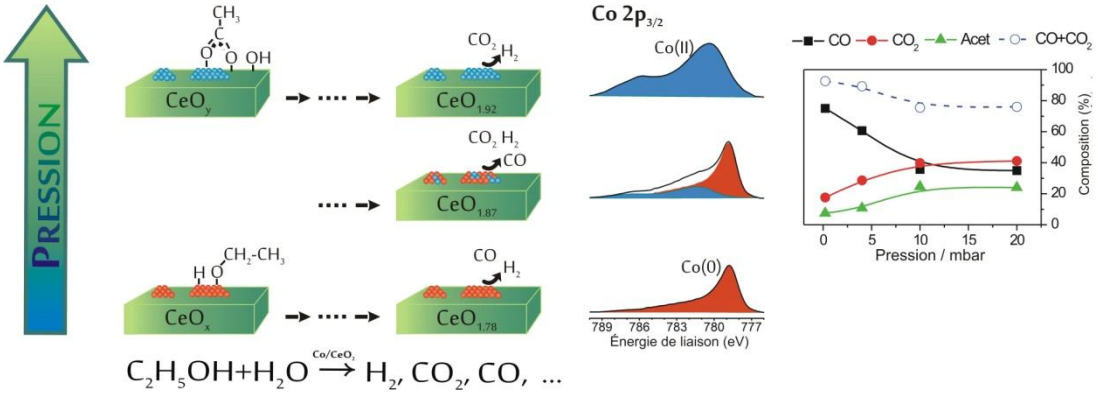

Fig.1 Influence de la pression (0.2–20 mbar) sur la surface et la distribution des cristallogènes (HS-Co/CeO_2, H_2O/EtOH = 3/1 mol/mol, 420ºC).

L'étude suivante sur le catalyseur HS-Co/CeO_2 a été menée sous une plus grande pression de vapeurs et avec de différentes concentrations des réactifs (H_2O/EtOH = 3/1, 9/1, 12/1 mol/mol, p= 57 mbar, 420ºC). Ella a montré que l'état d'oxydation du cobalt dans le catalyseur supporté sur l'oxyde de cérium n'est pas le facteur principal influant sur la sélectivité catalytique. C'est la concentration des groupes hydroxyles adsorbés à la surface qui joue un rôle essentiel. Cela ne surprend pas car on peut s'attendre à ce que, selon les conditions de la réaction, les groupes de l'oxygène adsorbés puissent être spectateurs, inhibiteurs ou même qu'ils puissent faciliter certaines voies réactionnelles.

Une étude pareille menée sur le catalyseur dont le support est de faible dispersion (la taille moyenne des cristallites de cobalt est de 39.3 nm) a abouti à une autre conclusion importante: outre la concentration des groupes de l'oxygène adsorbés à la surface, les facteurs comme la morphologie catalytique ou bien les sites où les groupes de l'oxygène sont adsorbés, peuvent également exercer une influence considérable.

Les analyses ont montré que le potassium crée un nouveau type de sites sélectifs, p. ex. $K^{\delta+}–O_{surf}^{\delta-}$, dont la concentration augmente avec l'excès de l'eau dans le mélange réactionnel. Ces sites favorisent la réaction du vaporeformage de l'éthanol. Ils constituent ainsi une source d'oxygène supplémentaire. Une influence manifeste des groupes OH et $K^{\delta+}–O_{surf}^{\delta-}$ sur la sélectivité d'ESR envers les produits gazeux, pour les catalyseurs promus et non promus, correspond aux limites thérmodynamiques de l'efficacité envers l'hydrogène et le dioxyde de carbone.

La tendance des catalyseurs à produire des dépôts carbonés a été particulièrement manifeste pendant la réaction menée avec le rapport stoechiométrique molaires des réactifs (3/1 mol/mol). Les résultats ont montré que le type de dépôt de carbone dépend en même temps de la morphologie du support et de la taille des particules de cobalt. Le catalyseur avec des particules de cobalt plus grandes favorise la croissance des nanotubes de carbone, pendant que sur la surface du nanocatalyseur le carbone est déposé progressivement sur les couches extérieures du catalyseur. La quantité de coke déposé a été considérablement diminuée suite à la promotion par le potassium du catalyseur supporté sur oxyde de cérium nanométrique.

Les essais de stabilité menés sur le rapport molaire H_2O/EtOH = 12/1 ont confirmé l'importance des groupes hydroxyles et K–O. La figure 2 indique que la concentration des groupes OH et K–O est modifiée pendant la réaction d'ESR, ainsi augmentant légèrement la sélectivité catalytique.

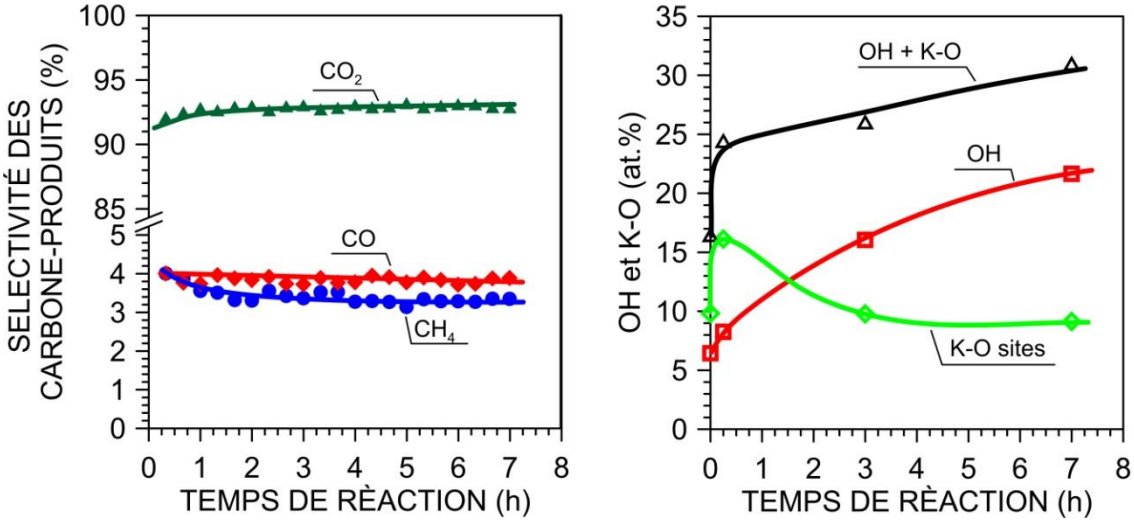

Fig.2 Influence du temps de la réaction d'ESR sur la sélectivité vers les produits de carbone et impact du changement de la concentration des groupes OH et KO sur le catalyseur supporté au cérium, promu par le potassium (H_2O/EtOH = 12/1 mol/mol, 420ºC, p = 57 mbar).

Les études ont permis de constater que tant les groupes OH et K–O que sont responsables de la diminution du coke formé et de l'inhibition de la création des formes de carbone déshydrogénées. Cette conclusion a été basée sur le fait qu'une concentration similaire des groupes hydroxyles n'entraîne pas nécessairement la formation du dépôt de carbone (Fig. 3).

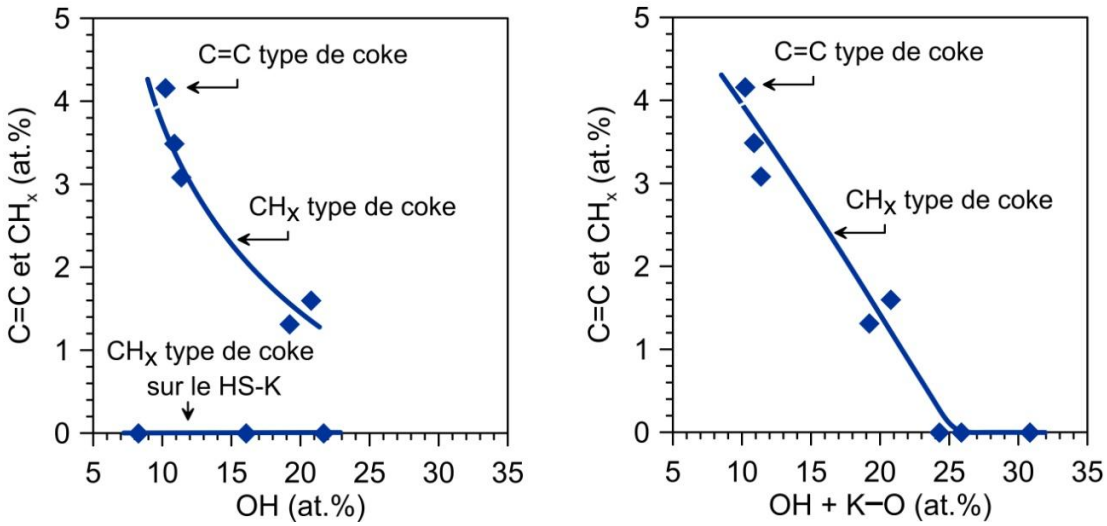

Fig. 3 Corrélation de la contribution des groupes C=C et CH_x (en pourcentage atomique), de la concentration des groupes hydroxyles et de la somme de groupes OH + K–O sur la surface du catalyseur supporté à l'oxyde de cérium.

Si nous prenons en considération l'influence des groupes K–O, outre les groupes hydroxyles, nous pouvons trouver une relation linéaire (Fig. 3, à droite) entre la quantité, le type de dépôt de carbone produit et la concentration des groupes de l'oxygène. D'après les résultats obtenus, il a été suggéré que si la surface du catalyseur

est couverte de groupes de l'oxygène (faiblement liés), de facile accès, comme p.ex. les groupes hydroxyles et K–O, il est possible d'éliminer ou de limiter la formation du coke.

Les études pareilles à celles susmentionnées ont été réalisées sur les catalyseurs supportés par le zirconium nano (HS) et micrométrique (LS). Les deux catalyseurs avec différentes dispersion de cobalt (respectivement 22.5 et 42.3 nm) ont été obtenus par imprégnation [3]. Une partie de catalyseur HS-Co/ZrO_2 a été promue au potassium (2% en masse).

Avant de discuter les résultats obtenus, il est important de mentionner que l'oxyde de zirconium, contrairement à l'oxyde de cérium, est difficilement réductible, a une mobilité de l'oxygène très faible et la nature acide de la surface plus importante. Nous pouvons donc nous attendre à de légères différences entre ces deux groupes de catalyseurs.

Les particules de cobalt déposées sur le support de zirconium présentent les comportements similaires à ceux qui ont été observés dans les catalyseurs supportés sur oxyde de cérium. Cela signifie que l'état d'oxydation du cobalt augmente avec l'excès de l'eau croissant dans le mélange réactionnel. Comme dans le cas des catalyseurs supportés sur oxyde de cérium, nous avons observé que l'état d'oxydation du cobalt n'est pas le facteur le plus important qui influence la sélectivité du catalyseur. En outre, il a été démontré que le pourcentage atomique des groupes hydroxyles et K–O sur la surface affecte la performance du catalyseur dans la production de l'hydrogène et du dioxyde de carbone. La Fig. 4 représente la corrélation entre l'efficacité de produire de l'hydrogène et du dioxyde de carbone et la concentration de groupes hydroxyles et K–O sur la surface des catalyseurs supportés sur oxyde de cérium et oxyde de zirconium. Le nombre de groupes hydroxyles augmente proportionnellement à l'excès de l'eau croissant dans le mélange réactionnel, selon le degré de dispersion du catalyseur. Dans le cas du catalyseur promu par le potassium, la concentration de groupes hydroxyles croissante est supplémentée par l'augmentation de nombre de groupes K–O.

En prenant en considération l'influence des groupes OH et K–O, la production de l'oxygène et du dioxyde de carbone crée une dépendance avec la valeur limite caractéristique pour les catalyseurs promus par le potassium. Ces limites concordent avec les limites thérmodynamiques de la production de l'oxygène et du dioxyde de carbone dans le vaporeformage de l'éthanol. Il ressort de la stoechiométrie de la réaction d'ESR que, s'il ne se produit pas une réaction secondaire, nous pouvons

obtenir 6.0 mol d'hydrogène et 2.0 mol de dioxyde de carbone [39] d'un mol d'éthanol. Sur les catalyseurs analysés l'efficacité de la production de l'hydrogène est de 5.55 mol/mol_{EtOH} et du dioxyde de carbone est de 1.85 mol/mol_{EtOH}.

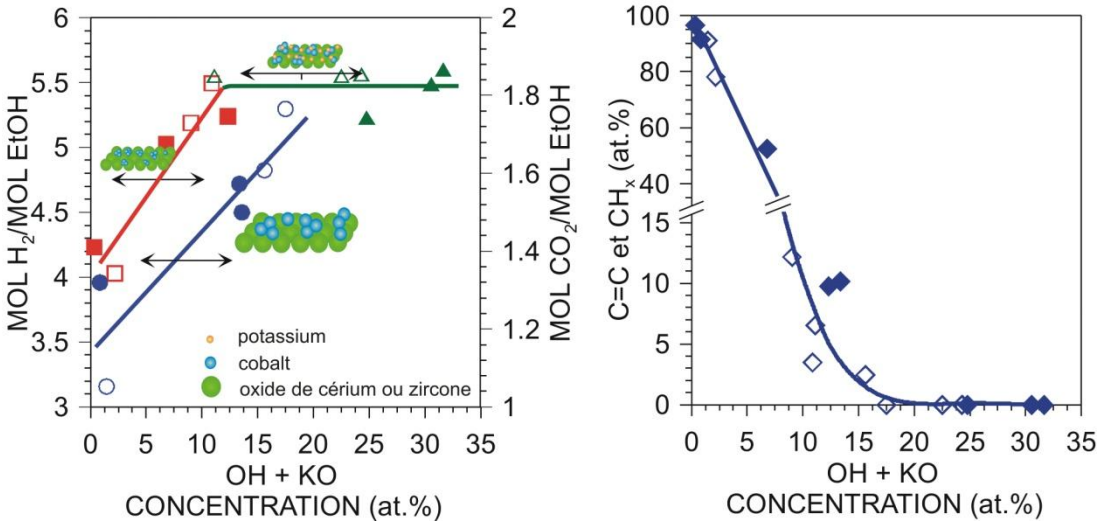

Fig. 4 Corrélation entre l'efficacité de la réaction d'ESR (420ºC) dans la production de H_2 et CO_2, le nombre de groupes C=C et CH_x sur toute la surface des catalyseurs et la concentration des OH + K–O. Chaque point se réfère à un différent rapport molaire. Les symboles ○, □, △ se réfèrent aux catalyseurs supportés sur oxyde de cérium LS-, HS- et HS-K. Les symboles remplis ●, ■, ▲ correspondent aux catalyseurs supportés sur oxyde de zirconium LS-, HS- et HS-K. Dans la figure à droite, les symboles ◇ correspondent à des données issues de spectres pour les catalyseurs supportés sur oxyde de cérium, alors que les symboles ◆ renvoient aux catalyseurs supportés sur oxyde de zirconium.

Outre de concentration des groupes OH + K–O à la surface, la taille des cristallites aussi influence la réaction d'ESR. La Fig. 5 montre que la promotion au potassium permet le déroulement sélectif de la réaction d'ESR, même si les cristallites de cobalt sont très grandes.

La susceptibilité au dépôt de carbone est une autre caractéristique qui distingue les catalyseurs supportés sur cérium de ceux supportés sur zirconium. Les derniers se sont révélés plus susceptibles à la formation du coke, ce qui est dû à une faible mobilité de l'oxygène, à une capacité limitée de stockage de l'oxygène par ce support, ainsi qu'à la nature acide de l'oxyde de zirconium [29]. La corrélation entre la contribution de carbone en pourcentage atomique et la concentration des groupes d'oxygène (Fig. 3, à droite) a démontré qu'une faible concentration des groupes OH et K–O sur la surface du catalyseur conduit à la formation de dépôt de carbone en quantité considérable sous une forme complètement (ou quasi complètement) déshydrogénée C=C, comme des fibres et des couches de carbone (conclusion basée sur les analyses microscopiques).

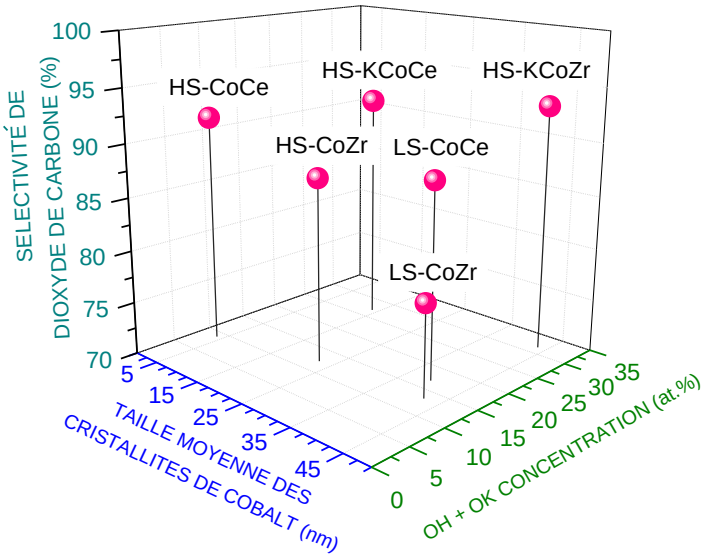

Fig. 5 Influence de la taille des cristallites de cobalt et de la concentration de groupes contenant les atomes d'oxygène (exprimé en pourcentage atomique) sur la sélectivité des catalyseurs supportés par l'oxyde de cérium et zirconium dans la production du dioxyde de carbone (H_2O/EtOH = 12/1 mol/mol, 420ºC, t = 1 h).

Conclusions

L'étude a démontré que l'état d'oxydation du cobalt et du cérium dépend des conditions réactionnelles (pression, rapport molaire des réactifs). De surcroît, l'état d'oxydation du cobalt dépend du type de support. Dans ce travail, les résultats ont montré que le rôle particulier de réduction et d'oxydation des composants principaux du catalyseur dans les conditions réactionnelles n'a aucun effet direct sur la sélectivité du catalyseur. A cet égard, la plus grande importance a été atribuée à la concentration des groupes d'oxygène (OH et O) adsorbés sur la surface, ce qui est une caractéristique de tous les catalyseurs, quel que soit le support. Outre la concentration de ces groupes, la dispersion de la phase active du cobalt est un autre facteur signifiant. Il a été observé que dans le cas des catalyseurs avec de petites cristallites de cobalt, la concentration inférieure des groupes d'oxygène adsorbés est nécessaire afin d'obtenir une bonne sélectivité et efficacité de production de l'hydrogène et du dioxyde de carbone, contrairement à des catalyseurs avec de grandes particules de cobalt. La promotion des catalyseurs par le potassium a considérablement augmenté la concentration des groupes OH + K–O sur la surface du catalyseur (et aussi la sélectivité de la réaction d'ESR), indépendamment de la taille de cristallites de cobalt. Pour cette raison, le promoteur du potassium améliore beaucoup plus les propriétés catalytiques des systèmes supportés sur oxyde de zirconium (avec de grandes cristallites de cobalt) que celles des catalyseurs supportés sur oxyde de cérium (avec de petites cristallites de cobalt).

La concentration des groupes d'oxygène influence l'intensité de la formation du coke. Dans le cas des catalyseurs supportés par le cérium la concentration plus élevée sur la surface des groupes d'oxyde influence aussi le type de carbone déposé, qui passe d'une forme complètement déshydrogénée à CH_x.

Streszczenie rozprawy doktorskiej pt. „Skład powierzchniowy katalizatorów kobaltowych do reformingu parowego etanolu”.

Wstęp

XXI wiek przyniósł wiele zmian, które dowiodły, że stabilność ekonomiczna świata jest jedynie pozorna. Eksperci ostrzegają przed nadchodzącym kryzysem energetycznym i sygnalizują, że to najwyższy czas, aby podjąć kroki w kierunku planowania nowych inwestycji, mających na celu zapewnienie bezpieczeństwa energetycznego. Obawy ekspertów nie są bezpodstawne. Dla przykładu, znaczące przerwy w dostawach energii eklektycznej, które w 2003 roku uderzyły Europę i Północną Amerykę, wskazały na potrzebę rozwoju bezpiecznego sektora energetycznego, co można osiągnąć zwiększając wydajność obecnie istniejących sieci, jak również i budowę nowych infrastruktur energetycznych [1, 2]. Kraje członkowskie Unii Europejskiej są „zachęcane” do korzystania z naturalnych źródeł energii, takich jak energia wody, wiatru czy słońca. Jednak ostatnio obserwowane zmiany klimatyczne mogą budzić słuszne obawy przed tego typu inwestycjami. Przykładem może być sytuacja jaka miała miejsce w Polsce, w sierpniu 2015 roku [3–6]. Fale upałów wykazały, że w Europie wciąż są kraje, które w pewnych sytuacjach, balansują na krawędzi ich możliwości energetycznych.

Ponadto, niektóre państwa takie jak Polska czy Francja są krajami wybitnie nizinnymi z niskim rocznym poziomem opadów deszczu, budowa nowych elektrowni wodnych w wielu przypadkach może być nieopłacalna. Według doniesień z 2015 roku [7–10], zainteresowanie sektorem energii słonecznej i wiatrowej cieszy się rosnącą popularnością na całym świecie, pomimo ograniczeń klimatycznych. Niestety, ostatnie doniesienia [11] wskazują, że z powodu jest ogólnego spadku cen energii opłacalność inwestycji związanych wykorzystaniem energii wiatru może ulec obniżeniu, stąd też np. rząd Danii zaniechał instalowania nowych turbin wiatrowych.

Innym, bardzo obiecującym źródłem energii, które może sprostać wymaganiom zrównoważonego źródła energii, jest biomasa. Fermentacja części roślin zawierających w składzie cukier i skrobię prowadzi do otrzymania bio-etanolu [12–15], który z kolei można zastosować jako czyste paliwo w silnikach spalinowych [16]. Jednak lepszą wydajność energetyczną można uzyskać gdy bio-etanol zostanie przetworzony na wodór, w wyniku reakcji katalitycznego reformingu parowego (*ESR, ethanol steam*

reforming) [17] ($CH_3CH_2OH_{(g)} + 3H_2O_{(g)} \rightarrow 6H_{2(g)} + 2CO_{2(g)}$). Uzyskany w ten sposób wodór można wykorzystać zarówno w stacjonarnych ogniwach paliwowych, jak i w rozwiązaniach transportowych [18–20]. Niewątpliwe zalety bio-etanolu i wodoru zostały wnikliwie przestawione we wstępie niniejszej pracy doktorskiej.

Jak już wspomniano, reakcja reformingu parowego etanolu jest procesem katalitycznym, stąd też wymaga katalizatora. Spośród różnych układów katalitycznych, te z kobaltową fazą aktywną są uważane za jedne z najbardziej obiecujących [21–23], stąd wiele zespołów badawczych skupia się na ich badaniu i rozwoju tychże katalizatorów. W celu stabilizacji cząstek kobaltu i uniknięcia ich spiekania katalizatora, naukowcy zasugerowali osadzanie kobaltu na nośnikach tlenkowych [24–26], takich jak: tlenek glinu, tlenek ceru, tlenek cyrkonu, tlenek cynku, itp. Badania właściwości kobaltu, osadzonego na wymienionych nośnikach, doprowadziły do wniosku, że nośniki z właściwościami redox [25, 27, 28], dużą mobilnością tlenu i możliwością jego magazynowania [29] (np. tlenek ceru), są jednymi z najlepszych kandydatów. Z drugiej strony, dobra stabilność termiczna tlenku cyrkonu również czyni go potencjalnym kandydatem dla nośnikowych katalizatorów kobaltowych, pomimo iż tlenek ten wykazuje niską mobilność tlenu i jest praktycznie nieredukowalny.

Niestety, katalizatory kobaltowe, nawet te z nośnikami o właściwościach redox, okazały się podatne na zawęglanie [30, 31]. Zminimalizowanie ilości tworzącego się węgla, a tym samym wydłużenie czasu pracy katalizatora, można osiągnąć poprzez dodatek metali alkaicznych (np. Na czy K) [22, 32–35]. Promocja metalami alkaicznymi pozwoliła na znaczną poprawę aktywności, selektywności i odporności katalizatora na tworzenie się depozytu węglowego [32, 33, 36–38].

W celu poprawy własności układów katalitycznych niezwykle ważne jest poznanie i zrozumienie stanu chemicznego i jego zmian zachodzących na powierzchni katalizatora w trakcie reakcji (stopienia utlenienia składników katalizatora, stężenia różnych cząstek zaadsorbowanych na powierzchni), tym samym mogących wpływać na skuteczność (aktywność, selektywność) pracy katalizatora. Zrozumienie stanu chemicznego „pracującego" katalizatora i jego ewentualnych zmian pozwoli na zasugerowanie racjonalnych strategii poprawy katalizatora i rzuci też nowe światło na rozwój układów katalitycznych.

Obecny stan wiedzy, znaczące zagadnienia i osiągnięcia dotyczące reformingu parowego etanolu prowadzonego na katalizatorach kobaltowych, zostały wnikliwie

przedstawione i omówione w przeglądzie literaturowym, zatytułowanym „*Otrzymywanie wodoru na drodze katalitycznego reformingu etanolu*".

Główne cele pracy doktorskiej

Praca ukierunkowana jest na poznanie i zrozumienie wpływu stanu powierzchni na właściwości katalityczne niepromowanych i promowanych katalizatorów kobaltowych z tlenkowymi nośnikami cerowymi i cyrkonowymi, różniącymi się rozmiarem cząstek (nano – HS (wysoko-powierzchniowy) i mikro – LS (nisko-powierzchniowy)). Część eksperymentalna rozprawy składa się z pięciu rozdziałów. Pierwszy poświęcony jest badaniom prowadzonym w warunkach niskiego ciśnienia (0.2 (*in-situ*), 4, 10, and 20 mbar) w 420ºC na wysoko-powierzchniowym katalizatorze Co/CeO_2. W kolejnych czterech rozdziałach zaprezentowano wyniki badań prowadzonych przy całkowitym ciśnieniu równym 1 atm. W dwóch z tych rozdziałów przedstawiono wpływ stosunku molowego $H_2O/EtOH$ (3/1, 9/1, 12/1 mol/mol, 420ºC) na stan powierzchni i właściwości katalityczne niepromowanych nisko- i wysoko-powierzchniowych katalizatorów Co/CeO_2 i Co/ZrO_2, jak również i promowanych potasem wysoko-powierzchniowych katalizatorów Co/CeO_2 i Co/ZrO_2. Pozostałe dwa rozdziały części eksperymentalnej poświęcone są badaniom reakcji reformingu parowego etanolu na niepromowanych i promowanych potasem katalizatorach z tlenkiem ceru i cyrkonu jako nośniki kobaltu, w reakcji ESR prowadzonej maksymalnie przez kilka godzin ($H_2O/EtOH$ = 12/1 mol/mol, 420ºC).

Główne cele pracy zostały przestawione we wstępie do rozprawy i zawierają:

(i) określenie stanu utlenienia składników katalizatora po jego kalcynacji, bezpośrednio po wstępnej redukcji wodorem i w trakcie reakcji ESR,

(ii) porównanie wpływu dyspersji nośników, cerowego i cyrkonowego, na stan utlenienia kobaltu w warunkach ESR, oraz na selektywność procesu,

(iii) zrozumienie wpływ warunków reakcji (ciśnienie, stosunek molowy $H_2O/EtOH$) na stan powierzchni, stopień przereagowania etanolu, selektywność oraz tworzenie się depozytu węglowego,

(iv) określenie która z form kobaltu Co(0) czy Co(II) dominuje w warunkach reakcji ESR,

(v) wyjaśnienie wpływu promotora potasowego na stan utlenienia fazy aktywnej i nośnika w warunkach ESR, stopień przereagowania etanolu, selektywność oraz tworzenie się depozytu węglowego,

(vi) określenie cząstek i miejsc specyficznych znajdujących się na powierzchni katalizatora i mogących wpływać na przebieg procesu ESR,

(vii) zrozumienie wpływu czasu reakcji ESR na stan powierzchni katalizatorów oraz ich właściwości katalityczne w reakcji ESR,

(viii) uzyskanie nowych informacji, które mogą przyczynić się do wyjaśnienia mechanizmu reakcji ESR na katalizatorach kobaltowych z tlenkiem ceru i cyrkonu jako nośnikami kobaltu,

(ix) rozwinięcie i uzupełnienie aktualnego stanu wiedzy.

Rolą tego streszczenia jest krótkie podsumowanie najważniejszych wyników badań eksperymentalnych, w kolejności w jakiej zostały przedstawione w rozprawie.

Dyskusja wyników badań eksperymentalnych

Katalizator kobaltowy z wysoko-zdyspergowanym (HS, wysoko-powierzchniowym) nośnikiem cerowym otrzymano metodą impregnacyjną [27] i scharakteryzowano z wykorzystaniem technik XRF, XRD, nisko-temperaturowej adsorpcji azotu i chemisorpcji wodoru. Średni rozmiar krystalitów kobaltu dla tego katalizatora, określony metodą chemisorpcji wodoru, był bardzo mały (3.8 nm). Główną techniką, która została wykorzystana w celu charakterystyki zmian stanu jego powierzchni w warunkach ESR była rentgenowska spektroskopia fotoelektronów (XPS). Skład produktów gazowych, takich jak wodór i związki zawierające węgiel, analizowano w trakcie przebiegu reakcji przy użyciu spektrometru masowego, w celu znalezienia korelacji pomiędzy chemicznym stanem powierzchni a efektami ESR.

Stan powierzchni i właściwości katalityczne katalizatora HS-Co/CeO_2 (pre-redukowanego wodorem) w warunkach ESR (H_2O/EtOH = 3/1 mol/mol, 420ºC) określono w zakresie ciśnień 0.2–20 mbar. Badania wykazały, że wzrost ciśnienia wpływa na stan utlenienia powierzchni katalizatora (Rys. 1), co w konsekwencji ma wpływ na dystrybucję produktów węglowych (Rys. 1). Pod ciśnieniem 0.2 mbar, kiedy powierzchnia katalizatora była silnie zredukowana, w składzie analizowanych produktów zawierających węgiel dominował tlenek węgla. Przewaga jonów Ce(III) była najprawdopodobniej związana z dużą ilością grup hydroksylowych

zaadsorbowanych na powierzchni katalizatora, które w warunkach niskiego ciśnienia (0.2 mbar) raczej hamowały niż promowały przebieg reakcji ESR. Może to sugerować, że w warunkach niskociśnieniowych, chemisorpcja z fazy gazowej jest faworyzowana na silnych centrach chemisorpcyjnych, ograniczających mobilność (dyfuzję) cząstek po powierzchni. Mniejsza mobilność grup hydroksylowych i innych zaadsorbowanych cząstek, ogranicza możliwość dalszych przemian i z powodu zajętych miejsc adsorpcyjnych hamuje adsorpcję reagentów.

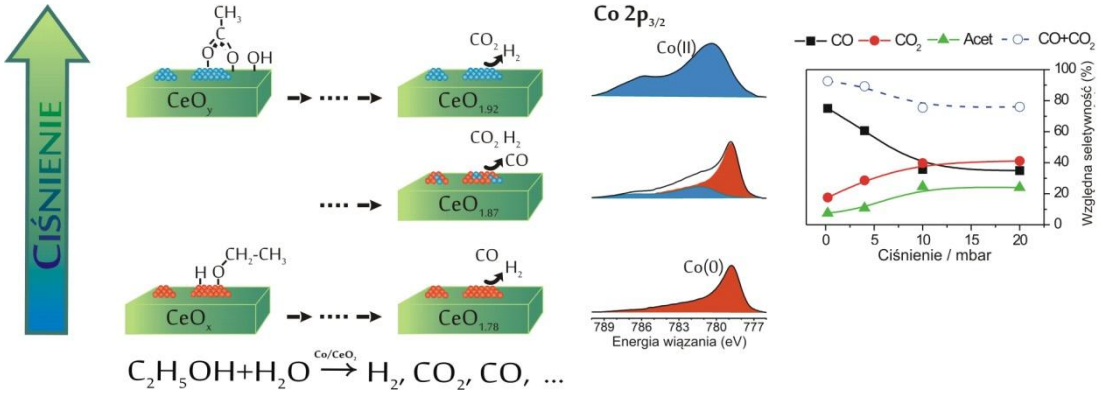

Rys. 1 Wpływ ciśnienia (0.2–20 mbar) na stan powierzchni i dystrybucję produktów węglowych (HS-Co/CeO_2, H_2O/EtOH=3/1 mol/mol, 420ºC).

Zwiększenie ciśnienia (4–20 mbar) spowodowało pojawienie się tlenkowej fazy kobaltowej – CoO_x (Rys. 1), wzrost ilości jonów Ce(IV) w strukturze powierzchni nośnika oraz zaadsorbowanych na powierzchni grup zawierających tlen. Zmiany te wpłynęły na wzrost udziału dwutlenku węgla w analizowanych produktach węglowych. Na tej podstawie stwierdzono, że większy udział dwutlenku węgla w produktach poreakcyjnych może być związany ze stanem utlenienia powierzchni; jednakże, może być również spowodowany dodatkowym zaangażowaniem słabych miejsc adsorpcyjnych w przemiany ESR.

Dalsze badania katalizatora HS-Co/CeO_2 były prowadzone przy większym ciśnieniu cząstkowym par i dla różnych stężeń reagentów (H_2O/EtOH = 3/1, 9/1, 12/1 mol/mol, $p_{cząstkowe}$ = 57 mbar, $p_{całkowite}$ = 1 atm, 420ºC). Wykazano, że stan utlenienia kobaltu w katalizatorach z tlenkiem ceru nie jest głównym czynnikiem wpływającym na selektywność katalizatora, podczas gdy obecność powierzchniowo-zaadsorbowanych grup hydroksylowych odgrywa bardzo istotną rolę. Nie jest to zaskakujące, ponieważ można oczekiwać, że w zależności od warunków reakcji, zaadsorbowane grupy zawierające w swoim składzie tlen, mogą hamować lub ułatwiać niektóre ścieżki reakcji, jak również mogą nie mieć na nie wpływu.

Podobne badania prowadzone na katalizatorze z nisko-zdyspergowanym nośnikiem cerowym (średni rozmiar krystalitów kobaltu 39.3 nm) doprowadziły do innego znaczącego wniosku. Oprócz ilości zaadsorbowanych grup zawierających tlen, duże znaczenie mogą mieć również inne czynniki, takie jak morfologia katalizatora czy miejsca, gdzie grupy tlenowe są zaadsorbowane.

Badania wykazały, że promotor potasowy wprowadza nowy typ selektywnych miejsc, $K^{\delta+}–O_{surf}^{\delta-}$ (dalej oznaczonych w formie skróconej: K–O), których ilość rośnie wraz ze wzrostem nadmiaru wody w mieszaninie reakcyjnej. Miejsca te promują reakcję reformingu etanolu, stanowiąc źródło dodatkowego tlenu. Wyraźny wpływ powierzchniowego stężenia grup OH i miejsc $K^{\delta+}–O_{surf}^{\delta-}$ na selektywność ESR do produktów gazowych, na promowanych i nie promowanych katalizatorach możliwy jest aż do uzyskania maksymalnych wydajności wodoru i dwutlenku węgla, wynikających z danych termodynamicznych.

Podatność katalizatorów na zawęglanie, była szczególnie wyraźna dla reakcji prowadzonej przy stechiometrycznym stosunku reagentów (3/1 mol/mol). Wyniki badań dowiodły, że rodzaj tworzącego się depozytu węglowego zależy zarówno od morfologii nośnika jak i wielkości cząstek kobaltu. Na katalizatorze z większymi cząstkami kobaltu faworyzowany jest wzrost włókien (wiskerów, *ang. whiskers*) węglowych, podczas gdy na powierzchni katalizatora nano-zdyspergowanego węgiel osadzany jest stopniowo na najbardziej zewnętrznych warstwach katalizatora. Ilość osadzonego węgla została zdecydowanie zmniejszona w wyniku promocji katalizatora z nośnikiem nano-cerowym potasem.

Znaczenie grup hydroksylowych i miejsc K–O potwierdziły badania stabilności właściwości katalizatorów w trakcie ESR, prowadzone przy stosunku molowym H_2O/EtOH = 12/1. Rys. 2 pokazuje, że w trakcie reakcji ESR ilość grup OH i K–O ulega zmianie, nieznacznie poprawiając w ten sposób selektywność reakcji ESR.

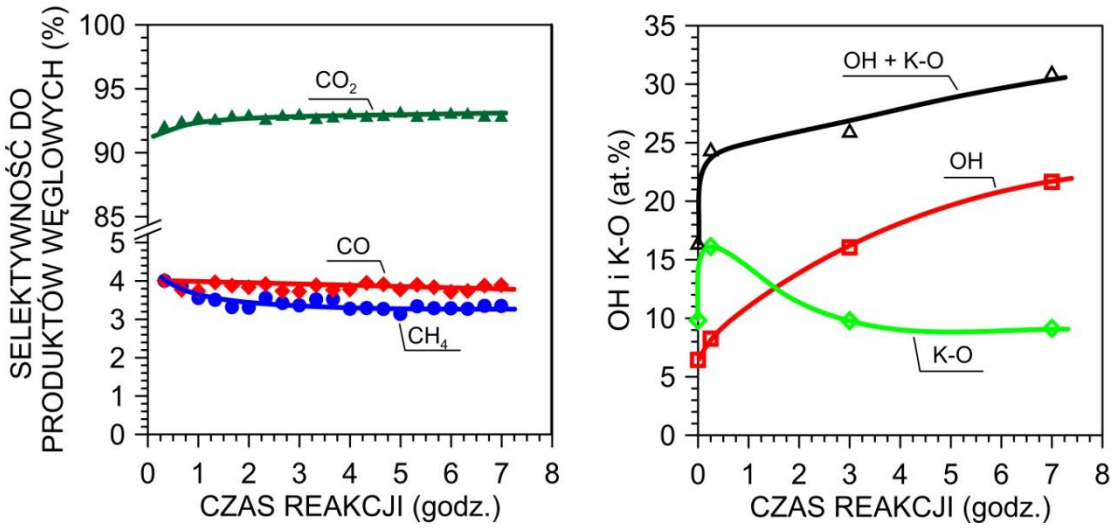

Rys. 2 Wpływ czasu reakcji ESR na selektywność do produktów węglowych oraz na zmiany procentowej ilości grup OH i miejsc K–O na promowanym potasem katalizatorze z nośnikiem cerowym (H_2O/EtOH = 12/1 mol/mol, 420ºC, $p_{częściowe}$ = 57 mbar, $p_{całkowite}$ = 1 atm).

Wyniki badań doprowadziły do wniosku, że zarówno grupy OH jak i miejsca K–O są odpowiedzialne za zmniejszenie ilości tworzącego się depozytu węglowego i zahamowanie powstawania odwodornionych form węgla. Wniosek ten oparto o fakt, że przy uwzględnieniu zmian na powierzchni wszystkich katalizatorów z nośnikami cerowymi, brak jednoznacznej korelacji pomiędzy ilością grup OH a zmniejszeniem ilości powstającego depozytu węglowego (Rys. 3, lewy wykres).

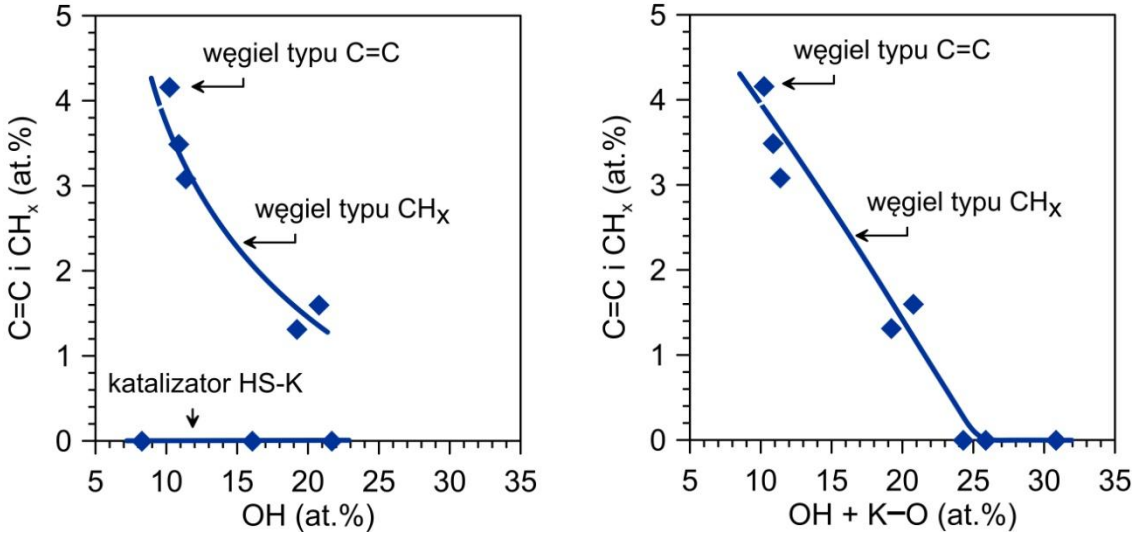

Rys. 3 Korelacja procentowego stężenia (w procentach atomowych) węgla typu C=C oraz CH_x ze stężeniem grup hydroksylowych (lewy wykres) i sumą grup OH + K–O (prawy wykres) na powierzchni katalizatorów z nośnikiem cerowym.

Jeśli poza grupami hydroksylowymi, rozważy się również wpływ miejsc K–O można znaleźć liniową zależność (Rys. 3, prawy wykres) pomiędzy ilością grup zawierających tlen, a ilością i rodzajem powstającego depozytu węglowego.

W oparciu o uzyskane wyniki zasugerowano, że jeśli powierzchnia katalizatora będzie pokryta łatwo dostępnymi (niezbyt silnie związanymi) grupami zawierającymi tlen, jak np. grupy hydroksylowe i K–O, można ograniczyć lub całkowicie wyeliminować proces zawęglania.

Badania podobne do wyżej przedstawionych, zostały przeprowadzone dla katalizatorów z nośnikami nano- (HS) i mikro-cyrkonowymi (LS). Dwa katalizatory, różniące się dyspersją kobaltu (22.5 and 42.3 nm, odpowiednio) otrzymano metodą impregnacyjną [3]. Część katalizatora HS-Co/ZrO_2 promowano potasem (2 wt.%).

Przed przystąpieniem do omówienia uzyskanych wyników warto nadmienić, że tlenek cyrkonu, w przeciwieństwie do tlenku ceru, jest bardzo słabo redukowalny, wykazuje bardzo niską mobilność tlenu i większą kwasowość powierzchni, toteż można było oczekiwać różnic pomiędzy tymi dwoma grupami katalizatorów.

Cząstki kobaltu osadzone na nośnikach cyrkonowych wykazują podobne zachowanie było obserwowana w katalizatorach z nośnikiem cerowym, tzn. że udział procentowy utlenionej formy kobaltu rośnie wraz ze wzrostem nadmiaru wody w mieszaninie reakcyjnej. Podobnie jak w przypadku katalizatorów z tlenkiem ceru jako nośnikiem, stwierdzono, że procentowy udział utlenionej formy kobaltu na powierzchni katalizatora nie jest najważniejszym czynnikiem wpływającym na selektywność katalizatora. Ponadto wykazano, że procentowy udział atomowy grup hydroksylowych i miejsc K–O na powierzchni ma wpływ na wydajność wodoru i dwutlenku węgla. Rys. 4 przedstawia zależność wydajności tworzenia wodoru i dwutlenku węgla od stężenia grup hydroksylowych i miejsc K–O na powierzchni obu grup katalizatorów, z nośnikiem cerowym i cyrkonowym. Stężenie grup hydroksylowych rośnie wraz ze wzrostem nadmiaru wody w mieszaninie reakcyjnej w stopniu zależnym od dyspersji katalizatora. W przypadku katalizatora promowanego potasem, rosnąca ilość grup hydroksylowych jest dodatkowo uzupełniona o wzrost ilości grup K–O.

Biorąc pod uwagę zarówno wpływ grup OH jak i K–O, uzyskane wydajności tworzenia wodoru i dwutlenku węgla tworzą zależność, której wartości graniczne wydajności stanowią wyniki uzyskane na katalizatorach promowanych potasem. Limity te są zgodne z limitami termodynamicznymi dla wydajności do wodoru i dwutlenku

węgla w reformingu parowym etanolu. Ze stechiometrii reakcji ESR wynika, że z jednego mola etanolu można uzyskać (przy braku reakcji ubocznych) 6 moli wodoru i 2 mole dwutlenku węgla [39]. Na badanych katalizatorach wydajność tworzenia wodoru wyniosła 5.55 mol/mol$_{EtOH}$, zaś dwutlenku węgla 1.85 mol/mol$_{EtOH}$.

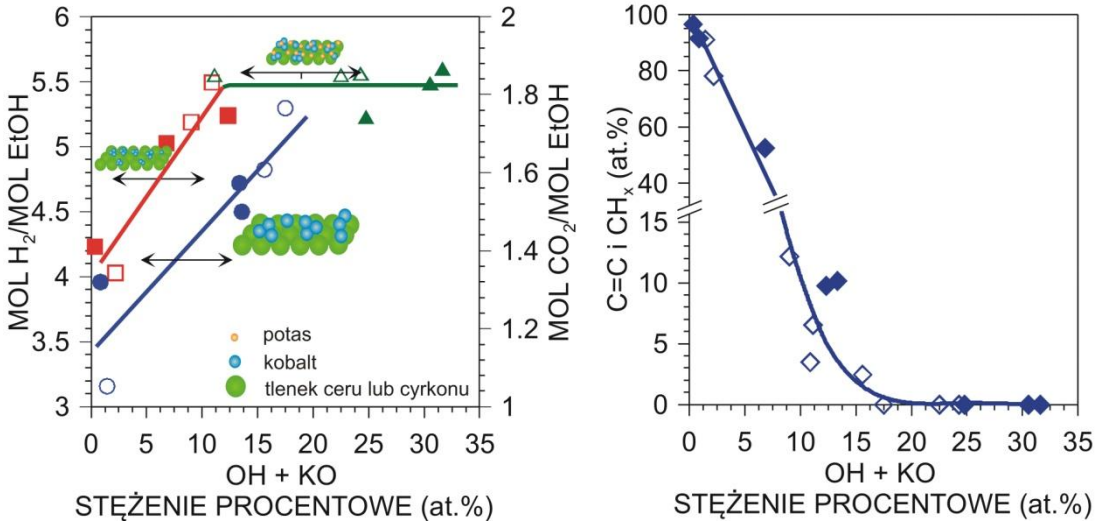

Rys. 4 Zależność wydajności reakcji ESR (420ºC) w kierunku tworzenia H_2 i CO_2, oraz ilości węgla typu C=C oraz CH_x na całej powierzchni katalizatorów, od stężenia OH + K–O. Każdy punkt odnosi się do innego stosunku molowego H_2O/EtOH. Symbole: ○, □, △ odnoszą się do katalizatorów z tlenkiem ceru LS-, HS- i HS-K, podczas gdy symbole wypełnione ●, ■, ▲ do katalizatorów z nośnikiem cyrkonowym LS-, HS- i HS-K. Na prawym rysunku symbole ◇ odpowiadają danym uzyskanym dla katalizatorów z tlenkiem ceru, zaś symbole wypełnione ◆ odnoszą się do katalizatorów z tlenkiem cyrkonu.

Poza ilością cząstek OH + K–O, na reakcję ESR również wpływa rozmiar krystalitów kobaltu. Rys. 5 pokazuje, że dodatek promotora potasowego umożliwia selektywny przebieg reakcji ESR, nawet w przypadku katalizatora o bardzo dużych krystalitach kobaltu.

Inną cechą, która odróżnia katalizatory z nośnikiem cyrkonowym od tych z nośnikiem cerowym, jest ich podatność na zawęglanie. Katalizatory z nośnikiem cyrkonowym okazały się bardziej podatne na zawęglanie, co w literaturze przypisywane jest słabej mobilności tlenu, niewielkich zdolności tego nośnika do magazynowana tlenu, jak również kwasowej naturze powierzchni tlenku cyrkonu [29]. Korelacja atomowego procentowego udziału węgla z ilością grup zawierających tlen (Rys. 3, prawy rysunek) wykazały, że niewielka ilość grup OH i miejsc K–O na powierzchni katalizatora skutkuje tworzeniem się znaczących ilości depozytu węglowego, występującego w formie całkowicie (lub prawie całkowicie) odwodornionej C=C, głownie w postaci włókien węglowych i warstw węgla, co stwierdzono w oparciu o badania mikroskopowe.

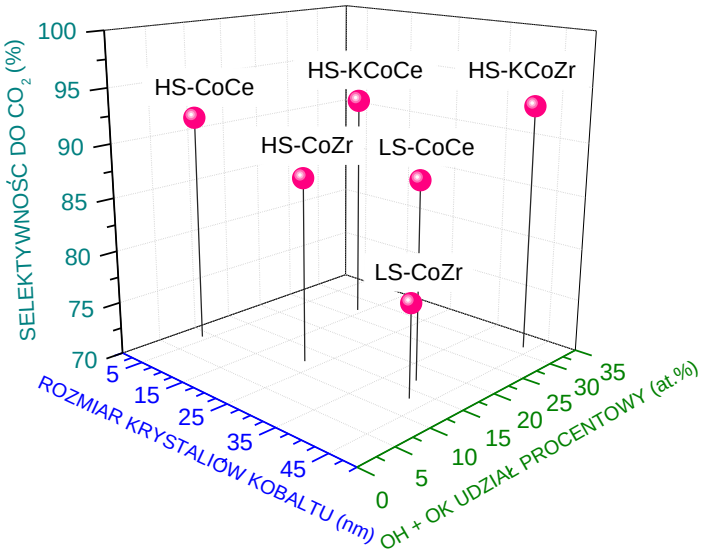

Rys. 5 Wpływ rozmiaru krystalitów kobaltu i ilości grup zawierających atomy tlenu (wyrażony w procentach atomowych) na selektywność ESR w kierunku tworzenia dwutlenku węgla na katalizatorach z nośnikami cerowymi i cyrkonowymi (H_2O/EtOH = 12/1 mol/mol, 420ºC, t = 1 godz.).

Wnioski

Badania wykazały, że stan utlenienia kobaltu i ceru zależy od warunków reakcji (ciśnienie, stosunek molowy reagentów). Dodatkowo, stan utlenienia kobaltu zależy od rodzaju nośnika. W pracy wykazano, że sugerowana w literaturze szczególna rola właściwości utleniająco-redukujących głównych składników katalizatora w warunkach reakcji nie ma bezpośredniego wpływu na selektywność ESR. Największe znaczenie, przypisano ilości zaadsorbowanych na powierzchni cząstek zawierających tlen (OH i O), co jest ogólną cechą wszystkich katalizatorów, niezależnie od rodzaju i dyspersji nośnika. Oprócz ilości cząstek zawierających w swoim składzie tlen, kolejnym istotnym czynnikiem jest dyspersja kobaltowej fazy aktywnej. Stwierdzono, że w celu uzyskania dobrej selektywności i wydajności do wodoru i dwutlenku węgla, w przypadku katalizatorów z małymi cząstkami kobaltu wymagana jest mniejsza ilość zaadsorbowanych grup tlenowych, niż ma to miejsce w przypadku katalizatorów o dużych krystalitach kobaltu. Promowanie katalizatorów potasem znacząco zwiększa procentowy udział grup OH i miejsc K–O na powierzchni katalizatora (przy tym także i selektywność reakcji ESR), niezależnie od wielkości krystalitów kobaltu. Z tego powodu promotor potasowy poprawia własności katalityczne układów z tlenkiem cyrkonu (z dużymi krystalitami kobaltu) w znacznie większym stopniu, niż ma to miejsce w przypadku katalizatorów z tlenkiem ceru (z małymi krystalitami kobaltu). Ilość grup zawierających tlen wpływa na intensywność procesu tworzenia się depozytu

węglowego, zaś w przypadku katalizatorów z nośnikiem cerowym wzrost procentowego udziału zaadsorbowanych na powierzchni cząstek zawierających tlen silnie wpływa również na rodzaj powstającego depozytu, zmieniając jego formę z całkowicie odwodornionej C=C na CH_x.

References/ Références/ Literatura

1. International Energy Agency, *Learning from the blackouts. Transmission System Security in Competitive Electricity Markets* 2005: Paris.
2. Siemens, *Answers for energy. Global Blackouts – Lessons Learned*. 2005: Milan.
3. W. Jakobik in Ekonomia, Energetyka, Polska *Polish blackout threat highlights network issues. Commentary for Interfax* 25 August 2005, Available from: https://wjakobik.com/2015/08/25/polish-blackout-threat-highlights-network-issues-commentary-for-interfax/.
4. Agnieszka Barteczko and Wojciech Zurawski; Edited by David Holmes *'Polish power generators call for urgent steps to avoid blackouts*' 8 September 2015; Available from: http://www.reuters.com/article/poland-electricity-idUSL5N11E38U20150908.
5. S. Udubasceanu *'Heatwave pushes Poland a 'whisker away from blackout'* 10 August 2015; Available from: http://www.icis.com/resources/news/2015/08/10/9912442/updated-heatwave-pushes-poland-a-whisker-away-from-blackout-/.
6. M. Olszewski '*The Polish Energy Drought'* 28 September 2015; Available from: http://energytransition.de/2015/09/the-polish-energy-drought/.
7. *Energetyka wiatrowa w Polsce (Wind energy in Poland)* 2015/2016, Avaiable from *www.paiz.gov.pl/files/?id_plik=23801*
8. Polskie Stowarzyszenie Energetyki Wiatrowej *Stan energetyki wiatrowej w Polsce w 2015 roku,* 2015, Avaliable from http://pliki.psew.pl/Marcin/Stan_energetyki_wiatrowej_w_Polsce_PL.pdf
9. The European Wind Energy Association *Wind in power 2015 European statistics*. 2016. http://www.ewea.org/fileadmin/files/library/publications/statistics/EWEA-Annual-Statistics-2015.pdf
10. REN21 2015. Renewables 2015 Global Status Report (Paris: REN21 Secretariat), Avaliable from http://www.ren21.net/wp-content/uploads/2015/07/REN12-GSR2015_Onlinebook_low1.pdf

11. Biznes Alert '*Dania rezygnuje z pięciu elektrowni wiatrowych ze względu na wysokie koszty'* 18 May 2016, Avaliale from http://biznesalert.pl/dania-rezygnuje-z-pieciu-wiatrakow-ze-wzgledu-na-wysokie-koszty/
12. H. Idriss *Platinum Metals Rev.* **48** (2004) 105–115.
13. P.R. de la Piscina, N. Homs *Chem. Soc. Rev.* **37** (2008) 2459–2467.
14. L.V. Mattos, G. Jackobs, H.D. Burtron, F.B. Noronha *Chem. Rev.* **112** (2012) 4094–4123.
15. M. Ni, D.Y.C. Leung, M.K.H. Leung *Int. J. Hydrogen Energy* **32** (2007) 3238–3247.
16. F. Auprêtre, C. Descorme, D. Duprez *Top Catal.* **30|31** (2004) 487–491.
17. E.Y. García, M.A. Laborde *Int. J. Hydrogen Energy* **16** (1991) 307–312.
18. P.K. Cheekatamarla, C.M. Finnerty *J. Power Sources* **160** (2006) 490–499.
19. S. Turczyniak, Y.T. Law, A. Machocki, S. Zafeiratos, ed. *Spektroskopia fotoelektronów badaniach katalizatorów reformingu parowego etanolu* in *Nauka i przemysł - metody spektroskopowe w praktyce, nowe wyzwania i możliwości,* ed. Z. Hubicki. 2013: Lublin, 617–624.
20. A. Machocki *Przem. Chem.* **86** (2006) 1045–1048.
21. E. Martono, J. M. Vohs *J. Catal.* **291** (2012) 79–86.
22. S. Ogo, T. Shimizu, Y. Nakazawa, K. Mukawa, D. Mukai, Y. Sekine Sekine *Appl. Catal., A* **495** (2015) 30–38.
23. J.A. Torres, J. Lorca, A. Casanovas, M. Domínguez, J. Salvadó, D. Montané *J. Power Sources* **169** (2007) 158–166.
24. S.S.-Y. Lin, D.H. Kim, M.H. Engelhard, S.Y. Ha *J. Catal.* **273** (2010) 229–235.
25. Zs. Ferencz, A. Erdőhelyi, K. Baan, A. Oszkó, L. Óvári, Z. Kónya, C. Papp, H.-P. Steinrück, J. Kiss *ACS Catal.* **4** (2014) 1205–1218.
26. J.C. Vargas, S. Libs, A.C. Roger, A. Kiennemann *Chem. Eng. Trans.* **4** (2004) 247–252.
27. A. Machocki, A. Denis, W. Grzegorczyk, W. Gac, *Appl. Surf. Sci.* **256** (2010) 5551–5558.
28. E. Martono, J.M. Vohs *ACS Catal.* **1** (2011) 1414–1420.
29. H. Song, U.S. Ozkan *J. Catal.* **261** (2009) 66–74.
30. P. Rybak, B. Tomaszewska, A. Machocki, W. Grzegorczyk, A. Denis *Catal. Today*, **176** (2011) 14–20.
31. H. Wang, Y. Liu, L. Wang, Y.N. Qin *Chem. Eng. J.* **145** (2008) 25–31.

32. B. Banach, A. Machocki *Appl. Catal., A* **505** (2015) 173–182.
33. M. Greluk, M. Rotko, A. Machocki *Catal. Lett.* **146** (2016) 163–173.
34. J. Llorca, P.R. de la Piscina, J.A. Dalmon, J. Sales, N. Homs *Appl. Catal., B* **43** (2003) 355–369.
35. J. Llorca, N. Homs, J. Sales, J.-L.G. Fierro, P.R. de la Piscina *J. Catal.* **222** (2004) 470–480.
36. G. Słowik, M. Greluk, A. Machocki, *Mater. Chem. Phys.* **173** (2016) 219–237.
37. M. Greluk, P. Rybak, G. Słowik, M. Rotko, A. Machocki, *Catal. Today* **242** (2015) 50–59.
38. M. Greluk, M. Rotko, A. Machocki, *Catal Lett* **146** (2016) 163-173.
39. K. Vasudeva, N. Mitra, P. Umasankar, S.C. Dhingra *Int. J. Hydrogen Energy*, **21 (**1996) 13–18.

Introduction

OUTLINE

Abstract

This chapter describes the role of hydrogen as an energy carrier and key factors in favour of bio-ethanol as a source of hydrogen. The main role of the introduction section is to explain the validity of carrying out the research on unpromoted and potassium-promoted cobalt-based systems with cerium and zirconium oxides supports and to present the main objectives of the doctoral thesis.

Inevitably depletion of fossil fuel's resources and increasing energy demand [1] due to rapid growth in population and industrial development [2] are driving forces for upgrading the world energy sector [3]. The criteria that should be taken into account while considering the development direction include availability of resources, market demand and competitiveness. Nowadays, the energy demand is fulfilled mostly by conventional sources like coal, natural gas and crude-oil. The energy that is produced by means of non-renewable resources results in undesirable climate changes. Inefficient atmospheric combustion of fossil fuels results in emission of greenhouse gases, i.e., sulphur dioxide, carbon dioxide and nitrogen oxides (NO_x), being a threat to the world climate [4] and human health. Today we are witnessing the increasing vulnerability of young generation for respiratory infections, like asthma [5] or lung disease. Heart disease and cancer are common as well. In further perspective, uncontrolled emission of greenhouse gases may cause some natural calamities like droughts, excessive rains and floods [6], earthquakes and massive volcanic activity.

Another important issue, that most of European economies need to face, is dependence of European Union (EU) Member States on energy imports, especially oil and gas (between 80% and 100%) [7]. Today, the EU imports gas mostly from unstable countries in the Middle East, Central Asia and Africa. However, as the situation in those places is getting worse, Russia appears to be the natural choice for being a gas supplier. From the other side, Gazprom's active expansion strategy does not help to lessen EU's energy security concerns. Hence, the attention that is paid to find alternative methods of energy obtaining is fully justified. The alternative energy sources like solar, wind, thermal, hydroelectric, biomass are inexhaustible, however, they are suited to particular regions.

Catalysis may play a major role in supporting the global vision of sustainable future since it is expected that hydrogen-based fuel cells technologies can overcome the energy and environmental challenges of the XXI century [8].

Hydrogen as an energy carrier

The key role of catalysis in a modern industry is undeniable fact. Only a few of chemical processes are carried out without catalysts. Many, important from the industrial point of view, reactions cannot be carried out without a catalyst. In most cases, catalysts are present at least on the one stage of the industrial process in the worldwide production [9]. Understanding the growing demand for energy and the increase of public awareness of environmental threats, the researchers focused on alternative methods of energy production. It has been assumed that “a new” source of energy should have minimal negative impact on the environment, being, at the same time, effective and accessible [10]. This assumption results from tightening regulations within the European Union (EU). Adopted and presented in 2008 the definitive EU 2020 climate and energy package [11] imposes the reduction of greenhouse gases and promote renewable energy. Since EU is well on the track to meet 2020 targets, in 2014 in Brussels EU set a new 2030 policy framework [12]. Within this framework EU has set three targets that should be fulfilled before the year 2030, i.e. a cut of at least 40% in greenhouse gases emissions, increasing to at least 27% share of renewable energy, and increasing by at least 27% in energy efficiency [13].

In the nearest future the great potential is attributed to the sources of energy which use the potential of wind, water, sun and biomass to satisfy an increasing energy demand. In the further perspective, hydrogen is considered as a source of “clean

energy" since it can be generated from low- or zero-carbon emissions sources [14] therefore, it will probably replace (to some extent) traditional liquid and gaseous fuels in stationary and transport applications. The idea of hydrogen use as an energy carrier is not new, however, currently this subject returns in the context of rapid development of fuel cells technology. According to the report of European Commission [15] it is expected that by 2020 hydrogen will have changed the face of global energy economy due to the market penetration of portable, stationary and transport applications based on hydrogen energy.

Hydrogen is the most wide spread element [16], therefore, its abundance makes hydrogen energy potentially affordable but the deciding factor in favour of hydrogen, are its good energetic properties. Hydrogen has the highest heat content per mass unit of all the conventional fuels and provides energy yield of 122 kJ/g which is 2.75 times greater than hydrocarbon fuels like petroleum and 4.06 times greater than coal [17]. Hydrogen has a wide range of flammability comparing to other fuels thus engines using hydrogen technology can be operated more effectively on excessively lean mixtures than gasoline engines. Moreover very low ignition energy (0.02 mJ), wide flammability range (4–74% in air) [18] and high diffusivity make hydrogen a good and safe fuel.

Nowadays research programs proved the technological feasibility of clean energy obtaining, that can be used in variety of stationery applications, as well as in transport systems. Hydrogen power cells are suggested to be used as a back-up power systems (uninterrupted power supply, UPS) for domestic use as well as in some public institutions, and complex production processes. The Japanese were pushed for what is called "hydrogen society" in which most of houses and institutions are provided with units used liquefied petroleum gas as the hydrogen feedstock, others – natural gas and some – kerosene. This solution allows to generate electricity on-site at houses bringing both environmental and economic benefits [19]. In accordance to the "hydrogen society" coming out, in 2015, bold headlines announced, that the big dream of hydrogen as a fuel of the future, came true thanks to Toyota, which launched production of "the first hydrogen fuel cell electric vehicle" [20] (it should be clarified that a lot of land, water and space vehicles can already run on hydrogen, so term "the first" refers to planned mass scale production probably). In 2017 it is expected that Toyota Mirai will be available in Great Britain, Denmark and Germany. Unfortunately, this amazing, breakthrough technological invention will cost 71 400 euro (in Germany), placing it out of reach of an ordinary people. It cannot be forgotten that developed by

Hyundai, the Hyundai ix35 Fuel Cell is also called "the first hydrogen-fuelled car" and according to the Hyundai official website its massive production was launched in 2013 [21]. News [22] from October 2015 suggests that Hyundai won the race since it is already available in Europe while Toyota is expected to follow it shortly. Costs of Hyundai ix35 Fuel Cell vary from 57 752 [23] to 85 317 euro [24] depending on a source of information.

Once hydrogen is produced it needs to be stored and then transmitted to customers, therefore, an essential key to developing a hydrogen economy on an industrial scale is undoubtedly the answer for issues as hydrogen storage and transport methods and costs. Hydrogen can be stored in three ways [25]: *(i)* as a compressed gas, *(ii)* as a liquid (stored at -252.8ºC) or *(iii)* as a solid combined with other compounds, e.g., physical adsorption on the surface of some alloys ($LaNi_5$, $ZrCr_2$), carbon nanotubes or chemical storage in the form of hydrides (KH, CaH_2 etc.). Apart from problems associated to hydrogen storage on board, it should be noted that at this time, for most countries, cost of running hydrogen fuelled vehicles is too high, i.a., due to energy expense required for fuel liquidation. Moreover, introduction of cars requiring filling up with compressed hydrogen present the issue of the construction of filling stations located every few kilometres (like average gasoline stations), meaning that countries interested in this solution should possess extensive infrastructure supporting the widespread use of hydrogen in motor vehicles. It will undoubtedly allow to create new workplaces, but their maintenance will be possible at first only in countries with highly developed economies. This clearly shows that the commercialization of hydrogen-powered vehicles in countries with less developed economies will by simply unprofitable. To overcome this problem, making the hydrogen economy more realistic and widely available at the same time, alternative methods of hydrogen production can be suggested.

Bio-ethanol as a hydrogen source

So far, there are many available methods of hydrogen production [26]. The reforming of natural gas, gasification of coal and refinery residues are one the most developed technology, while others, like e.g., steam reforming of ethanol (ESR) are still developing. The ESR process fulfils all the criteria imposed by the EU. First of all, ethanol (EtOH) can be produced by fermentation of sugars derived from biomass such

as wheat, corn, sugar beets, sugar cane, molasses [27], therefore, it can be defined by the prefix "*bio*-" to highlight its friendliness and recycled nature.

Secondly, bio-ethanol is harmless for the environment, since carbon dioxide emitted into the atmosphere during combustion or steam reforming is balanced by the amount of carbon dioxide absorbed by plants and forests. Another advantage of bio-ethanol is the fact that it contains no sulphur compounds and heavy metals, and also its storage and transportation does not cause difficulties. Moreover, the biomass processing will help to utilize the wastelands which, taking into account agricultural potential of Poland, is undoubted advantage. The listed advantages are not in a conflict with the overall stringent environmental criteria set by EU directives, actually perfectly fitting into their standards.

Ethanol can be directly used as a fuel, however, its transformation via ethanol steam reforming is strongly recommended. The most important advantage of ethanol transformation is the process efficiency. Heat combustion of hydrogen is 29 kcal/g while in the case of ethanol it is only 7 kcal/g [28].

First, limited reports about the ethanol steam reforming came from 1926. Later the process was systematically, although not very intensively, studied by few authors. Extensive reports about catalytic systems suggested for the ESR emerged after 2000. From that moment the interest in this field is constantly growing. Today, we are witnessing the intensive research towards determining the most beneficial chemical composition for the ESR catalyst. Objectively looking at today's achievements, the most important goals should be both: discovering of new materials and finding rational strategies to improve properties of promising catalysts, proposed in literature. Among so far examined catalysts the greatest interest has been placed in these based on noble metals (palladium, platinum, rhodium) and less expensive transition metals – mainly on cobalt and nickel. The base for studies of cobalt-based systems were literature reports suggesting a high cobalt activity for C–C bond cleavage in the temperature range of 350–400ºC and selectivity towards hydrogen comparable to noble metals. Disadvantages of cobalt catalysts such as sintering or deactivation owing the coke formation are believed to be limited by selection of a suitable support, dispersion of the active phase or by the ESR process parameters.

From 1970 cerium oxide has emerged as one of the most industrially interesting oxides [29, 30], due to its high oxygen storage capacity and excellent redox properties related to oxygen mobility. As for zirconium oxide, its good thermal stability made it

a potential candidate for catalysts' support. Ceria- and zirconia-supported cobalt catalysts were widely studied in literature using various techniques, like temperature-programmed measurements, infrared spectroscopic investigations, microscopic studies, and, of course, analysis of post reaction products. Recently the new trend in using X-ray Photoelectron Spectroscopy (XPS), especially combined with the gas chromatography (GC) or mass spectrometry (MS), has been observed.

Meeting current trends, predominating on the scientific field and understanding the big potential of the XPS technique, it was suggested that this method will help to understand the influence of the surface state on ceria- and zirconia-supported cobalt catalysts' activity and selectivity.

Main goals of the doctoral thesis

The thesis consists of two main parts *(i)* literature review and *(ii)* experimental section. In the first part a brief summary of current knowledge about the ESR and cobalt catalysts supported on ceria and zirconia support has been presented. The second part concerns fundamental catalysts characterization and XPS studies of pre-reduced catalysts' under the ESR, combined with *on-line* post-reaction products analysis.

The doctoral thesis was carried out in three research institutions: *(i)* University of Maria Curie-Skłodowska (UMCS) in Lublin (Poland), *(ii)* Institut de Chimie et Procédés pour l'Énergie, l'Environnement et la Santé (ICPEES) in Strasbourg (France) and *(iii)* BESSY Synchrotron facility in Berlin (Germany). The used experimental setup, the measurements procedure, and analysis of results were carried out in a different way; therefore, typical construction of the experimental section would lead to a voluminous chapter. Therefore, to avoid it, and to make easier tracking various problems considered in the thesis, the results of experimental studies, together with appropriate experimental procedures, were presented as drafts of articles, easy also for their future submission to scientific journals for their publication.

The main goals of the experimental part were:

(i) determination of the oxidation state of catalysts' components on different stages of their life; in the initial stages prior to the ESR reaction and their changes under the ESR conditions,

(ii) determination which form of cobalt Co(0) or Co(II) dominates under the reaction conditions,

(iii) comparison of the influence of ceria and zirconia support dispersion on the oxidation state of cobalt under the ESR, and on the ESR selectivity,

(iv) understanding the influence of the reaction conditions (pressure, the H_2O/EtOH molar ratio) on the surface's state, ethanol conversion selectivity and carbonaceous deposit formation,

(v) understanding the influence of the reaction time on catalysts' surface state and their ESR catalytic performance,

(vi) explanation the influence of potassium promoter on the oxidation state of the active phase and support under the ESR, ethanol conversion selectivity and carbonaceous deposit formation,

(vii) detection the catalyst's surface species and sites which influence the course of the ESR,

(viii) providing new data in order to shed a light into the ESR reaction mechanism over ceria- and zirconia-supported cobalt catalysts,

(ix) supplement currently available knowledge.

References

1 M.Y. Youn, J.G. Seo, S. Park, J.C. Jung, D.R. Park, I.K. Song *Int. J. Hydrogen Energ.* **33** (2008) 7457–7463.

2 J.A. Torres, J. Lorca, A. Casanovas, M. Domínguez, J. Salvadó, D. Montané *J. Power Sources* **169** (2007) 158-166.

3 M.A. Sigurbjornsdottir, J. Orlygsson, *Appl. Energy* **97** (2012) 785–791.

4 K. Mazloomi, C. Gomes *Renew. Sust. Energ. Rev.* **16** (2012) 3024–3033.

5 *The Global Asthma Report 2014.* (2014). Auckland, New Zealan: The Global Asthma Network. Available at: http://www.globalasthmareport.org/ resources/Global_Asthma_Report_2014.pdf .

6 R.C. Saxena, D.K. Adhikari, H.B. Goyal *Renew. Sust. Energ. Rev*. **13** (2009) 167–178.

7 E. Christie (2007). *Oil and Gas Dependence of EU-15 Countries (Research Report 343).* Vienna Institute for International Economic Studies. Available at: https://www.bankaustria.at/files/oilgas_4-07_e.pdf].

8 V. Subramani, C. Song, *Catalysis* **20** (2007) 65–106.

9 E. Farnetti, R.D. Monte, J. Kašpar, Inorg. Bio-inorg. Chem vol. II (Chapter 2) *Homogeneous and heterogeneous catalyst*, in Encyclopedia of Life Support Systems. 2004.

10 A. Machocki *Przem. Chem.* **85** (2006) 1045–1048.

11 European Commission (2008). *Memo on the Renewable Energy and Climate Change Package, MEMO/08/33*. Brussels. Available at: http://europa.eu/rapid/press-release_MEMO-08-33_en.pdf [Accessed 23 Jan. 2008].

12 European Commission (2014). *Communication from the Commission to the European Parliament, the Council, the European Economic and Social Committee and the Committee of the Regions. A policy framework for climate and energy in the period from 2020 to 2030*, COM(2014) 15 final. Brussels. Available at: http://eur-lex.europa.eu/legal-ontent/EN/TXT/PDF/?uri=CELEX:52014DC0015 & from=EN [Accessed 22 Jan. 2014].

13 Retrived from: http://ec.europa.eu/clima/policies/strategies/2030/index_en.htm.

14 G.F. Naterer, I. Dincer, C. Zamfirescu (2013) Hydrogen as a Clean Energy Carrier. In: Hydrogen Production from Nuclear Energy, Springer London, 1–20.

15 European Commission (2006). *Introducing Hydrogen as an energy carrier. Safety, regulatory and public acceptance issues*. Belgium. Available at: https://ec.europa.eu/research/energy/pdf/hydrogen_22002_en.pdf.

16 S. Dunn *Int. J. Hydrogen Energ.* **3** (2002) 235–264.

17 P.P. Edwards, V.L. Kuznetsov, W.I.F. David, N.P. Brandon *Energy Policy* **36** (2008) 4356–4362.

18 S.A. Sherif, F. Barbir, T.N. Veziroglu (2007) Hydrogen energy technology. In: D. Yogi Goswami, Frank Kreith ed. Handbook of Energy Efficiency and Renewable Energy. CRC Press, 1–12.

19 J. Gangi '*Home sweet home'* 1 June 2008 Retrieved from http://www.altenergymag.com/content.php?issue_number=08.06.01&article=injapan.

20 '*Toyota Mirai Takes to the Track'* 23 April 2015 Retrived from http://www.rir.com/Articles/2015/04/Toyota-Mirai-at-Richmond.aspx.

21 Retrived from: http://www.hyundai.com.au/why-hyundai/design-and-innovation/fuel-cell.

22 A. Crawford '*Hyundai ix35 Fuel Cell Review, Is this the car of the future?'* 19 October 2015 Retrived from: http://www.caradvice.com.au/389702/hyundai-ix35-fuel-cell-review-is-this-the-car-of-the-future/.

23 '*Hyundai ix35 Fuel Cell: wodór przyszłością motoryzacji?'* 11 December 2015 Retrived from: http://moto.onet.pl/ekomoto/hyundai-ix35-fuel-cell-wodor-przyszloscia-motoryzacji/4nzkm6.

24 J. Taylor '*Hydrogen-powered Hyundai ix35 Fuel Cell costs £53,000'* 5 May 2015 Retrived from: http://www.carmagazine.co.uk/car-news/industry-news/hyundai/hydrogen-powered-hyundai-ix35-fuel-cell-costs-53000/.

25 L. Zhou *Renewable and Sustainable Energy Reviews* **9** (2005) 395–400.

26 O. Bicáková, P. Straka *Int. J. Hydrogen Energy* **37** (2012) 11563–11578.

27 H. Idriss *Platinum Metals Rev*. **48** (2004) 105–115.

28 E.Y. García, M.A. Laborde *Int. J. Hydrogen Energy* **16** (1991) 307–312.

29 A. Trovarelli *Cat. Rev. Sci. Eng*. **38** (1996) 439–520.

30 F. Sadi, D. Duprez, F. Gérard, A. Miloudi *J. Catal.* **213** (2003) 226–234.

part I

LITERATURE REVIEW

CHAPTER

1

Hydrogen production via catalytic ethanol steam reforming

OUTLINE

Abstract

In this section it has been taken an overview of knowledge about the typical catalysts proposed for the steam reforming of ethanol, and widely discussed in the literature. The chapter is divided into short introduction and two main parts. The first one is devoted to noble metals-based catalysts, the second – discusses in details the role of cobalt particles size, cobalt oxidation state and supports nature in the ESR. The second part is mainly focused on cobalt catalysts with ceria and zirconia supports, which are the subject of this thesis.

Steam reforming of ethanol

The ethanol steam reforming is a widely studied, highly endothermic catalytic process ($\Delta°H^{298}$ = +174 kJ/mol) [1] involving reaction between ethanol and water, producing 6 moles of hydrogen per a mole of reacted ethanol (Eq. 1), if ethanol reacts in the most desirable way.

$$CH_3CH_2OH_{(g)} + 3H_2O_{(g)} \rightarrow 6H_{2(g)} + 2CO_{2(g)} \quad \textbf{(Eq. 1)}$$

Nevertheless, the ESR process is very complex and several competing reactions may occur, generating undesirable by-products (e.g., CO, CH_4 or CH_3CHO), therefore, influencing hydrogen yield. The reaction network may include: *(i)* ethanol dehydrogenation (Eq. 2), *(ii)* ethanol decomposition (Eq. 3), *(iii)* ethanol dehydration (Eq. 4), *(iv)* incomplete ethanol steam reforming (Eq. 5), *(v)* ethanol hydrogenolysis (Eq. 6), *(vi)* acetaldehyde decomposition (Eq. 7), *(vii)* acetaldehyde (Eq. 8), carbon(II) oxide (Eq. 9) and methane conversion (Eq. 10), *(x)* methanation (Eq. 11), and *(xi)* reactions resulting in coke formation (Eq. 12).

$$CH_3CH_2OH_{(g)} \rightarrow CH_3CHO_{(g)} + H_{2(g)} \quad \textbf{(Eq. 2)}$$

$$CH_3CH_2OH_{(g)} \rightarrow CO_{(g)} + CH_{4(g)} + H_{2(g)} \quad \textbf{(Eq. 3)}$$

$$CH_3CH_2OH_{(g)} \rightarrow C_2H_{4(g)} + H_2O_{(g)} \quad \textbf{(Eq. 4)}$$

$$CH_3CH_2OH_{(g)} + H_2O_{(g)} \rightarrow 2CO_{(g)} + 4H_{2(g)} \quad \textbf{(Eq. 5)}$$

$$CH_3CH_2OH_{(g)} + 2H_{2(g)} \rightarrow 2CH_{4\,(g)} + H_2O_{(g)} \quad \textbf{(Eq. 6)}$$

$$CH_3CHO_{(g)} \rightarrow CO_{(g)} + CH_{4(g)} \quad \textbf{(Eq. 7)}$$

$$CH_3CHO_{(g)} + H_2O_{(g)} \rightarrow CO_{2(g)} + H_{2(g)} \quad \textbf{(Eq. 8)}$$

$$CO_{(g)} + H_2O_{(g)} \leftrightarrow CO_{2(g)} + H_{2(g)} \quad \textbf{(Eq. 9)}$$

$$CH_{4\,(g)} + H_2O_{(g)} \rightarrow CO_{(g)} + 3H_{2(g)} \quad \textbf{(Eq. 10)}$$

$$CO_{(g)} + 3H_{2(g)} \rightarrow CH_{4(g)} + H_2O_{(g)}$$
$$CO_{2(g)} + 4H_{2(g)} \rightarrow CH_{4(g)} + 2H_2O_{(g)} \quad \textbf{(Eq. 11)}$$

$$CH_{4(g)} \rightarrow C_{(s)} + 2H_{2(g)}$$
$$2CO_{(g)} \rightarrow C_{(s)} + CO_{2(g)} \quad \textbf{(Eq. 12)}$$
$$C_2H_{4(g)} \rightarrow \text{polymers} \rightarrow \text{coke}$$

The contribution of each reaction (Eq. 1–12) in the overall process, strongly depends on reaction conditions (e.g., reaction temperature, pressure, time on stream,

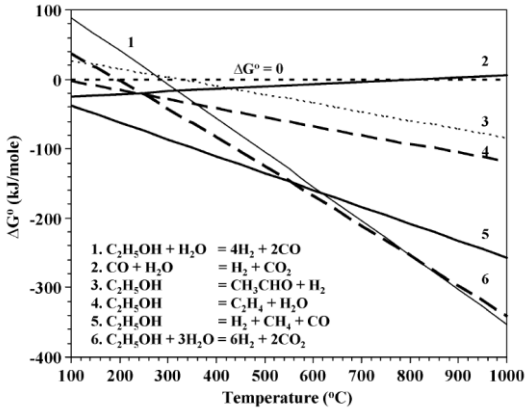

Fig. 1.1 Free energy (ΔG) changes in steam reforming, decomposition, dehydrogenation and dehydration reactions of ethanol [2].

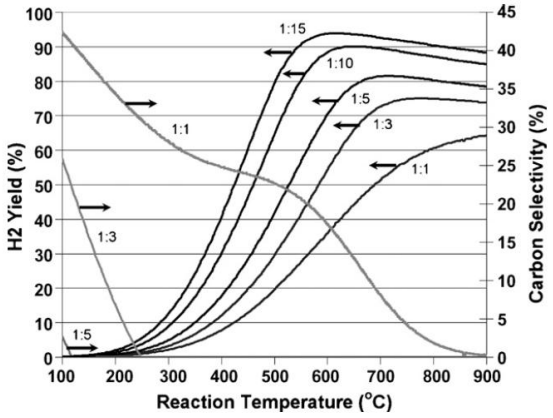

Fig. 1.2 Effect of H_2O/EtOH molar ratio on equilibrium hydrogen yield and carbon selectivity (no dilution) [4].

gas space velocity, contact time, feed composition, like H_2O/EtOH molar ratio, and the catalyst chosen [3–5].

It is worth to point out that there is number of publications (including exhaustive reviews) dealing with both: theoretical [4–12] and experimental [3, 13–18] aspects of the ESR. From the thermodynamical point of view, the reaction of ethanol steam reforming is favoured when the temperature and the excess of water in the system increase or pressure is lowered [6], preferably to 1 atm [2]. In fact, at the temperatures lower than 200ºC the most favourable reaction is ethanol decomposition (Fig. 1.1), while the ESR does not proceed spontaneously (ΔG>0) [2, 19]. The thermodynamic evaluations results [5] have shown that, in the temperature range of 100–1000ºC, by the increase of water excess, the selectivity towards hydrogen and carbon dioxide can be increased, while the selectivity to methane exhibits the opposite tendency. The maximum of hydrogen and carbon dioxide formation for the H_2O/EtOH molar ratio higher than 3/1 mol/mol was found within a temperature range of 550–700ºC (Fig. 1.2) [4]. However, it should be noted that the temperature increasing favours reverse water gas-shift (RWGS) reaction [11, 16, 20]. This effect is strongly marked for the ESR carried out with low excess of water. The selectivity towards carbon monoxide was found to be almost not influenced by the H_2O/EtOH molar ratio in the temperature range from 100ºC to 400ºC [4]. Therefore, while thinking about fuel cells, the temperature region below 400ºC seems to be the most interesting from technological point of view, since both carbon monoxide and thermal duty reduction will result in lowering the costs [21].

Another important issue in the ESR, is the influence of the overall (total) reaction pressure and the partial pressure of reactants (Fig. 1.3) on hydrogen production.

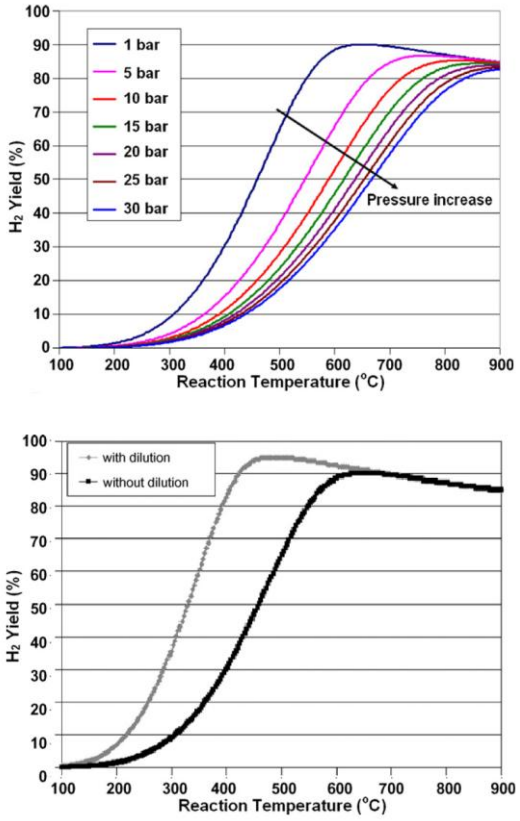

Fig. 1.3 Effect of pressure (H_2O/EtOH = 10/1 mol/mol) (top) and dilution (inert/H_2O/EtOH = 25:10:1) (down) on equilibrium hydrogen yield [4].

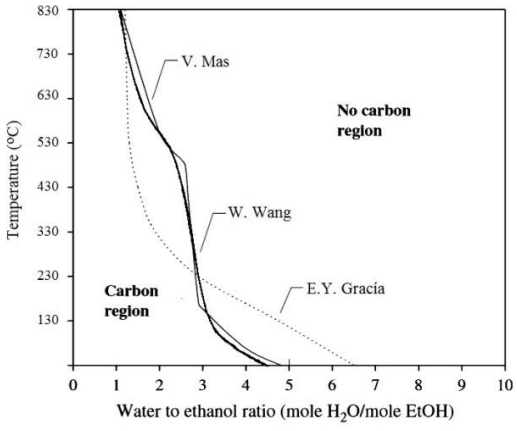

Fig. 1.4 Range of conditions for carbon formation Data from E.Y. García and M. Laborde [6], W. Wang and Y.Q. Wang [11], were added to the Fig. 9 from V. Mas et al. work [7].

H. Song et al. [4] have noted that the increase of the total pressure from 1 to 30 bar has a negative effect on hydrogen production. Whereas, lowering of the partial pressure of reactants by the addition of an inert gas at temperatures lower than 600ºC, results in the increase of hydrogen yield. The authors [4] explained this by the fact that diluting the system favours the methane steam reforming, hence an observable difference at low temperatures. At higher temperatures (>600ºC) the RWGS reaction has a significant influence on hydrogen yield. Equilibrium of this reaction is not affected by dilution (generally, by the pressure).

The thermodynamic calculations have been also performed for various H_2O/EtOH molar ratios [4, 6–8, 11]. The analysis suggests that, with higher excess of water, formation of carbon monoxide and methane can be minimized [6]. Moreover, E.Y. García and M. Laborde [6] have suggested that at least the H_2O/EtOH= 2/1 mol/mol and the temperatures higher than 330ºC are needed to operate within no carbon region. The Authors carried out their calculations considering only ethanol, water, carbon monoxide, methane, carbon dioxide, and hydrogen in equilibrium, which

raised an objection of K. Vasudeva et al. [8], since other liquid products like, e.g., acetaldehyde are also formed during the ESR. Fig. 1.4 presents the comparison of thermodynamic calculations of E.Y. Gracía and M. Laborde [6], V. Mas et al. [7], and W. Wang and Y.Q. Wang [11]. It appears, that in order to work in the free of coke formation region for the H_2O/EtOH = 2/1 molar ratio, the operating temperature must be higher than 630ºC, whereas in the case of the H_2O/EtOH = 3/1 molar ratio the temperature higher than 330ºC is required [7, 11]. In further sections of this chapter will be shown that thermodynamic calculations concerning carbon free zone are not entirely reflected in the experimental studies.

The thermodynamics does not consider the concept of time, thus it does not provide any indicators about reactions rate. Most the aforementioned reactions (Eq. 1–12), are slow, hence a catalyst plays a pivotal role in the efficiency of the ESR. Numerous experimental investigations have been performed to determine the best catalyst's composition. A wide variety of catalysts have been examined so far. A close look at literature reveals that, the ESR catalysts can be divided in three groups, according to the type of the active phase: *(i)* those based on noble metals, like Pt, Pd, Rh, Ru, Ir, *(ii)* transition metals (mainly Co, Ni and Cu) and *(iii)* metal alloys (e.g., Cu-Ni [22–26], Pt-Ni and Pt-Co [27], Ni-Co [28–30], and others [31, 32]).

The catalytic performance of supported noble metal catalysts for the ESR have been investigated in a wide temperature range, under the different H_2O/EtOH molar ratios, with respect to the metal loading and the nature of a support. The main difficulties, when comparing the ESR catalysts described in literature, are *(i)* different reaction conditions (temperature, the H_2O/EtOH molar ratio and dilution), *(ii)* differences in the preparation procedure, which also strongly affect catalytic properties of a catalyst.

1.1. Catalysts based on noble metals

Number of papers addressed to the production of hydrogen by the ESR have considered catalysts based on noble metals, such as rhodium [33–44], ruthenium [33, 42], platinum [33, 42, 43, 45–51], iridium [42, 52], palladium [33, 42] deposited on various oxide supports (γ-Al_2O_3 [33, 49, 53], ZnO [54], MgO [33], TiO_2 [33, 48], CeO_2 [48–50, 52], CeO_2-ZrO_2 [44, 51, 55], ZrO_2 [48, 53, 56]). A high catalytic performance obtained for catalysts with a noble metal as an active phase is ascribed to its remarkable capability in C–C bond cleavage.

Despite many differences between noble-metal catalysts with similar chemical composition it can be concluded that among examined noble metals, rhodium is one of the most active in C–C bond cleavage. Rhodium was found to be more active than ruthenium, palladium and platinum of similar metal loading [33], though the main drawback of this metal is its low water gas-shift (WGS) activity (compared with other metals, e.g., platinum or palladium) [57].

One of the most frequently studied catalytic system based on rhodium is Rh/γ-Al_2O_3. The catalytic performance of rhodium (0.5, 1, 2 wt.%), platinum (1 wt.%), palladium (1 wt.%) and ruthenium (1, 3, 5 wt.%) supported on γ-Al_2O_3 in the temperature range of 600–850ºC with the H_2O/EtOH molar ratio of 3/1 was compared by D.K Liguras et al. [33]. It was found that rhodium-catalyst exhibited the highest activity and that the order of catalysts' activity was following: Rh>>Pt>Pd>Ru, whereas the selectivity towards hydrogen and carbon dioxide could be presented as: Rh>>Pt>Ru≈Pd. Lower selectivities of platinum, palladium and ruthenium were attributed to the poorer reforming capabilities of these metals. However, it should be noted that the presented orders were not the rule [58]. The catalytic performance of catalysts based on rhodium and ruthenium was improved with the increase of metal contents, which was significantly marked in the case of the ruthenium-based catalysts. The ruthenium-catalysts are far less expensive than the ruthenium-based one, however, they are leading to ethene formation, therefore, the ruthenium-based catalysts, even based on different supports than alumina, require additionally a suitable promoter.

The platinum-, palladium-, rhodium-, ruthenium-based catalysts, with different metal loading, supported on γ-Al_2O_3, were also the main concern of A.C. Basagiannis et al. [58] studies. However, contrary to the group of D.K. Linguras [33], they carried out the ESR in the low-temperature regime (300–400ºC). It was found that the platinum- and palladium-catalysts exhibited the highest activity and selectivity to hydrogen, despite the lowest metal percent content. Over these catalysts both ethanol conversion and selectivity to hydrogen increased with increasing temperature. For the platinum-based catalyst in the temperature range of 300–400ºC the increase of ethanol conversion from 75 to 97%, and selectivity to hydrogen from 38–47% was noted. At the same time the palladium catalyst exhibited higher ethanol conversion between 300–340ºC (90–96%) compared to the platinum-based catalyst, to reach 97% at 360ºC. This difference is obviously related to lower WGS activity of palladium catalyst than the platinum-based one [58]. As for selectivity to hydrogen over these two catalysts, for the

palladium-based one it remained stable (37%) over the entire temperature range, whereas for the platinum catalyst the increase of selectivity to hydrogen from 38% to 47% was observed. None of these catalysts exhibited ethane formation, suggesting that dehydration reaction did not take place. The ruthenium- and rhodium-based catalysts were less active as well as less selective to hydrogen in the temperature range of 300–400ºC. The ethanol conversion was increasing with the increase of the temperature from 30–85% for the ruthenium catalyst, and from 40–70% for the rhodium-based one. A higher selectivity to hydrogen of platinum and palladium-based catalysts under the low-temperature steam reforming was also confirmed by A. Erdőhelyi et. al. [42]. Better platinum-catalyst's performance at low temperatures is not surprising since platinum has higher WGS activity than ruthenium. For the platinum-, ruthenium- and rhodium-based catalysts' selectivity to both methane and carbon dioxide was increasing with the temperature increase, whereas for the palladium-based catalyst slight decrease in selectivity to these products was observed [58].

It is very difficult to present in a short review the detailed current state of knowledge on noble metal catalysts proposed to the ESR. The summary of achievements in this field can be found in a few very extent reviews [3, 15, 17, 59].

Even though noble metals such as platinum, palladium, rhodium are very interesting candidates for the ESR, their high cost (Table 1) is a driving force for searching of less expensive alternatives.

Table. 1 The prices in euro (troy ounce, 1 ozt = 31.012g) of selected noble metals.

noble metal	**price for troy ounce (ozt) in euro***
Ru	36.86
Pd	496.67
Ir	456.39
Rh	649.48
Pt	841.11

*Actual data taken from *www.infomine.cominvestment/metal-prices* for 25 January 2016.

1.2. Catalysts based on transition metals (Co, Ni and Cu)

So far, most studies in the ESR have been dedicated to examine cobalt- and nickel-containing catalysts, inasmuch as they are far less expensive alternative for noble metals; however, some interesting studies have been also performed on Cu-based catalysts. Though catalysts based on copper-zinc oxide are interesting for methanol

steam reforming due to their good activity and selectivity [60], they showed rather poor properties towards C–C bonds cleavage in the low and medium-temperature ESR (EtOH conversion was between 4–30% at the temperature of 340–400ºC [61]). It was suggested that more interesting would be operating at higher temperatures [61], however, at high temperatures copper-based catalysts undergo a relatively fast deactivation, mainly due to metal sintering [60].

Also, the Cu/CeO_2 [62] catalyst did not attract much attention, since it was highly selective towards acetone. Contrary, both cobalt [29, 30, 63, 64] and nickel [29], [30, 65] were found to be effective catalysts for the cleavage of O–H, C–C and C–H bonds. Moreover, a lot of studies have shown better nickel's ability for cleaving C–C bonds [20, 28. 66].

A few works have been devoted to comparison of cobalt- and nickel-based catalysts with following oxides as a support: Al_2O_3 [67, 68], SiO_2 [68], MgO [69–71], CeO_2 [20, 72], ZrO_2 [28, 73], $LaAlO_3$ and $SrTiO_3$ [71].

The M/MgO catalysts (where, M = Co or Ni) were the main concern of S. Freni and F. Frusteri teams studies [69, 70]. Group of S. Freni [69] prepared, by incipient wetness impregnation, a total of four nickel- and cobalt-based catalysts with different metal loadings (5 and 20 wt.%) with commercial magnesia support. In this work authors found that regardless of metal loading, the pre-reduced at 725ºC Ni/MgO catalysts exhibited higher activity and selectivity to hydrogen and carbon monoxide, carbon dioxide, methane, and acetaldehyde (further named as C_1-products), than the cobalt-based counterparts (H_2O/EtOH = 8.4/1 mol/mol, 650ºC, GHSV = 80,000h^{-1}). After 10 h on stream, ethanol conversions over the cobalt-based catalysts were nearly 10 and 30% for catalysts with 5 and 20 wt.% metal loading, respectively. At the same time, for the nickel-based counterparts, ethanol conversion achieved nearly 40 and 45% for catalysts with 5 and 20 wt.% loading of nickel. As for catalysts' selectivity towards C_1-products, the catalyst with 5 wt.% of cobalt was found to be highly selective towards acetaldehyde (100% after 10 h of reaction), whereas over its 20 wt.% loaded counterpart, more than 40% of carbon dioxide was detected.

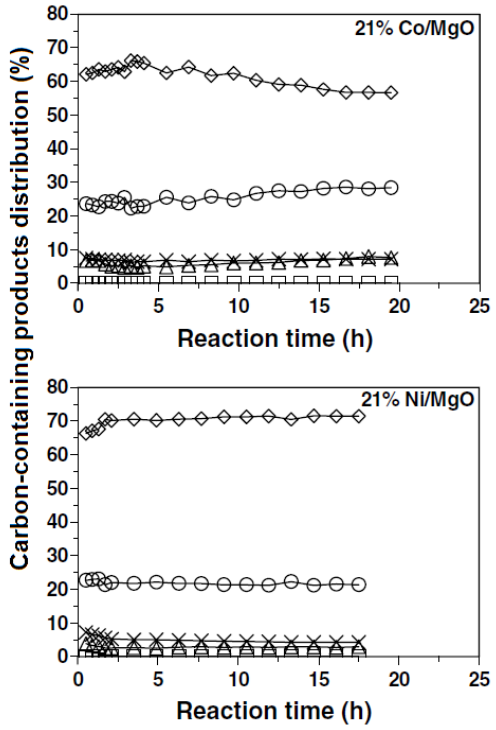

Fig. 1.5 Product distribution vs. time on stream (N_2/H_2O/EtOH = 24/68/8 vol.%, 650ºC, GHSV = 40 000 h^{-1}). Part of Fig. 2 from F. Frusteri et al. studies [70]. (◊) CO_2, (○) CO, (x), CH_4, (Δ) CH_3CHO, (□) C_2H_4.

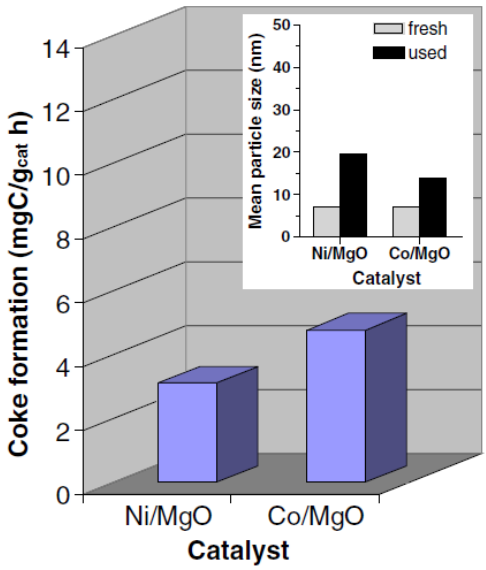

Fig. 1.6 Coke formation (evaluated by Carlo-Erba elementary analyser) and mean particle size (evaluated by TEM) of Ni/MgO and Co/MgO catalysts after 20 h ESR. Based on Fig. 5 and 6 from F. Frusteri et al. studies [70].

The selectivity of other carbon-containing products were about 33, 20, 5% for acetaldehyde, carbon monoxide, and methane, respectively. The nickel-based catalysts showed slightly better selectivity to carbon dioxide (45 and around 50% for the catalyst with 5 and 20 wt.% of nickel loading). Contrary to the cobalt-based catalysts, carbon monoxide was the second most important by-product on the nickel-based catalysts'. Regardless of nickel's loading, the selectivity neither to acetone nor to methane never exceed 15%.

The authors [69] concluded that the nickel-catalysts are more active and selective to hydrogen than the cobalt-based catalysts due to higher resistance of metallic nickel to oxidation in the presence of water. A higher resistance to oxidation of nickel than cobalt was confirmed by the XPS studies of Y.T. Law et al. [30, 74].

Another publication [70] has confirmed better selectivity of Ni/MgO to hydrogen and carbon dioxide than Co/MgO (Fig. 1.5). However, contrary to the studies of F. Frusteri et al. [69] the cobalt-based catalyst showed in the ESR ($EtOH/H_2O$ = 1/4.2 mol/mol, 650ºC, GHSV = 40,000h^{-1}) higher ethanol conversion (19 mol%) than the nickel-based one (10.36 mol%) [70]. After 10 h of the ESR, the ethanol conversion was nearly 50% and 40% for the Co/MgO and Ni/MgO (with 21 wt.% of metal loading),

respectively [70]. In the previous cited studies [69], depending on metal loading, ethanol conversion was 45 and 40% for Ni/MgO and 30 or less than 10% for Co/MgO, for the catalyst with low and high metal loading. The differences between the results may be attributed to different reaction conditions.

Catalytic tests carried out over pre-reduced (600ºC) Co/MgO and Ni/MgO (5 wt.% of cobalt and nickel) catalysts with the $H_2O/EtOH = 10/1$ mol/mol also confirmed higher selectivity to hydrogen of the nickel-based catalyst [71].

In all so far cited publications concerning nickel- and cobalt-catalysts with magnesia as a support it was concluded that both catalysts suffer for coke formation and metal sintering. F. Frusteri et al. [70] observed slightly higher amount of coke on the spent Co/MgO catalyst than on the nickel-based one (Fig.1.6), while K. Urasaki et al. [71] obtained the opposite result. The amount of deposited coke in the case of studies of the first group [70] was evaluated by Carlo-Erba elementary analyser instrument, while the second group [71] quantified it by the temperature oxidation (TPO) measurements.

Application of the support with basic nature, like magnesium oxide, significantly slowed down the rate of coke formation, as compared to results obtained by other authors on nickel- and cobalt-based catalysts with alumina as a support [67]. Large amounts of coke on catalysts with acidic oxides as a support, is a result of high activity of such systems towards ethanol dehydration reaction (Eq. 4) leading to formation of ethene, which is well-known precursor of coke formation (Eq. 10) [68, 75]. In order to attenuate the dehydrogenating ability of alumina and slightly decrease a catalyst's coking by gasification of coke precursors, the addition of lanthana to the catalyst's support was suggested [68, 75, 76]. Studies of F.L.S. Carvalho et al. [77] showed also that the rate of coking can slowed down by lanthana doping to ceria (due to the increase of the oxygen species mobility, including OH species) in the case of the $Co_3O_4/La_2O_3/CeO_2$ catalysts synthesized by one-step polymerization. It was found that lanthana enhances the ESR and WGS [68], as well as, methane steam reforming [77] over the ethanol decomposition reaction.

Studies provided by L. Chen et al. [28] showed that cobalt supported on calcium doped alumina exhibited higher activity compared to the zirconia-supported one, probably due to the higher availability of surface adsorbed –OH groups. The authors, of above mentioned publication [28], discussed the role of metal (cobalt and nickel) and the support (Ca-γ-Al_2O_3 and ZrO_2) in the ESR. They concluded that the activity of

zirconia supported catalysts was much lower than those of Ca-γ-Al_2O_3-supported (Fig. 1.7) meaning, that a support has a significant influence on the catalyst's activity. As it is shown in Fig. 1.7 the nickel-catalysts were more selective to hydrogen as compared to the cobalt-based catalysts, which is in agreement with previous reports [69, 71]. The difference is more evident at temperatures higher than 600ºC. Another interesting conclusion from that work concerns the nature of coke deposited on both catalysts. On the basis of the TPO of experiment after temperature-programmed desorption (TPD) of ethanol study the authors [28] suggested that, on the surface of cobalt-based catalysts carbon formed through ethene polymerization is less crystalline, therefore, easy to remove via oxidation. While, carbon formed through methane decomposition is more stable.

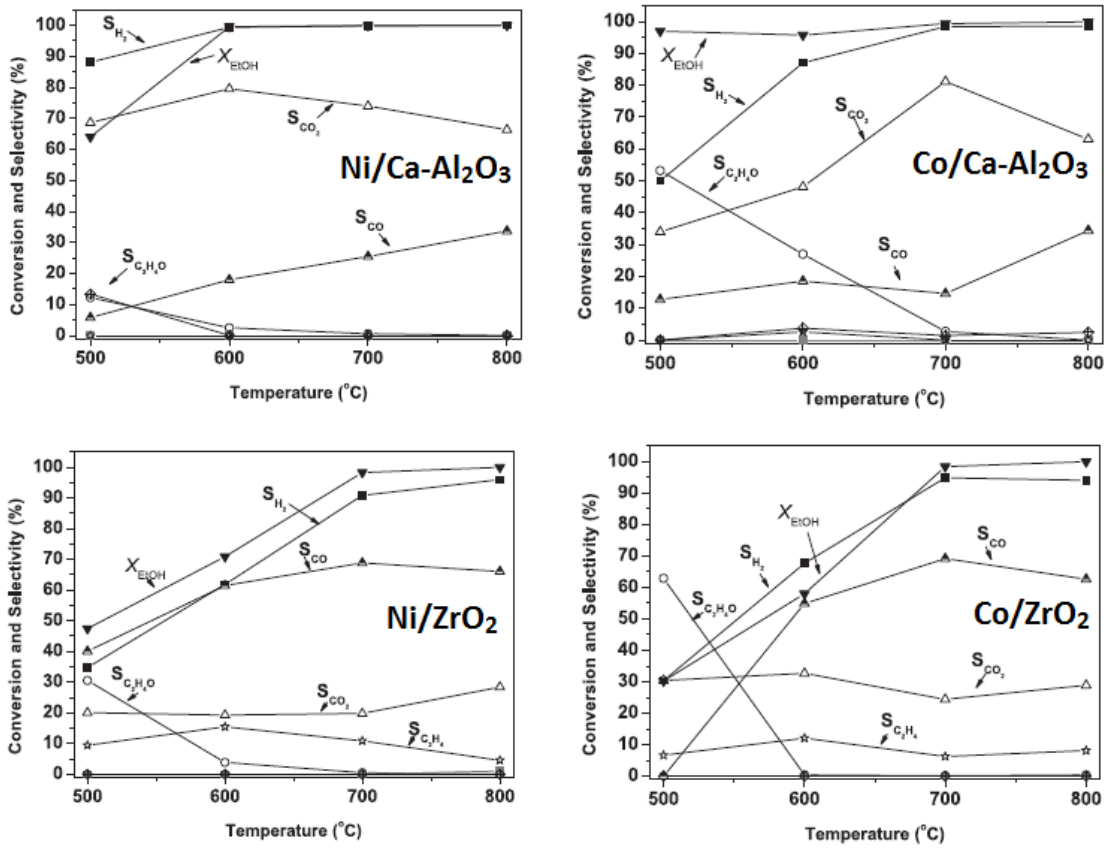

Fig. 1.7 Effect of reaction temperature on ethanol conversion and product selectivities over nickel- and cobalt-based Ca-γ-Al_2O_3 and ZrO_2 supported catalysts. Based on Fig. 5 and 6 from L. Chen et al. studies [28].

B. Zhang et al. [20] suggested ceria as a suitable support for cobalt- and nickel-catalysts, because of its high oxygen storage capacity. The catalytic behaviour of pre-reduced (400ºC) catalysts was tested within the temperature range of 300–700ºC with the H_2O/EtOH = 3/1 mol/mol. For the low temperatures (<400ºC) ethanol dehydrogenation and decomposition were the primary pathways, depending on the

nature of the active metal (Fig. 1.8). In the temperature range of 300–400ºC carbon dioxide and relative abundant amounts of acetone were detected over the Co/CeO_2. The Ni/CeO_2 catalyst at temperatures lower than 400ºC gave traceable amounts of acetone, while methane and carbon monoxide were the major carbon-containing products (Fig. 1.8). The authors [20] suggested that acetone, produced over the examined catalyst was probably a result of acetaldehyde decarbonylation (Eq. 13):

$$2CH_3CHO_{(g)} \rightarrow CH_3COCH_{3(g)} + CO_{(g)} + H_{2(g)} \quad \textbf{(Eq. 13)}$$

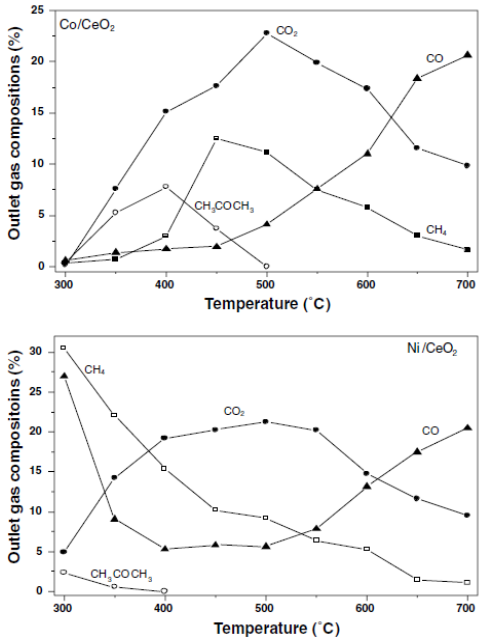

Fig. 1.8 Effect of the reaction temperature on products distribution over Co/CeO_2 and Ni/CeO_2 catalysts for the $H_2O/EtOH$ = 3/1 mol/mol. Part of Fig. 5 from B. Zhang et al. studies [20].

Moreover, at higher temperatures (>500ºC) the increase of the amounts carbon monoxide and gradual decrease of methane formation indicates (according to the authors [20]) that RWGS and steam reforming of methane were major reactions determining the outlet gas composition (Fig. 1.8). After the long-term stability tests (not shown here) at 450ºC (27 h) for the Ni/CeO_2 and 500ºC (24 h) for the Co/CeO_2 catalysts, the significant heavy coke deposit (with filamentous structure) was found on the surface of both catalysts. The coke formation was related to the polymerization of acetone, appearance of which in the products was observed after 18 h of the ESR. Detailed views on the mechanism of coke formation in the ESR are presented in the section 1.2.1.4 of this chapter.

Concluding this very short review, both nickel- and cobalt-catalysts were found to be active and selective alternatives of noble-metal catalysts for ethanol steam reforming [20, 28, 67, 69–71]. The catalytic performance of these catalysts can be modified by acid-base properties of a support [28, 68, 73, 75–78]. There are a few drawback of both nickel- and cobalt-catalysts. First of all, they suffer for metal sintering [20, 70] (more than noble-metal catalysts [70]) and for coking [20, 66, 70, 71]. Secondly, cobalt-catalysts have higher tendency (than nickel-based one) to get oxidized [30, 69] leading to the formation of acetaldehyde [20, 30, 74] and acetone [20], whereas

the selectivity to hydrogen over nickel-catalysts can be lowered as a consequence of higher amounts of methane formed [66]. Both active phases are very interesting, however, most researchers focused on cobalt-based catalysts.

1.2.1. Cobalt-based catalysts for the ESR – current state-of-the-art

Any catalyst's performance is followed by many variables like: *(i)* metal loading, *(ii)* metal precursor and support nature, *(iii)* method of preparation, *(iv)* synthesis parameters, *(v)* calcination temperature, *(vi)* activation (reduction) temperature, and finally *(vii)* reaction parameters such as temperature, pressure and reactants composition. Of all the mentioned parameters, some are not easy to control. For example, it is difficult to manage a metal particle size (its dispersion).

It should be remembered that cobalt particles size and cobalt oxidation state, may be important variables for the ESR, that are directly related to the support (its nature, morphology and textural properties) and cobalt–support interactions.

Since real catalytic systems are complex and distinguishing the contribution of individual factor to catalytic phenomena is difficult, it is helpful to consider first the influence of each variable at least more or less separately in order to better understand the way of catalysts' functioning and suggest rational strategies of catalysts' improvements.

1.2.1.1 The role of cobalt particles size in the ESR and possible ways to tune the particle size up

Until now, a few papers have been devoted to examination of the effect of cobalt particles size in the ethanol steam reforming [79–82]. The number of publications, towards understanding the effect of cobalt particles size on catalyst's activity, selectivity and stability in the ESR, is rather limited and most of them are devoted to studies of cobalt particles located on catalytically active supports, e.g., ceria or ceria-zirconia solid solution [79–81, 83–86]. It was found that ethanol conversion is greatly influenced by a support (nature, dispersion, and morphology) [78, 83, 87–90]. Therefore, before discussing current studies of supported cobalt-based systems, it is worth to mention about the results of studies which were aimed to elimination of the effect of a support, in order to determine the intrinsic cobalt particle size effects on the ESR.

The authors [82] studied, in the ESR, behaviour of cobalt (with different particle sizes 2.6–6 nm) supported on carbon nanofiber (CNF). It was noted that only initial ethanol conversion was affected by particles size, whereas the difference in products distribution was rather small. The smallest cobalt particles exhibited rather a stable ethanol conversion, while the larger cobalt particles (Co size > 4 nm) showed a significant decrease of conversion in first hours of the ESR (H_2O/EtOH = 3/1 mol/mol, 500ºC). The loss of activity (caused by filaments carbon deposition) was more pronounced while particle size increased (Fig. 1.9 A). The growth of particle size was concomitant with the increase of number of terrace sites (Fig. 1.9 B), meaning that the growth of carbon filaments starts on terraces. Basing on these results, it can be concluded that the metal particle size determine carbonaceous deposit accumulation.

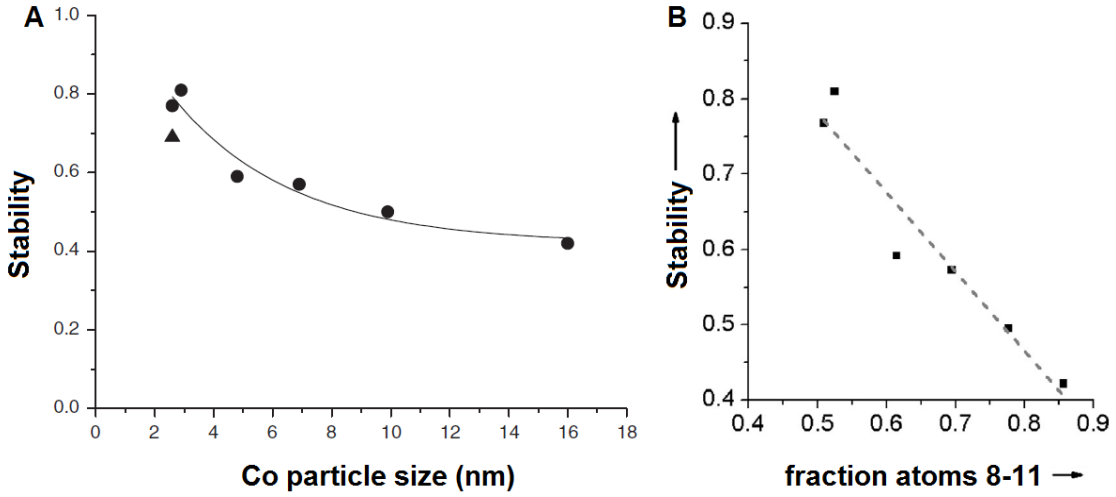

Fig. 1.9 Stability of Co/CNF A) as a function of cobalt particle size (EtOH/H_2O = 1/3 mol/mol, 500ºC), B) as a function of the fraction of surface atoms with coordination number 8–11, like in terraces. Combined Fig. 3 and 6b from A.L.M. da Silva et al. studies [82].

The easiest way to "tune a metal particle size", using the conventional impregnation, is the application of high- and low-dispersed supports. Obviously in the case of impregnation method the term "particle size tuning" is rather exaggerated since this method does not allow obtaining a catalyst with a highly homogeneous dispersion. However, this method allows controlling the particle size in two scales, generally named nano- and micro-range. Experimental studies have shown higher selectivity towards hydrogen and carbon dioxide of cobalt-catalysts with high-dispersed oxides supports [79–81].

A. Machocki et al. [81] studied the catalytic performance of pre-reduced nano- and micro- ceria- and zirconia-supported cobalt-catalysts in the ESR (H_2O/EtOH = 21/1 mol/mol) within the temperature range of 350–600ºC. It turned out that at 420ºC the

nano-ceria-supported cobalt-catalyst achieved the highest selectivity to hydrogen (93%) among the examined samples, whereas, the selectivity of the ESR to hydrogen on its micro-counterpart support was significantly lower (76%). The selectivity to hydrogen of the Co/ZrO_2 catalysts was around 85 and 77% for the nano- and micro-zirconia supported systems, respectively. It was concluded that when the distance from a centre of cobalt crystallites to the cobalt–support border is too long and water is not strongly activated on the support, the nonselective ethanol transformations take place. There are some studies [91, 92] proving that water activation depends on cobalt particle size. The researchers [81] suggested that a low surface concentration of activated water adsorbed on the surface of the micro-supports in the close contact with cobalt particles is also responsible for high selectivity of the mirco-dispersed catalyst towards acetaldehyde (28 and 31% for the micro-Co/CeO_2 and Co/ZrO_2 catalysts, respectively).

I.I. Soykal et al. [80] carried out the ESR reaction over nano- and micro-Co/CeO_2 ($H_2O/EtOH$ = 10/1 molar ratio, 300–500ºC) observing higher selectivity of the nano-catalyst towards hydrogen. The authors [80] observed that nano-Co/CeO_2 exhibited higher selectivity towards acetaldehyde than its the micro-counterpart. Similar phenomenon was observed when ethene production was considered. The authors [80] noted that despite the high ethene selectivity of the nano-Co/CeO_2, this catalyst was highly resistant to coking, whilst its micro- counterpart showed a high affinity for ethene decomposition, hence for coke formation. The coke formed on the surface of the nano-Co/CeO_2 was primarily amorphous, while more than 90% of carbon accumulated on the micro-Co/CeO_2 catalyst surface was graphitic.

More recent work of I.I. Soykal team's [79], concerning the ESR reaction ($H_2O/EtOH$ = 10/1 molar ratio, 350–450ºC) carried out over activated cobalt catalysts with nano- and micro-ceria supports, confirmed higher selectivity to hydrogen and carbon dioxide of nano-catalyst [79–81], however, the selectivities towards acetaldehyde and ethene were this time (comparing with [80]) higher on the catalyst denoted as micro-. In both works [79, 80] the nano- and micro-Co/CeO_2 catalysts were prepared via incipient wetness impregnation method, however, the differences were found in the support preparation procedure, resulting in a different ceria particle size distribution (Fig. 1.10).

I.I. Soykal et al. [80] employing X-ray absorption spectroscopic (XAS) technique observed easier reducibility of cobalt supported on the nano-ceria (94% of metallic cobalt) than the micro-ceria (88% of metallic cobalt), which was attributed to

the small particles size. Also the bare nano-ceria was found to be reduced more easily by both hydrogen and the H_2O/EtOH vapours [79]. Therefore, comparison of the results [79–81] led to conclusion, that apart from the particles size of cobalt and ceria, the catalyst's morphology and reducibility play an important role.

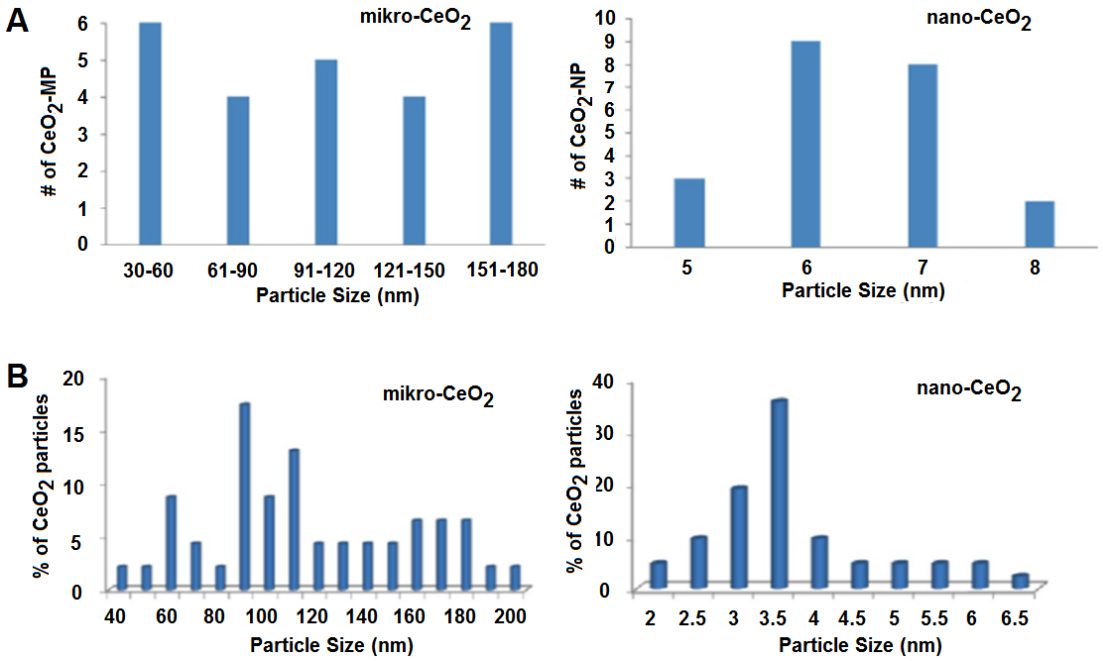

Fig. 1.10 Particle size distribution histograms of the micro- and nano-Co/CeO_2. Combined figures from the studies of I.I. Soykal et. al A) [80] (Fig. 1) and B) [79] (Fig. 3).

The XAS studies of B. Bayram et al. [84] and I.I. Soykal et al. [83] carried out over pre-reduced (3.6 % H_2/He, 400ºC, 1 h) cobalt catalysts, prepared by impregnation of a commercial ceria powder (Aldrich, 5μm), yielded with 62% of metallic cobalt, whereas, in the case of cobalt supported on ceria nano-rods and nano-cubes it was 51% and 79%, respectively. The reduction extent of cobalt supported on ceria nano-cubes was ascribed to the crystal plane structure of the support, that allowed for higher number of anion vacancies, hence, a higher mobility of oxygen. The plane structure of the micro-ceria crystals may cause higher reducibility of cobalt particles than in the case of cobalt supported on nano-ceria.

Comparison of the steady-state catalytic activity of the samples from B. Bayram et al. [84] and I.I. Soykal et al. [83] studies is impossible. The work of B. Bayram et al. [84] did not provide data on selectivity to hydrogen and carbon dioxide. I.I. Soykal et al. [83] studies showed that ethanol conversion, selectivities to hydrogen and carbon dioxide obtained over cobalt supported on ceria nano-cubes were definitely higher that these found for cobalt supported on ceria nano-rods, meaning that ceria morphology influences the catalyst's properties. The different orientation of crystal planes of ceria

may result in different orientation of cobalt species [83], therefore, affecting the catalyst's activity and products distribution.

The influence of the support morphology on cobalt-catalyst's properties will be discussed also in the section 1.2.1.3 of this chapter.

The Co/CeO_2 catalysts with different metal dispersion, thus, different reducibility were obtained by H. Song et al. using *(i)* different cobalt precursor [93], *(ii)* different impregnation medium [94], and *(iii)* various preparation techniques [95]. All these experiments were inspired by the idea that any parameter that would give a high cobalt dispersion is likely to improve the catalytic performance.

To examine the effect of a different cobalt precursor on metal dispersion and the performance of Co/CeO_2 catalysts, researchers [93] prepared a few catalysts by incipient wetness impregnation, using various organometallic and inorganic salts. The dispersion of cobalt, depending on the precursor type, varied in the following order: cobalt(II) acetyl acetonate ~ octacarbonyldicobalt > cobalt(II) carbonate hydrate > cobalt(II) nitrate hexahydrate > cobalt(II) oxalate dehydrate > cobalt chloride hexahydrate ~ cobalt(II) sulphate heptahydrate. The steady-state reaction experiments (H_2O/EtOH = 10/1 mol/mol, 450ºC) showed the highest stability and the highest selectivity to hydrogen and carbon dioxide of the catalysts prepared using organometallic cobalt precursors, suggesting that the organic ligands surrounding cobalt ions keep the particles segregated, leading to the better dispersion and stability. In the case of inorganic precursors, the authors [93] observed a significant level of acetone (74.5%, 52.9%, and 14.2% for the catalysts obtained using cobalt(II) sulphate heptahydrate, cobalt chloride hexahydrate, and cobalt(II) carbonate hydrate as precursors, respectively) [93]. This was ascribed to the poisoning effect of the inorganic anions (Cl^-, SO_4^{2-}) and different cobalt particles distribution.

Even though preparation of catalysts in inorganic or organic media has no effect on Co_3O_4 crystallite size [94], the crystallite size of reduced and spent samples showed a significant difference, meaning that an impregnation medium plays an important role in suppressing particle growth under the ESR conditions. Comparison of the reduction behaviour (TPR technique) of the catalysts prepared in an aqueous and organic medium showed that the sample synthesized in ethanol exhibited better reducibility and a higher ESR activity. The same observation was made by M. Greluk et al. [96], who prepared the Co/CeO_2 catalysts via impregnation using different impregnation media (water, methanol, ethanol, and isopropyl alcohol).

The impregnation is the simplest and the most convenient method of heterogeneous catalysts' preparation, thus widely used. The main drawback of this method is a possibility of the non-homogenous distribution of the active metal. This may be overcome employing co-precipitation or sol-gel methods, however, catalysts prepared by these methods are generally less active [85, 95] due to embedding of metal atoms into the support matrix. However, the cases in which the impregnated catalysts were less active that co-precipitated ones in the ESR are also known.

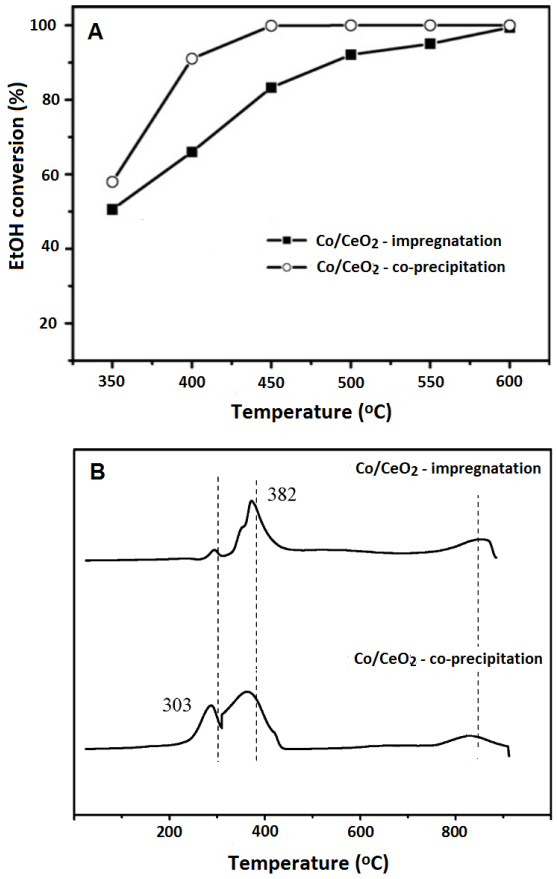

Fig. 1.11 The ethanol conversion vs. reaction temperature A) and TPR profiles B) for the Co/CeO_2 catalysts prepared via impregnation and co-precipitation techniques. Part of Fig. 4 and Fig. 9 from H. Wang et al. [97] studies.

H. Wang et al. [97] compared Co/CeO_2 catalysts prepared by impregnation and co-precipitation methods. By comparison of ceria lattice parameters the authors came to the conclusion that more cobalt entered into ceria lattice in the case of co-precipitated catalyst. This resulted, according to authors, in weaker interaction between cobalt and ceria on the surface of the Co/CeO_2 and had a beneficial effect for catalyst's reducibility, hence activity (Fig. 1.11A and B), and resistance to carbon deposition. At this point it should be clarified that it is generally accepted that cobalt–ceria interactions are getting stronger when cobalt enters into ceria lattice. The authors [97] also found that even though higher surface area and higher cobalt dispersion were achieved for the catalyst prepared by impregnation, the co-precipitated catalyst was more active (Fig. 1.11 A) and selective towards hydrogen and carbon dioxide at 450ºC (H_2O/EtOH = 3/1 mol/mol). The higher activity of the co-precipitated catalyst can be attributed to its higher reducibility and increased oxygen mobility of ceria, which was achieved by replacement of some Ce(IV) ions with cobalt ions.

Slightly better reducibility of the Co/CeO_2 catalyst, caused by substitution of cobalt in ceria lattice, was also found for a catalyst prepared by ultrasonic-assisted

co-precipitation method [98]. It was proved that this method gave more promising results than hydrothermal co-precipitation, due to the facilitation of metal dispersion, increasing the amounts of oxygen vacancies, hence promoting oxygen storage capacity of ceria, and increasing its ionic conductivity. Greater accessibility of oxygen chemisorbed on oxygen vacancies was suggested to play a significant role in suppressing carbon deposition and increasing the ESR performance of catalysts. Basing on XPS studies of O 1s core level, the authors [98] found that higher concentration of the component located at 532–533 eV was present on the spectrum recorded for the catalyst prepared by ultrasonic-assisted co-precipitation method. The presence of this component was attributed to oxygen chemisorbed on surface vacancies, therefore, suggesting abundance of sites capable to oxidize, e.g., carbon monoxide. Moreover, it was noted that in the temperature range of 250–400ºC for the H_2O/EtOH molar ratio of 13/1, the catalyst with a higher cobalt dispersion exhibited higher selectivity to hydrogen and a lower selectivity to acetaldehyde and acetone.

According to H. Song et al. [95], better dispersion, maintaining good catalysts activity, can be achieved using reverse micro-emulsion technique. The results show [95] that this method allows achieving a catalyst with improved cobalt dispersion; therefore, exhibiting superior catalytic activity and selectivity (hydrogen and carbon dioxide selectivities obtained in the ESR (carried out with the H_2O/EtOH = 10/1mol/mol, 450ºC) were equal 94.7 and 94%, respectively.

The one conclusion emerging from so far presented studies is that the catalytic activity is definitely related to cobalt dispersion [79–82], which strongly depends on the preparation method [93–95, 97, 98] and the support morphology [79–81, 84]. Superior performance of cobalt-based catalysts is a combination of a few factors, i.e. increased reducibility [93, 97, 98], and as well as accessibility of active sites, e.g., abundance of oxygen adsorbed species on the support surface [98].

1.2.1.2 Importance of cobalt oxidation state in ethanol transformations

The metal particle size is also a determining factor in cobalt susceptibility to oxidation under the ESR. The effect of cobalt oxidation state on catalytic performance under the ESR has been investigated over unsupported [19, 99, 100] and supported [101] systems. However, till now, the nature of cobalt active sites and their role in the reaction pathways is still under discussion [102]. In some publications authors suggested that metallic form of cobalt is the most active form of cobalt in the ESR [100,

101, 103–107]. However, there are some supporters of the theory that oxidized cobalt species (CoO_x) can be highly active in the ESR [108–110], but these species can be also responsible for coke deposition.

It should be expected that during the ESR reaction, the redox atmosphere is generated. A catalyst may undergo oxidation (due to presence of water [111]) and/or reduction (due to formation of reducing agents such as hydrogen, carbon monoxide, and methane) during the reaction.

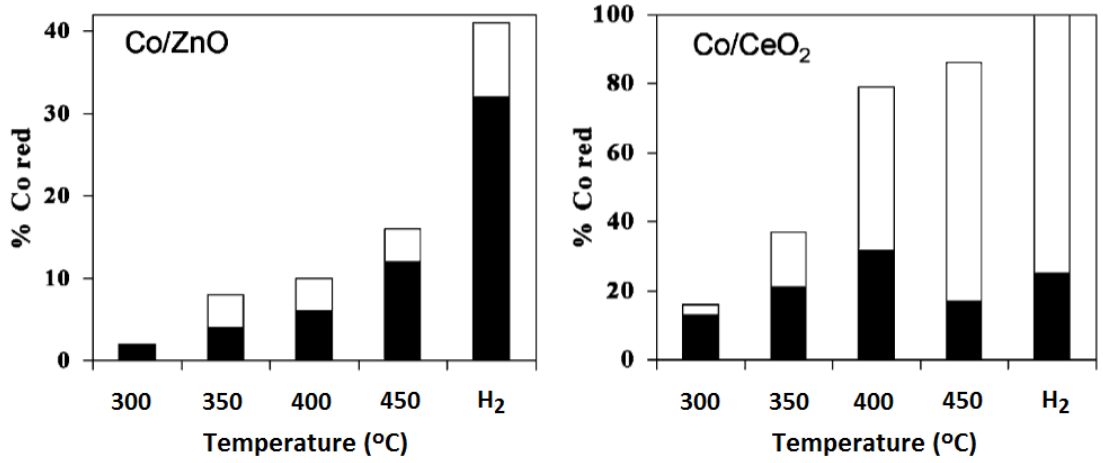

Fig. 1.12 Amount of metallic cobalt in particles dispersion (■) and bigger (□) than the critical diameter obtained after the ESR (300–450ºC) and after H_2 treatment at 450ºC. Part of Fig 3 from J. Llorca et al. [101].

The studies of J. Llorca et al. [101], provided an evidence for the co-existence of both forms of cobalt Co(0) and Co(II) under the ESR carried out over supported (MgO, Al_2O_3, SiO_2, TiO_2, V_2O_5, ZnO, La_2O_3, CeO_2 and Sm_2O_3) cobalt-catalysts. These authors demonstrated that the extent of cobalt reduction in both, hydrogen and the H_2O/EtOH, depends on a support nature (Fig. 1.12), and that catalysts are re-oxidized in the ESR conditions.

To gain a better understanding the role of cobalt species J. Lorca et al. [99] and V.A. de la Peña O'Shea et al. [100] carried out studies of Co_3O_4 transformations under the ESR conditions (H_2O/EtOH = 13/1 [99] and 6/1 [100] mol/mol). Even though both studies (of J. Lorca et al. [99] and V.A. de la Peña O'Shea et al. [100]) differ in terms of the H_2O/EtOH molar ratio, both groups of researchers proved the progressive reduction of Co_3O_4 to CoO and Co(0) in the reaction mixture (Fig. 1.13). At 300ºC in both papers, samples exhibited a low activity and selectivity to hydrogen and acetaldehyde, which were the only products. In line with Fig. 1.13 at the temperature of 300ºC, Co_3O_4 and CoO were present. At 400ºC, when Co(0) and CoO dominate, ethanol conversion increased and the sample became selective towards hydrogen and carbon dioxide.

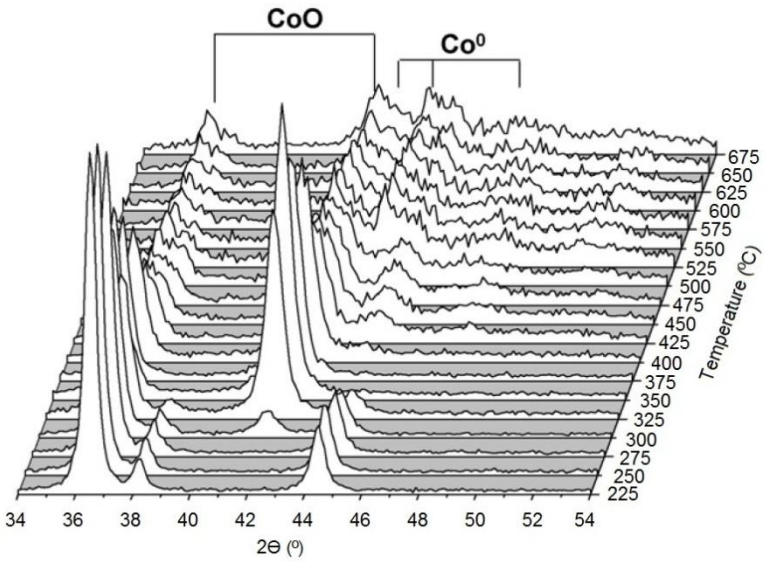

Fig. 1.13 XRD patterns corresponding to the transformation of Co_3O_4 under *operando* ESR as a function of the temperature [100].

Information on the difference of behaviour between an unsupported Co_3O_4 and oxide-supported cobalt particles have additionally been provided by studies of J. Lorca et al. [99]. The degree of reduction of cobalt active phase in the case of the unsupported Co_3O_4 was higher than for supported systems, even though similar reaction conditions to these used in their previously quoted publication [101], were applied.

The different reducibility of a supported (Co/MgO) and unsupported cobalt was also confirmed by studies of S. Tuti and F. Pepe [19]. The cited work additionally discuses the influence of the pre-treatment (oxygen or hydrogen) on the catalytic activity (H_2O/EtOH = 3.5/1 mol/mol, 250–550ºC) of the unsupported cobalt. It was confirmed that the pre-oxidized Co_3O_4 is not active in the ESR in the temperature range of 250–300ºC [100]. In this study [19] the conversion of ethanol, over the pre-oxidized Co_3O_4, was equal 2.8% at 250ºC, 6.1% at 300ºC, and 68.1% at 350ºC. In the same temperature range (250–350ºC) the activity of the pre-reduced sample was higher (27.1%, 55.3%, and 98.2%), as compared to the pre-oxidized Co_3O_4. Both samples (the pre-oxidized and the pre-reduced one) exhibited 100% conversion of ethanol at temperatures higher than 400ºC. The efficiency of the overall ESR reaction, determined as the H_2/EtOH molar ratio, showed that the pre-reduced sample exhibited higher hydrogen yield in the temperature range of 250–400ºC; however, the final H_2/EtOH molar ratio (at 550ºC) reached a higher value (5.4 mol H_2/mol EtOH) in the case of the pre-oxidized Co_3O_4 (Fig. 1.14). The authors [19] explained obtained result

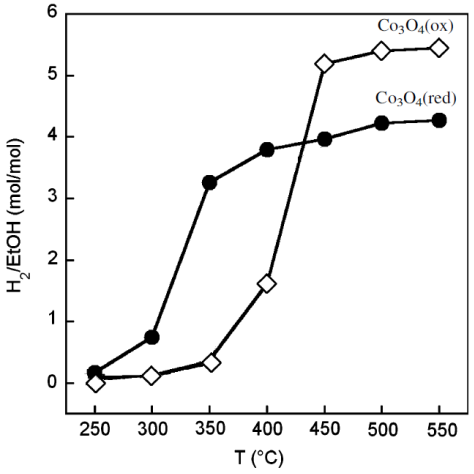

Fig. 1.14 Efficiency of ethanol steam reforming over the pre-oxidized and the pre-reduced Co_3O_4 under the H_2O/EtOH = 3.5/1 mol/mol carried out at 250–550ºC. Part of Fig. 3 from studies of S. Tuti and F. Pepe [19].

by reduced sintering effect of metallic cobalt particles in the case of the pre-oxidized sample. As for carbon-containing products selectivity of the pre-reduced Co_3O_4, it was found that below 300ºC acetaldehyde was the main product, suggesting that dehydrogenation of ethanol was the primary pathway. Above 350ºC the formation of acetaldehyde was suppressed and carbon dioxide was the main carbon-containing product, meaning that the sample promoted mainly the ESR. It was suggested [19] that the formation of acetaldehyde is related to the presence of Co(II) species. It is very probable that the pre-reduced sample was slightly re-oxidized to Co(II) by water [19, 100, 112, 113] at low temperatures, since it was found that the exposition of cobalt-catalysts to water at higher temperature (400ºC) also causes their oxidation [114]. This is also in agreement with theoretical studies [12], which suggest that under the ESR conditions, metallic cobalt can be re-oxidized to Co(II) to a limited extent. Regarding the role of metallic cobalt in the ESR, the authors [19] proposed that metallic cobalt can be responsible not only for the ethanol steam reforming (and generally reactions leading to the cleavage of C–C bonds), but also for the WGS reaction [19, 106, 115] and methane steam reforming [19].

So far cited works have concerned the pre-oxidized and pre-reduced unsupported Co_3O_4 or pre-reduced supported cobalt-catalysts. It was proved that the gradual reduction of Co_3O_4 in the reaction mixture allows to obtain satisfactory selectivity to hydrogen and carbon dioxide at temperatures higher than 400ºC.

Team of P. Rybak et al. [86] carried out the ESR (H_2O/EtOH = 21/1 mol/mol, 420ºC) on unreduced cobalt-based systems supported on cerium, zirconium and mixed cerium-zirconium oxides. The researchers reported that selectivities were in the range of 56–64% and 18–25% for hydrogen and carbon dioxide, respectively. Whereas. the initial ethanol conversion was between 72–42%, depending on the support used. The Co/ZrO_2 catalyst was initially highly selective towards acetaldehyde (20%) and ethene (10%), to reach the selectivity around 35% for acetone and 12% for ethane after 20 h in the stream. The Co/CeO_2 catalyst was found to be very selective towards

acetone (65%). The catalysts supported on mixed CeO_2-ZrO_2 in terms of selectivity towards acetone showed very similar behaviour to the Co/CeO_2 catalyst. Analysing the results obtained by this research group, with respect to the above-presented results [99–101], it may be concluded that both Co(0) and Co(II) were present at 420ºC. The presence of Co(0) is supported by the noticeable conversion of ethanol (and water), while acetaldehyde and acetone may suggest the predominance of Co(II) species.

Good catalytic performance of a pre-reduced Co/ZnO catalyst was presented in J. Llorca et al. [116] studies. The pre-reduced catalyst exhibited 100% ethanol conversion even at a temperature as low as 350ºC, whilst over the as calcined sample it was just 3.8%. At this temperature over the oxidized sample the main products were hydrogen and acetaldehyde (50.1 and 45.9%, respectively). Over the pre-reduced Co/ZnO acetaldehyde (30.6%) appeared only at the lowest temperature (300ºC). Better ethanol conversion over the as calcined sample was achieved at 450ºC (97.6%); however, the selectivity to hydrogen was still lower (62.2%) than over the pre-reduced sample (73%). Moreover, acetaldehyde was constantly present as a by-product (8.9%).

The importance of the Co(0)/Co(II) ratio on the reaction pathways over unsupported and supported cobalt systems is undeniable. However, so far presented research can only suggest a role of Co(0) and Co(II) species. Studies of possible ethanol transformations were carried out over a model cobalt foil [117], cobalt films and cobalt particles supported on single crystal metal oxides [118–121], as well as on real catalytic systems based on cobalt supported on various oxides [106, 122–124]. In order to determine the reaction of ethanol on metallic and oxidized cobalt surfaces M.P. Hyman and J.M. Vohs [117] oxidized cobalt foil to a various extent. As prepared samples were characterized by the XPS (Fig. 1.15). The main peak on the Co 2p spectra, which appeared at 778.0 eV was ascribed to the

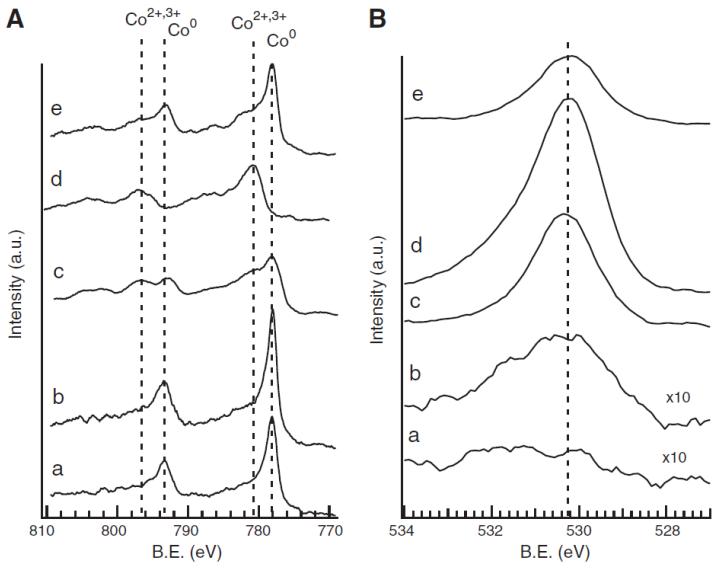

Fig. 1.15 A) Co 2p and B) O 1s XPS spectra of (a) clean Co foil; (b) Co foil exposed to 60 L O_2 at 25ºC, (c) Co foil exposed to 9000 L O_2 at 730ºC, (d) Co foil exposed to10^7 L O_2 at 300ºC, (e) sample d annealed at 830ºC for 10 min [117].

presence of metallic cobalt and this at 781.0 eV was referenced to Co(II) species or a mixture of Co(II) and Co(III). The exposition of the clean foil (Fig. 1.15A) to 60 L of oxygen at room temperature did not produce significant changes on the Co 2p spectrum, however, a small peak could be noticed on the O 1s spectrum. This peak was assigned to the presence of oxygen adatoms on the metallic sample. After the exposition of the foil on 9000 L O_2 at around 730ºC (Fig. 1.15B), the thin film of CoO_x was formed. The exposition of the foil on 10^7 L of O_2 at around 300ºC allowed the formation of more oxidized sample (Fig. 1.15C). So prepared samples were subjected to ethanol TPD experiments (Fig. 1.16).

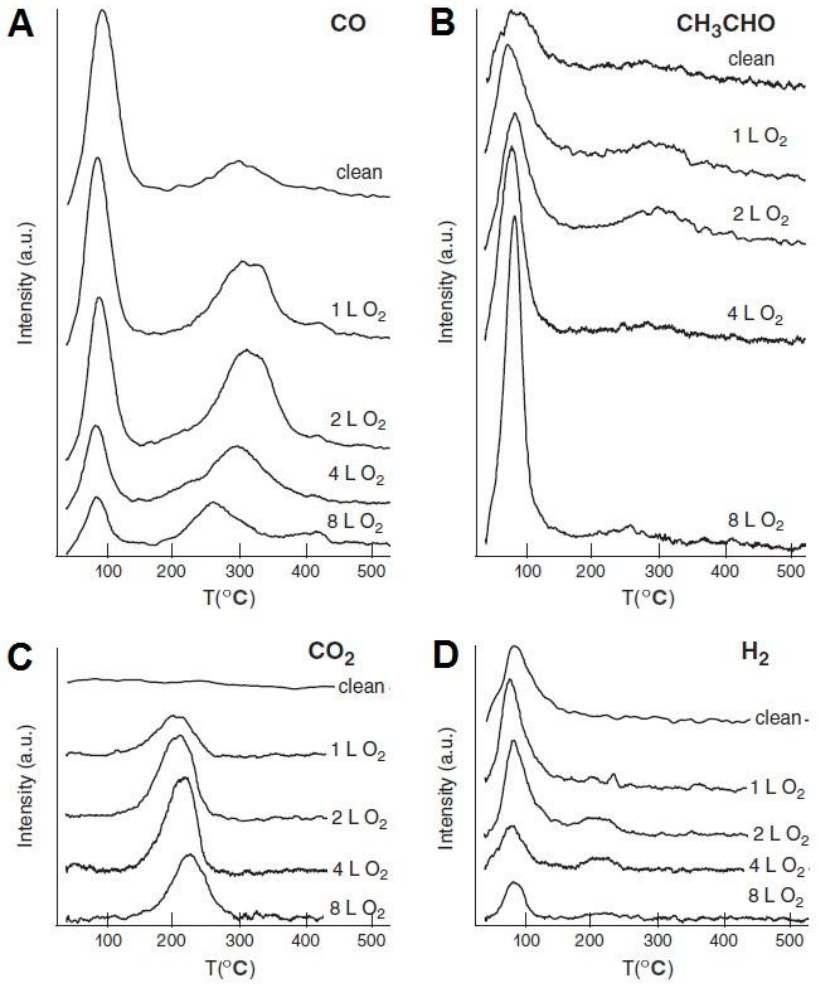

Fig. 1.16 The TPD spectra for CO, CH_3CHO, CO_2 and H_2 products obtained during ethanol TPD from O_2-dosed Co foils. An ethanol dose of 4 L was used in each experiment and the O_2 exposures are as indicated in the figure. CO, m/z = 28; CH_3CHO, m/z = 29; CO_2 m/z = 44; H_2, m/z = 2. Picture retrived from M.P. Hyman J.M. Vohs [117] studies.

On the clean cobalt foil ethanol was not observed as a desorption product. This confirmed previous reports that ethanol, like other alcohols, adsorbs on metallic cobalt surface forming ethoxide species [125]. The most intense peak on the TPD spectra appearing at ~100ºC was related to carbon monoxide desorption, suggesting

decarbonylation as the primary pathway on cobalt metallic sites. The authors [117] suggested that decarbonylation proceeds through an oxametallacycle intermediate. The increase of the amount of desorbed acetaldehyde observed on more oxidized sample suggested, that Co(II) sites have relatively high selectivity for α-hydrogen abstraction from adsorbed ethoxide.

That studies [117] did not provided any insight into hydrogen and carbon dioxide production from acetaldehyde. It was only suggested that the low-temperature (220ºC) desorption peak of carbon dioxide may mean, that further acetaldehyde transformations can proceed through an acetate ESR intermediate. Acetate species are recognized as important intermediates which may decompose to carbon dioxide [126–128].

Ambient Pressure Photoemission Spectroscopy (APPES) studies combined with *on-line* mass spectroscopy analysis, carried out over the pre-reduced in hydrogen cobalt nano-powder, during the ESR (H_2O/EtOH = 3/1 mol/mol, p_{total} = 0.2 mbar) were presented in the doctoral thesis of Y.T. Law [129]. It was found that under the reaction condition at 350ºC cobalt was completely reduced to the metallic state, which affected the relative products distribution. It was observed that over metallic cobalt, carbon monoxide was the major reaction product, proving that decomposition of ethanol was the most important reaction pathway [130]. The relative selectivity towards carbon dioxide was incomparably lower than that to carbon monoxide, indicating that the presence of some amounts of Co(II) is important for selective transformations of ethanol.

Studies of E. Martono and J.M. Vohs [118], which were focused on the reaction of ethanol on Co/CeO_2/YSZ(100) model catalysts, are consistent with the observations from above mentioned publications. Additionally, the authors came to the conclusion, that the facile transfer of oxygen from ceria to cobalt allows for formation of CoO_x species ($Co + 2CeO_2 \rightarrow CoO + Ce_2O_3$). B. Bayram et al. [84] specified that cobalt re-oxidation can be caused by the migration of labile oxygen species from the support to cobalt moieties. This phenomenon, according to the both researchers groups [84, 118], may play an important role in the ESR. As it can be expected the oxygen transfer results also in ceria support reduction [118, 119]. It was mentioned [117, 118, 121], that CoO_x species can promote ethanol dehydrogenation, thus the support may influence the overall activity of a catalyst, providing the oxygen required for the dehydrogenation of

$–O–C_2H_5$ to acetaldehyde. Facile transfer of oxygen from the support to cobalt was observed also in a model Co/ZnO catalyst [120].

The same research team [120, 130, 131] performed a very simple experiment to examine the thermal and chemical stability of as deposited cobalt on zinc oxide, and yttria-stabilized zirconia (YSZ). The samples were progressively heated in ultra high vacuum (UHV) at higher temperatures and examined by the XPS. In the initial state of both samples, cobalt remained preliminary in metallic form (778.0 ± 0.2 eV). However, in the case of the Co/ZnO, annealing caused gradual appearance of the feature at 780.5 ± 0.5 eV, suggesting cobalt oxidation. The Co/YSZ sample was found to exhibit relatively high stability during heating. Note, that at the same temperature (427ºC) for the Co/YSZ sample (Fig. 1.17) no features, indicating for cobalt oxidation were found. Those results showed that a support nature may dramatically change cobalt oxidation state due to cobalt–support interactions. E. Martono and J.M. Vohs [130] also concluded that cobalt supported on reducible oxides (zinc oxide, and ceria) exhibits higher activity compared to that of cobalt deposited on more refractory supports (zirconia, and magnesia). It is noteworthy, that oxygen from the reducible supports was found to hinder carbon build-up [118, 121, 123, 132], while in the case of non-reducible supports, oxygen had to be provided from the gas phase to remove deposited carbon [130].

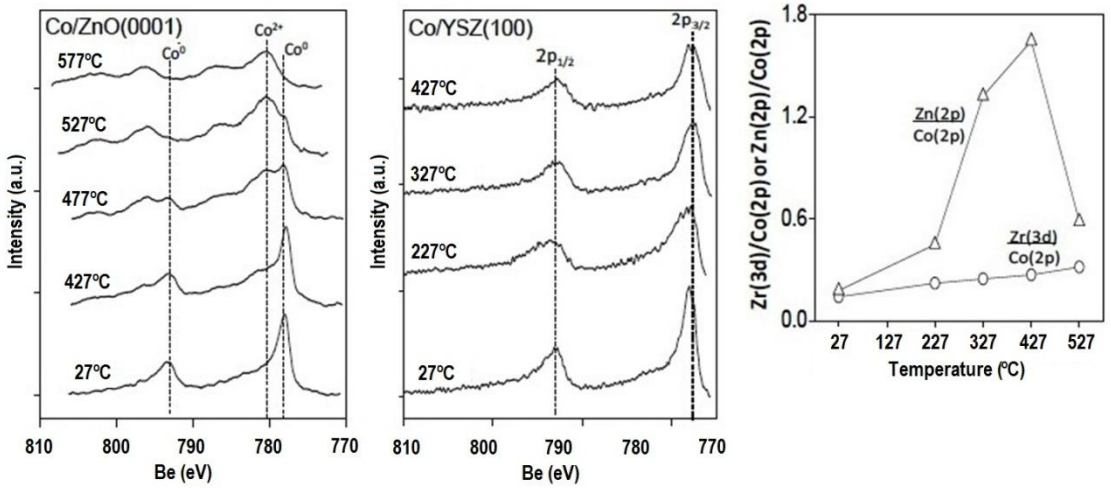

Fig. 1.17 XPS-spectra of 2 ML Co/ZnO(0001) and Co/YSZ(100) samples as a function of the annealing temperature and Zr 3d/Co 2p and Zn 2p/Co 2p peak area ratios as a function of the sample annealing temperature for both samples. Pictures taken from Ph.D. dissertation of E. Martono [131]. Combined Fig. 3.3 and 5.2.

The cited publication [130] provided also a new insight into active sites on cobalt-based catalysts. According to the authors [130] CoO_x species do not appear to provide the active sites for acetaldehyde production. The studies demonstrated that

oxygen-covered metallic cobalt is much more active for ethoxide dehydrogenation than CoO_x.

In terms of different support's capacities towards cobalt oxidation also the latest studies of E. Varga et. al. [123] should be mentioned. The authors were pre-treated a Co/CeO_2 catalyst in a high-pressure cell connected to the XPS chamber via a gate valve. After each pre-treatment (reduction and the ESR) the high-pressure cell was evacuated and the sample was transferred to the analysis chamber in UHV. The catalytic reaction was also carried out in a fixed-bed continuous reactor. The products were detected by means of a gas chromatograph. The XPS studies, carried out over the pre-reduced Co/CeO_2 catalyst used in the ESR (H_2O/EtOH = 3/1 mol/mol), showed the presence of noticeable amounts of CoO_x species up to 500ºC (Fig. 1.18).

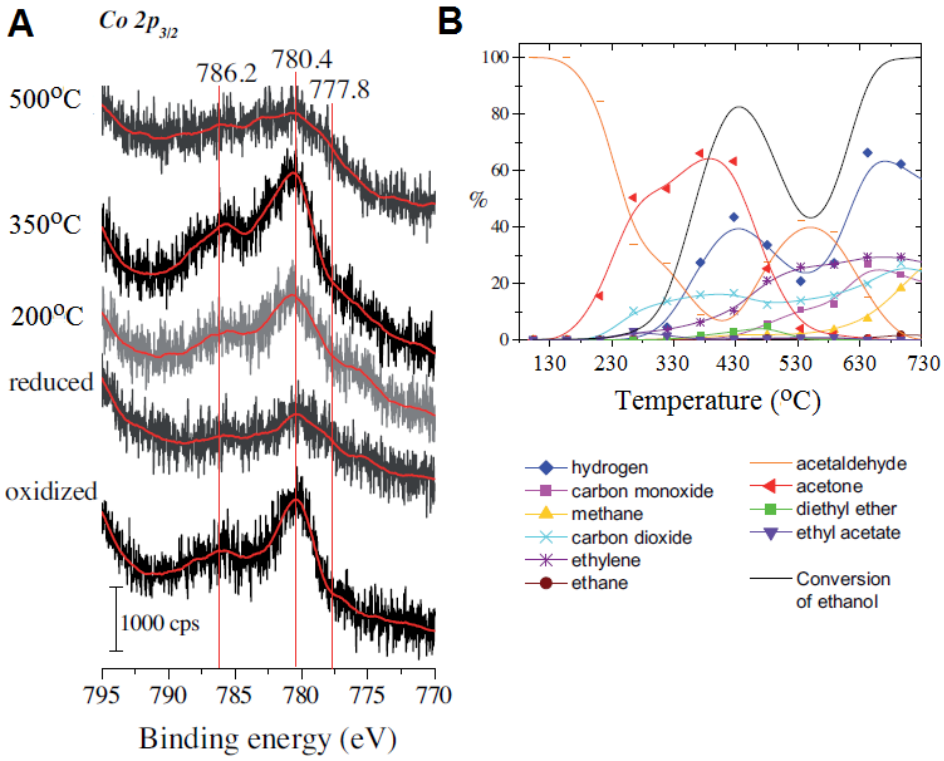

Fig. 1.18 Co 2p spectra after the ESR at different temperatures on 2% Co/CeO_2 catalyst A) and selectivities as a function of temperature B). Combined Figs. 2a and 4a from E. Varga et al. studies [123].

Correlation of information from the XPS spectra and catalytic tests shows that the oxidized catalyst is highly selective towards acetone in the temperature range of 200–500ºC (which is in agreement with studies of P. Rybak et al. [86]). After the ESR carried out at 500ºC, the small feature at 777.8 eV on the Co 2p spectrum appeared (Fig. 1.18 A), indicating for the presence of metallic cobalt species [133].

D. Zanchet et al. [134], in the quite extensive review about metal-catalyzed ethanol steam reforming, mentioned that in principle the molar ratio of Co(0)/Co(II)

can be manipulated by changing the reaction mixture composition [84, 114], the temperature of reaction [122], as well as by manipulating cobalt particle size, and also cobalt-loading [135]. In so far available works, the ratio between Co(0) and Co(II) has been manipulated by changing the calcination temperature [122] or cobalt loading [106, 135]. As presented above, the extent of cobalt particles oxidation can be additionally influenced by interaction with a support. Therefore, it is very important to obtain the complete catalysts' characterization under *in-situ (operando)* conditions in order to understand the structural and electronic information, that can be combined with activity and selectivity of a catalyst.

The catalytic role of Co(0) and Co(II) during the ESR was widely studied on real cobalt-catalysts with the magnesia, alumina, ceria and zirconia supports [106, 122–124, 135], by means of XPS combined with gas chromatographic studies. The authors of those papers agreed that Co(0) is more active for C–C bonds cleavage and in the WGS reaction than Co(II) (which is in agreement with previous cited works [19, 106, 115]), as well as that acetaldehyde might be a very important intermediate during the ESR.

The team of A.M. Karim [106] found the correlation of Co(0) fraction towards methane selectivity in the ESR. Their results show that a higher percentage contribution of metallic cobalt results in lower selectivity towards methane. The researchers [106], therefore suggested, that formation of methane may proceed through *(i)* ethanol decomposition (Eq. 3) and/or *(ii)* methanation of carbon monoxide and carbon dioxide (Eq. 12), which could be more favoured on oxidized cobalt species. The second explanation is rather unlikely since methanation proceed faster on the metal than on the oxide.

A.R. Passos et al. [122] showed that on a catalyst with lower Co(0)/Co(II) ratio the increase of acetaldehyde formation is followed by the increase of methane selectivity, indicating that probably methane is formed via acetaldehyde decomposition. What is quite important, the authors of abovementioned publication [122], suggested that stabilisation of metallic cobalt species is crucial in order to achieve a catalyst exhibiting a high selectivity towards hydrogen. A.R. Passos et al. [122] postulated that there is an evidence that the molar ratio of Co(0)/Co(II) around 3 results in a stable catalyst, thus there are reasons for controlling Co(0)/Co(II) ratio under the reaction conditions.

The presented results were a driving force for a deeper understanding of cobalt active sites nature since it was clearly showed, that both Co(0) and Co(II) species play a very important role during the ESR. Another aspect, that has already appeared several times, is the interaction of cobalt with different oxides which can be used as a support. Selected supports may differ in view of the acid-base properties, oxygen storage capacity, oxygen mobility, ability for water dissociation, all of which affect the activity, selectivity and stability of a catalyst.

It was discovered that another important factor influencing on catalyst's components oxidation state is an addition of a promoter. Promoters (e.g., alkali metals such as sodium [136–138], potassium [110, 139–143] or noble metals, like rhodium [123, 124], platinum [144]). are widely used to improve catalysts activity [116, 138, 142], extent catalysts' lifetime: making sintering [145] and carbon formation [110, [138–140, 142] more difficult.

Very recently it was found, that traces of rhodium promoter altered cobalt and ceria oxidation state after reduction (Fig. 19), the ESR (Fig. 1.20A), and changed the reaction pathways [123, 124]. In literature devoted to XPS studies [117, 146–156] it was shown that features denoted as v' and u' on the Ce 3d spectrum (located on Fig. 19B at 885.3 eV and 903.9 eV) confirm the presence of Ce(III) ions, whereas peak characteristic for metallic cobalt usually was found around 778.3 eV. In the presence of rhodium the percentage contribution of Co(0) and Ce(II) on the surface was more prominent, therefore, the authors [124] concluded that the rhodium promoter first helps to improve catalyst's reducibility and to keep cobalt in metallic state during the ESR. Additionally, rhodium promotes cleavage of C–C bonds in ethanol molecule, which was supposed to be supported by the presence of $–CH_3$ species on the catalyst's surface and higher catalyst's selectivity towards methane, as compared to the unpromoted catalyst. Moreover, addition of small amounts of rhodium (0.1 wt.%) to the Co/CeO_2 promoted catalyst's selectivity to hydrogen [123, 124]. A higher selectivity of the rhodium-promoted Co/CeO_2 catalyst (than the unpromoted one) to carbon dioxide was explained by the demethanation of acetate to carbonate species, decomposition of which resulted in appearance of carbon dioxide [124].

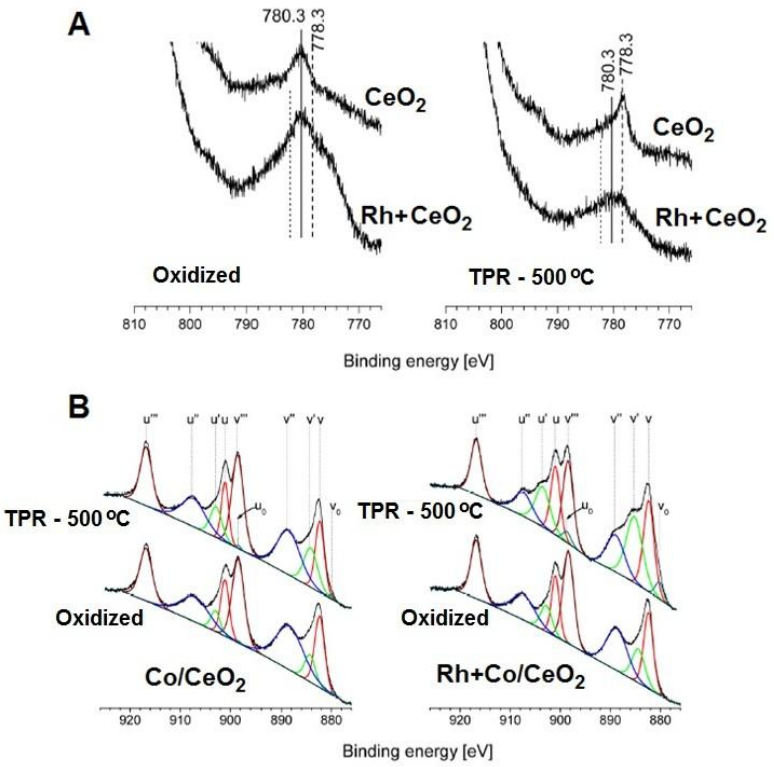

Fig. 1.19 A) Co 2p XPS spectra on ceria support after oxidation at 400ºC for 30 min and after linear heating (20ºC/min) in H_2 to 500ºC, B) Ce 3d XPS spectra taken on a 2% Co/CeO_2 catalyst and 0.1% Rh + 2% Co/CeO_2 catalyst after oxidation at 400ºC and after reduction with the TPR run up to 500ºC. Part of Fig. 2 from Zs. Ferencz et al. studies [124].

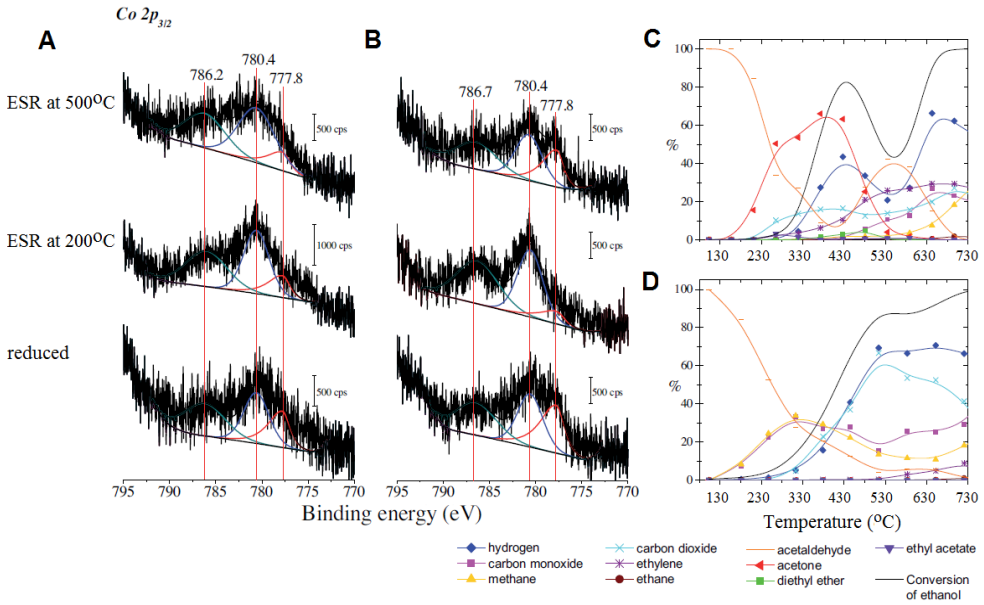

Fig. 1.20 The peak fitting of Co $2p_{3/2}$ spectra after reduction and after ESR at 200ºC and 500ºC for 2% $CoCeO_2$ A) and 0.1% Rh + 2% Co/CeO_2 B). And selectivities as a function of temperature for 2% $CoCeO_2$, C) - repeated Fig. 1.17A) and 0.1% Rh + 2% Co/CeO_2 D). Combined Figs. 2 and 6 from E. Varga et al. studies [123].

According to the authors [124] this process might be an additional source of hydrogen. The amounts of acetaldehyde formed over the rhodium-promoted Co/CeO_2 catalyst were lower, whereas acetone production was hindered as compared to the unpromoted Co/CeO_2 catalyst. It was suggested that oxidized cobalt centres promote aldol condensation [123].

The addition of the same promoter to cobalt catalysts with different supporting oxides resulted in different oxidation behaviour of cobalt. The modification of a Co/CeO_2 catalyst with zinc oxide, lowered activity of the catalyst towards C–C bonds cleavage and affected on C_1-products distribution (Fig. 1.21) [157]. The TPO investigation demonstrated, that the addition of zinc oxide facilitated the oxidation of metallic cobalt, presumably via enhancement of ceria oxygen mobility. In addition, zinc oxide promotion changed acid-base properties of ceria resulting in the decrease of the selectivity to C_2-products. This was caused by the suppression of ethanol dehydration on the surface acid sites and slightly improvement of pathways leading to formation of C_3-products, like acetone.

Some reports indicating that potassium addition influences the increase of the amount of CoO_x species [109, 110] are also available in literature.

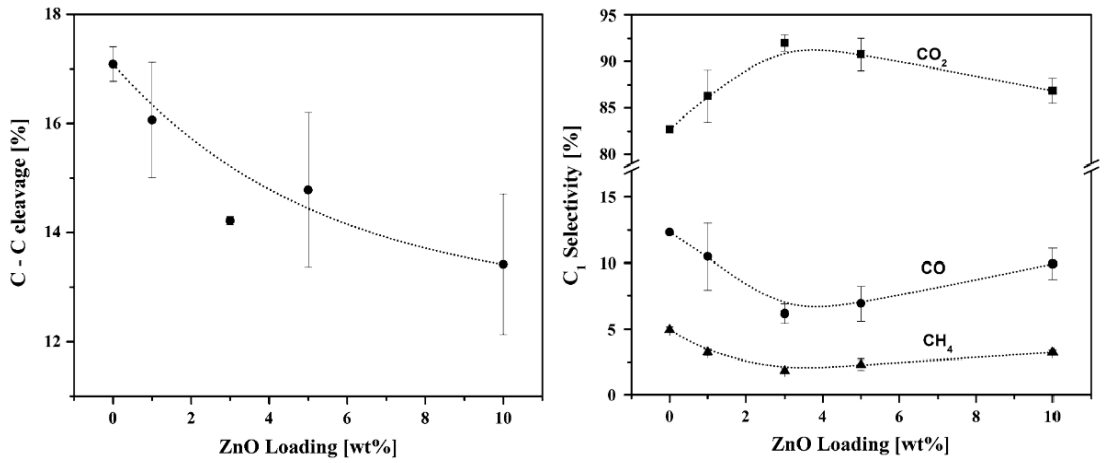

Fig. 1.21 The C–C cleavage conversion and C_1-products selectivity for different zinc oxide loading in the cobalt catalysts. Combined Fig. 6 and 7 from S. Davidson et al. studies [157].

In the case of zinc oxide-promoted Co/ZrO_2 catalyst [107], oxidation of metallic cobalt particles was suppressed. Insight research of S. Davidson et al. [158] showed that the addition of zinc oxide inhibited ability of the Co/ZrO_2 for water dissociation, therefore, resulting in a higher Co(0)/Co(II) ratio. The results of catalytic studies [107] revealed that addition of zinc oxide to the Co/ZrO_2 suppressed ethene, acetaldehyde,

and acetone formation and enhanced selectivity towards hydrogen and carbon dioxide. Experimental data demonstrated, that higher Co(0) contribution results in lower selectivity to methane, which was in agreement with studies of A.M. Karim et al. [106] devoted to Co/MgO catalysts. Similar effect of enhanced reducibility of cobalt(II) species was found on Co/ZnO catalyst after sodium promotion [138].

The discrepancy between studies in ref. [107, 157] and with that of S. Davidson et al. [157] is attributed to the different oxygen mobility of ceria and zirconia supports [132].

The results of TPR studies carried out by M. Greluk et al. [139] showed that the reducibility of a Co/CeO_2 catalyst was improved after potassium promotion. Therefore, even though the authors did not performed studies of cobalt oxidation state it might be expected, that similar to rhodium promoter [123, 124], potassium will improve the catalyst's reducibility under the ESR. From the other hand, the TPO studies showed that the addition of potassium caused greater oxygen-consumption [139]. The studies carried out under the ESR (H_2O/EtOH = 9/1 mol/mol, 420ºC) revealed that potassium addition did not influence on selectivity to carbon dioxide, while the evident decrease of the amount of methane formed was observed [139].

Basing on the XPS studies, M. Sun et al. [159] suggested that addition of the potassium promoter to cobalt catalyst accelerated the adsorption of oxygen and encouraged the formation of surface O^- species (component on the O 1s spectra located at 531.4 eV). These species might be responsible for hindering coke formation (consuming carbon and forming carbonate species [159]), observed by M. Greluk et al. [139] on the potassium-promoted catalyst.

Summing up this part of the literature review it can be said that both forms of cobalt are regarded as important for the ESR. Metallic cobalt is reported to be more active for C–C and C–H bonds rapture [19, 106, 115, 121–124, 135], the WGS reaction [19, 106, 115], and methane steam reforming [19] than Co(II), but from the other side, metallic species are believed to be active centres for coke formation [110]. Cobalt(II) oxide species can be responsible for dehydrogenation of ethanol into acetaldehyde [19, 123, 124], although it was demonstrated that oxygen-covered metallic cobalt exhibits higher activity for dehydrogenation of ethoxide than CoO_x [130]. The next question requiring clarification is the role of a promoter in cobalt oxidation. Usually, addition of a promoter improves catalyst's properties [116, 138, 142], but as it was shown a promoter may facilitate or hinder cobalt reduction [107, 123, 124, 139, 158].

Therefore, scientists should answer whether CoO_x reduction into Co(0) should be suppressed or not [108, 110, 122, 138, 160] to improve the catalyst's activity and stability.

Hence, in view on presented research, it seems that the discussion which form of cobalt Co(0) [100, 101, 103–107] or CoO [108–110] is more active in the ESR, is still open.

1.2.1.3 The role of metal oxides supports in cobalt-catalysts

Numerous studies in literature have presented the reactivity trends of cobalt catalysts as a function of supports [118], such as MgO [19, 87, 101, 106, 161], ZnO [101, 116, 161, 162], γ-Al_2O_3 [87, 88, 101, 124, 161, 163–165], SiO_2 [87, 101, 124, 161, 163], TiO_2 [101, 161], V_2O_5 [101, 161], La_2O_3 [101, 161], Sm_2O_3 [101, 161], CeO_2 [80, 88, 101, 124, 127, 161] and ZrO_2 [87, 88, 104, 127].

So far, several advantages of cobalt supporting on metal oxides have been presented. First of all, supports play a role of a dispersion medium and in preventing metal particles from sintering [132].

Support is also responsible not only for physical stabilisation of cobalt crystallites, but also for their chemical stability. Some supports, like ceria or zinc oxide, facilitate the oxidation of cobalt through release of lattice oxygen [114, 120, 130] leading to the formation of CoO_x species, which have lower C–C cleavage activity than metallic cobalt [117, 130, 157]. Oxygen storage and release capacity of a support are very important to hinder the formation of carbonaceous deposit by its gasification [130, 132]. It can be said that support's oxygen mobility may define the stability of a catalyst under the reaction conditions [132, 166–168].

As already mentioned, supporting oxides play an important role in modifying the formation of active cobalt species [130, 135] and in alternating the reaction pathways [81, 85, 169]. Most metal oxides take also part in intermediate steps of ethanol transformations [4, 87, 170–172] and in activation of water molecules [127, 171], meaning that they are chemically active (even though, barely). For example, some studies indicate that ceria and zirconia exhibit some catalytic performance in water, ethanol [79, 167, 173, 174] (Fig. 1.22) and other carbon-containing products (like ethane, ethene, acetaldehyde, acetone) transformations [79, 173–175].

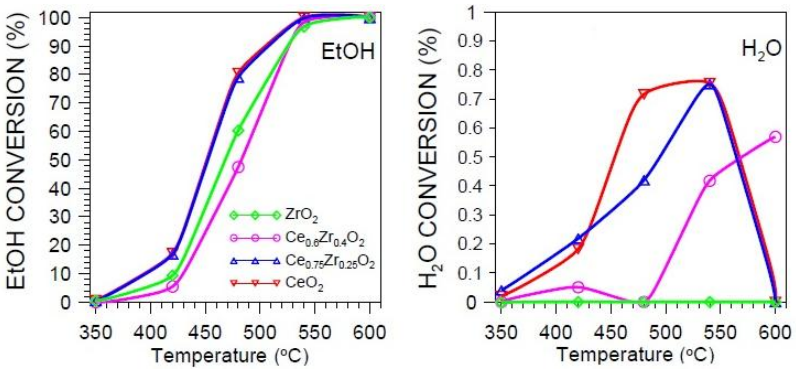

Fig. 1.22 Conversion of ethanol and water at temperatures 350–600ºC over high-surface area ceria, zirconia and binary ceria-zirconia oxides [174].

It was found that the share of thermodynamically possible directions of ethanol transformations strongly depend on acid-base support's properties, therefore, affecting on selectivity of the ESR process [88]. It was widely accepted [81, 169] and proved [87, 101, 161, 163–165] that oxides with acidic surface (e.g., alumina) strongly favour the reaction of ethanol dehydration [88, 101, 103], producing ethene (Eq. 4), which is recognised as a coke precursor [68–88]. From the other side, employment of support oxides of the strong basic nature (e.g., magnesia) cause ethanol condensation to higher oxygenates like acetaldehyde [19, 161].

Table 2. Catalytic Performance of supported cobalt-catalysts after 20 h at 450ºC under the H_2O/EtOH/Ar = 13/1/70 molar ratio) at p = 1 atm and GHSV=5000 h^{-1} [161].

talyst	Conv. (%)	Selectivity (%)*							
		H_2	CO	CO_2	CH_4	C_2H_4	C_3H_6	CH_3CHO	Me_2CO
Co/MgO	29.3	55	0.4	8.2	2.1	2.5	4.2	27.6	—
Co/Al_2O_3	100	0.8	—	0.3	0.1	98.8	—	—	—
Co/SiO_2	87	49.8	2.9	3.9	2.1	3.4	0.2	37.7	—
Co/TiO_2	16.4	47.4	—	4.4	0.3	13.5	—	34.4	—
Co/V_2O_5	100	53.5	—	16.1	1.2	19.9	0.3	6.4	2.6
Co/ZnO(1)	100	66	—	20.8	0.7	1.1	0.5	4.8	6.1
Co/ZnO(2)	100	71.3	—	20.2	0.8	0.6	0.1	0.2	6.8
Co/La_2O_3	85	63.1	—	21.5	1.3	1.1	0.1	0.5	12.4
Co/CeO_2	93.7	69.6	—	21.1	0.1	1.9	0.1	0.8	6.4
Co/Sm_2O_3	85.9	64.7	—	21	1.6	7.3	0.1	—	5.3

* In fact – products distribution (S. Turczyniak remark)

However, studies of J. Llorca et al. [161] argue against the thesis that support acid-base properties are the sole factor in controlling a catalyst's selectivity to hydrogen and carbon dioxide. In their studies [161] (H_2O/EtOH = 13/1 mol/mol, 450ºC), the Co/ZnO catalyst was found to be much more active and selective than the Co/MgO (Table 2). The authors [118] pointed that both oxides have comparable basicity, which was supported by the work of M.H. Youn et al. [176]. In literature exists disagreement

regarding the basicity of these two supports. Some authors believe that magnesia is a strong basic support, while zinc oxide posses only a weakly basic properties [81]. There are also reports indicating, that the basicity of magnesia varies with the temperature increasing, while the basicity of zinc oxide remains constant [177]. Thus, the results of J. Llorca et al. [161] should not be regarded as an evidence declining the importance of a support acid-base properties. However, it should be remembered that both cobalt catalysts were found to form MgO-CoO [161] and ZnO-CoO [101, 116, 178, 179] solid solutions, where CoO_x substituted cation ion in the support lattice. Formed solid solutions may exhibit different reducibility [130] and performance under the ESR, which also can explain obtained [161] results.

Comparing cobalt catalysts with different supporting oxides it can be seen, that these with weak basic and/or redox properties exhibit better catalytic performance. H. Song et al. [88] found that the activity, selectivity to hydrogen and stability decrease in the order $Co/CeO_2 > Co/ZrO_2 > Co/Al_2O_3$, while the reverse order of surface acidity was found. Their work is not the only one that proved the promising properties of redox oxides [80, 96, 124, 132, 139] thus, attention that has been given to examine them is definitely understood.

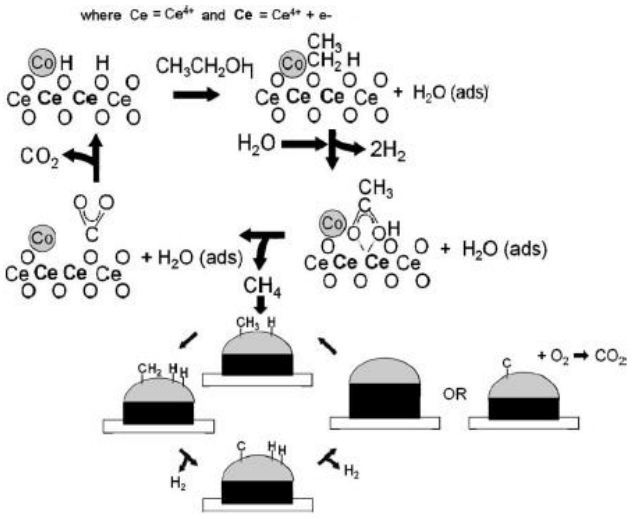

Fig. 1.23 Reaction mechanism suggested by S. M. de Lima et al. for ethanol conversion reactions [167].

A large number of studies have been devoted to comparison of Co/CeO_2, Co/ZrO_2 and $Co/Ce_xZr_{1-x}O_2$ catalysts [81, 86, 132, 180] or just to the characterization of the catalytic performance of each one separately. The Co/CeO_2 and Co/ZrO_2 differ regarding support's reducibility and oxygen storage and releasing capacity. Ceria is known for its high oxygen storage capacity and it is believed to preserve the catalyst's surface area and the catalytic activity [181]. Redox reaction between Ce(IV) and Ce(III) contributes to the remarkable catalytic properties of ceria [151, 182, 183]. Examples are oxidation of carbon monoxide to carbon dioxide [152, 184, 185] or sooth combustion. Contrary to

ceria, zirconia shows no reducibility and no oxygen uptake [132], however, its good thermal stability [186] encourages its application in catalysis.

The papers of S. M. de Lima et al. [51, 55, 167, 187] were mostly devoted to studies of ceria- and zirconia-supported platinum-based catalysts. Only one, from cited works, was dedicated to studies of a cobalt-based catalyst. Despite this, insightful analyze of these works may led to the conclusion that no matter what is the active phase platinum or cobalt, the metal particles may assist in *(i)* hydrogen dissociation, *(ii)* ethanol dissociation, *(iii)* acetate species demethanation and *(iv)* coke formation (Fig. 1.23). However, the presented scheme may be misleading. I can suggest that: *(i)* dissociated ethanol molecule *spill over* on the support and further transformations proceed on the support surface, or *(ii)* that the process takes place on cobalt–ceria boundary, since ethoxy species are located on the support in the nearest neighbourhood of cobalt particles. Furthermore, the proposed scheme seems to diminish the role of cobalt on different oxidation states and over highlighting the importance of ceria as a catalyst's component.

Some studies have shown that addition of zirconia to ceria improves the support thermal stability, redox properties [168, 188] and oxygen storage capacity [189, enhancing e.g., carbon monoxide and sooth oxidation as well as methane combustion 180]. The oxygen mobility in ceria and/or zirconia can be enhanced also by doping of the oxide with other metals or metal oxides [107, 190, 191]. Addition of some dopants to the support was found to influence a catalyst's oxidation. For example, the zinc oxide addition to zirconia-supported cobalt catalyst was found to inhibit metal oxidation [107], decreasing the ability of Co/ZrO_2 to water dissociation [158].

Not only the support nature is substantial in the overall ESR process. Another important factors influencing on a catalyst's activity and selectivity are morphology and textural properties of a support [80, 81, 150, 173, 192].

The morphology [151], specific surface area and crystallity [147] of a support is integrally linked to its reducibility, which was shown by L. Qiu et al. [151]. These authors investigated the differences in a surface's reduction between a nano- and micro-ceria after Ar^+ bombardment and X-ray irradiation. The Ce 3d spectra showed a clear evidence of higher reduction degree of the mico-ceria. It is believed that lower reduction level of the nano-ceria was caused by a higher diffusion degree of oxygen from the bulk to the surface and a higher defect concentration.

The support oxide morphology influences also transformation of various compounds. The different crystal planes result in pronounced differences in ceria activity. Studies of the adsorption and reaction of acetaldehyde (which is regarded as an important intermediate in the ESR) on oxidized and reduced bare ceria (111) and (100) thin films [193, 194] showed, that acetaldehyde reacts on oxidized ceria (100) producing carbon dioxide, carbon monoxide, and water as primary products, while on reduced ceria (100) surface it forms mainly hydrogen and carbon. In the case of ceria (111), acetaldehyde reacts only on the reduced surface forming hydrogen, ethene and ethyne.

1.2.1.4 Cobalt-catalysts deactivation

Changes occurring on a catalyst's surface under working ESR conditions lead to the gradual decrease of a catalyst's activity with time on stream. Among various processes causing a catalyst's deactivation *(i)* coke formation, *(ii)* sintering, *(iii)* active component and promoter volatilisation [195] and *(iv)* metal oxidation [69], can be listed. Generally, deactivation of cobalt catalysts is attributed either to sintering and coke formation [196] or to metal particles oxidation.

Prolonged exposure of a catalyst to a high temperature lead the decrease of the surface area of a catalyst, due to sintering [94, 104, 197]. Small crystallites of the active phase gradually migrate along the support's surface (or by gas phase) (Fig. 1.24) and merge together (coalescence), resulting in the increase of particles size and lowering a surface area. Diminution of the active phase and its support dispersion influences a catalyst's selectivity.

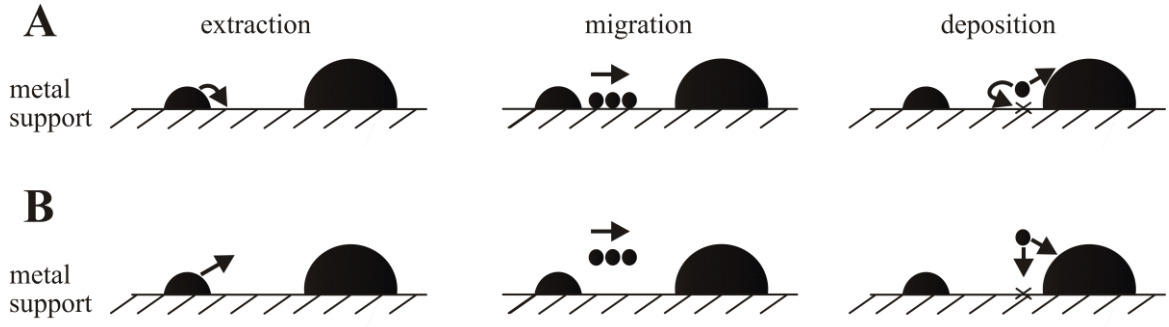

Fig. 1.24 Ostwald's ripening; A) migration of metal atoms ● on a support surface and B) transport in a gas phase, x – not occupied places on a support surface [198].

Sintering processes of the active phase can be inhibited (but not eliminated) by deposition of a metal on a highly dispersed and thermally stable oxide supports [132,

145], whereas a support's resistance to sintering can be improved by addition of small amounts of e.g., alumina [162].

Catalysts' deactivation due to coking is a severe problem, as reported in literature [67, 86, 88, 103, 162, 196, 199, 200]. Thermodynamic considerations on coke formation were briefly presented in the first section to this chapter (entitled "*Steam reforming of ethanol*"). In short, general conclusion is that for working in carbon free zone for the $H_2O/EtOH = 3/1$ mol/mol at least the temperature higher than 330ºC [7, 11] is required (Fig. 1.4). However, simplified thermodynamic calculations are not necessarily consistent with experimental results, whereas a catalyst is loaded to a reactor and then the ESR in carried out.

The aim of the group of H. Wang et al. [201] was at first, to examine the activity and selectivity of the Co/CeO_2 catalyst under reaction conditions ($H_2O/EtOH = 3/1$ mol/mol) carried out at different temperatures, and secondly, to determine how the temperature influences the nature of coke formed during the ESR, and thirdly, to suggest which reactions leading to coke formation at a given temperature are dominant. Based on obtained data the authors [201] concluded, that on the reaction temperature lower than 450ºC coke is formed through the following sequence of ethanol transformation: EtOH → MeCHO → coke and/or EtOH → MeCHO → $(Me)_2CO$ → coke. As the reaction time on stream increases, another pathway becomes more prominent: EtOH →C_2H_4 → polymers→ coke. At this temperature coke formed encapsulates catalyst's particles, contributing to severe catalyst's deactivation. When the temperature is higher (500ºC or 550ºC), reactions such as methane cracking (dissociation) and carbon monoxide disproportionation (Boudouard reaction) (Eq. 12) take place [200]. At these temperatures formed coke is transformed into fiber- (whiskers) or tube-like carbon. However, whiskers of carbon were also observed in the ESR at 420ºC [140]. At temperatures higher than 600ºC coke formation is rather slight.

The above-cited publication [140] clearly shows, that generally two forms of carbon should be expected on working ESR catalyst. First, carbon in the form of nanotubes (Fig. 1.25A) and the second one, condensed carbon encapsulating catalyst's particles (Fig. 1.25B and C). Filamentous carbon is suggested to be generated via Boudouard reaction and methane decomposition (Fig. 1.23), even at lower temperature than suggested in ref. [200].

Carbon whiskers are generated by the diffusion of dissolved carbon through metal crystallite structure [140, 196, 200, 202]. This process causes lifting up of a metal

crystallite from the catalyst's surface, eventually resulting in a catalyst's fragmentation [140, 196, 200]. This kind of coke does not necessarily result in catalyst deactivation [67, 140, 196, 201, 203]. Nonetheless, the formation of filamentous carbon can result in build-up of the pressure in a catalyst's bed, a reactor blockage, fragmentation of a catalyst and plugging of its pores and further coking [140, 196, 200]. Metal particle located at the top of carbon whisker is still active (Fig. 1.25A), if it is not encapsulated (Fig. 1.25B). G. Słowik et al. [140] suggested that in ceria-supported catalysts cobalt particles located on the top of carbon whiskers start acting as Co/C catalyst or KCo/C (in the case of potassium-promoted catalyst). The lost of the contact of cobalt particles with ceria support may alter the ESR selectivity.

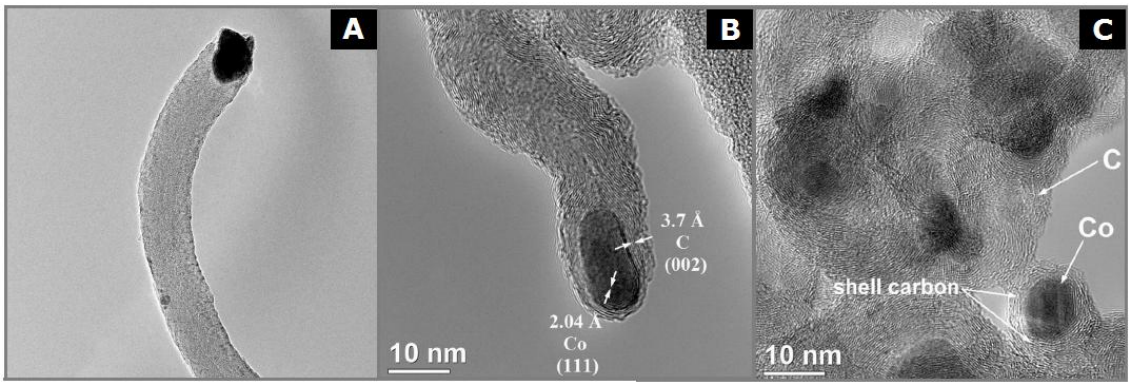

Fig. 1.25 Chosen TEM images of the KCo/CeO_2 catalyst after 33 h in the ESR at 420ºC. A) fiber carbon deposit, B) encapsulating carbon deposit, C) shell carbon encapsulating cobalt particle [140].

The encapsulating carbon deposit (Fig. 1.25B and C) is more harmful type of the coke. It is formed mainly from ethene, acetaldehyde and acetone, like it was suggested in the previous paragraph devoted to studies of H. Wang et al. [201]. Cobalt particles encapsulated in this type of coke and a support's surface covered by it, become completely inaccessible to the reactants, therefore a catalyst starts to be inactive [140].

The change of operating conditions e.g., *(i)* addition of water excess, *(ii)* temperature increase, *(iii)* contact time, *(iv)* co-feeding with oxygen [141] or catalysts' modification like *(v)* manipulation with support oxygen mobility contribute to the attenuation of the problem with coking. Another way to alter a catalyst's susceptibility for coking, is noble metals or alkali metals promotion [139]. Addition of potassium was found to improve catalyst's stability [139–142] by coke gasification, however, the tendency of potassium hydroxide to volatilise in steam stream at high temperatures results in potassium lost. Therefore, potassium should preferentially exist on

a catalyst's surface as e.g., nonvolatile potassium carbonate, potassium-aluminosiliate or potassium-aluminate to be liberated slowly to ensure a good alkali contact with the coke and improve its gasification [200, 204].

References

1 V.D. Parkash, A.E. Rodrigues *Chem. Eng. J.* **117** (2006) 39–49.

2 V. Subramani, C. Song *Catalysis* **20** (2007) 65–106.

3 L.V. Mattos, G. Jackobs, H.D. Burtron, F.B. Noronha *Chem. Rev.* **112** (2012) 4094–4123.

4 H. Song, L. Zhang, R.B. Watson, D. Braden, U.S. Ozkan *Catal. Today* **129** (2007) 346–354.

5 V. Palma, F. Castaldo, P.Ciambelli, G.Iaquaniello *Sustainable hydrogen production by catalytic bio-ethanol steam reforming* in *Greenhouse gases — Capturing, Utilization and Reduction*; 7:137–184.

6 E.Y. García, M. Laborde *Int. J. Hydrogen Energy* **16** (1991) 307–312.

7 V. Mas, R. Kiproes, N. Amadeo, M. Laborde *Int. J. Hydrogen Energy* **31** (2006) 21–28.

8 K. Vasudeva, N. Mitra, P. Umasankar, S.C. Dhingra *Int. J. Hydrogen Energy* **21** (1996) 13–18.

9 C.C.R.S. Rossia, C.G. Alonso, O.A.C. Antunes, R. Guirardello, L. Cardozo-Filho *Int. J. Hydrogen Energy* **34** (2009) 323–332.

10 I. Fishtik, A. Alexander, R. Datta, D. Gean *Int. J. Hydrogen Energy* **25** (2000) 31–45.

11 W. Wang, Y.Q. Wang *Int. J. Energy Res.* **32** (2008) 1432–1443.

12 C.N. de Ávila, C.E. Hori, A.J. de Assis *Energy* **36** (2011) 4385–4395.

13 S. Freni, N. Mondello, S. Cavallaro, G. Cacciola, V.N. Parmon, V.A. Sobyanin *React. Kinet. Catal. Lett.* **71** (2000) 143–152.

14 A. Iulianelli, S. Liguori, T. Longo, S. Tosti, P. Pinacci, A. Basile *Int. J. Hydrogen Energy* **35** (2010) 3159–3164.

15 J.L. Contreras, J. Salmones, J.A. Colín-Luna, L. Nuño, B. Quintana, I. Córdova, B Zeifert, C. Tapia, G.A. Fuentes *Int. J. Hydrogen Energy* **39** (2014) 18835–18853.

16 P.R. de la Piscina, N. Homs *Chem. Soc. Rev.* **37** (2008) 2459–2467.

17 P.D. Vaidya, A.E. Rodrigues *Chem. Eng. J.* **117** (2006) 39–49.

18 M. Ni, D.Y.C. Leung, M.K.H. Leung *Int. J. Hydrogen Energy* **32** (2007) 3238–3247.

19 S. Tuti, F. Pepe *Catal Lett.* **122** (2008) 196–203.

20 B. Zhang, X. Tang, Y. Li, W. Cai, Y. Xu, W. Shen *Catal. Commun.* **7** (2006) 367–372.

21 V. Palma, F. Castaldo, P. Ciambelli, G. Iaquaniello, G. Capitani *Int. J. Hydrogen Energy* **16** (2013) 6633–6645.

22 A. Carrero, J.A. Calles, A.J. Vizcaíno *Chem. Eng. J* **163** (2010) 395–402.

23 L.-C. Chen, S.D. Lin *Appl. Catal., B* **148–149** (2014) 509–519.

24 L. Zhang, J. Liu, W. Li, C. Guo, J. Zhang *Journal of Natural Gas Chemistry* **18** (2009) 55–65.

25 A.J. Vizcaíno, A. Carrero, J.A. Calles *Int. J. Hydrogen Energ.* **32** (2007) 1450–1461.

26 L.-C. Chen, S.D. Lin *Appl. Catal., B* **106** (2011) 639–649.

27 V. Palma, F. Castaldo, P. Ciambelli, G. Iaquaniello, G. Capitani *Int. J. Hydrogen Energy* **38** (2013) 6633–6645.

28 L. Chen, C.K.S. Choong, Z. Zhong, L. Huang, Z. Wang, J. Lin *Int. J. Hydrogen Energy* **37** (2012) 16321–16332.

29 X. Zhao, G. Lu Int. *J. Hydrogen Energy* **41** (2016) 3349–3362.

30 Y.T. Law, W.H. Doh, W. Luo, S. Zafeiratos *J. Mol. Catal. A* **381** (2014) 89–98.

31 A. Casanovas, C. de Leitenburg, A. Trovarelli, J. Llorca, *Chem. Eng. J.* **154** (2009) 267–273.

32 M.H. Youn, J.G. Seo, P. Kimb, I.K. Song *J. Mol. Catal. A* **261** (2007) 276–281.

33 D.K. Liguras, D.I. Kondarides, X.E. Verykios *Appl. Catal., B* **43** (2003) 345–354.

34 F. Auprêtre, C. Descorme, D. Duprez *Top Catal.* **30|31** (2004) 487–491.

35 E. Gucciardi, V. Chiodo, S. Freni, S. Cavallaro, A. Galvagno, J.C.J. Bart *Reac. Kinet. Mech. Cat.* **104** (2011) 75–87.

36 S. Cavallaro *Energy & Fuels* **14** (2000) 1195–1199.

37 R. Wang, H. Xu, X. Liu, Q. Ge, W. Li *Appl. Catal., A* **305** (2006) 204–210.

38 K. Hashimoto,N. Toukai, R. Hamada, S. Imamura *Catal Lett.* 50 (1998) 193–198.

39 H. Cordatos, T. Bunluesin, J. Stubenrauch, J M. Vohs, R.J. Gorte *J. Phys. Chem.* **100** (1996) 785–789.

40 A. Birot, F. Epron, C. Descorme, D. Duprez *Appl. Catal., B* **79** (2008) 17–25.

41 A. Platon, H.-S. Roh, D.L. King, Y. Wang *Top. Catal* **46** (2007) 374–379.

42 A. Erdőhelyi, J. Raskó, T. Kecskés, M. Tóth, M. Dömök, K. Baán *Catal. Today* **116** (2006) 367–376.

43 M. Bilal, S.D. Jackson *Catal. Sci. Technol.* **3** (2013) 754–766.

44 H.-S. Roh, Y. Wang, D.L. King *Top Catal.* **49** (2008) 32–37.

45 R.M. Navarro, M.C. Álvarez-Galván, M. Cruz Sánchez-Sánchez, F. Rosa, J.L.G. Fierro *Appl. Catal., B* **55** (2005) 229–241.

46 M. Dömök, M. Tóth, J. Raskó, A. Erdőhelyi *Appl. Catal., B* **69** (2007) 262–272.

47 M. Dömök, K. Baán, T. Kecskés, A. Erdőhelyi *Catal Lett.* **126** (2008) 49–57.

48 Z. He, M. Yang, X. Wang, Z. Zhao, A. Duan *Catal. Today* **194** (2012) 2–8.

49 P. Ciambelli, V. Palma, A. Ruggiero *Appl. Catal., B* **96** (2010) 18–27.

50 P. Ciambelli, V. Palma, A. Ruggiero *Appl. Catal., B* **96** (2010) 190–197.

51 S.M. de Lima, A.M. Silva, U. M. Graham, G. Jacobs, B. H. Davis, L.V. Mattos, F.B. Noronha *Appl. Catal., A* **352** (2009) 95–113.

52 B. Zhang, W. Cai, Y. Li, Y. Xu, W. Shen *Int. J. Hydrogen Energy* **33** (2008) 4377–4389

53 P. Panagiotopoulou, X.E. Verykios *Int. J. Hydrogen Energy* **37** (2012) 16333–16345.

54 A. Casanovas, J. Llorca, N. Homs, J.L.G. Fierro, P.R. de la Piscina *J. Mol. Catal. A* **250** (2006) 44–49.

55 S.M. de Lima, A.M. Silva, I.O. da Cruz, G. Jacobs, B.H. Davis, L.V. Mattos, F.B. Noronha *Catal. Today* **138** (2008) 162–168.

56 T. Yamazaki, N. Kikuchi, M. Katoh, T. Hirose, H. Saito, T. Yoshikawa, M. Wada *Appl. Catal., B* **99** (2010) 81–88.

57 T. Bunluesin, R.J. Gorte, G.W. Graham *Appl. Catal., B* **15** (1998) 107–114.

58 A.C. Basagiannis, P. Panagiotopoulou, E. Verykios, *Top Catal.* **51** (2008) 2–12.

59 M.N. Dennis, Y.C. Leung, M.K.H. Leung *Int. J. Hydrogen Energy* **32** (2007) 3238–3247.

60 B. Lorenzut, T. Montini, L. De Rogatis, P. Canton, A. Benedetti, P. Fornasiero *Appl. Catal., B,* **101** (2011) 397–408.

61 W. Grzegorczyk, A. Denis, W. Gac, T. Ioannides, A. Machocki *Catal Lett.* **128** (2009) 443–448.

62 T. Nishiguchi, T. Matsumoto, H. Kanai, K. Utani, Y. Matsumura, W.-J. Shen, S. Imamura *Appl. Catal. A* **279** (2005) 273–277.

63 J. Llorca, N. Homs, P.R. de la Piscina, *J. Catal.* **227** (2004) 556–560.

64 C.N. Ávila-Neto, J.W.C. Liberatori, A.M. da Silva, D. Zanchet, C.E. Hori, F.B. Noronha, J.M.C. Bueno *J. Catal.* **287** (2012) 124–137.

65 C. Zhang, S. Li, G. Wu, Z. Huang, Z. Han, T. Wang. J. Gong *AIChE Journal* **60** (2014) 634–644.

66 P.K. Seelam, S. Liguori, A. Iulianelli, P. Pinacci, V. Calabrò, M. Huuhtanen, R. Keiski, V. Piemonte, S. Tosti, M. De Falco, A. Basile *Catal. Today* **193** (2012) 42–48.

67 P. Bichon, G. Haugom, H.J. Venvik, A. Holmen, E.A. Blekkan *Top Catal.* **49** (2008) 38–45.

68 A.G. Gayubo, J. Vicente, J. Ereña, C. Montero, M. Olazar, J. Bilbao *Catal Lett.* **144** (2014) 1134–1143.

69 S. Freni, S. Cavallaro, N. Mondello, L. Spadaro, F. Frusteri *Catal. Commun.* **4** (2003) 259–268.

70 F. Frusteri, S. Freni, L. Spadaro, V. Chiodo, G. Bonura, S. Donato, S. Cavallaro *Catal. Commun.* **5** (2004) 611–615.

71 K. Urasaki, K. Tokunaga, Y. Sekine, M. Matsukata, E. Kikuchi *Catal. Commun.* **9** (2008) 600–604.

72 M.S. Yakimova, V.K. Ivanov, O.S. Polezhaeva, A.S. Lermontov, Y.D. Tretyakov *Doklady Chemistry* **427** (2009) 190–193.

73 R. Padilla, M. Benito, L. Rodríguez, A. Serrano, G. Muñoz, L. Daza *Int. J. Hydrogen Energy* **35** (2010) 8921–8928.

74 Y.T. Law, T. Skála, I. Pís□, V. Nehasil, M. Vondrác□ek, S. Zafeiratos *J. Phys. Chem. C* **116** (2012) 10048–10056.

75 A.N. Fatsikostas, X.E. Verykios *J. Catal.* **225** (2004) 439–452.

76 J.W.C. Liberatori, R.U. Ribeiro, D. Zanchet, F.B. Noronha, J.M.C. Bueno *Appl. Catal., A* **327** (2007) 197–204.

77 F.L.S. Carvalho, Y.J.O. Asencios, A.M.B. Rego, E.M. Assaf *Appl. Catal., A* **483** (2014) 52–62.

78 J.F. Da Costa-Serra, R. Guil-López, A. Chica *Int. J. Hydrogen Energ.* **35** (2010) 6709–6716.

79 I.I. Soykal, H. Sohn, D. Singh, J.T. Miller, U.S. Ozkan *ASC Catal.* **4** (2014) 585–592.

80 I.I. Soykal, H .Sohn, U.S. Ozkan *ACS Catal.* **2** (2012) 2335–2348.

81 A. Machocki, A. Denis, W. Grzegorczyk, W. Gac *Appl. Surf. Sci.* **256** (2010) 5551–5558.

82 A.L.M. da Silva, J.P. den Breejen, L.V. Mattos, J.H. Bitter, K.P. de Jong, F.B. Noronha *J. Catal.* **318** (2014) 67–74.

83 I.I. Soykal, B. Bayram, H. Sohn, P. Gawade, J.T. Miller, U.S. Ozkan, *Appl. Catal., A* **449** (2012) 47–58.

84 B. Bayram, I.I. Soykal, D. von Deak, J.T. Miller, U.S. Ozkan *J. Catal.* **284** (2011) 77–89.

85 S.S.-Y. Lin, H. Daimon, S.Y. Ha *Appl. Catal., A* **366** (2009) 252–261.

86 P. Rybak, B. Tomaszewska, A. Machocki, W. Grzegorczyk, A. Denis, *Catal. Today* **176** (2011) 14–20.

87 F. Haga, T. Nakajima, H. Miya, S. Mishima *Catal Lett.* **48** (1997) 223–227.

88 H. Song, L. Zhang, U.S. Ozkan *Top. Catal.* **55** (2012) 1324–1331.

89 N. Yu, H. Zhang, S.D. Davidson, J. Sun, Y. Wang *Catal. Commun.* **73** (2016) 93–97.

90 A.M. da Silva, K.R. de Souza, G. Jacobs, U.M. Graham, B.H. Davis, L.V. Mattos, F.B. Noronha *Appl. Catal., B* **102** (2011) 94–109.

91 X.-Q. Gong, R. Raval, P. Hu *Mol. Phys.* **102** (2004) 993–1000.

92 J. Sun, D. Mei, A.M. Karim, A.K. Datye, Y. Wang *ChemCatChem* **5** (2013) 1299–1303.

93 H. Song, B. Mirkelamoglu, U.S. Ozkan *Appl. Catal., A* **382** (2010) 58–64.

94 H. Song, U.S. Ozkan *J. Mol. Catal. A* **318** (2010) 21–29.

95 H. Song, B.Tan, U.S. Ozkan, *Catal Lett.* **132** (2009) 422–429.

96 M. Greluk, M. Rotko, B. Banach, G. Słowik, A. Machocki, *Reforming parowy etanolu na katalizatorach otrzymanych w środowisku niewodnym, 58 Zjazd PTChem,* Gdańsk 2015, S06KS15, [Acces On-line] http://ptchem2015.ug.edu.pl/img/uploadFiles/materialy_zjazdowe/58ptchem__materialy_zjazdowe_s06.pdf.

97 H. Wang, J.L. Ye, Y. Liu, Y.D. Li, Y.N. Qin *Catal. Today* **129** (2007) 305–312.

98 S.-W. Yu, H.-H. Huang, C.-W. Tang, C.-B. Wang Int. *J. Hydrogen Energy* **39** (2014) 20700–20711.

99 J. Llorca, P.R. de la Piscina, J.A. Dalmon, N. Homs *Chem. Mater.* **16** (2004) 3573–3578.

100 V.A. de la Peña O'Shea, N. Homs, E.B. Pereira, R. Nafria, P.R. de la Piscina *Catal. Today* **126** (2007) 148–152.

101 J. Llorca, J.A. Dalmon, P.R. de la Piscina, N. Homs *Appl. Catal., A* **243** (2003) 261–269.

102 W. Luo, A. Asthagiri *Catal. Sci. Technol.* **4** (2014) 3379–3389.

103 M.S. Batista, K.S. Santos, E.M. Assaf, E.A. Ticianelli *J. Power Sources* **124** (2003) 99–103.

104 H. Song, L. Zhang, U. S. Ozkan *Green Chem.* **9** (2007) 686–694.

105 M. Domínguez, E. Taboada, H. Idriss, E. Molins, J. Llorca *J. Mater. Chem.* **20** (2010) 4875–4883.

106 A.M. Karim, Y. Su, M.H. Engelhard, D.L. King, Y. Wang *ACS Catal.* **1** (2011) 279–286.

107 V.M. Lebarbier, A.M. Karim, M.H. Engelhard, Y. Wu, B.-Q. Xu, E.J. Petersen, A.K. Datye, Y. Wang, *ChemSusChem* **4** (2011) 1679–1684.

108 L. del Río, G. Marbán *Appl. Catal., B* **150–151** (2014) 370–379.

109 R. Espinal, E. Taboada, E. Molins, R.J. Chimentao, F. Medina, J. Llorca *Appl. Catal., B* **127** (2012) 59–67.

110 S. Ogo, T. Shimizu, Y. Nakazawa, K. Mukawa, D. Mukai, Y. Sekine *Appl. Catal., A* **495** (2015) 30–38.

111 W. Gac *Catal. Today* **176** (2011) 131–133.

112 P.J. van Bergea, J. van de Loosdrecht, S. Barradas, A.M. van der Kraan *Catal. Today* **58** (2000) 321–334.

113 A. Sirijaruphan, A. Horváth, J.G. Goodwin Jr., R. Oukaci *Catal Lett*. **81** (2003) 89–94.

114 S.S.-Y. Lin, D.H. Kim, M.H. Engelhard, S.Y. Ha *J. Catal.* **273** (2010) 229–235.

115 L.P.R. Profeti, E.A. Ticianelli, E.M. Assaf *Appl. Catal., A* **360** (2009) 17–25.

116 J. Llorca, P.R. de la Piscina, J.A. Dalmon, J. Sales, N. Homs *Appl. Catal., B* **43** (2003) 355–369.

117 M.P. Hyman, J.M. Vohs, *Surf. Sci.* **605** (2011) 383–389.

118 E. Martono, J.M. Vohs *J. Catal.* **291** (2012) 79–86.

119 L. Óvári, S.K. Calderon, Y. Lykhach, J. Libuda, A. Erdőhelyi, C. Papp, J. Kiss, H.-P. Steinrück *J. Catal.* **307** (2013) 132–139.

120 M.P. Hyman, E. Martono, J. Vohs, *J. Phys. Chem. C* **114** (2010) 16892–16899.

121 E. Martono, M.P. Hyman, J. M. Vohs *Phys. Chem. Chem. Phys.* **13** (2011) 9880–9886.

122 A.R. Passos, L. Martins, S.H. Pulcinellin, C.V. Santilli, V. Briois *Catal. Today* **229** (2014) 88–94.

123 E. Varga, Z. Ferencz, A. Oszkó, A. Erdöhelyi, J. Kiss, *J. Mol. Catal. A* **397** (2015) 127–133.

124 Zs. Ferencz, A. Erdöhelyi, K. Baan, A. Oszkó, L. Óvári, Z. Kónya, C. Papp, H.-P. Steinrück, J. Kiss *ACS Catal*. **4** (2014) 1205–1218.

125 A. Bshish, Z. Yaakob, B. Narayanan, R. Ramakrishnan, A. Ebshish *Chem Papers* **65** (2011) 251–266.

126 J.M. Guil, N. Homs, J. Llorca, P.R. de la Piscina *J. Phys. Chem*. **109** (2005) 10813–10819.

127 H. Song, X. Bao, C.M. Hadad, U.S. Ozkan *Catal Lett.* **141** (2011) 43–54.

128 M. Virginie, M. Araque, A.-C. Roger, J.C. Vargas, A. Kiennemann *Catal. Today* **138** (2008) 21–27.

129 Y.T. Law *Investigation of reaction networks and active sites in ethanol steam reforming reaction over Ni and Co-based catalysts*, in École doctorale des sciences chimique UMR 7515 — Institut de Chimie et Procédés pour l'Énergie, l'Environnement et la Santé 2013, Université de Strasbourg: Strasbourg.

130 E. Martono, J.M. Vohs *ACS Catal.* **1** (2011) 1414–1420.

131 E. Martono *Mechanistic Studies of Alcohol Steam Reforming Catalysts*. 2013, University of Pennsylvania: Pennsylvania.

132 H. Song, U.S. Ozkan *J. Catal*. **261** (2009) 66–74.

133 V. Papaefthimiou, T. Dintzer, V. Dupuis, A. Tamion, F. Tournus, A. Hillion, D. Teschner, M. Hävecker, A. Knop-Gericke, R. Schlögl, S. Zafeiratos *ACS Nano* **5** (2011) 2182–2190.

134 D. Zanchet, J.B.O. Santos, S. Damyanova, J.M.R. Gallo, J.M.C. Bueno *ASC Catal.* **5** (2015) 3841–3863.

135 J. Sun, A.M. Karim, D. Mei, M. Engelhard, X. Bao, Y. Wang *Appl. Catal., B* **162** (2015) 141–148.

136 J. Llorca, N. Homs, J. Sales, J.-L.G. Fierro, P.R. de la Piscina *J. Catal.* **222** (2004) 470–480.

137 A. Casanovas, M. Roig, C. de Leitenburg, A. Trovarelli, J. Llorca *Int. J. Hydrogen Energy* **35** (2010) 7690–7698.

138 K.-S. Kim, H.-R. Seo, S.Y. Lee, J.-G. Ahn, W.Ch. Shin, Y.-K. Lee *Top Catal.* **53** (2010) 615–620.

139 M. Greluk, M. Rotko, A. Machocki *Catal. Lett.* **146** (2016) 163–173.

140 G. Słowik, M. Greluk, A. Machocki *Mater. Chem. Phys.* **173** (2016) 219–237.

141 M. Greluk, P. Rybak, G. Słowik, M. Rotko, A. Machocki *Catal. Today* **242** (2015) 50–59.

142 B. Banach, A. Machocki, *Appl. Catal., A* **505** (2015) 173–182.

143 A. Machocki, T. Ioannides, E. Papadopoulou, B. Banach *Fuel Processing Technol.* **148** (2016) 341–349.

144 J.Y.Z. Chiou, W.-Y. Wang, S.-Y. Yang, C.-L. Lai, H.-H. Huang, C.-B. Wang, *Catal Lett.* **143** (2013) 501–507.

145 S.S.-Y. Lin, D.H. Kim, S.Y. Ha *Appl. Catal., A* **355** (2009) 69–77.

146 M.V. Rama Rao, T. Shripathi *J. Electr. Spectrosc. Rel. Phen.* **87** (1997) 121–126.

147 C. Padeste, N.W. Cant, D.L. Trimm *Catal Lett.* **18** (1993) 305–316.

148 C. Padeste, N.W. Cant, D.L. Trimm *Catal Lett.* **28** (1994) 301–311.

149 F. Zhang, P. Wang, J. Koberstein, S. Khalid, S.-W. Chan *Surf. Sci.* **563** (2004) 74–82.

150 M.M. Natile, G. Boccaletti, A. Glisenti *Chem. Mater.* **17** (2005) 6272–6286.

151 L. Qiu, F. Liu, L. Zhao, Y. Ma, J. Yao *Appl. Surf. Sci.* **252** (2006) 4931–4935.

152 D.R. Mullins, S.H. Overbury, D.R. Huntley *Surf. Sci.* **409** (1998) 307–319.

153 S. Zafeiratos, F. Paloukis, G. Papakonstantinou, D. Teschner, M. Hävecker, E. Vass, P. Schnörch, A. Knop-Gericke, R. Schlögl, B. Moreno, E. Chinarro, J.R. Jurado, S.G. Neophytides *Catal. Today* **157** (2010) 250–256.

154 S. Zafeiratos, T. Dintzer, D. Teschner, R. Blume, M. Hävecker, A. Knop-Gericke, R. Schlögl *J. Catal.* **269** (2010) 309–317.

155 A. Galtayries, J. Grimblot *J. Electr. Spectrosc. Rel. Phen.* **98–99** (1999) 267–275.

156 M.C. Biesinger, B.P. Payne, A.P. Grosvenor, L.W.M. Lau, A.R. Gerson, R.St.C. Smart *Appl. Surf. Sci.* **257** (2011) 2717–2730.

157 S. Davidson, J. Sun, Y. Wang *Top Catal.* **56** (2013) 1651–1659.

158 S.D. Davidson, J. Sun, Y. Wang *Top Catal.* **269** (2015) 140–147.

159 M. Sun, L.Wang, B. Feng, Z. Zhang, G. Lu, Y. Guo *Catal. Today* **175** (2011) 100–105.

160 L. del Río, G. Marbán *Appl. Catal., B* **126** (2012) 39–46.

161 J. Llorca, N. Homs, J. Sales, P.R. de la Piscina *J. Catal.* **209** (2002) 306–317.

162 B. Banach, A. Machocki, P. Rybak, A. Denis, W. Grzegorczyk, W. Gac *Catal. Today* **176** (2011) 28–35.

163 M.S. Batista, R.K.S. Santos, E.M. Assaf, J.M. Assaf, E.A. Ticianelli *J. Power Sources* **134** (2004) 27–32.

164 D.R. Sahoo, S. Vajpai, S. Patel, K.K. Pant *Chem. Eng. J.* **125** (2007) 139–147.

165 F. Haga, T. Nakajima, H. Miya, S. Mishima *Reac Kinet Catal. Lett.* **63** (1998) 253–259.

166 A.M. da Silva, L.V. Mattos, J.P. de Breejen, J.H. Bitter, K.P. de Jong, F.B. Noronha *Catal. Today* **164** (2011) 234–239.

167 S.M. de Lima, A.M. da Silva, U.M. Graham, G. Jacobs, B.H. Davis, L.V. Mattos, F.B. Noronha *J. Catal.* **268** (2009) 268–281.

168 T. Mondal, K.K. Pant, A.K. Dalai *Int. J. Hydrogen Energy* **40** (2015) 2529–2544.

169 A.M. de Silva, L.O.O. da Costa, K.R. de Souza, L.V. Mattos, F.B. Noronha *Catal. Commun*. **11** (2010) 736–740.

170 F. Auprêtre, C. Descorme, D. Duprez *Catal. Commun.* **3** (2002) 263–267.

171 W. Xu, Z. Liu, A.C. Johnston-Peck, S.D. Senanayake, G. Zhou, D. Stacchiola, E.A. Stach, J.A. Rodriguez *ACS Catal.* **2** (2013) 975−984.

172 H. Idriss, E.G. Seebauer *J. Mol. Catal. A* **152** (2000) 201–212.

173 N. Laosiripojana, S. Assabumrungrat *Appl. Catal., B* **66** (2006) 29–39.

174 P. Rybak *Konwersja etanolu do wodoru na nośnikowych katalizatorach kobaltowych (Ethanol conversion to hydrogen on supported-cobalt-catalysts).* 2013, Uniwerystet Marii Curie-Skłodowskiej, Lublin: Poland.

175 S.D. Senanayake, W.O. Gordon, S.H. Overbury, D. R. Mullins *J. Phys. Chem. C* **113** (2009) 6208–6214.

176 M.H. Youn, J.G. Seo, H. Lee, Y. Bang, J.S. Chung, I.K. Song *Appl. Catal., B* **98** (2010) 57–64.

177 K. Tanabe, T. Yamaguchi *Journal of the research institute for catalysis Hokkaido University* **11(3)** (1964) 179–184.

178 J.A. Dumont, M.C. Mugumaoderha, J. Ghijsen, S. Thiess, W. Drube, B. Walz, M. Tolkiehn, D. Novikov, F.M. F. de Groot, R. Sporken *J. Phys. Chem. C* **115** (2011) 7411–7418.

179 M.A. Martin-Luengo, P.A. Sermon, Y. Wang *J. Catal.* **135** (1992) 263–268.

180 T.A. Maia, H.M. Assaf, E.M. Assaf *Mater. Chem. Phys.* **132** (2012) 1029–1034.

181 G.R. Rao, B.G. Mishra *Bulletin of the Catalysis Society of India* **2** (2003) 122–134.

182 A. Trovarelli *J. Am. Chem. Soc.* **124** (2002) 12923–12924.

183 S.M.F. Shahed, T. Hasegawa, Y. Sainoo, Y. Watanabe, N. Isomura, A. Beniya, H. Hirata, T. Komeda *Surf. Sci.* **628** (2014) 30–35.

184 T.X.T. Sayle, S.C. Parker, C.R.A. Catlow *Surf. Sci.* **316** (1994) 329–336.

185 G. Kim *Ind. Eng. Chem. Prod. Res. Dev.* **21** (1982) 267–274.

186 P.D.L. Mercera, J.G. van Ommen, E.B.M. Doesburg, A.J. Burggraaf, J.R.H. Ross *Appl. Catal.* **71** (1991) 363–391.

187 S.M. de Lima, I.O. da Cruz, G. Jacobs, B.H. Davis, L.V. Mattos, F.B. Noronha *J. Catal.* **257** (2008) 356–368.

188 E.S. Putna, T. Bunluesin, X.L. Fan, R.J. Gorte, J.M. Vohs, R.E. Lakis, T. Egami *Catal. Today* **50** (1999) 343–352.

189 R. Di Monte, J. Kašpar *Top Catal.* **28** (2004) 47–57.

190 H. Song, U.S. Ozkan *J. Phys. Chem. A* **114** (2010) 3796–3801.

191 X. Pang, Y. Cen, R. Dai, P. Cui *Chinese Journal of Catalysis* **33** (2012) 281–289.

192 W.-I. Hsiao, Y.-S. Lin, Y.-C. Chen, C.-S. Lee *Chem. Phys. Lett.* **44** (2007) 294–299.

193 T.-L. Chen, D.R. Mullins *J. Phys. Chem. C* **115** (2011) 3385–3392.

194 D.R. Mullins, P.M. Albrecht *J. Phys. Chem. C* **117** (2013) 14692–14700.

195 B.G. Świerkosz *Zmiany aktowności katalitycznej i zmiany katalizatora w czasie reakcji katalitycznej (Changes of catalytic activity and changes of the catalyst during catalytic reaction),* in Elementy katalizy heterogenicznej, W.N.PWN, Editor. 1993: Warszawa, 159–168.

196 D.L. Trimm *Catal. Today* **49** (1999) 3–10.

197 J. Barcicki in *Podstawy katalizy heterogenicznej (Basis of heterogenous catalysis).* 1998, Wydawnictwo Uniwersytetu Marii Curie-Skłodowskiej: Lublin, 179–182.

198 G.A. Fuentes and R.E. Salinas *Realistic particle size distributions during sintering by Ostwald ripening*, in J.J.Spivey, G.W. Roberts, and B.H. Davis, eds. *"Catalysts Deactivation 2001"*, Studies in Surface Science and Catalysis, v.139, 503–510, Elsevier, Amsterdam 2001.

199 F. Frusteri, S. Freni, V. Chiodo, S. Donato, G. Bonura, S. Cavallaro *Int. J. Hydrogen Energy* **31** (2006) 2193–2199.

200 H. Wang, Y. Liu, L. Wang, Y.N. Qin *Chem. Eng. J.* **145** (2008) 25–31.

201 D.L. Trimm *Catal. Today* **37** (1997) 233–238.

202 J. Rostrup-Nielsen, D.L. Trimm *J. Catal*. **48** (1977) 155–165.

203 J. Vicente, C. Montero, J. Ereña, M.J. Azkoiti, J. Bilbao, A.G. Gayubo *Int. J. Hydrogen Energ*. **39** (2014) 12586–12596.

204 M. Carlsson *Johnson Matthey Technol. Rev.* **59** (2015) 313–318.

205 R.C. Weast, M.J. Astle (Eds), CRC Handbook of Chemistry and Physics 63 rd, CRC Press, Boca Raton, FL, 182 p. D-51

part II

EXPERIMENTAL PART

CHAPTER

2

Effect of the surface state on the catalytic performance of Co/CeO_2 ethanol steam reforming catalyst

OUTLINE

Abstract

This chapter has been published in *J. Catal* **340** (2016) 321–330**: *Effect of the surface state on the catalytic performance of Co/CeO_2 ethanol steam reforming catalyst***

This work examines the impact of the Co/CeO_2 catalysts' surface oxidation state and composition on the ethanol steam reforming (ESR) reaction performance. To this purpose, in situ and ex-situ X-ray Photoelectron Spectroscopy (XPS) combined with on-line mass spectrometry were applied at a wide pressure range (0.2 mbar to 20 mbar). When the reaction was performed at 0.2 mbar metallic cobalt and partly reduced cerium oxide was found regardless the catalysts pre-treatment conditions.

This surface state favors CO and H_2 production, indicating that C–C bonds cleavage is the most important pathway in this pressure regime. A higher reduction degree of ceria gave rise to a higher population of adsorbed hydroxyl groups, which counterintuitive to the expected behavior, suppressed the activity and the C–C bond cleavage yield A higher reduction degree of ceria gave rise to a higher population of adsorbed hydroxyl groups, which counterintuitive to the expected behavior, suppressed the activity and the C–C bond cleavage yield. Under higher pressure (4–20 mbar) gradual oxidation of cobalt and ceria was noted. The presence of ionic cobalt species appears to enhance CO_2 and acetaldehyde yields. On the basis of the present results and available literature a plausible, pressure-dependent, reaction mechanism is proposed.

Introduction

Increasing demand for energy and concerns about the environmental impact of fossil fuels, call for alternative energy sources and efficient energy carriers. Hydrogen is an ideal energy carrier and, when is produced from sustainable energy sources, has a relatively low environmental impact. Among the possible ways of hydrogen production (i.e. reforming of hydrocarbons, electrolysis, photolytic and biological conversion), the ethanol steam reforming (ESR) seems to be very attractive [1–7]. Cobalt-based catalysts have become one of the most promising ESR catalysts because they have comparable activity with noble metals for C–C bond cleavage in the medium temperatures range, but considerably lower price. Primary disadvantages of cobalt catalysts, such as sintering or deactivation owing to the coke formation, can be limited by selection of a suitable support. From the 70's cerium oxide has emerged as one of the most prominent oxides in catalysis [8] due to its high oxygen storage capacity and its ability to form non-stoichiometric sub-oxides CeO_{2-x} ($0<x<0.5$). It was found that defects in the oxygen lattice of cerium oxide promote CO oxidation [9] and may be activate water in water-gas shift reaction [10, 11].

The effect of ceria particles size on Co/CeO_2 catalysts have been thoroughly investigated by several groups [1, 4, 12–21]. A. Machocki et al. [12] examined the influence of the support morphology on the catalytic performance and showed that the size of the support particles has an effect on the dispersion of cobalt active phase and hence, on the catalytic activity and selectivity. The catalyst supported on nano-ceria

exhibited 100% ethanol conversion and water conversion close to the stoichiometric (13%). The effect of the support particle size of Co/CeO_2 catalysts in the ESR was also the subject of I.I. Soykal et al. [4] research. After hydrogen pre-treatment X-ray Absorption Spectroscopy (XAS) studies showed the presence of almost completely reduced cobalt for the catalyst supported on nano-dispersed ceria and around 88% metallic phase for the catalyst on micro-dispersed ceria. The authors stated that the degree of cobalt reduction is related to the cobalt particles size. In all the above studies high selectivity towards H_2 and CO_2 and low amounts of CO, CH_4, C_2H_4, CH_3CHO were noted. At temperatures below 500ºC, severe deactivation of cobalt-based catalyst was observed, leading H. Wang and co-workers [19] to study the nature of carbon deposit formed during the ESR process. Upon the ESR at 450ºC cobalt particles were encapsulated by coke. The deactivation of the catalyst due to coke formation and catalyst encapsulation was assigned to reactions of dehydrogenation and/or dehydratation of ethanol. Some authors [22] suggested that the presence of –OH groups on the surface of Co/CeO_2 facilitate coke-removal.

The nature of the active cobalt phase during the ESR reaction was the focus of studies dealing with unsupported [23–25] and supported [5, 7, 26, 27] cobalt catalysts. The Co_3O_4 spinel phase was not active for the ESR at least in the temperature range of 250–350ºC [24]. J. Llorca et al. [23] studied Co_3O_4 transformation during the ESR and observed progressive activation of the sample under the reaction feed. Initially, on the oxidized sample, hydrogen and acetaldehyde were the major products but after 2 h of reaction at 400ºC, activation of cobalt occurred, and almost 100% conversion of ethanol to H_2 and CO_2, was achieved. In the *operando* XRD study of V.A. de la Peña O'Shea et al. it was found that a mixture of both CoO and metallic Co phases was active and very selective in the ESR reaction [25]. However, numerous other publications assumed that the metallic cobalt is the most active form of cobalt in the ESR [27–29] even if in some cases, promotes catalyst deactivation [30]. Recently, the idea that different cobalt oxidation states might favor different reaction paths is gaining ground. Metallic cobalt is associated to ethanol decarbonylation to CO and CH_4 [30], or formation of the acetaldehyde [31, 32], while ionic Co^{2+} sites seems to be responsible for selective oxidation of ethoxide species to acetaldehyde [33]. However, B. Bayram et al. [34] showed that under the ESR CO_2 and H_2 were the major products even if both forms of cobalt Co^0 and Co^{2+} were present.

Although the crucial role of cobalt and ceria surface state during the ESR reaction is recognized, definition of the chemical state of the active catalyst remains a key challenge. Reliable information can be provided when the surface characterization of the catalyst under working ESR conditions is combined with the evaluation of the catalytic performance. In this work the Co/CeO_2 ethanol steam reforming catalyst was analysed *in-situ* by synchrotron based XPS and absorption spectroscopies combined with *on-line* mass spectrometry. On account of the pressure limits of this method, the *in-situ* results are complemented with higher-pressure XPS studies where the working catalyst is quenched by rapid exposure to vacuum conditions. These findings reveal some new insights about the role of ceria and cobalt in the ESR reaction.

1. Experimental

1.1. Catalyst preparation

The Co/CeO_2 catalyst was prepared by the impregnation method. The commercial nano-dispersed ceria support (Aldrich) was initially dried at 120ºC for 3 h and consequently impregnated with a 1/1 molar cobalt nitrate and citric acid solutions. After impregnation, the catalyst precursor was dried at 120ºC for 12 h and then calcined at 400ºC for 1 h.

1.2. Catalyst characterization

The in-situ synchrotron-based X-ray photoelectron (in situ-XPS) and absorption spectroscopies (XAS) were performed at ISISS beamline at BESSY in Berlin, in a set-up described in details elsewhere [35]. The soft X-ray absorption spectra of the Co $L_{3,2}$ and Ce $M_{4,5}$ edges were recorded in the Total Electron Yield (TEY) mode. The gas phase composition was monitored *on-line* by a differentially pumped quadrupole mass spectrometer (QMS), which was connected to the experimental cell through a leak valve. The catalyst was initially pre-treated in the XPS cell in oxygen (0.2 mbar O_2 at 250ºC) to remove all residual surface carbon. A similar procedure was repeated after each reaction cycle to "refresh" the surface and eliminate carbon deposit as confirmed by C 1s XPS spectrum. The ESR reaction was performed in several cycles at the same catalytic specimen under identical reaction conditions. Prior to any reaction cycle the sample was treated in reducing (0.2 mbar H_2 at 250ºC or EtOH at 420ºC) or

oxidative (0.2 mbar O_2 at 250ºC) environments. The aim of this pre-treatment was to induce modifications at the catalysts' surface state during the subsequent ESR reaction cycle. This is feasible since the kinetics of surface transformation under the reaction mixture are relatively slow, allowing for different surface states to maintain for periods comparable to the XPS acquisition time (e.g. 30 min). In this way under reaction conditions the predominant bulk characteristics of the catalysts remain similar while the surface state might vary considerably [36].

The water/ethanol mixture (3/1 mol/mol) with an overall pressure of 0.2 mbar was introduced after cooling down the sample to 50ºC. Consequently the sample was heated to 420ºC (by 5 C min^{-1}), and spectra were recorded after about 15 min, where QMS signal showed a stable catalytic performance. Spectra were recorded using appropriately selected photon energies, resulting in photoelectrons with two characteristic kinetic energies (180 and 465 eV) and therefore two different analysis depths (ca. 1.7 and 2.9 nm). Quantitative calculations were performed taking into account the photon-energy dependence of the atomic subshell photo-ionization cross-sections.

The ex situ laboratory-based XPS measurements were carried out in an ultrahigh vacuum (UHV) setup combined with an attached variable-pressure 0.6 l reactor (VPR). The analysis chamber of the UHV setup is equipped with a hemispherical electron analyzer and a dual X-ray source. The AlKα line at 1486.6 eV was used for the ex situ XPS measurements. The powder sample was pressed into a 13 mm pellet and mounted on a sample holder with boron nitrate heater and a temperature sensor attached to it, which can be used both in UHV and VPR chambers. The gas inlet and gas detection systems were analogous of those in the synchrotron-based XPS setup. Prior to the reaction the samples were reduced in hydrogen (10 mbar) at 420ºC during 1 h and then exposed to the reaction mixture at various pressures. Catalytic experiments in the VPR chamber were performed in 3 distinct pressure regimes, namely 4, 10 and 20 mbar. After about 30 min under ESR reaction conditions at 420ºC, the state of the reacting surface was quenched by cooling down rapidly and pumping off the gas mixture ($p<1x10^{-7}$ mbar) from the VPR chamber. Consequently the sample was rapidly transferred under UHV from the reactor to the analysis chamber for XPS characterization.

The conversion of EtOH and H_2O under the ESR conditions was calculated from the change of QMS EtOH (m/z = 31) and H_2O (m/z = 18) intensities. The product

yields were calculated by the increase of the H_2 (m/z = 2), CO (m/z = 28), CH_3COH (m/z = 29) and CO_2 (m/z = 44) QMS intensities induced by the catalytic reaction. A correction of the ion current signals due to fragmentation was also taken into account. Since QMS signals were not calibrated to the sensitivity factor of each gas, the product yields are used in a % comparative basis and therefore described as relative (products) yields. For more details about the calculation method of conversion and the product yields please refer to Supporting Information 1. The blank experiment, performed under mbar conditions for the H_2O/EtOH = 3/1 mol/mol showed low ethanol and water conversions which do not exceed 20% of those found with the catalyst loaded in the reactor. The contribution of the background conversion was taken into account during the QMS data processing.

Transmission electron microscopy images were obtained with the FEI Titan G2 60-300 kV microscope at an electron beam accelerating voltage of 300 kV. Elemental mapping was carried out in the *scanning transmission electron microscopy (*STEM) mode by collecting point by point Energy-dispersive X-ray spectra (EDS) at each pixel in the map. More details about the experimental procedure followed in this paper can be found in Supporting Information 1.

2. Results

2.1 Textural and morphological characteristics of the fresh catalyst

Table 1 shows structural characteristics of the ceria support and cobalt–ceria catalyst. The total surface area of the CeO_2 support was about 73 m^2/g and after cobalt deposition decreased slightly to 67 m^2/g. The average size of CeO_2 particles increased from 22 to 30 nm after cobalt deposition, as calculated on the basis of XRD results. The absence of cobalt-related peaks on the XRD pattern suggests highly dispersed cobalt oxide on the support. The average cobalt crystallite size (in the reduced catalyst) as calculated on the basis of hydrogen chemisorption measurement was about 14 nm.

Table 1. Support and catalyst textural characterization results.

	Pore volume (cm^3/g)	**Pore diameter (nm)**	**Total surface area (m^2/g)**	**Support crystallite size (nm)[a]**	**Co content (wt.%)**	**Cobalt surface area (m^2/g)**	**Average cobalt crystallite size (nm)[b]**
CeO_2	0.331	14.2	72.9	22	-	-	-
Co/CeO_2	0.191	8.8	66.9	30	7.9 ± 0.3	3.82	14.0

[a] On the basis of the XRD measurements.
[b] On the basis of hydrogen chemisorption measurements.

Prior to the XPS measurements the morphology of ceria support and cobalt/ceria catalyst was examined by AFM, STEM, and STEM-EDS methods. In general, cobalt deposition did not change significantly the morphology of the support (see Supporting Information 2). The average ceria crystallite size for the Co/CeO_2 calculated from TEM images (see Supporting Information 2) was 24.5 nm close to the result obtained from the XRD measurements (30 nm). The difficulty in distinguishing between ceria and cobalt oxide crystallites in the TEM images suggests that cobalt is well-dispersed on the support and does not form large aggregates. This is further supported by EDS mapping of Ce, Co and O in the STEM mode (STEM-EDS) shown in Fig. 1. From the compositional image it can be seen that the distribution of cobalt oxide on the support is almost homogenous, with rare agglomerates. Although microscopy images were obtained from catalyst calcined at 400ºC, one cannot exclude that the morphological characteristics are modified under the reaction conditions. However, it is recognized that the state of the ESR catalyst prior to the reaction has a notable impact on the catalytic behavior [15].

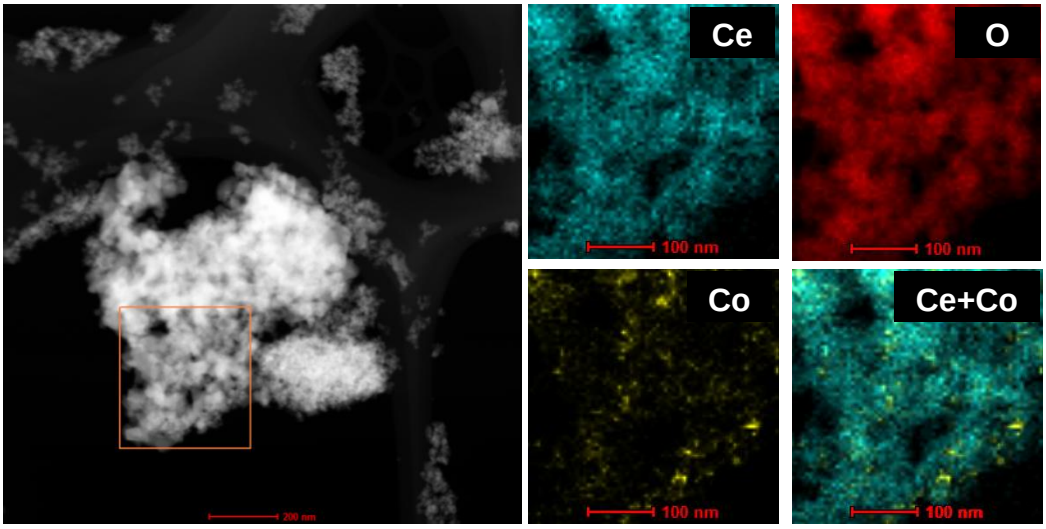

Fig. 1. STEM image with selected area mapping and STEM-EDS spectrum images showing the elemental composition of calcined Co/CeO_2 catalysts.

2.2. The Co/CeO_2 oxidation state under the ESR reaction at 0.2 mbar

Before the ESR reaction the Co/CeO_2 catalyst was conditioned in the spectrometer under oxidative (O_2) or reductive (H_2 or ethanol vapor) gas phase environments. Fig. 2a and b show the Ce 3d and Co $2p_{3/2}$ synchrotron-based XPS spectra recorded during the various pretreatment atmospheres and the following-up ESR reaction. In O_2 the Co $2p_{3/2}$ peak at 779.7 eV (bottom spectrum) is assigned to the Co_3O_4 spinel phase [37], as also confirmed by the Co L_3-edge XAS spectrum shown in Supporting Information 3 [36, 38–40], while the Ce 3d peak corresponds to CeO_2 [41–42] (Fig. 2b). In reducing pretreatment conditions (0.2 mbar H_2 or ethanol vapors at 420ºC) cobalt is fully reduced to the metallic state (Co^0) as shown by the characteristic Co 2p peak at 778.3 eV, while ceria is partially reduced to a mixture of Ce(III) and Ce(IV) (Fig. 2a and 2b). Please note that in EtOH atmosphere the background of the Co $2p_{3/2}$ spectrum is perturbated due to severe carbon deposition as will be discussed below. However the Co L-edge spectrum presented in *Supporting Information 3*, confirms the metallic state of cobalt. In addition the differences in the Ce 3d spectra suggest that ceria is more reduced in ethanol atmosphere as compared to H_2.

During the ESR reaction (H_2O/EtOH = 3/1 mol at 420ºC) the Co $2p_{3/2}$ photoemission (Fig. 2a) and Co $L_{3,2}$-edge XAS spectra (see Supporting Information 3) [40] are characteristic of metallic Co^0, independently of the prior surface state under the pretreatment atmosphere. On the other hand, in agreement with previous reports [41], the Ce 3d spectrum corresponds to partially reduced ceria composed by a mixture of Ce(III) and Ce(IV) oxides (see Table 2) [42–45]. In contrast to cobalt, the valence of ceria is influenced by the pre-treatment, as indicated by the small but notable differences in the Ce 3d spectra. It is also interesting to note that similar oxidation states of cobalt and ceria were observed even if the pre-treated catalyst was exposed in the ESR mixtures with H_2O excess (8/1 mol/mol) (data not shown), showing that the mixing ratio has limited effect on the oxidation state under these conditions.

The quantitative analysis of the XPS spectra provides information about the surface composition under the ESR conditions. In the results presented in Table 2 the Co 2p to Ce 3d atomic ratio was used in order to estimate relative modifications on the cobalt surface distribution, while spectra from different analysis depths can indicate possible surface segregation or layered structure. Please note that even if the ESR reaction mixture modifies the oxidation state compared to the pretreatment, the slow kinetics of ceria modification, induce a "*memory effect*" on the catalyst and helps to

maintain different ceria oxidation states under ESR. The percentage contribution of Ce(III) was determined after deconvolution of Ce 3d spectra into Ce(III) and Ce(IV) components. This was done for spectra recorded using two excitation photon energies and thus two information depths (EK_1 = 180 eV [information depth ~1.7 nm] and EK_2 = 465 eV [~2.9 nm]) (Supporting Information 4). As shown in Table 2 reduced ceria is systematically enhanced at the lower analysis depth, indicating that there is a gradient of Ce^{3+} species from the surface towards the interior. In addition, the pre-treatment of catalysts in pure oxygen, hydrogen or ethanol did not have a significant effect on the measured Co/Ce atomic ratio under the ESR, suggesting that the pretreatment has limited influence on the surface composition during the ESR reaction.

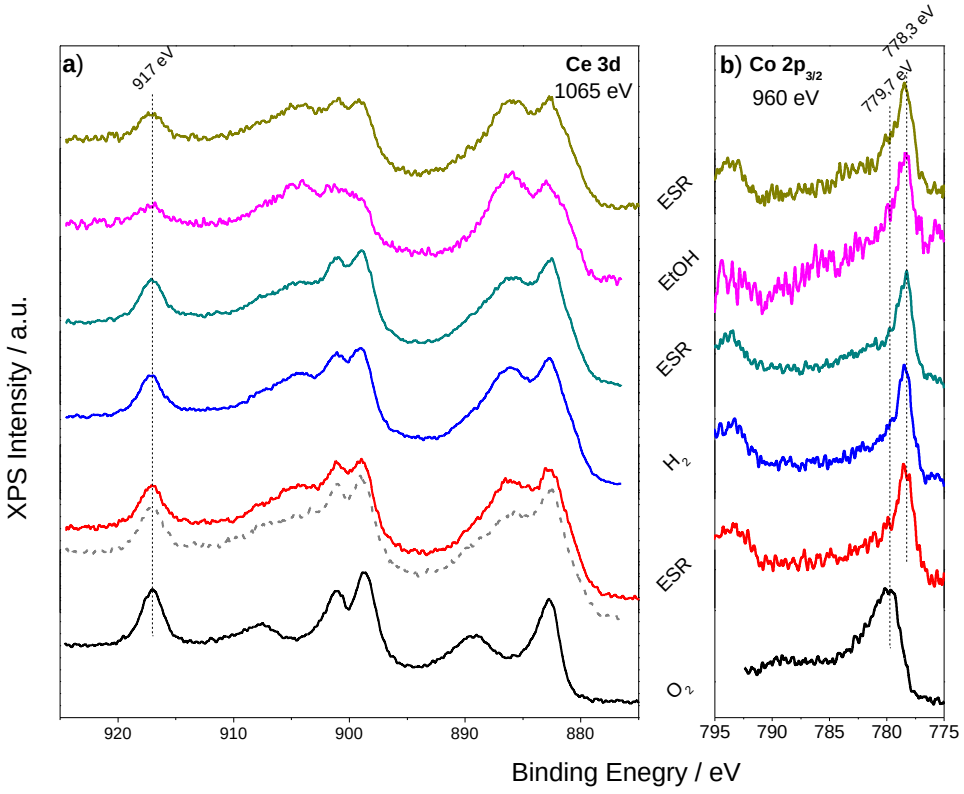

Fig. 2. *Synchrotron-based* XPS (a) Ce 3d (*hv* = 1065 eV) (b) Co $2p_{3/2}$ (*hv* = 960 eV) spectra of the Co/CeO_2 catalyst in (*from bottom to the top*): O_2 at 250ºC, subsequent ESR reaction (2 experiments with different O_2 pre-treatment duration), H_2 at 420ºC, subsequent ESR reaction, EtOH at 420ºC, subsequent ESR reaction. The ERS reaction condition were H_2O/EtOH = 3/1 mol/mol at 420ºC and the overall pressure was 0.2 mbar.

Finally, comparison of the Co/Ce peak area ratio in the two analysis depths does not show substantial differences. Accordingly one can rule out extended surface segregation phenomena and propose homogenous mixing of cobalt and ceria in the

outer 3 nm of the catalyst. Overall, our results reveal that under the ESR conditions the surface oxidation state and composition of the catalyst adapts primarily to the ESR reaction mixture and is moderately influenced by the prior oxidation state.

Table 2: The percentage of Ce (III) species as well as the Co/Ce and C/(Ce+Co) surface atomic ratios obtained by *in-situ* synchrotron XPS measurements of Co/CeO_2 catalyst during ESR. Prior to the reaction the catalyst had undergone different pre-treatments in O_2, H_2 or EtOH. Spectra were measured using selected photon energies, so as to obtain measurements at two different information depths (i.d.).

Pre-treatment	Ce(III) (%)		Co/Ce*		C/(Ce*+Co)
	i.d.** 1.7 nm	2.9 nm	1.7 nm	2.9 nm	1.7 nm
O_2 250ºC(1)	41.6	28.3	0.15	0.18	0.10
H_2 420ºC(2)	44.9	33.4	0.15	0.16	0.02
O_2 250ºC(3)	51.1	37.7	0.14	0.16	0.02
EtOH 420ºC(4)	64.1	43.5	0.17	0.18	3.36

*Ce = Ce_2O_3+CeO_2, **Estimated information depth, (1)Pre-calcined sample treated at the indicated conditions for 60 min, (2)Sample treated at the indicated conditions for 30 min, (3)Pre-reduced sample treated at the indicated conditions for 10 min, (4)Sample treated at the indicated conditions for 10 min.

The O 1s and C 1s core level spectra recorded during ESR reaction on samples which were subjected to different pre-treatments are shown in Fig. 3. Analysis of the O 1s peak indicate three O 1s components at 530.0, 531.2 and 533.0 ± 0.1 eV due to ceria lattice oxygen (O_{lat}), adsorbed hydroxyl [7, 46–48] and water [46–48] species respectively (the addition of both hydroxyl and water species is abbreviated as OH_{ads}). Please note that the O 1s components at 533 eV has been also assigned to surface lattice defects [49, 50], however this is less likely here since the relative intensity of 533 eV component is not increasing for more reduced samples. The C 1s region (Fig. 3b) recorded under ESR conditions shows a broad peak at 289.5 eV due to the Ce 4s core level and a peak at 284.8 ± 0.2 eV typically assigned to graphite and/or C=C [51, 52] and $–CH_x$ species [53]. Oxygenated carbon species (e.g. CO_3^{2-}[54]) are not observed and therefore their contribution to the O 1s spectra should be excluded.

The relative amount of O_{lat} and OH_{ads} species can be estimated from the O 1s peak analysis and combined with the ceria oxidation state (Ce(III)) as shown in Fig. 3c. As expected, the O_{lat}/Ce ratio decreases when ceria is reduced, while the OH_{ads}/Ce ratio increases, with the only exception of the state in which severe carbon deposition occurred (Ce(III) ca. 62%). The increase of relative amount of OH_{ads} species with parallel reduction of ceria suggests the partial replacement of ceria lattice oxygen by OH_{ads} species formed due to water and/or ethanol dissociation. In addition, the drastic reduction of OH_{ads} upon severe carbon deposition indicates that adsorbed carbon and OH_{ads} species compete for the same adsorption sites on ceria surface. Please note that

the O_{lat}/Ce stoichiometry shown in y-axis of Fig. 3c is systematically higher than that expected from the Ce(III) value. This might be an effect of systematic errors in the O_{lat}/Ce calculations arising from uncertainties at the sensitivity factors and the O 1s deconvolution procedure. However, the trend between O_{lat}/Ce stoichiometry and Ce(III) species is consistent in both cases implying the reduction of ceria.

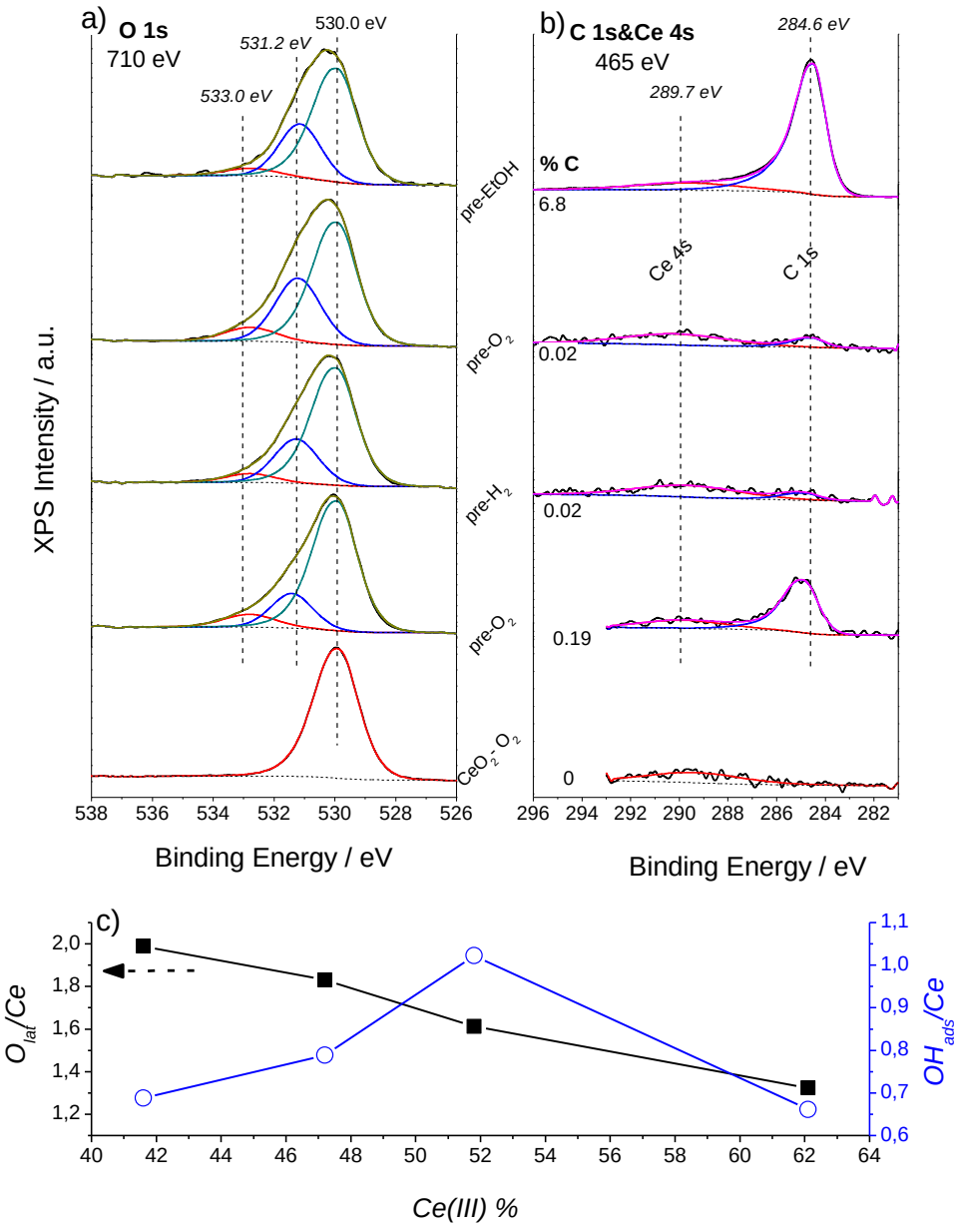

Fig. 3. *Synchrotron-based* XPS (a) O 1s (hv= 710 eV) and (b) C 1s & Ce 4s (hv= 465 eV) core level spectra during the ESR reaction (H_2O/EtOH = 3/1 mol/mol at 420ºC, p = 0.2 mbar) over Co/CeO_2 samples undergone different pretreatments. Reference spectra recorded on pure CeO_2 under oxidative atmosphere are shown at the bottom. (c) The evolution of the lattice (O_{lat}) and adsorbed (OH_{ads}) oxygen species acquired after the O 1s peak deconvolution as a function of the percentage contribution of Ce(III) species in the overall Ce 3d spectrum.

2.3. Correlation of the surface state with the catalytic conversion and the products yield

Having shown the correlation of ceria oxidation state with the population of the adsorbed oxygen species, it is interesting to investigate its effect on the activity and selectivity of the catalyst. By means of *on-line* QMS analysis, mass fragments due to reactants and potential products of the ESR reaction, were recorded. The activity of the catalyst is demonstrated by the consumption of ethanol and water, as well as by the detection of mass fragments due to various reaction products (Supporting Information 5). Taking into consideration the blank experiment and after fragment correction four main reaction products are detected in the gas phase, namely H_2 (m/z = 2), CO (m/z = 28), CO_2 (m/z = 44) and CH_3CHO (m/z = 29). Due to the particular conditions of the experiments other products like CH_4 (m/z = 16), acetone (m/z = 43), or ethylene (m/z = 27), etc. typically referred as ethanol steam reforming byproducts, if present, were below the detection limit of *on-line* gas phase analysis.

In Fig. 4a and 4b we present the conversion of ethanol (m/z = 31) and water (m/z = 18) recorded by *on-line* mass spectrometry as a function of Ce(III) percentage and the relative abundance of OH_{ads}, (OH/(Co+Ce)) obtained from the *synchrotron-based* XPS. Both ethanol and water conversions are enhanced on more oxidized ceria substrate (Fig. 4a), while the population of OH_{ads} groups has the reverse effect. As mentioned above (Fig. 3c) carbon deposition limits the relative abundancy of OH_{ads} species and probably replaces them with hydrocarbon species. This can explain why the liner correlation between EtOH and water conversion with OH_{ads} is perturbated in the case of severe carbon deposition (Fig. 4b). However, evidently the influence of carbon deposit on the H_2O conversion is less as compared to that of EtOH conversion.

In Fig. 4c and d the relative yield of each carbon product is presented as a function of % Ce(III) and the amount of adsorbed species. The relative yield of CO_2 is practically independent of the oxidation state of ceria and the amount of adsorbed oxygen species. However, CO and acetaldehyde show an opposite tendency. In particular, CO is enhanced as ceria becomes more oxidized and the amount of OH_{ads} species decreases, while acetaldehyde shows the reverse trend.

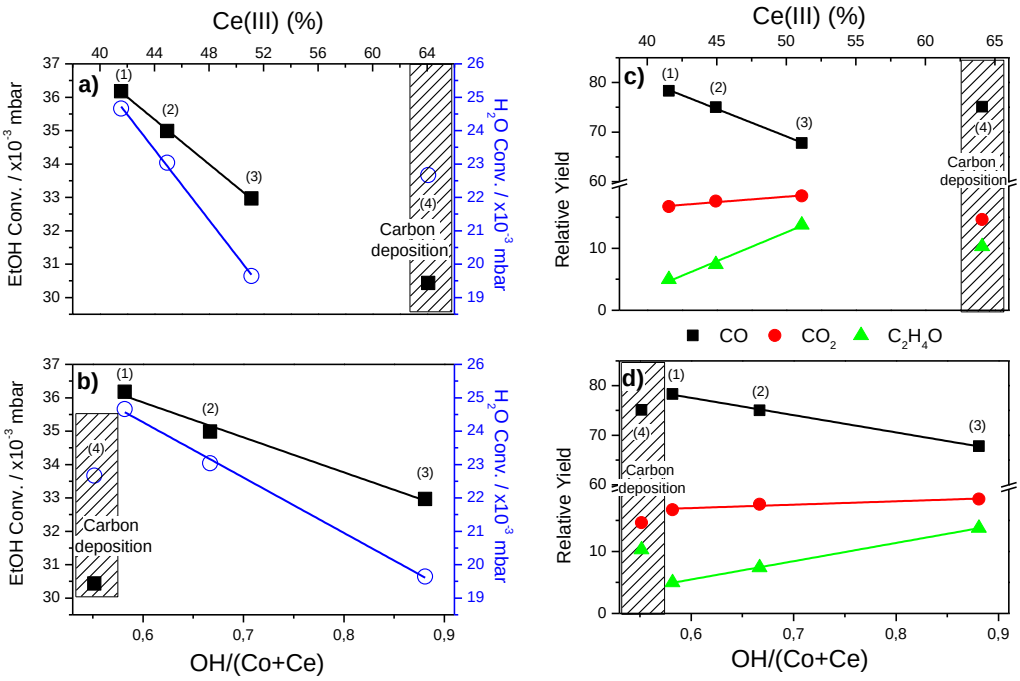

Fig. 4. (a) Correlation of the % Ce(III) fraction to the overall ceria (b) the relative amount of adsorbed hydroxyl species (OH/(Co+Ce)), with ethanol and water conversion. (c) Correlation of the % Ce(III) fraction to the overall ceria and (d) the relative amount of adsorbed hydroxyl species (OH/(Co+Ce)), with carbon products yields (the ESR reaction conditions 420ºC, 0.2 mbar H_2O/EtOH = 3/1 mol/mol). The % Ce(III) and OH/(Co+Ce) values were obtained from synchrotron-based XPS spectra with estimated information depth 1.7 nm. The dashed areas highlight ESR reaction on samples with severe carbon deposition. Each point represents reaction performed after different pretreatment of the Co/CeO_2 catalyst. The numbers in parenthesis correspond to the treatment before ESR reaction: [(1)]Pre-calcined sample treated at 250ºC in O_2 for 60 min, [(2)]Sample treated at 420ºC in H_2 for 30 min, [(3)]Pre-reduced sample treated at 250ºC in O_2 for 10 min, [(4)]Sample treated at 420ºC in EtOH for 10 min.

2.4. Effect of the reaction pressure on the oxidation state and the product selectivity

As shown above during the *in-situ* synchrotron-based XPS experiments relatively high yield to CO was observed, which was not the case when the catalyst was tested in a flow fixed-bed reactor at atmospheric pressure [2]. In addition, metallic cobalt was always the valence state observed under the employed ESR reaction conditions (even in water-rich mixture), while in the past several authors gave evidences for the presence of oxidized cobalt species. Therefore, a justified question is whether the high CO yield and metallic cobalt observed at the low pressure XPS experiments are interrelated. Accordingly the ESR reaction was performed up to two orders of magnitude higher pressure in a combined high-pressure reactor/UHV set up, which allowed the characterization of the catalyst just after reaction without exposure to air. Samples from the same batch were pre-reduced in the reactor at 420ºC in H_2 prior to the ESR reaction. Apart from the overall pressure, care was taken that the other

reaction conditions (pre-treatment, temperature, H_2O/EtOH mixing ratio and reaction time) are identical to those of the synchrotron studies. The Co $2p_{3/2}$ and Ce 3d spectra indeed indicated that the reaction pressure has a prominent effect over the surface oxidation state (see Fig. 5). Increasing the ESR reaction pressure enhances oxidation of cobalt and ceria. Although a post reaction re-oxidation of cobalt by residual water in the high pressure reactor cannot be excluded, there is a clear trend between the cobalt oxide formation and the reaction pressure, allowing linking the low pressure *synchrotron-based* XPS experiments with the real ESR conditions.

In Fig. 5e we present the product yields as a function of the reaction pressure (from 0.2 to 20 mbar) and the cobalt and ceria oxidation state. From the graph, it is clear that as the reaction pressure increases from 0.2 to 20 mbar cobalt and ceria are gradually oxidized. This has also a direct effect on the carbon product selectivity with CO gradually replaced by relatively higher CO_2 and acetaldehyde production. Please note that in the synchrotron XPS experiments of Fig. 4c, the CO yield drops with the increase of Ce(III) species, which is the reverse trend as compared to the pressure-dependent experiments of Fig. 5d. This discrepancy can be explained by the differences in the oxidation state of cobalt observed in the two cases. In particular at low pressure experiments (Fig. 4c) cobalt is metallic, while at higher pressure (Fig. 5d) cobalt is partly oxidized. Since the catalytic performance depends both on ceria and cobalt oxidation states, one can anticipate that differences in the cobalt oxidation state will have a prominent effect on the ESR products. This argument can qualitatively explain the differences in the various pressure regimes and confirm that the catalytic performance is a complex interplay between ceria and cobalt oxidation states.

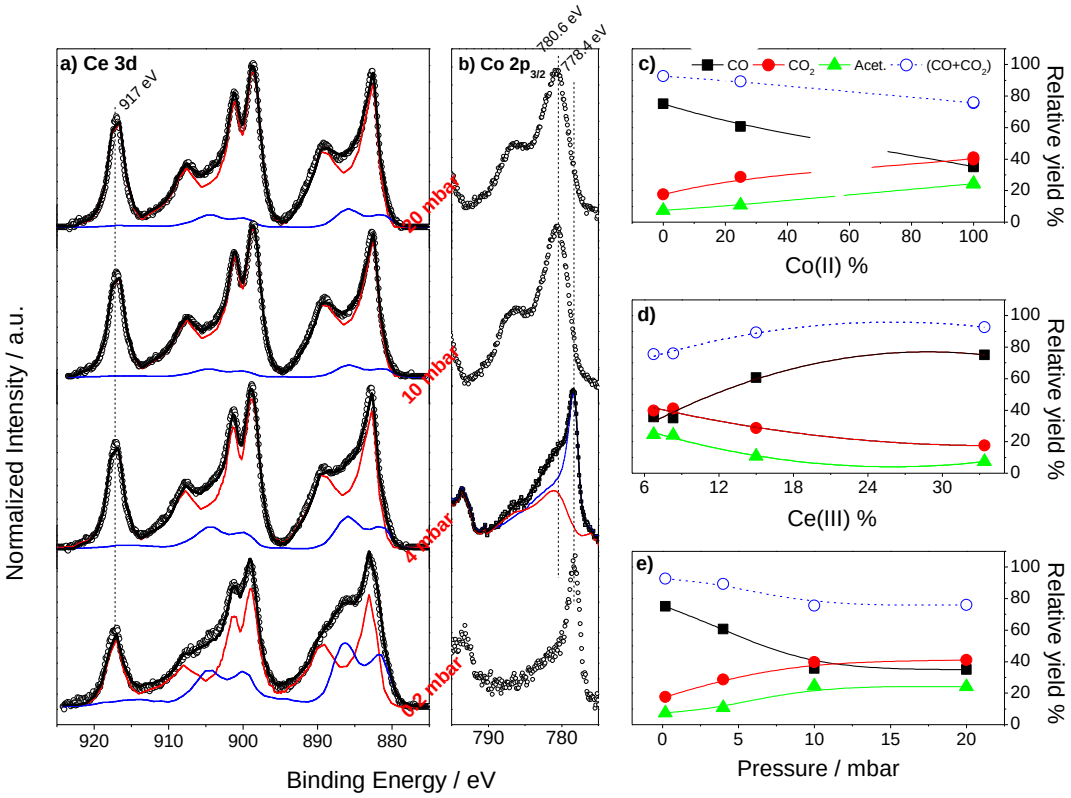

Fig. 5. (a) Ce 3d and (b) Co $2p_{3/2}$ XPS spectra recorded over Co/CeO_2 catalysts after the ESR reaction (H_2O/EtOH = 3/1 mol/mol at 420ºC) at different pressures (p = 0.2–20 mbar). The bottom XPS spectra are recorded *in-situ* at a synchrotron setup (using hv = 1350 and 1245 eV), while higher pressure results are *ex-situ* from a high-pressure reactor attached to UHV set up using an AlKα source. The product yields are obtained by the QMS analysis as a function of (c) Co(II) (d) Ce(III) and (e) reaction pressure. Please note that the Ce(III) and Co(II) % at 0.2 mbar (synchrotron-XPS) was calculated from spectra recorded using 1350 and 1245 eV excitation photon energy.

It is very difficult to determine the effect of overall pressure on the product selectivity, since the Co/CeO_2 adapts fast its oxidation state to the ESR mixture pressure. Nevertheless, Fig. 5 shows that there is a net monotonic correlation between the oxidation states of ceria and cobalt and various products, which is a very important fact for the ESR reaction.

3. Discussion

3.1. Effect of the surface state to the conversion of ethanol and water

The results of Fig. 3c evoke that reduction of ceria during the ESR reaction is accompanied by the replacement of lattice oxygen from adsorbed oxygen species (mainly OH groups), in accordance with previous reports [51]. Since the oxidation state and the relative amount of cobalt are stable, the drop of EtOH and H_2O conversion can be correlated with the decrease of the oxidation state of ceria which induces a collateral

increase of adsorbed oxygen species (Fig. 4). Therefore, contrary to the common conception, adsorbed OH groups are not promoting, but rather inhibiting, the ESR reaction under low pressure conditions. This inhibitory effect should be explained by the occupancy of adsorption sites by strongly bonded, stable OH species, which are unable to participate in ethanol transformations. On the other hand, the abundance of ceria lattice oxygen species (ca. 530 eV in O 1s spectrum) is evidently promoting the catalytic conversion. It can be also seen in Fig. 4b that carbon deposition drastically reduces the amount of OH_{ads} species suppressing primarily ethanol conversion, and to a less extent, water conversion. This observation indicates that the mechanism of water and ethanol activation involves, to some extent, different surface sites.

3.2. *Effect of the surface state to the ESR reaction products yield*

The correlation between experiments at the various pressure regimes may be used to propose the pressure-dependent reaction scheme shown in Fig. 6. Literature does not provide a direct answer on the nature of active species under the ESR [33, 55] however, it is often assumed that metallic cobalt is the active site [25–27, 29, 31, 56]. Therefore, the adsorption of ethanol (as ethoxy species) on metallic particles [30, 57] is considered as the initial step of EtOH transformation (1) [31, 58]. Ethanol, similar to other alcohols also dissociatively adsorbs on ceria [7, 59, 60, 61], however, studies of I.I. Soykal et al. [4, 62] and H. Song et al. [16] have shown that bare ceria exhibits rather poor activity in C–C bonds cleavage in temperature range of 400–450ºC. Studies of A.M. da Silva suggest that an EtOH conversion of ~50% can be achieved at 500ºC with H_2O/EtOH = 3/1 mol/mol [61, 63]. Therefore, metallic cobalt particles were considered as the most significant EtOH adsorption sites in the proposed mechanism. As for H_2O activation, it is expected that it occurs mainly on cobalt particles and either forms a oxidized cobalt layer or transfer to the support and reduce ceria to Ce(III). Recent DFT studies [64] suggest that water dissociation is strongly promoted on Co nanoparticles, meaning that water can be easily converted into atomic O releasing H_2. Furthermore, ceria lattice oxygen can spillover to cobalt [33]. If this oxygen layer is very thin and do not induce modifications at the Co 2p spectrum, it will be difficulty detectable by XPS, but it will still influence the catalyst selectivity [65]. Since there is no evidence of cobalt oxidation at 0.2 mbar and cobalt dispersion is high, it can be assumed that in that case most of –OH species are located on the support surface.

The adsorbed ethoxy species can undergo scission of the Cα–H bond (2) and desorbs as CH_3CHO (3) [30, 66, 67] or undergo C–C bond scission [66] which will lead to CO and/or CO_2 [30] (please recall that CH_4 production was negligible here) with parallel H_2 production. Results in Fig. 5 indicate interdependence between CO + CO_2 and CH_3CHO yields suggesting that these products are formed by two antagonistic reaction paths. As mentioned before, ceria itself can also participate in EtOH and H_2O transformations [4, 61–63, 68] and influence the reaction pathways. Some authors highlight ceria importance, whereas the role of metal particles is rather diminished [21, 61, 63, 69], even though unsupported cobalt was found to be very selective in the ESR [25, 70]. We suggest that the main role of ceria at low pressure is to provide mobile oxygen to cobalt–ceria interface [33]. High reduction degree of ceria may led to formation of C_2H_4 which is well known coke precursor [51, 71]. This can be supported by the decrease of CO_2 formation and increase of the mass signal 28 which can be ascribed to CO and C_2H_4.

At low pressure experiments (0.2 mbar) CO is the major product; therefore the cleavage of C–C bonds is proposed as the most favourable pathway (4–10), what is in agreement with the studies of H.P. Hyman and E. Martono [30]. The negligible amounts of CH_4 can be explained by scission of C–H bonds leading to C deposition (8) [61, 63, 66], which is subsequently oxidized by water (9–10) [61, 63], since carbon deposition was limited over catalysts pre-treated in O_2 or H_2. Fig. 4d shows that the abundance of adsorbed oxygen species enhances the yield of CH_3CHO in the expense of CO, even if CO_2 production remained practically constant. Therefore, at 0.2 mbar, further oxidation of CO to CO_2 is suppressed, despite a considerable amount of adsorbed OH groups indicated by the XPS results. Formation of CO_2 under examined conditions can be a result of the presence of a surface layer of adsorbed oxygen containing species (e.g. in form of –OH species or atomic O). Studies of E. Martono and J. Vohs [65] suggest that even if cobalt remains predominantly metallic, some oxygen adlayer may exist and promote CO_2 formation. In agreement L. De Rio et al. [70] suggest that CoO_x phase is required in order to obtain sufficient CO_2 selectivity. At higher pressure (4–20 mbar) ESR reaction on Co/CeO_2 catalysts proceeds mainly through the formation of acetate species (CH_3COO–), as has been reported based on *in situ* DRIFT studies [17, 34, 31]. This pathway is possible due to the presence of oxidized cobalt (12–14) and weakly bonded –OH species on the support (16–18). The transformation of ethoxy species to acetate in the presence of CoO has been previously

suggested in literature [34]. The transformation of $–CH_3$ species advance through pathways (14) and/or (7–10) [61, 63]. We note that the proposed reaction steps are the main reaction pathways in each pressure without excluding a lesser participation of the other steps.

The relatively high concentration of CO among C-containing products can be rationalized taking into account the influence of the pressure on the chemisorption properties of the catalyst surface. In general two main sites responsible for reagents chemisorption can be distinguished *(i)* strong adsorption sites, such as low-coordinated centres (corners, edges, lattice defects) and *(ii)* weak sites, such as terraces on the crystallites surface. It is well known that depending on the reaction conditions, adsorbed oxygen-containing species can be spectators, inhibitors or they can facilitate some reaction pathways. Usually, as a first step of the ESR, ethanol adsorption (mainly on metal particles) and water (dissociation on metal and ceria support) are considered [66, 72, 73]. At very low pressure, chemisorption from the gas phase occurs preferentially on the strong chemisorption centres, while with the increase of the pressure also weak centres are populated and involved in the ESR reaction. Strongly chemisorbed species restrain mobility (diffusion) over the surface, therefore there is a lower possibility to react with other species. In addition, further dissociation of ethanol and water will be inhibited, due to occupancy of the absorption sites.

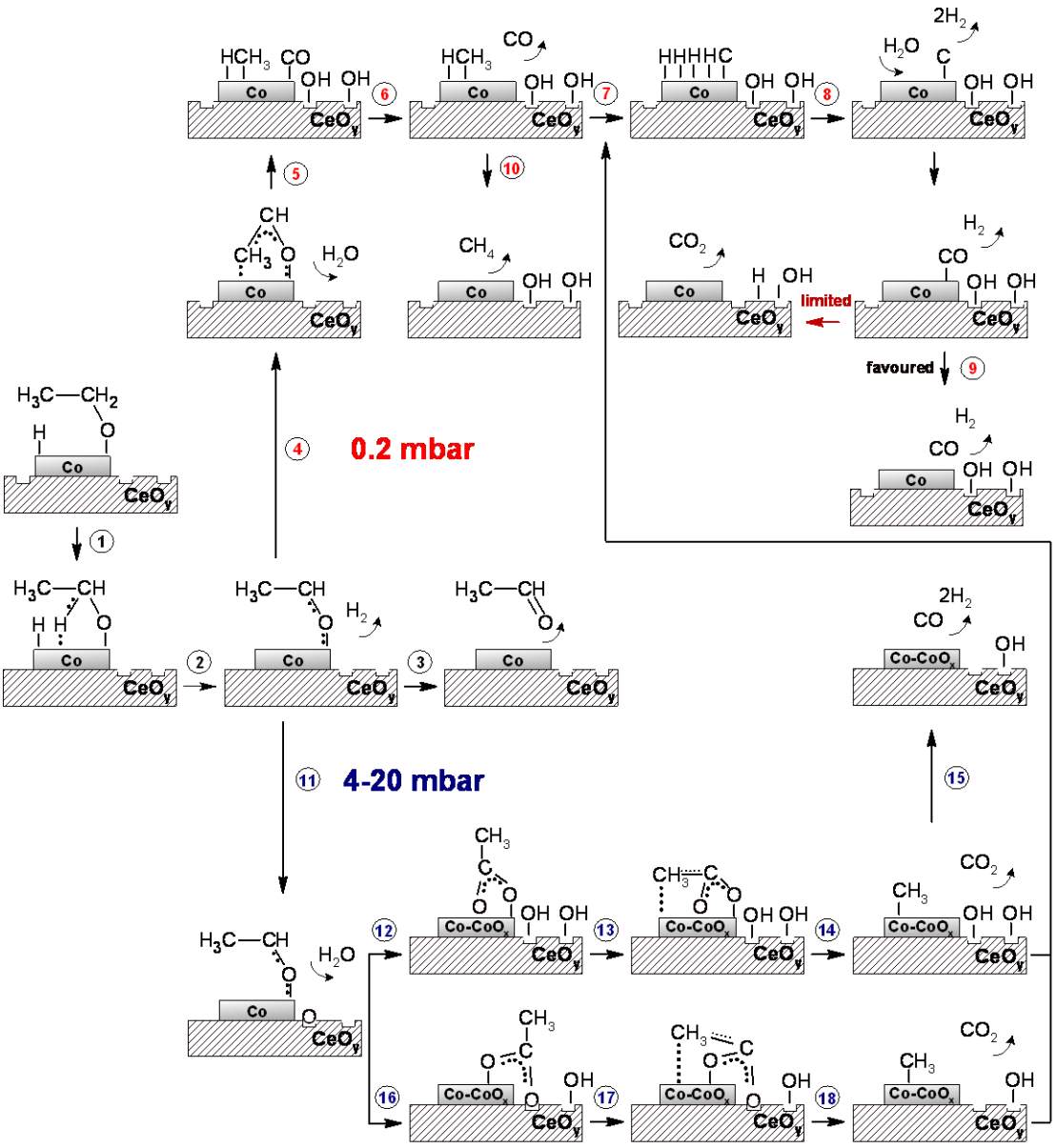

Fig. 6. Proposed reaction paths of ESR reaction over Co/CeO_2 catalyst in various pressure regimes. For clarity of the scheme, –OH species adsorbed on cobalt surface are omitted.

The *ex situ* studies performed at higher reaction pressure (4–20 mbar) show the enrichment of the surface with Co^{2+} and Ce^{4+} species, with parallel increase of the yield towards CO_2 and CH_3CHO (Fig. 5). The increase of CH_3CHO yield is not surprising since ionic Co^{2+} is known to be less active in C–C bonds cleavage than metallic Co [30, 74]. Further transformation of formed acetaldehyde may presumably proceed on cobalt–ceria interface. Studies have shown that depending on both: morphology and oxidation state, ceria may exhibit different performance toward acetaldehyde transformations. [51, 75] Acetaldehyde reacts on oxidized CeO_2 (100) producing CO_2, CO and H_2O as primary products, while on reduced CeO_2 (100) surfaces it forms

mainly H_2 and C. However, even at the elevated reaction pressure (20 mbar) substantial amount of CO was present within the products. Therefore, one cannot exclude the existence of metallic cobalt species under the ESR conditions [76], which do not withstand the sample transfer to the analysis chamber and oxidize. Higher CO_2 yield can be assigned both to the presence of Co^{2+} species [70] and to more reactive/mobile –OH groups on the support and cobalt as well.

Conclusions

A high surface area Co/CeO_2 catalyst prepared by impregnation method was investigated using combined *in-situ* and *ex-situ* XPS in seeking to understand the implications of the surface state to the ESR catalytic performance. It was found that the active surface state is formed primarily under the ESR reaction mixture and the catalytic pretreatment has a limited effect on the surface characteristics. In the presence of metallic cobalt and reduced ceria CO production is favored, while ionic cobalt species promotes CO_2 and CH_3CHO yields. A higher population of adsorbed hydroxyl groups is build up with the reduction degree of ceria however, under the examined low pressure conditions, hydroxyl groups' act more as inhibitors rather than promoters of the ESR reaction rate. Finally, at constant cobalt oxidation state, the cleavage of C–C ethanol bond is favored on more oxidized ceria supports.

Acknowledgements

S.T. acknowledges support from Campus France, PHC Polonium, Project No. 27700SJ. The research leading to these results has received funding from the European Community's Seventh Framework Programme (FP7/2007-2013) under grant agreements n.312284 and n.226716. We thank G. Słowik from University of Maria Curie-Skłodowska in Lublin for his help with the microscopic studies which were carried out at an equipment purchased thanks to the financial support of the European Regional Development Fund in the framework of the Polish Innovation Economy Operational Program (contract no. POIG.02.01.00-06-024/09 Center of Functional Nanomaterials). Finally, we acknowledge the Inorganic Chemistry department of the Fritz-Haber- Institut der MPG, in particular M. Ha□vecker and A. Knop-Gericke for the opportunity to use ISISS beamline and HZB for the allocation of synchrotron radiation beamtime.

References

1 P. Rybak, B. Tomaszewska, A. Machocki, W. Grzegorczyk, A. Denis *Catal. Today* **176** (2011) 14–20.

2 B. Banach, A. Machocki, P. Rybak, A. Denis, W. Grzegorczyk, W. Gac *Catal. Today* **176** (2011) 28–35.

3 S.S.Y. Lin, D.H. Kim, S.Y. Ha *Catal. Lett.* **122** (2008) 295–301.

4 I.I. Soykal, H.Sohn, U.S. Ozkan *ACS Catal.* **2** (2012) 2335–2348.

5 S.-W. Yu, H.-H. Huang, C.-W. Tang, C.-B. Wang, *Int. J. Hydrogen Energy* **39** (2014) 20700–20711.

6 A.R. Passos, L. Martins, S.H. Pulcinelli, C.V. Santilli, V. Briois *Catal. Today* **229** (2014) 88–94.

7 L. Óvári, S. Krick Calderon, Y. Lykhach, J. Libuda, A. Erdőhelyi, C. Papp, J. Kiss, H.-P. Steinrück *J. Catal.* **307** (2013) 132–139.

8 F. Sadi, D. Duprez, F. Gerard, A. Miloudi *J. Catal.* **213** (2003) 226–234.

9 T.X.T. Sayle, S.C. Parker, C.R.A. Catlow *Surf. Sci.* **316** (1994) 329–336.

10 W. Xu, R. Si, S.D. Senanayake, J. Llorca, H. Idriss, D. Stacchiola, J.C. Hanson, J.A. Rodriguez *J. Catal.* **291** (2012) 117–126.

11 R.J. Gorte, S. Zhao *Catal. Today* **104** (2005) 18–24.

12 A. Machocki, A. Denis, W. Grzegorczyk, W. Gac *Appl. Surf. Sci.* **256** (2010) 5551–5558.

13 H. Song, L. Zhang, U.S. Ozkan *Top. Catal.* **55** (2012) 1324–1351.

14 H. Song, L. Zhang, U.S. Ozkan *Ind. Eng. Chem. Res.* **49** (2010) 8984–8989.

15 H. Song, U.S. Ozkan *J. Mol. Catal. A* **318** (2010) 21–29.

16 H. Song, B. Mirkelamoglu, U.S. Ozkan *Appl. Catal. A* **382** (2010) 58–64.

17 H. Song, U.S. Ozkan *J. Catal.* **261** (2009) 66–74.

18 H. Song, B. Tan, U.S. Ozkan *Catal Lett.* **132** (2009) 422–429.

19 H. Wang, Y. Liu, L. Wang, Y.N. Qin *Chem. Eng. J.* **145** (2008) 25–31.

20 A.S.P. Lovón, J.J. Lovón-Quintana, G.I. Almerindo, G.P. Valença, M.I.B. Bernardi, V.D. Araújo, T.S. Rodrigues, P.A. Robles-Dutenhefner, H.V. Fajardo *J. Power Sources* **216** (2012) 281–289.

21 S.M. de Lima, A.M. Silva, U.M. Graham, G. Jacobs, B.H. Davis, L.V. Mattos, F.B. Noronha *Appl. Catal., A* **352** (2009) 95–113.

22 A.M. da Silva, K.R. de Souza, L.V. Mattos, G. Jacobs, B.H. Davis, F.B. Noronha *Catal. Today* **164** (2011) 234–239.

23 J. Llorca, P.R. de la Piscina, J.-Al. Dalmon, N. Homs *Chem. Mater.* **16** (2004) 3573–3578.

24 S. Tuti, F. Pepe *Catal Lett.* **122** (2008) 196–203.

25 V.A. de la Peña O'Shea, N. Homs, E.B. Pereira, R. Nafria, P.R. de la Piscina *Catal. Today* **126** (2007) 148–152.

26 A.M. Karim, Y. Su, M.H. Engelhard, D.L. King, Y. Wang *ACS Catal.* **1** (2011) 279–286.

27 J. Llorca, J.-A. Dalmon, P.R. de la Piscina, N. Homs *Appl. Catal., A* **243** (2003) 261–269.

28 H. Song, L. Zhang, R.B. Watson, D. Braden, U.S. Ozkan *Catal. Today* **129** (2007) 346–354.

29 M.S. Batista, R.K.S. Santos, E.M. Assaf, J.M. Assaf, E.A. Ticianelli *J. Power Sources* **124** (2003) 99–103.

30 M.P. Hyman, J.M. Vohs *Surf. Sci. Lett.* **605** (2011) 383–389.

31 Z. Ferencz, A. Erdőhelyi, K. Baán, A. Oszkó, L. Óvári, Z. Kónya, C. Pap, H.-P. Steinrüc, J. Kiss *ACS Catal.* **4** (2014) 1205–1218.

32 T. Herranz, X. Deng, A. Cabot, J. Guo, M. Salmeron *J. Phys. Chem. B* **113** (2009) 10721–10727.

33 E. Martono, J.M. Vohs *J. Catal.* **291** (2012) 79–86.

34 B. Bayram, I.I. Soykal, D. von Deak, J.T. Miller, U.S. Ozkan *J. Catal.* **284** (2011) 77–89.

35 V. Papaefthimiou, T. Dintzer, V. Dupuis, A. Tamion, F. Tournus, D. Teschner, M. Haevecker, A. Knop-Gericke, R. Schloegl, S. Zafeiratos *J. Phys. Chem. Lett.* **2** (2011) 900–904.

36 S. Zafeiratos, T. Dintzer., D. Teschner, R. Blume, M. Hävecker, A. Knop-Gericke, R. Schlögl *J. Catal.* **269** (2010) 309–317.

37 A. Tuxen, S. Carenco, M. Chintapalli, C.-H. Chuang, C. Escudero, E. Pach, P. Jiang, F. Borondics, B. Beberwyck, A. Paul Alivisatos, G. Thornton, W.-F. Pong, J. Guo, R. Perez, F Besenbacher, M. Salmeron *J. Am. Chem. Soc.* **135** (2013) 2273–2278.

38 V. Papaefthimiou, T. Dintzer, V. Dupuis, A. Tamion, F. Tournus, A. Hillion, D. Teschner, M. Hävecker, A. Knop-Gericke, R. Schlögl, S. Zafeiratos *ACS Nano* **5** (2011) 2182–2190.

39 S.C. Petitto, E.M. Marsh, G.A. Carson, M.A. Langell *J. Mol. Catal. A* **281** (2008) 49–58.

40 M.C. Biesinger, B.P. Payne, A.P. Grosvenor, L.W.M. Laum A. R. Gerson, R.St.C. Smart *Appl. Surf. Sci.* **257** (2011) 2717–2730.

41 W. Xu, Z. Liu, A.C. Johnston-Peck, S.D. Senanayake, G. Zhou, D. Stacchiola, E.A. Stach, J.A. Rodriguez *ACS Catal.* **3** (2013) 975–978.

42 V. Papaefthimiou, M. Shishkin, D.K. Niakolas, M. Athanasiou, Y.T. Law, R. Arrigo, D. Teschner, M. Hävecker, A. Knop-Gericke, R. Schlögl, T. Ziegler, S.G. Neophytides, S. Zafeiratos *Adv. Energy Mater.* **3** (2013) 762–769.

43 C. Padeste, N.W. Cant, D.L. Trimm *Catal Lett.* **24** (1994) 95–105.

44 L. Qiu, F. Liu, L. Zhao, Y. Ma, J. Yao *Appl. Surf. Sci. A* **252** (2006) 4931–4935.

45 E. Paparazzo *Surf. Sci. Lett.* **234** (1990) 253–259.

46 D.A. Creaser, P.G. Harrison *Catal Lett.* **23** (1994) 13–24.

47 B.E. Koel, G. Praline, H.-I. Lee, J.M. White, R.L. Hance *J. Electron. Spectrosc. Relat. Phenom.* **21** (1980) 31–46.

48 Y. Wu, J.T. Mayer, E. Garfunkel, T.E. Madey *Langmuir* **10** (1994) 1482–1487.

49 A. Pfau, K.D. Schierbaum *Surf. Sci.* **321** (1994) 71–80.

50 J.P. Holgado, G. Munuera, J.P. Espinós, A.R. González-Elipe *Appl. Surf. Sci.* **158** (2000) 164–171.

51 T.-L. Chen, D.R. Mullins *J. Phys. Chem. C* **115** (2011) 3385–3392.

52 M. Nagai, R. Isoe, K. Ishiguro, H. Tominaga, M. Shimizu *Chem. Eng. J.* **207** (2012) 938–942.

53 J. Światowska, V. Lair, C. Pereira-Nabais, G. Cote, P. Marcus, A. Chagnes *Appl. Surf. Sci*. **257** (2011) 9110–9119.

54 D. Rosenthal, M. Ruta, R. Schlögl, L. Kiwi-Minsker,*Carbon* **48** (2010) 1835–1843.

55 W. Luo, A. Asthagiri *Catal. Sci. Technol.* **4** (2014) 3379–3389.

56 H. Song, L. Zhang, U.S. Ozkan *Green Chem.* **9** (2007) 686–694.

57 A. Bshish, Z. Yakoob, B. Narayanan, R. Ramakrishnan, A. Ebshish *Chem Papers* **65** (2011) 251–266.

58 L.V. Mattos, G. Jacobs, B.H. Davis, F.B. Noronha *Chem. Rev.* **112** (2012) 4094–4123.

59 R. M. Ferrizz, G. S. Wong, T. Egam, J. M. Vohs *Langmuir* **17** (2001) 2464–2470.

60 A. Yee, S.J. Morrison, H. Idriss *J. Catal.* **191** (2000) 30–45.

61 A.M. da Silva, K.R. de Souza, G. Jacobs, U.M. Graham, B.H. Davis, L.V. Mattos, F.B. Noronha *Appl. Catal. B* **102** (2011) 94–109.

62 I.I. Soykal, H. Sohn, D. Singh, J.T. Miller, U.S. Ozkan *ASC Catal.* **4** (2014) 585–592.

63 S.M. de Lima, A.M. da Silva, L.O.O. da Costa, U.M. Graham, G. Jacobs, B.H. Davis, L.V. Mattos, F.B. Noronha *J. Catal* **268** (2009) 268–281.

64 J.M. Sun, D.H. Mei, A.M. Karim, A.K. Datye, Y. Wang *ChemCatChem* **5** (2013) 1299–1303.

65 E. Martono, J.M. Vohs *ASC Catal.* **1** (2011) 1414–1420.

66 E. Varga, Z. Ferencz, A. Oszkó, A. Erdöhelyi, J. Kiss *J. Mol. Catal. A* **397** (2015) 127–133.

67 S.S.-Y. Lin, D.H.K., S.Y. Ha *Appl. Catal., A* **355** (2009) 69–77.

68 N. Laosiripojana, S. Assabumrungrat *Appl. Catal., B* **66** (2006) 29–39.

69 S.M. de Lima, A.M. Silva, I.O. da Cruz, G. Jacobs, B.H. Davis, L.V. Mattos, F.B. Noronha *Catal. Today* **138** (2008) 162–168.

70 L. del Río, I. López, G. Marbán *Appl. Catal., B* **150–151** (2014) 370–379.

71 T.-L. Chen and D. R. Mullins *J. Phys. Chem. C* **115** (2011) 3385–3392.

72 R. Padilla, M. Benito, L. Rodríguez, A. Serrano, G. Muñoz, L. Daza *Int. J. Hydrogen Energy* **35** (2010) 8921–8928.

73 D. Zanchet, J.B.O. Santos, S. Damyanova, J.M.R. Gallo, J.M.C. Bueno *ASC Catal.* **5** (2015) 3841–3863.

74 E. Martono, M.P. Hyman, J.M. Vohs *Phys. Chem. Chem. Phys.* **13** (2011) 9880–9886.

75 D.R. Mullins, P.M. Albrecht *J. Phys. Chem. C* **117** (2013) 14692–14700.

76 C.N. de Ávila, C.E. Hori, A.J. de Assis *Energy* **36** (2011) 4385–4395.

Supporting Information

Supporting information 1: Experimental details

Textural and morphological characterization

X-ray powder diffraction patterns (XRD) of the support and catalyst were collected by a Zeiss HZG-4 diffractometer using Mn-filtered CuKα radiation. The measured patterns were compared with the JCPDS (Joint Committee on Powder Diffraction Standards) database for phase identification. The average size of the support and cobalt oxide crystallites was estimated from X-ray diffraction line broadening, using the Scherrer equation.

X-ray fluorescence technique (XRF) was used to determine the bulk cobalt content in the catalyst. The spectra were collected with Canberra 1510 fluorescence spectrometer equipped with a liquid N_2-cooled Si(Li) detector and the AXIL software was used for the calculation of the cobalt content.

The porosity and the total Brunauer–Emmett–Teller BET surface area of the support and catalyst were measured by the low-temperature nitrogen adsorption in the ASAP 2405N v1.0 analyzer (Micromeritics), assuming that one nitrogen molecule occupies the area of 0.162 nm^2. The pore volume and their average diameter were evaluated applying the Barrett–Joyner–Halenda (BJH) method.

The active metal surface area, dispersion and mean size of cobalt particles in *in-situ* pre-reduced (with hydrogen at 400ºC for 1 h catalyst were calculated from hydrogen chemisorption data obtained in AUTOSORB-1CMS apparatus (Quantachrome Instruments) at 40ºC. The amount of surface Co atoms was calculated from the amount of hydrogen chemisorbed, assuming that one hydrogen atom is adsorbed on the area occupied by one surface cobalt atom (the stoichiometry of chemisorption was Co/H = 1/1) and that the surface area occupied by one atom of hydrogen is equal to 0.065 nm^2. The uptake of hydrogen due to its chemisorption was determined by extrapolating the straight-line portion of the total chemisorption isotherm to zero pressure.

The morphology of the support and catalyst were investigated by means of atomic force microscopy (AFM). Measurements were carried out in ambient air in NanoScope V (Bruker) controlled by NanoScope ver 8.15 software and operated in the tapping mode. The size and shape of the particles were determined in the dark field

TEM mode and the average size was calculated according to: $d_{average} = \frac{N_i D_i}{N_i}$ where: N_i – the numbers of metal crystallites in a specific size range, D_i – the average diameter in each diameter range.

Synchrotron-based spectroscopic characterization

For the *synchrotron-based* XPS experiments the powder catalyst was pressed into pellet (0.5 mm thick and 5 mm diameter) and placed on a sample holder. The temperature was controlled by a K-type thermocouple mounted on the sample surface. The flow rate of EtOH and H_2O vapors into the reaction cell was controlled by calibrated mass flow controllers. In case where various oxidation states were superimposed in one spectrum (Ce 3d or Co 2p) a linear peak fitting analysis using reference spectra of the pure phases was performed. The percentage of the Ce(III) and Co(II) oxidation states to the overall ceria and cobalt amount was calculated using the peak areas emerged by the linear fitting procedure according to the formulas : $Ce\ III = \frac{\text{Ce III}}{\text{Ce III} + \text{Ce IV}} \cdot 100$ and $Co\ II = \frac{\text{Co II}}{\text{Co II} + \text{Co 0}} \cdot 100$.

The total conversion of ethanol X_{EtOH}, conversion of water $X_{\text{H}_2\text{O}}$ were calculated on the basis of their concentrations before and after the reaction, from the equations: $X_{EtOH} = \frac{I_{EtOH}^{in} - I_{EtOH}^{out}}{I_{EtOH}^{in}} \times 100\%$ and $X_{H_2O} = \frac{I_{H_2O}^{in} - I_{H_2O}^{out}}{I_{H_2O}^{in}} \times 100\%$, where I_{EtOH}^{in}, $I_{H_2O}^{in}$ and I_{EtOH}^{out}, $I_{H_2O}^{out}$ are ethanol and water QMS signals in the reaction mixture and in the post-reaction mixture respectively. The relative distribution of carbon containing, for brevity called as the relative (product) yields, was expressed as $Y_{CP} = \frac{I_{CP}}{I_{CP}} \times 100\%$, where Y_{CP} is a percent contribution of given carbon containing product, I_{CP} is a difference between QMS signal for a given C-product before and after reaction mixture introduction.

Ex-situ laboratory-based XPS catalyst characterization

The inlet of the variable pressure reactor is connected with a gas/vapor source unit consisting of four mass flow controllers. A LabVIEW-based software is used to control the inlet flow and the mixing ratio of the gasses/vapors. The pressure is measured by 2 capacitance manometers (pressure range $1x10^{-4}$ - $1x10^{3}$ mbar), while the outlet flow is controlled by a variable flow valve. The inlet and outlet flow of the VPR

was properly selected so as to maintain the required reactor pressure. The gas composition was measured *on-line* by a differentially pumped quadrupole mass spectrometer (Pfeiffer QMS; channeltron detector) attached to the VPR through a leak valve. The QMS signal was recorded for m/z = 31 and 45 for EtOH, 18 for H_2O, 2 for H_2, 44 for CO_2, 28 for CO and for CH_3CHO at 29 amu.

Supporting information 2

The textural characteristic and morphology of the surface of the high surface ceria support and catalysts, characterized by AFM method, are shown in Fig. S2. Silicon tip NS G30 (NT-MDT) with force constant 20 N/m was used to examine the surface of the sample. Samples were scanned with the scan rate 0.3 Hz. The images presented in this paper are plotted as high and amplitude data with a resolution of 256 × 250 pixels. Analysis of the pictures was carried out using NanoScope Analysis 1.40 software.

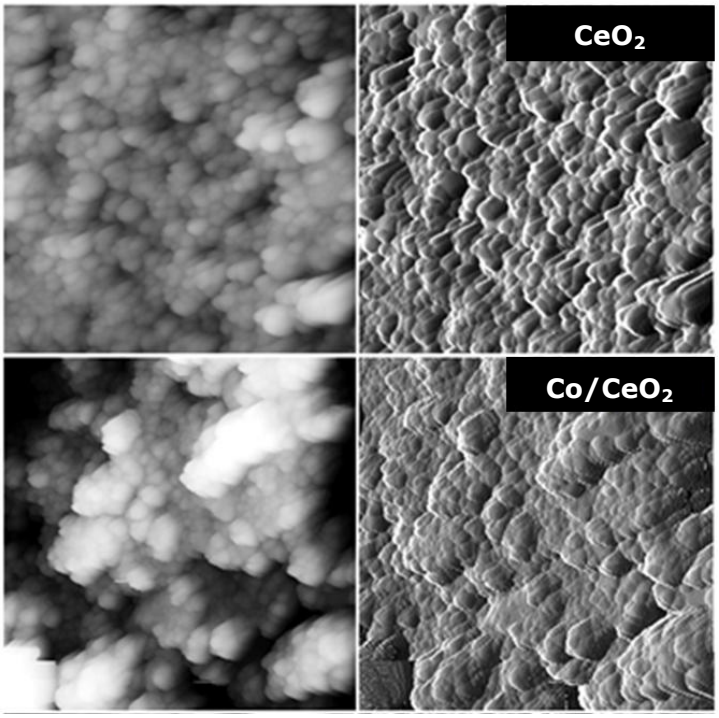

Fig S2.1. AFM images of CeO_2 (top), Co/CeO_2 catalyst (bottom) (side of the picture is 1 μm).

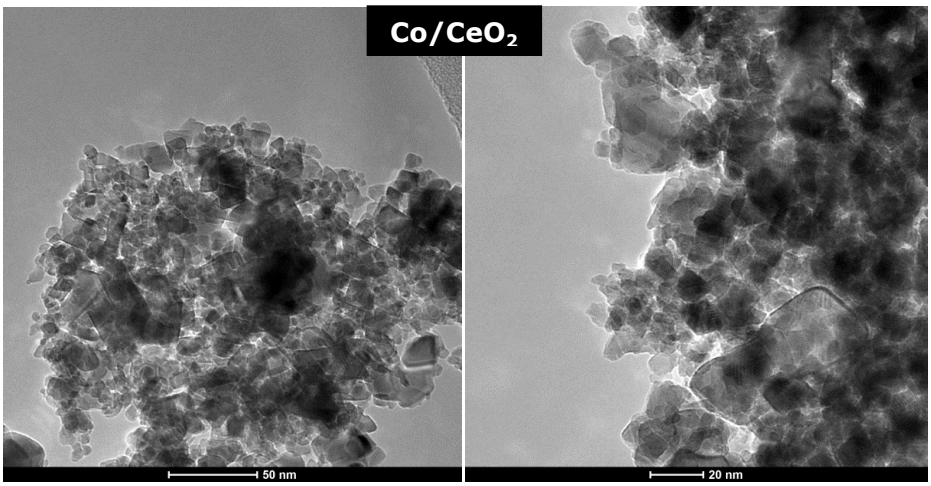

Fig. S2.2. TEM images of Co/CeO_2.

Supporting information 3

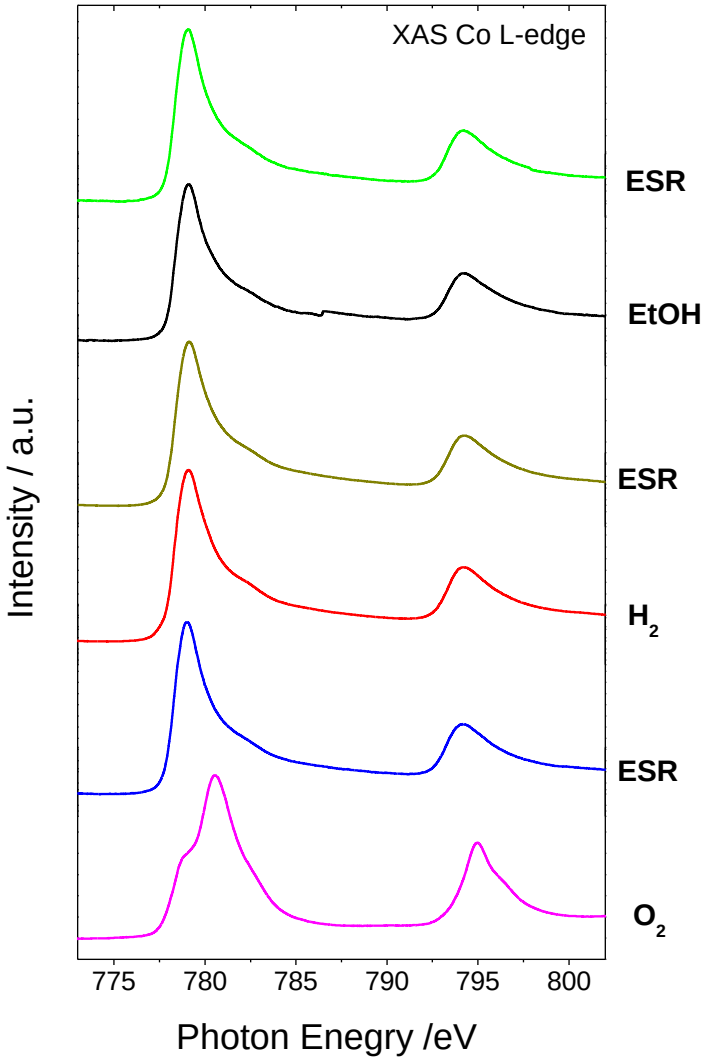

Fig. S3. Total electron yield (TEY) mode Co L-edge XAS spectra of Co/CeO_2 catalysts recorded at conditions the same conditions with the Co $2p_{3/2}$ XPS spectra presented in Fig. 2 in the main text. Namely (from bottom to the top) 0.2 mbar of O_2 at 250ºC, subsequent ESR reaction (H_2O/EtOH = 3/1 mol/mol) at 420ºC, 0.2 mbar of H_2 at 420ºC, subsequent ESR reaction, 0.2 mbar of EtOH at 420ºC, subsequent ESR reaction.

Supporting information 4

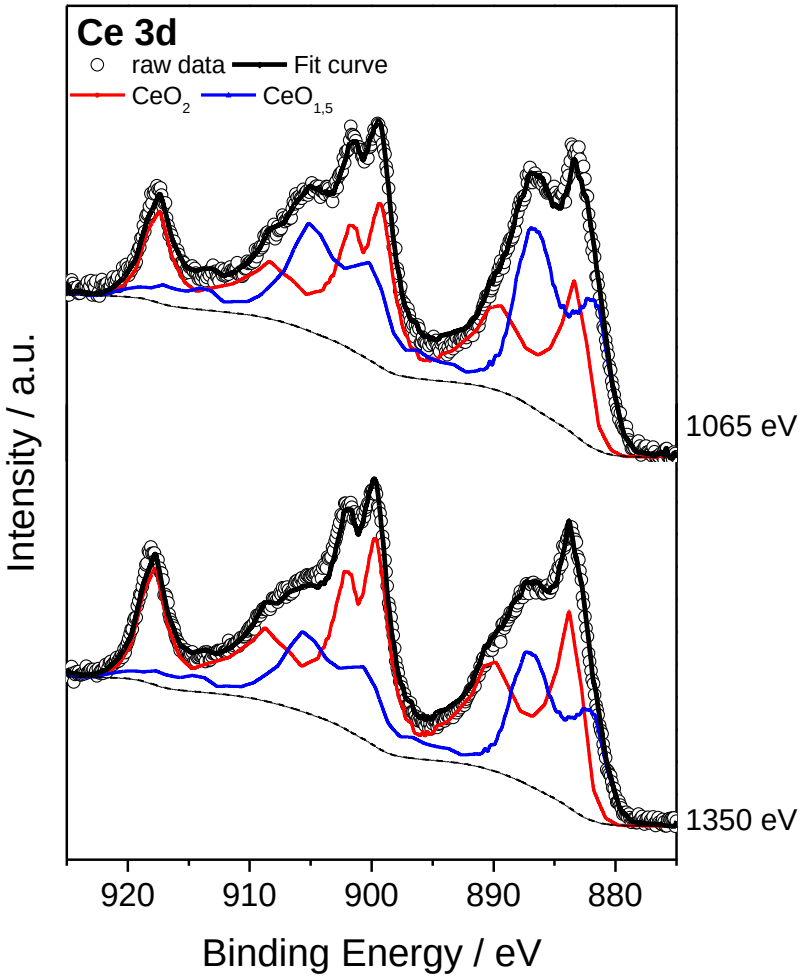

Fig. SI4 Example of Ce 3d spectra deconvolution using Ce 3d components recorded on reference samples. Spectra recorded using different photon energies are shown. Please note the relatively higher $CeO_{1.5}$ component at the spectrum recorded using 1065 photon energy.

Supporting information 5

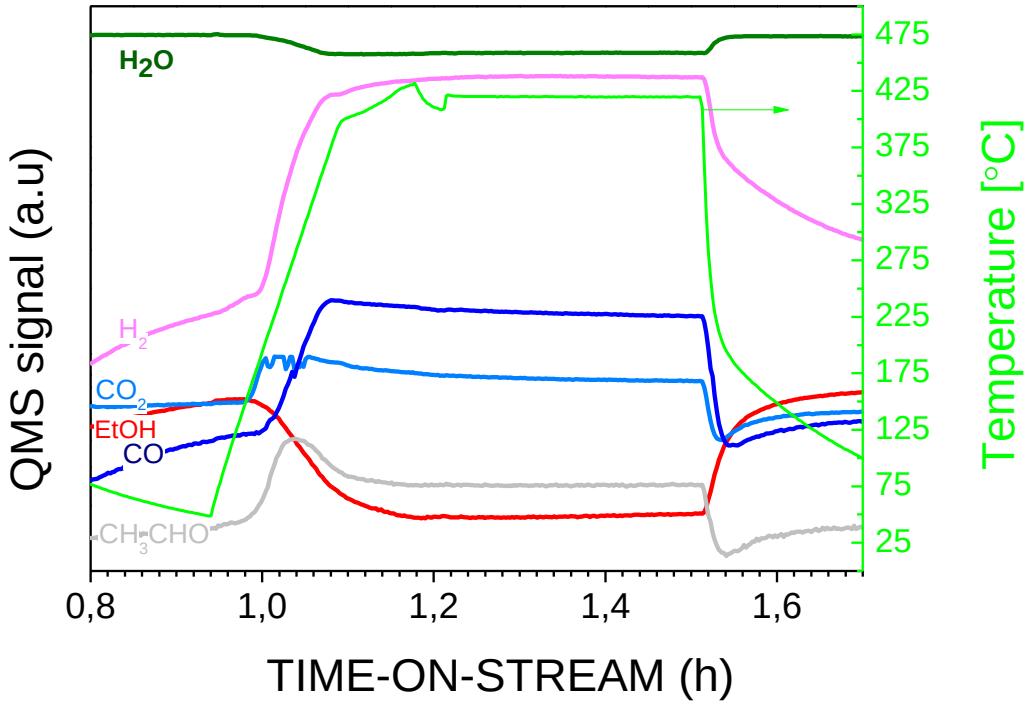

Fig. SI5. Characteristic *on-line* mass spectrometry data (after fragment correction) recorded upon heating the Co/CeO_2 catalyst in the ESR reaction mixture ($EtOH/H_2O$ = 1/3 mol/mol, 420ºC, 0.2 mbar). The green line is the sample temperature corresponding to the right y-axis.

CHAPTER

3

How reactants mixing ratio, cobalt and support particles size, and potassium promoter affect surface state and selectivity of Co/CeO_2 ethanol steam reforming catalyst

OUTLINE

Abstract

The surface state, and the catalytic performance of cobalt supported on micro- and nano-dispersed cerium oxides were investigated under the steam reforming of ethanol (ESR) at 420 °C for the H_2O/EtOH molar ratios equal to 3/1, 9/1 and 12/1. In the case of the nano-catalyst the effect of potassium promotion was also examined. The XPS results revealed two oxidation states of cobalt, Co(0) and Co(II), with more prominent the metallic form. The surface oxidation of cobalt depends on the H_2O/EtOH molar ratio. It increases with the water excess; after potassium promotion — only in very low extent. Relationship between catalyst surface chemical state and ESR effects was established. The ceria support in the unpromoted catalysts was progressively oxidized with increasing excess of water,

whereas in the case of potassium-promoted catalyst, the reverse tendency was observed. Regardless of the surface oxidation state of the catalyst, the ESR reaction selectivity is critically influenced by the surface–adsorbed oxygen–containing species (OH and $K^{\delta+}-O_{surf}{}^{\delta-}$*). These species are also required to lower the amount of deposited coke, and transform it from fully dehydrogenated C=C to* CH_x *type. The catalyst morphology, and sites where oxygen–containing species are chemisorbed may be equally important as their abundance. The high-selective ceria–supported cobalt catalyst is that with well dispersed cobalt particles deposited on the well dispersed (high surface area) support.*

Introduction

In recent years cobalt-based catalysts for the ethanol steam reforming (ESR) reaction are in the focus of numerous studies seeking understanding the catalysts' function under working conditions. The aim is to provide rational improvement strategies so as to develop a low-cost, active and sustainable ESR catalyst [1]. Among the critical issues previously reported are *(i)* the effect of the H_2O/EtOH molar ratio [2], *(ii)* the influence of the support (i.e., surface acidity, morphology, particle size, oxygen-storing and releasing capacity and oxygen mobility) [3–10], *(iii)* the nature of cobalt active sites [11–14], *(iv)* the capability of cobalt [15–17], support [18–20], and their interface to convert ethanol and water, and finally *(v)* the role of alkali metal promotion [21–23].

The oxidation state of cobalt under the ESR reaction has been a subject of several studies [4, 7, 11, 13, 14, 24, 25]. Using model Co/ZnO (0001) catalysts, E. Martono and J.M. Vohs [26] showed that metallic cobalt is active for ethoxide decarbonylation into carbon monoxide and hydrogen, while CoO provides the active sites for ethanol dehydrogenation. However, as yet there is no consistency in what is the most active and selective form of cobalt under the ESR and all combinations *(i)* a mixture of Co(0) and Co(II) [11–13, 26–28], *(ii)* metallic cobalt [16, 29] or *(iii)* Co(II) [14, 23] have been proposed in the so far published results.

The role of the support is also of major importance and to date ceria-supported catalysts are considered to be one of the most promising. This is assigned mainly due to the facility of ceria to reversible change of its oxidation state between Ce(IV) and Ce(III) [30–32] and its remarkable oxygen storage capacity [10, 33–35]. I.I. Soykal [20]

and co-workers investigated the behaviour of particles size (3.5 nm and 120 nm) on ceria reducibility and its catalytic performance under the ESR. They found that whether ceria was pre-reduced or not, it converge to the same oxidation state (mixture of Ce(IV) and Ce(III)) at given temperature and exhibited similar ESR performance; however, a highly dispersed ceria produced much more ethylene than its low-dispersed counterpart.

Whereas a great number of publication is focused on the role of cobalt and ceria oxidation state in the ESR only in a few the attempt was made to explain the role of surface adsorbed hydroxyl species or generally speaking surface adsorbed oxygen-containing species. The group of A.M. de Silva et al. [33] suggested that hydroxyls adsorbed on ceria's surface assist in coke removal from cobalt, whereas another paper [1] suggests that a high concentration of surface adsorbed oxygen-containing species may also induce oxidation of metal surface. In the second case it is obvious that adsorbed species would influence a catalyst's selectivity [36], therefore, playing an important role in the ESR. S.M de Lina et al. [37] presented a scheme of ethoxy species transformation in which dehydrogenated species (acetyl species) undergo support-induced oxidation by oxygen-containing species (OH or surface oxygen adatoms) forming acetates. Acetate species can be further oxidized by surface adsorbed oxygen-containing species to carbonates followed by decomposition to carbon dioxide.

It is generally accepted that alkali metal promoters improve the stability of catalysts. The group of J.-W. Snoeck [38] examined the effect of potassium loading on nickel-catalysts on the rate of carbon gasification and showed that the most satisfying results were obtained with 1.6–2 wt.% of K_2O content. Besides, S. Ogo et al. [23] showed that 1-2 wt.% potassium addition improved both the activity and selectivity of the Co/Al_2O_3 catalyst which stays in lines with results of other researchers [21, 39. 40]. The authors [23] deduced that beneficial properties of potassium addition are related to the reduction of Co(II) into Co(0), stabilization of acetate species, and suppression of methane formation, whereas in ref. [41] it was suggested that potassium prevents ethylene formation, which is well-known coke precursor [3, 41], consequently hindering coke formation.

The catalyst's stability is in the core of the effort to develop new advanced catalysts for the ESR. Although Co/CeO_2 catalysts are very promising candidates for the ESR they exhibit loss of the activity and selectivity in long-testing experiments

even after alkali metal promotion, which is commonly attributed to coke deposition. Apart from the use of alkali promoters, the increase of the water to ethanol molar ratio in the feed can be also used to moderate carbon accumulation with time on stream [2]. K. Vasudeva et al. [42] suggested that carbon formation on catalysts' surface occurs only at low H_2O/EtOH molar ratios (<2/1), whereas the group of V. Mas [43], that the H_2O/EtOH = 3/1 mol/mol and T>230ºC are required to avoid coke formation. Other group of researchers [44] suggested that the steam to carbon molar ratio up to 10/1 is needed to obtain the best production of hydrogen, minimize the formation of carbon monoxide and methane, and to avoid carbon deposition.

Although cobalt-based catalysts have been in the focus of many research groups, there are no works dealing with more than one or two variable factors at a time. Moreover, there were no attempts to characterize by surface sensitive methods potassium-promoted Co/CeO_2 systems under the different H_2O/EtOH molar ratios. The present work aims to show the influence of the above factors in a holistic approach focusing mainly on the surface influence. The main objectives of this study was to find *(i)* cobalt and ceria oxidation state after activation in hydrogen and under the ESR, *(ii)* the effect of ceria support and cobalt active phase particles size on catalyst's reducibility and its behaviour under the ESR, *(iii)* the effect of potassium promotion on the catalyst's surface state after reduction and the ESR, *(iv)* the influence of the H_2O/EtOH molar ratio on the surface state of the Co/CeO_2 catalysts, and *(iv)* the impact of the Co/CeO_2 catalysts' surface state on their catalytic performance under the ESR.

1. Experimental

1.1. Catalysts preparation

The Co/CeO_2 catalysts were prepared by impregnation of the commercial nano- (HS) and micro- (LS) dispersed ceria support (<25 nm and <5 μm, respectively, Aldrich). Prior to the impregnation, the supports were dried at 120ºC for 3 h. The solution of cobalt nitrate and citric acid – CA (the relative molar concentration of Co and CA was 1/1) was used for impregnation. After impregnation, the catalysts' precursor were dried at 120ºC for 12 h, then calcined at 400ºC with a heating rate of 2ºC/min up to the calcination set point and maintained for 1 h at this temperature. The catalysts were denoted as LS- and HS-Co/CeO_2. Next, the obtained HS-Co/CeO_2 catalyst's precursor was impregnated with potassium nitrate solution in order to introduce 2 wt.% of potassium promoter to the catalyst (further abbreviated as HS-K) and again it was dried at 110ºC for 12 h, then calcined at 400ºC with a heating rate of 2ºC/min up to the calcination set point and maintained for 1 h at this temperature.

1.2. Catalysts characterization

X-ray fluorescence technique (XRF) was used to determine the bulk cobalt content in the catalyst. The measurements were performed by Axios^{mAX} (PANalytical) spectrometer fitted with a Rh (4 kW) tube.

The X-ray powder diffraction patterns of the support and catalysts were recorded using an Empyrean X-ray (PANalytical) diffractometer equipped with a PIXcel^{3D} detector using Cu Kα radiation (λ = 0.154 nm). Data were acquired from 10 to 110º(2θ) with a 0.026º(2θ) step size. The measured patterns were compared with the International Centre for Diffraction Data (ICDD) PDF-4+ database for phase identification and the crystallite size was calculated using the Scherrer equation. A correction for instrumental broadening was applied using a reference standard (LaB_6).

The porosity and BET total surface area of catalysts were measured by the low temperature (-196ºC) nitrogen adsorption in the ASAP 2420 (Micromeritics) analyzer after degassing the samples at 200ºC. The average pore diameter and the volume of pores were calculated from desorption data using Barret-Joyner-Halenda (BJH) method.

The active metal surface area, dispersion and mean cobalt particles size of catalysts pre-reduced in situ in hydrogen at 420ºC (1 h), were calculated from hydrogen

chemisorption data obtained at an ASAP 2020 (Micromeritics) analyzer at 130ºC. The H/Co stoichiometry of 1/1 and the spherical particles of cobalt were used for calculation of the mean size. The detailed description of the calculation method has been given elsewhere [8].

The temperature-programmed reduction study of the catalysts was carried out in an AutoChem II 2920 (Micromeritics) apparatus using 0.05 g of the catalyst (0.15–0.3 mm) placed in a quartz flow reactor with an internal diameter 7 mm. Before reduction the catalyst were dried in the reactor for an hour in argon flow (150ºC). A 5% H_2/Ar mixture at a flow rate of 30 cm^3/min was used as a reducing gas. The temperature raised from 20 to 800ºC with a ramp rate of 10ºC/min. The water vapour formed during the reduction process was removed by a cold trap (immersed in a liquid nitrogen-isopropanol slush, at -98ºC) placed in front of the thermal conductivity detector (TCD).

The gravimetric studies of catalysts' coking in the ESR were carried out on TG121 microbalance system (CAHN), under dynamic conditions in a quartz reactor with a continuous flow of H_2O/EtOH vapours diluted with He (He 50 cm^3/min + 3 cm^3/min mixture) at 420ºC for 21 hours. The molar ratio of H_2O/EtOH was equal 3, 9 and 12. Prior to the reaction, catalysts (0.05 g of the catalyst (0.15–0.3 mm)) were reduced by passing 10% H_2/He flow (70 cm^3/min) at the temperature of 420ºC for 1 hour (the linear temperature increase to 420ºC was 10ºC/min). In all studies 96% bio-EtOH was used for the reaction mixture preparation.

1.3. Combined XPS and catalytic performance experiments

X-ray Photoelectron Spectroscopy (XPS) studies were performed in a multi-chamber UHV system (PREVAC, Poland) equipped with a monochromatized Al source (XM 650 X Ray Monochromator) source operating at 360 W and a hemispherical electron analyzer (Scienta R4000). The pass energy of the analyser was set at 200 eV (energy step 0.5 eV) for survey scan and 50 eV (energy step 0.1 eV) for high resolution Co 2p, Ce 3d, O 1s, C 1s, Ce 4s and K 2p spectra. The base pressure in the analysis chamber was $5 \cdot 10^{-8}$ mbar. Data processing was performed with the CasaXPS software (v 2.3.16 PR 1.6). After Shirley background subtraction the Co 2p and Ce 3d regions were fitted using spectra recorded over Co(0), CoO, CeO_2 and Ce_2O_3 reference samples. The ceria valence state (CeO_y) and CoO_x oxidation state were calculated using the peak areas emerged by the linear fitting procedure according to the formulas:

$y = 2 \cdot \frac{Ce(IV)}{Ce\ III\ + Ce(IV)} + 1.5 \cdot \frac{Ce(III)}{Ce\ III\ + Ce(IV)}$ and $x = \frac{Co(II)}{Co\ II\ + Co(0)}$. In the text CeO_y was also expressed as a percentage contribution of Ce(III) in the overall Ce 3d spectra, calculated as $Ce\ III\ = \frac{Ce(III)}{Ce\ III\ + Ce(IV)} \cdot 100\%$.

Catalytic tests were performed in a high pressure flow reactor connected through the radial distribution chamber with the analysis chamber. The samples were pressed into 10 mm diameter pellets and attached on a dedicated sample holder (PTS HPC RES/C-K RG). The temperature of the sample was measured with a thermocouple in contact with the sample holder and regulated by HEAT2-PS power supply. Prior to the reduction samples were heated in a load lock chamber by halogen lamp for 1.5 h to remove volatile surface adsorbed impurities. The reduction was carried out in the flow reactor at 420ºC for 1 h, by hydrogen diluted in argon (50/50 cm^3/min, p = 1 atm). The samples were cooled down to 200ºC in the flow of H_2/Ar and then the flow of hydrogen was stopped. Further cooling down (to 80ºC) was in the flow of Ar only. The water/ethanol vapours (3 cm^3/min) diluted in Ar (50 cm^3/min) were introduced to the reactor (by heated lines) at the reaction temperature (420ºC) by a Controlled Evaporation and Mixing (CEM) System (Bronkhorst). Before the reaction, samples were heated in the flow of Ar (50 cm^3/min) with the ramp rate 10ºC/min. The ESR was carried out over 1 h, next the flow of vapours was stopped and samples were quenched in the flow of Ar till 80ºC and transferred to the XPS analysis chamber.

In the course of the ESR reaction, carried out in the high pressure cell, the composition of gas phase products (H_2, CO_2, CO, CH_4) was monitored *on-line* by means of a micro-GC (Agilent, 490-GC).

1.4. Catalytic tests in a fixed-bed reactor

In order to gain a better insight into catalytic properties (activity as well as selectivity towards gas and liquid products) of the examined catalysts, the ESR reaction (H_2O/EtOH molar rations 3/1, 9/1 and 12/1) was carried out also in a fixed-bed continuous-flow quartz reactor (Microactivity Reference unit, PID Eng & Tech.) under atmospheric pressure. The pre-treatment and reaction conditions were kept identical to those described above for reactor attached to the UHV setup. The analysis of the reaction mixture and the reaction products (all in the gas phase) were carried out *on-line* by means of two gas chromatographs. One of them, Bruker 450-GC was equipped with

two columns, the first filled with a porous polymer Porapak Q (for all organics, CO_2 and H_2O vapour) and the other one – capillary column CP-Molsieve 5Å (for CH_4 and CO analysis). Helium was used as a carrier gas and a TCD detector was employed. The hydrogen concentration was analyzed by the second gas chromatograph, Bruker 430-GC, using a Molsieve 5Å, argon as a carrier gas and a TCD detector.

The total conversion of ethanol X_{EtOH}, water X_{H_2O} and conversions of ethanol into individual carbon-containing products (X_{CP}) were calculated from their concentrations before and after the reaction, taking into account changes in the gas volume during the reaction, from the equations:

$$X_{EtOH} = \frac{C_{EtOH}^{in} - C_{EtOH}^{out} \cdot K}{C_{EtOH}^{in}} \cdot 100\% ,$$

$$X_{H_2O} = \frac{C_{H_2O}^{in} - C_{H_2O}^{out} \cdot K}{C_{H_2O}^{in}} \cdot 100\% ,$$

$$X_{CP} = \frac{C_{CP}^{out} \cdot K}{n/2 \cdot C_{EtOH}^{in}} \cdot 100\% ,$$

where:

C_{EtOH}^{in} and $C_{H_2O}^{in}$ – is the molar concentration of EtOH and H_2O in the reaction mixture (mol%); C_{EtOH}^{out} and $C_{H_2O}^{out}$ – is the molar concentration of EtOH and H_2O in the post-reaction mixture (mol%); C_{CP}^{out} – is the molar concentration of carbon-containing products in the post-reaction mixture (mol%); n - is number of carbon atoms in carbon-containing molecule of the reaction product; K – is the volume contraction factor (K = C_C^{in}/C_C^{out} where C_C^{in} and C_C^{out} are the molar concentrations of carbon in the ethanol feed to the reaction and in all carbon-containing compounds which were present in post reaction gases, respectively). The selectivity of ethanol conversion into individual carbon-containing products was expressed as $(X_{CP}/X_{EtOH}) \cdot 100\%$.

The selectivity of hydrogen formation was determined as:

$$H_2\ \text{selectivit}\ y = \frac{C_{H_2}^{out}}{C_{H_2}^{out} + 2 \cdot C_{CH_4}^{out} + 2 \cdot C_{CH_3CHO}^{out}} \cdot 100\%$$

where:

C^{out} - is the molar concentration of the hydrogen-containing products in the post-reaction mixture (mol%). Hydrogen, methane and acetaldehyde were the only hydrogen-containing products of the ESR.

1.5. Post-reaction TEM catalysts' characterization

The spent catalysts (after 1 h of the ESR) were grinded to a fine powder in an agate mortar and then mixed with 99.8% ethanol into the ultrasonic homogenizer for 20 s. The slurry containing the catalyst was pipetted on a 200 mesh copper grid covered with lacey formvar and stabilized with carbon (Ted Pella Company) and left on a filter paper to evaporate ethanol. Subsequently, the sample deposited on the grid was inserted to the sample holder and transferred to the electron microscope. The images were recorded in a transmission electron microscope (Tecnai G^2 20 X-TWIN FEI Company), equipped with LaB_6 emitter and using 200 kV electron beam accelerating voltage.

2. Results

2.1. Reduction of the catalysts in hydrogen

As shown in Table 1 the BET surface area of HS- and LS-catalysts differs by about one order of magnitude, while after addition of potassium the surface area of HS decreases considerably. In addition, although the cobalt wt.% content is comparable in all catalysts (8–9 wt.%), the cobalt surface area is significantly higher for the HS-catalyst (47.2 m^2/g) in accordance to the much lower cobalt particle size (3.8 nm). The potassium promotion increases average cobalt particle size (13.9 nm) and lowers cobalt surface area (4.1 m^2/g) as compared to the unpromoted HS-catalyst, making it comparable to this obtained for the LS-catalyst (1.5 m^2/g). However, one should note that cobalt crystallites in the LS-catalyst were much bigger (39.3 nm) as compared to other catalysts.

Table 1. Results of the Co/CeO_2 catalysts characterization.

Catalyst	BET surface area[a]	Volumes of pores[a]	Pore diameter[a]	Cobalt content[b]	Average crystallite size[c]		Average cobalt crystallite size[d]	Cobalt dispersion[d]	Cobalt surface area[d]
	m^2/g	cm^2/g	nm	wt.%	nm		nm	%	$m^2/g_{cat.}$
					Co_3O_4	CeO_2			
LS-Co/CeO_2	5.3	0.03	28.2	9.00±0.27	23.3	87.1	39.3	2.5	1.5
HS-Co/CeO_2	47.2	0.15	11	9.55±0.38	8.4	25.6	3.8	26.6	17.1
HS-KCo/CeO_2	29.6	0.12	12.4	8.44±0.34	9.3	26.5	13.9	7.2	4.1

[a] Determined by the low-temperature N_2 adsorption.
[b] Determined by XRF.
[c] Determined by XRD.
[d] Determined by the hydrogen chemisorption measurements.

The temperature programmed reduction (TPR) profiles are shown in Fig. 1. The unsupported Co_3O_4 reduction occurs in two main temperature regions: the first peak up to 320ºC and the other one with the maximum rate of the reduction at 380ºC. The reduction of Co_3O_4 is typically referred as a two-step reduction according to following scheme: $Co_3O_4 \rightarrow CoO \rightarrow Co(0)$ [7, 9, 11, 13, 45–47]. Similar TPR profile is observed for the LS-catalyst (Fig. 1) however, the peak maximum was found at 350ºC. In the TPR profiles of the HS-catalyst several peaks, which are expanding to a much larger temperature region, were resolved. The addition of potassium improves the HS-catalyst' reducibility, as reflected by the shift of the high temperature peak to lower temperatures. Based on the TPR results complete reduction of cobalt in the HS-K catalyst is expected to take place around 500ºC.

Some authors [48, 49] suggested that the addition of alkali metals may weaken the strength of the cobalt–oxygen bond and promote reduction. This effect would be observed as a shift of TPR profile towards lower temperatures. The bare ceria TPR profile indicates that the support's reduction occurs around 400ºC and above 700ºC. However, the TPR experiments do not allow distinguishing between reduction of cobalt oxides and ceria in the catalysts below the former temperature.

The reducibility of cobalt oxides is strongly related to the cobalt crystallite size, as well as to the presence of additives. It is expected that large cobalt oxide particles are easier to reduce than the smaller ones [46]. Therefore, the reduction of the HS-catalyst at higher temperature can be rationalized on the basis of cobalt oxide crystallites size (Table 1). In the presence of potassium, apart from the cobalt crystallites size, additional effects might influence the reducibility of the catalyst.

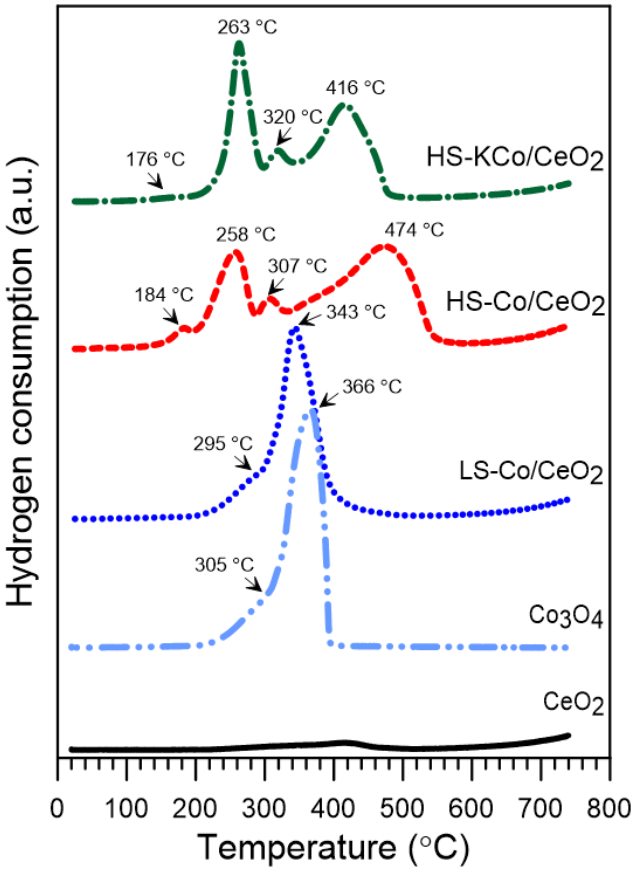

Figure 1. H_2-TPR profiles of as calcined ceria support, Co_3O_4 and cobalt-based catalysts.

Fig. 2 shows the XPS core level spectra of the surface elements after reduction at 420ºC in hydrogen (detailed characterization of the pristine samples can be found in the Supplementary Information Fig. S1). For the deconvolution of the Ce 3d region (Fig. 2a) reference spectra of CeO_2 (\\\) and Ce_2O_3 (///) recorded over oxidized and reduced cerium foil were used. In the same way two components recorded on reference samples were also used for Co $2p_{3/2}$ (Fig. 2b) deconvolution: one for metallic cobalt (///), located at 778.6 eV, and a second around 781.4 eV – formally ascribed to oxide-like component (CoO and/or Co–OH), further abbreviated as CoO_x (\\\). In literature [50] metallic cobalt is fitted with a characteristic asymmetric main peak and two plasmon loss peaks (located at 3.0 and 5.0 eV higher binding energy than the main component) [50].

From Fig. 2(a-b) it is evident, that after hydrogen treatment the surface of all catalysts was reduced, however, to a different extent. From the spectra deconvolution it was found that the reduction of cobalt oxides on the surface of the LS-catalyst was complete, while on the HS and HS-K small amounts of CoO_x remain after the hydrogen treatment. The XPS results are in a good agreement with the TPR profiles shown in

Fig. 1. Some authors postulate that persistent Co(II) species can be a result of a strong metal-support interaction and/or penetration Co^{2+} ions into the support lattice [51–53]. This effect is related to the cobalt crystallite size shown in Table 1.

It is well known that pure ceria is difficult to reduce in hydrogen at relatively low temperatures [54], however, in the presence of cobalt it can be partially reduced due to hydrogen *spill-over* effect [8, 54–56]. The Ce 3d spectra shown in Fig. 2a indicate that the ceria support of the LS-catalyst was partially reduced to $CeO_{1.76}$ (Ce(III) = 48.85%), while the supports of promoted and unpromoted HS-catalysts remained practically fully oxidized. Higher diffusion ability of oxygen atoms for the HS-ceria support due to the higher defects' concentration leads to the different reduction level between the HS-ceria and LS-ceria [30].

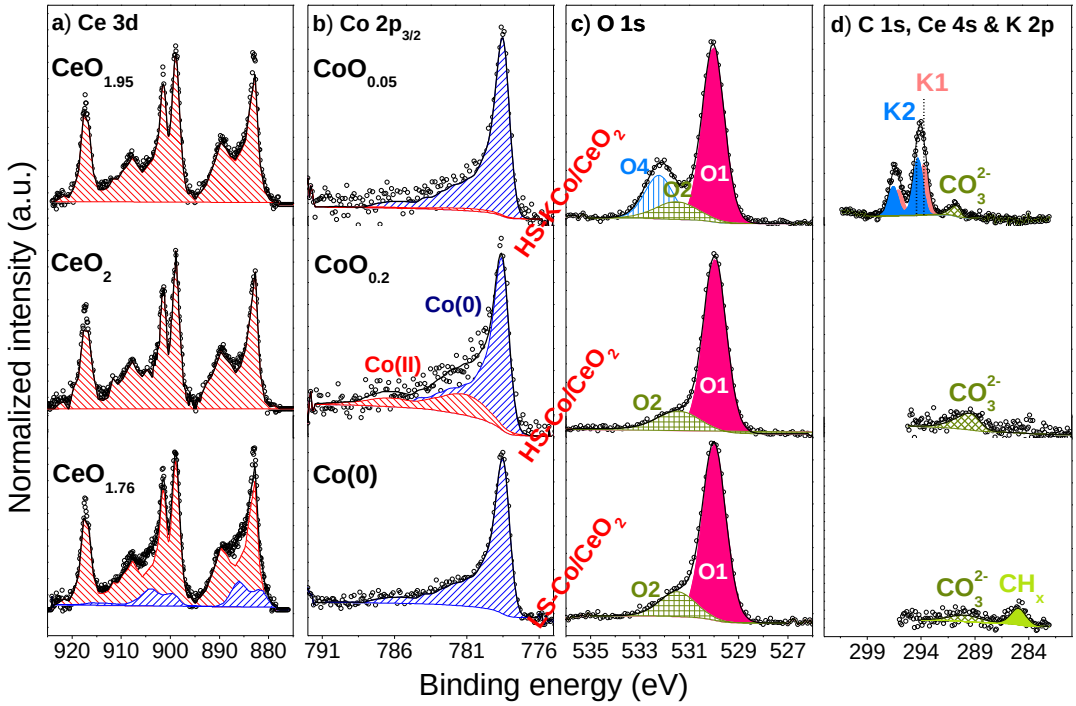

Figure 2. The high resolution XPS spectra of Ce 3d (a), Co $2p_{3/2}$ (b), O 1s (c) and C 1s, Ce 4s & K 2p (d) collected after the reduction (H_2/Ar= 50/50 cm^3, T = 420ºC, p_{total} = 1 atm, 1 h) of the LS-Co/CeO_2, HS-Co/CeO_2 and HS-KCo/CeO_2 catalysts; a) Ce(IV) (\\\), Ce(III) (///), b) Co(II) (\\\), Co(0) (///), c) O1 – lattice oxygen, O2 – hydroxyl and carbonate species, O4 – carbonate species bonded to potassium, d) K1 – KCO_3, K–O species, K2 – change of potassium electronic properties.

The O 1s spectra (Fig. 2c) of the unpromoted catalysts are very similar. The detailed information of each component contribution in the overall spectra can be found in Supplementary Information – Table S1. The main peak (530 eV) can be safely assigned to ceria lattice oxygen (O1) [57–60], while the assignment of the high binging

energy component at 531.5 eV (O2) is controversial. Some authors assign it directly to the presence of –OH groups [61–64], while some others identify them as adsorbed oxygen ions (O^- species) on surface oxygen vacancies [49, 58, 65]. It should be mentioned that quite recently Z. Liu et al. [57] suggested that in ceria-supported systems the peak located at 1.4 eV higher binding energy than the main component is probably related to ceria hydroxide layer $Ce^{3+}(OH)_x$. On the spectra of the potassium-promoted catalyst, an additional peak at 532.2 eV (O4) was found. In literature this peak is regarded as the fingerprint of the presence of amorphous layer of potassium oxides [66], potassium hydroxide [67] or potassium carbonate [68, 69].

The presence of amorphous potassium oxides on the surface of ESR catalysts was recently confirmed by S. Ogo et.al. [23]. The nature of potassium oxides is still under discussion. B. Lamontagne et al. [70] have studied the alkali metal promotion of silicon oxidation and their measurements revealed the existence of four potassium oxides formed during increasing oxygen exposure. They assigned the peak at 531.0 eV to K_2O_2, 532.0 eV to K_2O_3 and 534.2 eV to KO_2. Contrary, G. Pirug et al. [71] have assigned the component at 531.7 eV to K_2O_2 surface species. Z. Hou et al. [67] have suggested that potassium on the surface exists as KOH. M. Carlsson [72] claimed that potassium forms hydroxide species resulting in the increase of the surface basicity. Despite difficulties in determining the exact nature of the potassium compounds, the increase of K 2p intensity and appearance of the O4 component at O 1s spectrum confirms the existence of potassium-oxygen bonds. In further part of this paper we will try to shed a light on the nature of K1 and O4 components.

Before reduction, carbonaceous deposit was detected on the surface of all catalysts (Supplementary Information, Fig. S.1). The reduction procedure allowed for the removal of adsorbed carbon impurities and purification of the surface (Fig. 2d). For the K-promoted catalyst the peaks at 294.3 and 297.0 eV are due to the presence of K^+ ions (K 2p core level). The intensity of these peaks increased after hydrogen pre-treatment (Fig. 2d), as compared to the as-calcined sample (Supplementary Information, Fig. S1d). The calculated contribution of potassium on the surface of the fresh sample was 2.7 at.%, whereas after reduction it increases to 12.1 at.% (Table 2), suggesting surface's enrichment in potassium (e.g., re-dispersion) after reduction. Analysis of the K 2p region (Fig. 2d) allowed observing small asymmetry and the shift of the peak towards higher binding energies (BE), as compared to further results (Fig. 3-5d). This may indicate the coexistence of two potassium related species (the

K $2p_{3/2}$ components located at 293.8 ± 0.2 eV and 294.6 ± 0.2 eV respectively were denoted as K1 and K2).

H.P. Bonzel et al. [73, 74] have presented the results of XPS studies of K-promoted surface of the Fe foil and they have suggested that the presence of K $2p_{3/2}$ component around 294 eV and oxygen at 532.2 eV is strongly supporting the hypothesis of KOH existence [73], however, only in the case of absence of the carbonate peak at ~290 eV [74]. In the presence of carbonates the oxygen peak at 532.3 eV can be assigned also to the existence of potassium carbonates [68]. It should be noted that BE's of the K $2p_{3/2}$ for as deposited KNO_2, K_2CO_3 and KOH films on the Fe foil were very close (293.7–293.8 eV) and the shift towards higher BE's (293.9–294.1 eV) were observed after samples' reduction [73, 74]. The work of G. Maniak et al. [75] confirms that regardless of potassium compound used for cobalt oxide promotion, shifts on the BE scale are not observed, therefore, we assigned the K1 component to potassium bonded to oxygen species.

Table 2. The percentage contribution (at.%) of elements on the surface of catalysts under the ESR calculated on the basis of high resolution XPS spectra after taking into account the atomic sensitivity factor of each element.

Catalyst	**H_2O/EtOH (mol/mol)**	**Contribution of an element (at. %)***				
		Co	**Ce**	**O**	**C**	**K**
LS-Co/CeO_2		20.3	31.4	40.8	7.5	0.0
HS-Co/CeO_2	H_2**	9.4	37.3	45.3	8.0	0.0
HS-KCo/CeO_2		5.7	27.8	49.9	4.4	12.1
LS-Co/CeO_2		1.3	3.0	4.6	91.1	0.0
HS-Co/CeO_2	3/1	3.1	7.9	10.7	78.3	0.0
HS-KCo/CeO_2		2.3	22.3	46.5	17.8	11.1
LS-Co/CeO_2		19.0	25.3	51.5	4.2	0.0
HS-Co/CeO_2	9/1	5.6	28.4	42.6	23.4	0.0
HS-KCo/CeO_2		1.9	15.9	51.5	11.4	19.2
LS-Co/CeO_2		22.2	25.6	50.5	1.8	0.0
HS-Co/CeO_2	12/1	9.1	33.6	48.1	9.2	0.0
HS-KCo/CeO_2		1.2	8.0	52.6	11.8	26.3

*Calculated as: $n_i = n_i/\sum n_{i-j} \cdot 100\%$, where n_i = [Co, Ce, O, C, K] and n_{i-j} = Co+Ce+O+C+K.

**Results obtained after the catalysts pre-reduction (H_2/Ar) at 420ºC for 1 h.

Even though at this point, the chemical nature of potassium species is not clear it is convincing that the potassium state would depend on the local chemical environment of the surface [74] and that potassium species can be easily transformed. In the view of the above discussion, in this work the shift of the K 2p (appearance of

the component K2) towards slightly higher BE's is suggested to be ascribed to the change of electronic properties of potassium.

2.2. XPS characterization of catalysts after the ESR with a stoichiometric H_2O/EtOH molar ratio

The XPS results recorded after the ESR reaction at a stoichiometric (3/1 mol/mol) H_2O/EtOH molar ratio (T = 420ºC, p_{total} = 1 atm, t = 1 h), show partially reduced ceria support and metallic cobalt with traces of CoO_x (Fig. 3a and 3b).

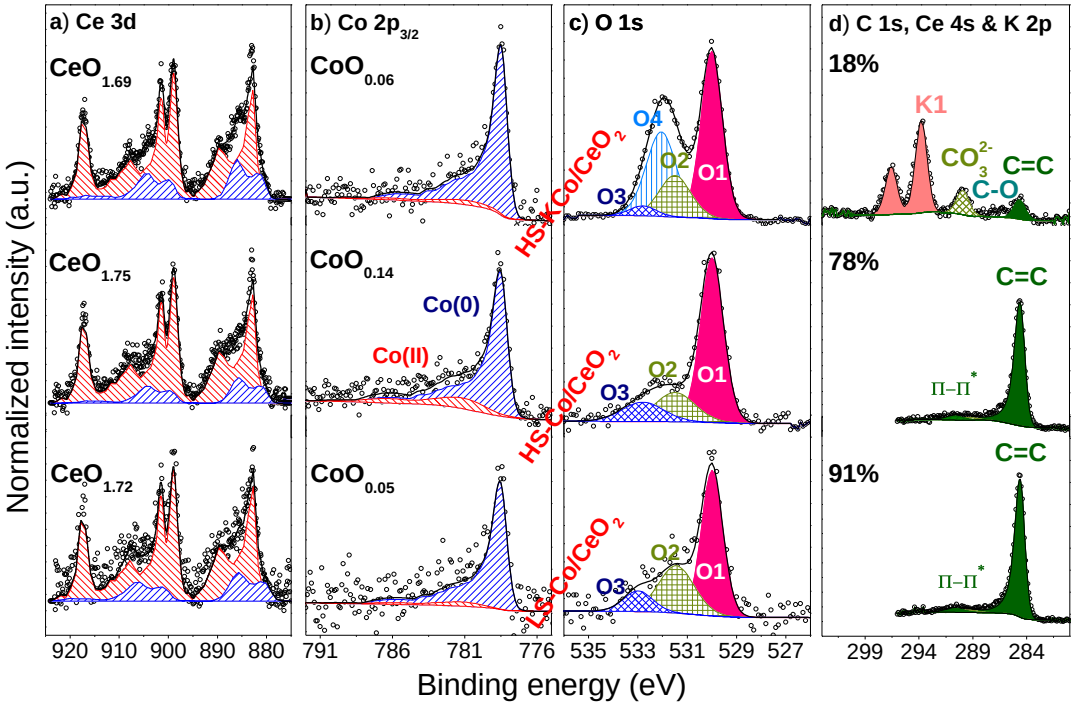

Figure 3. The high resolution XPS spectra of Ce 3d (a), Co $2p_{3/2}$ (b), O 1s (c) and C 1s, Ce 4s & K 2p (d) collected after the ESR (H_2O/EtOH = 3/1 mol/mol, T = 420ºC) carried out over the pre-reduced (H_2, T = 420ºC) LS-Co/CeO_2, HS-Co/CeO_2 and HS-KCo/CeO_2 catalysts; a) Ce(IV) (\\\), Ce(III) (///), b) Co(II) (\\\), Co(0) (///), c) O1 – lattice oxygen, O2 – hydroxyl and carbonate species, O3 – water, O4 – carbonate species bonded to potassium, d) K1 – KCO_3, K–O species. On the picture (d) also the percentage atomic contribution of carbon on the surface was given.

It is interesting to note that as compared to the state prior to the ESR (reduced samples, Fig. 2), the stoichiometric reaction mixture seems to be more efficient in ceria's reduction than hydrogen. On the other hand, for cobalt it is not the case since its oxidation state remains almost the same as before the reaction (please compare Fig. 2b and 3b). Significant re-oxidation of metallic cobalt to CoO_x accompanied by ceria's reduction has been reported by S.S.Y. Lin et al. [27], over the pre-reduced 10% Co/CeO_2-ZrO_2 catalyst, exposed to the H_2O/EtOH mixture molar ratio of 4/1 at 450ºC. It was also found that water content has a limited effect on cobalt re-oxidation process.

The higher reduction degree of ceria, as calculated by Ce 3d spectra, was found for the HS-K catalyst ($CeO_{1.69}$, 61.72% of Ce(III)). In addition, as compared to the unpromoted HS catalyst, cobalt of HS-K catalyst is more reduced ($CoO_{0.05\pm0.01}$). Therefore, potassium loading facilitates catalyst's reduction under the ESR reaction, contradicting previous reports of L. del Río et al. [76, 77].

Comparison of the O 1s spectra of the samples after hydrogen pre-treatment (Fig. 2c) and the ESR reaction (Fig. 3c) shows, that the relative intensity of the O2 component (531.5 eV) increases, while a new component located around 532.8 ±0.2 eV (denoted as O3), appears. According to its binding energy the O3 component can be assigned to surface adsorbed water species [58, 78, 79]. Moreover, it can be seen that concentration of surface adsorbed hydroxyl species (O2) is higher for the LS and HS-K catalysts.

The unpromoted catalysts after 1 h of the ESR were covered by carbon deposit, as seen in the C 1s region (Fig. 3d). The C 1s peak position at 284.6 eV, as well as its characteristic asymmetric shape, indicates for the presence of graphitic carbon species [80]. The higher binding energy component (289.4 eV) is characteristic for both Ce 4s region [81] and carbonate-type species [57, 74]. Carbon dominates the surface with 91 and 78% atomic concentration for the LS- and HS-catalysts, respectively (Table 2). Potassium inhibits carbon deposition (formation of C=C and CH_x species) down to <10%; however, a new peak at 290 eV indicates for the presence of CO_3^{2-} species (total carbon-containing species coverage including carbonates was <20% as shown in Table 2). The K 2p spectrum of the HS-K catalyst shows a doublet at 293.8 and 296.6 eV which is very close to the BE of the K 2p doublet (293.9 and 296.6 eV), recorded by E. de Smit et al. [82]. In this case the peak was assigned to metastable basic potassium carbonate species. The noticeable intensity increase of the C 1s peak at 290 eV allows assuming that the K1 component at least partially is related to the presence of potassium carbonates, e.g., $2K^+CO_3^{2-}$ or $K^+CO_2^-$. In order to determine the origin of K1 and O4 components analysis of the percentage of the surface adsorbed CO_3^{2-} species (after subtracting of the Ce 4s contribution) was done. The contribution of these species in O 1s and K 2p regions led us to the conclusion that O4 peak is related to KCO_3 species (the amount of potassium species for the H_2O/EtOH molar ratio of 3/1 is insufficient to form K_2CO_3 species). Because the percentage contribution of potassium on the surface is higher than that of KCO_3 species in the K 2p spectra for

all H_2O/EtOH molar ratios it is suggested that the rest of the potassium may occur on the surface as $K^{\delta+}–O_{surf}^{\delta-}$.

Potassium containing species are rather difficult to characterize, especially when they are highly dispersed [84, 83], therefore, knowledge about them is limited [83]. The XPS studies cannot provide direct information whether potassium is bonded through oxygen to the surface, or it just occurs as a compound with oxygen (e.g., KOH layer). N. Hou et al. [83] suggested that $K^{\delta+}–O_{surf}^{\delta-}$ species might be formed due to decomposition of potassium carbonates initiated by hydroxyls adsorbed on the surface.

2.3. XPS characterization of catalysts after the ESR at high H_2O/EtOH molar ratios

The catalysts' resistance to coke formation can be improved by increasing the water to ethanol molar ratio in the reaction feed. In Fig. 4 the XPS spectra of catalysts in the H_2O/EtOH = 9/1 mol/mol mixture are shown. The surface of the unpromoted catalysts is more oxidized as compared to the 3/1 molar ratio. The valence state of cerium for H_2O/EtOH = 9 mol is 1.76 (Ce(III) = 47.12%) and 1.83 (Ce(III) = 33.65%) for the LS- and HS-catalyst respectively, while the concentration of Co(II) species increases considerably. At the HS-K catalyst the molar ratio of 9/1 induce more oxidized cobalt, but notably has the reverse effect on cerium, which is more reduced than in the molar ratio of 3/1. In addition, the atomic fraction of potassium (Table 2) increases considerably followed by simultaneous increase of the O 1s component at 532.2 eV (Fig. 4c). The excess of water had a beneficial effect on suppression of carbon formation. The carbon atomic fraction, which was 91-78% in the H_2O/EtOH = 3/1 molar ratio, drops down to 4 and 23% for the LS- and HS-catalysts, respectively. However, one should note that the given carbon percentage contribution is considered to the whole C 1s core level, meaning that C=C, CH_x, and chemisorbed C–O and CO_3^{2-} species are also included. Potassium addition decreases the carbon fraction at the HS-K catalyst from 23% (for HS) to 11%, while the sole C 1s component around 290 eV (Fig. 4d) is characteristic for carbonate species as discussed in the previous section.

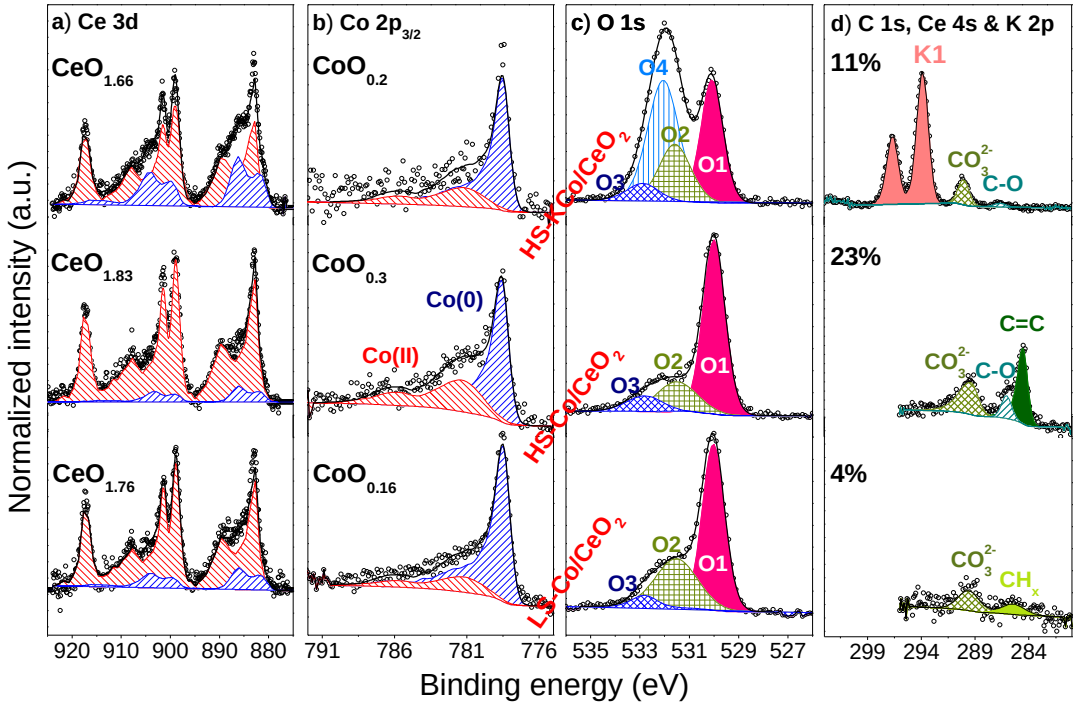

Figure 4. The high resolution XPS spectra of Ce 3d (a), Co $2p_{3/2}$ (b), O 1s (c) and C 1s, Ce 4s & K 2p (d) collected after the ESR (H_2O/EtOH = 9/1 mol/mol, T = 420ºC) carried out over the pre-reduced (H_2, T = 420ºC) LS-Co/CeO_2, HS-Co/CeO_2 and HS-KCo/CeO_2 catalysts; a) Ce(IV) (\\\), Ce(III) (///), b) Co(II) (\\\), Co(0) (///), c) O1 – lattice oxygen, O2 – hydroxyl and carbonate species, O3 – water, O4 – carbonate species bonded to potassium, d) K1 – KCO_3, K–O species. On the picture (d) also the percentage atomic contribution of carbon on the surface was given.

Further increase of the H_2O/EtOH molar ratio to 12/1 (Fig. 5) induces cobalt oxidation ($CoO_{0.34}$) for both LS- and HS-catalysts. In the case of the HS-K catalyst, the Co 2p peak after 1 h of the ESR has been in the signal noise level, indicating that cobalt particles were buried underneath a thick layer (around 3 to 4 nm) which attenuates Co 2p signal. The intense signal of the K1 (K 2p) and O4 (from the O 1s) components suggests that cobalt particles were most probably covered by the potassium bonded to oxygen layer (KCO_3 and K–O).

The Ce 3d peak was also barely detectable, indicating that KCO_3/K–O is deposited without apparent distinction over cobalt and ceria support areas. In order to estimate the time dependence of KCO_3/K–O layer formation, ESR at shorter reaction period (15 min) was carried out (inset of Fig. 5b). In this case the Co 2p signal directly suggests that KCO_3/K–O layer was thinner than after 1 h of the ESR, therefore its formation is time-depended.

Our experiments show that for the HS-K catalyst more potassium species were observed in water rich reactants mixtures, suggesting segregation of potassium due to

its stronger affinity to water. These experiments also allow us to conclude that the oxidation state of cobalt is the same like for the unpromoted catalysts ($CoO_{0.34}$). Ceria valence state for the LS- and HS-catalysts were the same like this recorded for the 9/1 molar ratio, while further reduction of cerium oxide was found for the potassium-promoted catalyst ($CeO_{1.61}$, 78.13% of Ce(III)).

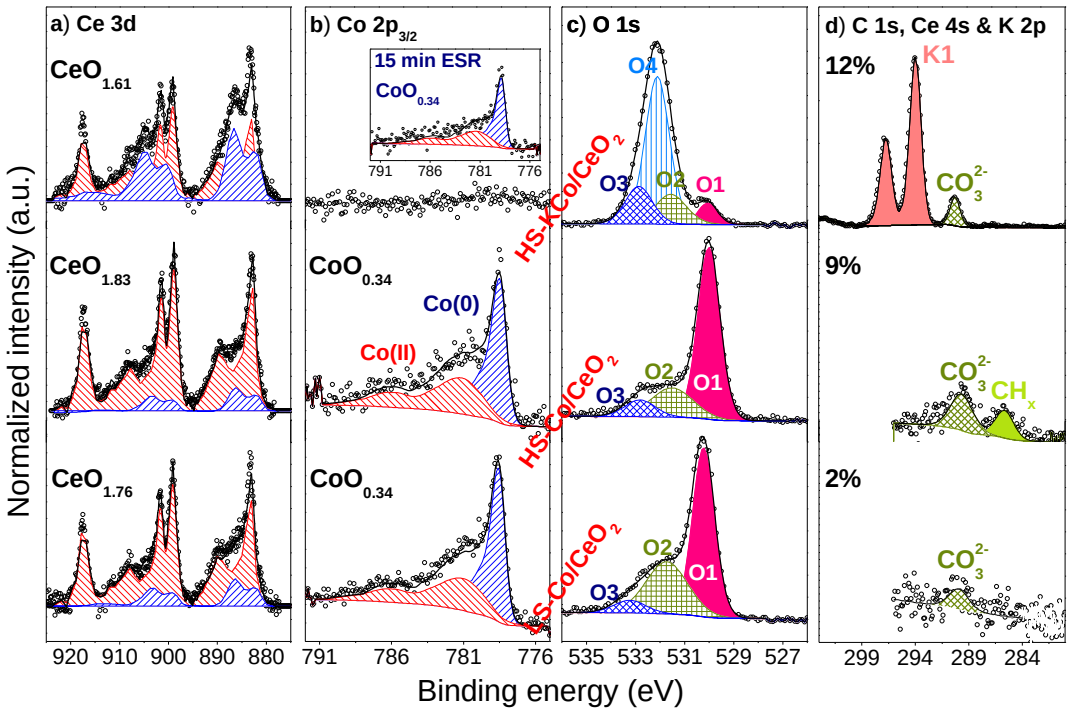

Figure 5. The high resolution XPS spectra of Ce 3d (a), Co $2p_{3/2}$ (b), O 1s (c) and C 1s, Ce 4s & K 2p (d) collected after the ESR (H_2O/EtOH = 12/1 mol/mol, T = 420ºC) carried out over the pre-reduced (H_2, T = 420ºC) LS-Co/CeO_2, HS-Co/CeO_2 and HS-KCo/CeO_2 catalysts; a) Ce(IV) (\\\), Ce(III) (///), b) Co(II) (\\\), Co(0) (///), c) O1 – lattice oxygen, O2 – hydroxyl and carbonate species, O3 – water, O4 – carbonate species bonded to potassium, d) K1 – KCO_3, K–O species. On the picture (d) also the percentage atomic contribution of carbon on the surface was given.

The common feature for all catalysts was decreased, almost negligible, carbon deposition. Notably at 12/1 molar ratio, the promoted HS-K catalyst shows higher carbon atomic fraction (Table 2) as compared to the unpromoted catalysts. This can be explained by the lower surface potential barrier of potassium-covered surfaces [75] which increases the adsorption energy of carbon monoxide. Adsorbed species were converted on the surface into carbonate-type species.

The presented results show that regardless of the H_2O/EtOH ratio, a mixed metallic-ionic form of cobalt is always present on the surface during the ESR reaction. As expected, reactant mixture, reach in water, enhances cobalt oxidation. Oxidation of cobalt in the excess of water has been reported previously for Co/Al_2O_3 catalysts tested

under H_2O/EtOH = 6/1 mol/mol [13] as well as for Co/CeO_2-ZrO_2 with the H_2O/EtOH molar ratio of 4 [27]. The higher excess of water allows for higher concentration of surface adsorbed –OH groups (O2) (as compared to the results obtained in the stoichiometric ratio of reactants), facilitating carbon removal.

2.4. The ESR performance of the catalysts

Table 3 shows the reactants conversions and the ESR reaction products selectivity obtained after 1 h at 420ºC for all three H_2O/EtOH molar ratios. It can be seen that, apart from the LS-catalyst at 3/1 molar ratio, 100% ethanol conversion is achieved in all cases. Water conversion (not shown in the table) at 3/1 molar ratio is between 37 and 54%, which is significantly lower than this expected from the ESR stoichiometry (100%). This indicates that non-selective ethanol transformations (without the participation of water molecules) occurred under the examined conditions. In the case of the ESR carried out in water excess (9/1 and 12/1 mol/mol), the water conversion over the LS- and HS-catalysts (38–41% and 21–28% respectively) is only a little higher in relation to the expected reaction stoichiometry (33 and 25%).

In all H_2O/EtOH molar ratios the ESR reaction products include H_2, CO_2, CO, CH_4 and some amounts of acetaldehyde observed only on the LS-Co/CeO_2. Over all samples selectivity to hydrogen was quite high and in general it increased with the increase of water excess, varying between 82% (3.16 $\mathrm{mol_{H_2}/mol_{EtOH}}$) and 98% (5.56 $\mathrm{mol_{H_2}/mol_{EtOH}}$).

Table 3. Activity and selectivity of catalysts after 1 h in the ESR at 420ºC.

Catalyst	H_2O/EtOH (mol/mol)	Conv. (%)	Selectivity (%)					H_2/EtOH	CO_2/EtOH
		EtOH	H_2	CO_2	CO	CH_4	MeCHO	(mol/mol)	(mol/mol)
LS-Co/CeO_2	3/1	92.4	82.5	52.6	19.7	15.0	6.3	3.16	1.05
HS-Co/CeO_2		100	84.6	67.2	10.6	22.2	0	4.03	1.34
HS-KCo/CeO_2		100	98.5	91.7	5.5	2.7	0	5.55	1.85
LS-Co/CeO_2	9/1	100	94.1	80.4	10	9.6	0	4.83	1.61
HS-Co/CeO_2		100	95.1	86.5	5.7	7.8	0	5.19	1.73
HS-KCo/CeO_2		100	98.4	90.7	6.6	2.7	0	5.55	1.85
LS-Co/CeO_2	12/1	100	96.5	88.3	6.3	5.4	0	5.30	1.77
HS-Co/CeO_2		100	97.1	91.6	3.9	4.5	0	5.49	1.83
HS-KCo/CeO_2		100	97.7	92.7	3.7	3.6	0	5.56	1.85

On the contrary, the selectivities of carbon-containing products show striking difference among the catalysts. Comparison of the LS- and HS-catalysts shows that the

HS is more selective towards CO_2 (and less to CO) than the LS-counterpart for all H_2O/EtOH molar ratios. At the 3/1 molar molar ratio both LS- and HS-catalysts have lower CO_2 and higher CO and CH_4 selectivities than the HS-K, though more CH_4 is observed for the HS- compared to LS-catalyst. In the excess of water, the increase of CO_2 selectivity over the LS- and HS-catalysts is accompanied with a decrease of CO and CH_4 formation. The results also show that in the case of the HS-K the influence of the H_2O/EtOH molar ratio on the catalyst's selectivity in the ESR is negligible.

2.5. The influence of the ESR conditions on the catalysts' coking

It is expected that the LS-catalyst should be more vulnerable to coking than its HS-counterpart due to the presence of bigger cobalt particles [85, 86]. The XPS spectra obtained at the 3/1 molar ratio are in agreement with this hypothesis, but in excess of water, less carbon was observed on LS-catalyst after 1 h ESR. This behaviour might be caused by the different kinetics of carbon deposition in that two cases. More information about the kinetics of carbon deposition under long ESR reaction periods is provided by gravimetric studies (Fig. 6). One should note that due to substantial differences in the catalytic reactors, quantitative comparison of gravimetric and the XPS results is impossible and only certain trends should be taken into account. Nevertheless, based on the XPS results the oxidation state of the catalysts was not dramatically different, therefore, the weight changes can be primarily assigned to coke deposition. In general, the weight change of the unpromoted catalysts (LS and HS) is significantly higher as compared to the HS-K catalyst, confirming that potassium inhibits carbon formation and catalyst's oxidation, in accordance with the XPS results.

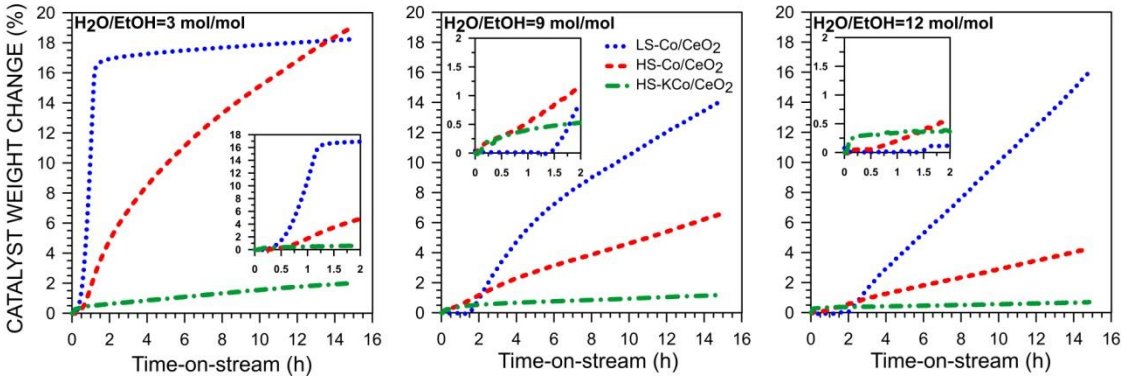

Figure 6. The gravimetric results for the LS-Co/CeO_2 (···), HS-Co/CeO_2 (---) and HS-KCo/CeO_2 (– · –) catalysts under the H_2O/EtOH = 3/1, 9/1 and 12/1 mol/mol.

Under the stoichiometric (3/1 mol/mol) reaction mixture the weight of the LS-catalyst has increased sharply to reach an almost constant value, while in the case of the HS-catalyst the weight gain was slower. However, note that the weight gain for both catalysts starts immediately after exposure to the ESR reactants (see insets of Fig. 6). On the other hand, at mixtures rich in water the weight gain does not start simultaneously for the LS- and HS-catalysts. In particular carbon deposition (and oxidation) on the LS-catalyst necessitates an induction period of 1 to 2 hours but after that increases rapidly. Conversely, catalyst's oxidation and carbon deposition on the HS-catalyst starts immediately and occurs gradually but with lower rate as compared to the LS-catalyst.

The explanation of the differences at the carbon deposition kinetics between the catalysts is out of the scope of this paper. However from Fig. 6 (insets) it is evident that during the reaction period used at XPS experiments (1 hour) carbon deposition for the LS-catalyst at water rich ESR mixtures is limited, in agreement with our the XPS studies.

The morphology of the spent catalysts after 1 h ESR reaction under the 3/1 molar ratio was studied by TEM, with emphasis on the carbon deposit formed during the ESR (Fig. 8-10). The TEM analysis of spent LS- and HS-samples revealed mainly graphitic carbon, although amorphous carbon was also detected, but to a lower extent. However, the morphology of carbon deposits differs among the catalysts. On the LS (Fig. 7) mostly carbon filaments in which encapsulated cobalt particles could be seen. Carbon detected on the HS looks more like a few atomic layers of carbon, mostly located at the boundary of cobalt and ceria crystallites, indicating that reaction occurs in this direction at the Co–CeO_x interface (Fig. 8). On the TEM images of the HS-K negligible amounts of carbon were found (Fig. 9), in accordance with the XPS results.

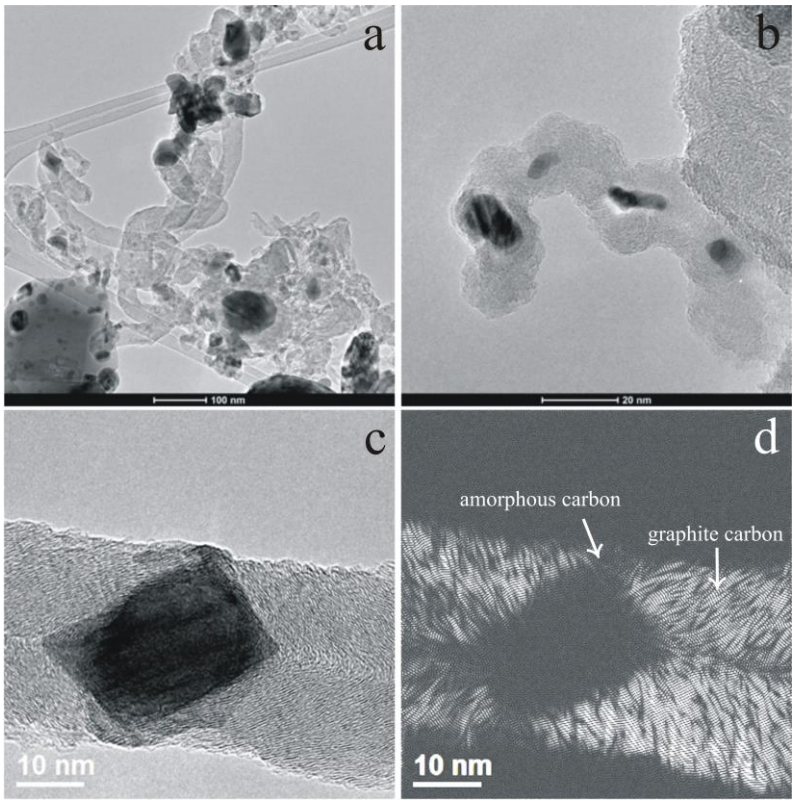

Figure 7. TEM images of the LS-Co/CeO_2 catalyst after 1 h ESR (T = 420ºC, H_2O/EtOH = 3/1 mol/mol).

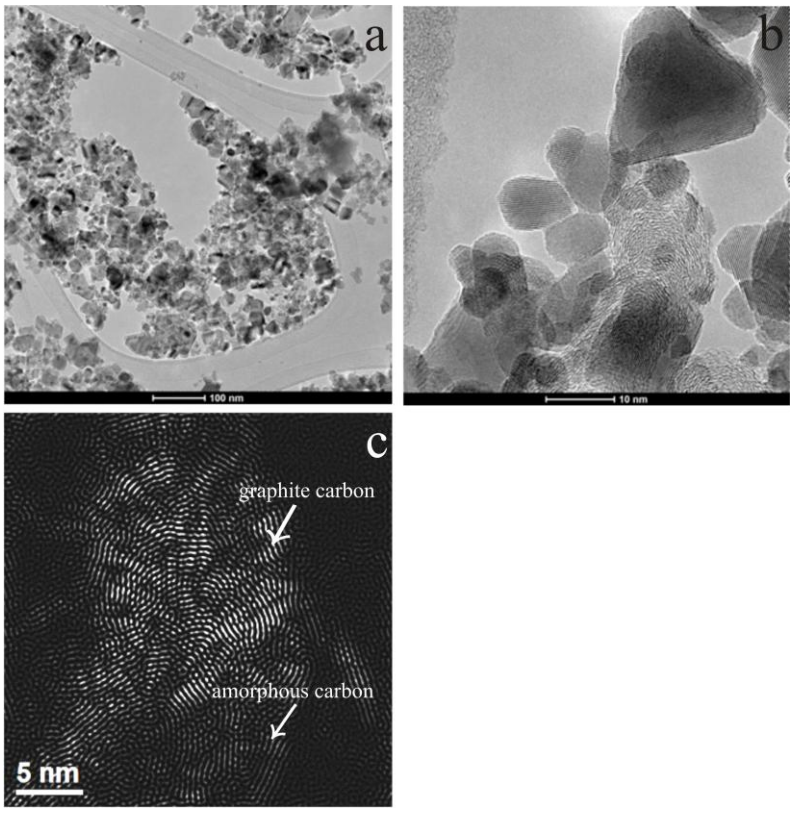

Figure 8. TEM images of the HS-Co/CeO_2 catalyst after 1 h ESR (T = 420ºC, H_2O/EtOH = 3/1 mol/mol).

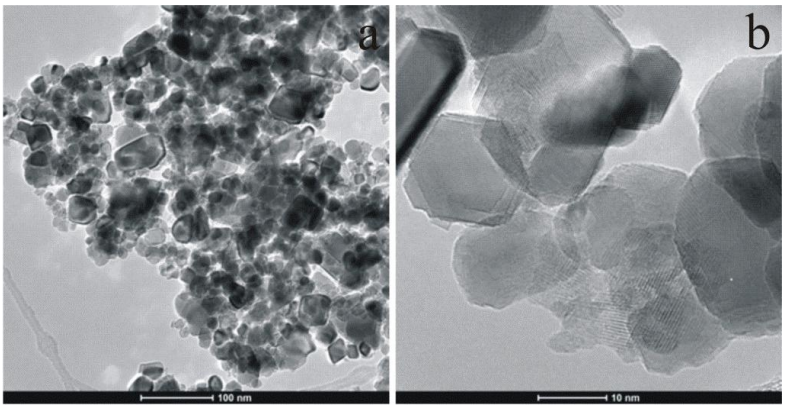

Figure 9. TEM images of the HS-KCo/CeO_2 catalyst after 1 h ESR (T = 420ºC, H_2O/EtOH = 3/1 mol/mol).

It can be concluded that the form of the carbon deposit depends on the support morphology and cobalt particles size. The catalyst with larger cobalt particles favours the growth of carbon nanofibers [86]. The XPS results show that the amount of coke on both LS- and HS-catalysts is comparable after 1 h ESR for the H_2O/EtOH = 3/1 mol/mol. On the contrary, TEM studies shows that significantly less carbon was found in the case of the HS-catalyst, what is also compatible with results of the gravimetric measurements (Fig. 6). TEM images prove that in the case of the LS-catalyst, carbon diffused inside cobalt crystallites, destroying the sample from the inner layers and it is deposited mainly in the whiskers form, while on its HS counterpart, carbon was deposited gradually only the outer layers of catalysts. Due to its high surface sensitivity, XPS cannot detect carbon diffused into cobalt particles, and thus justify the similar coke amounts found in the two catalyst types.

3. Discussion

3.1. The influence of the H_2O/EtOH molar ratio on the catalysts' surface

Fig. 10 shows how the reactants composition influences the catalysts' surface state. It can be seen that the catalysts' surface undergoes reorganization under conditions of the steam reforming of ethanol to a degree dependent on the H_2O/EtOH molar ratio. The ceria support in the unpromoted catalysts is progressively oxidized (Fig. 10a) with increasing excess of water. Ceria with the higher surface area (smaller ceria crystallites) is oxidized to a larger extent (on its surface the concentration of Ce(III) ions is lower) than that of the low-surface area. Moreover, the water excess facilitates oxidation of cobalt (Fig. 10b). As in the case of ceria, the more intensive

oxidation of cobalt (the larger Co(II)/(Co(0)+Co(II)) atomic ratio) occurs when the small cobalt crystallites were deposited on the high-surface area ceria support. Those results prove that higher dispersion (smaller crystallites) of both ceria support and cobalt in the unpromoted catalyst makes easier its oxidation under ESR conditions – this catalyst was also more resistant to reduction, as it is shown in Fig. 1.

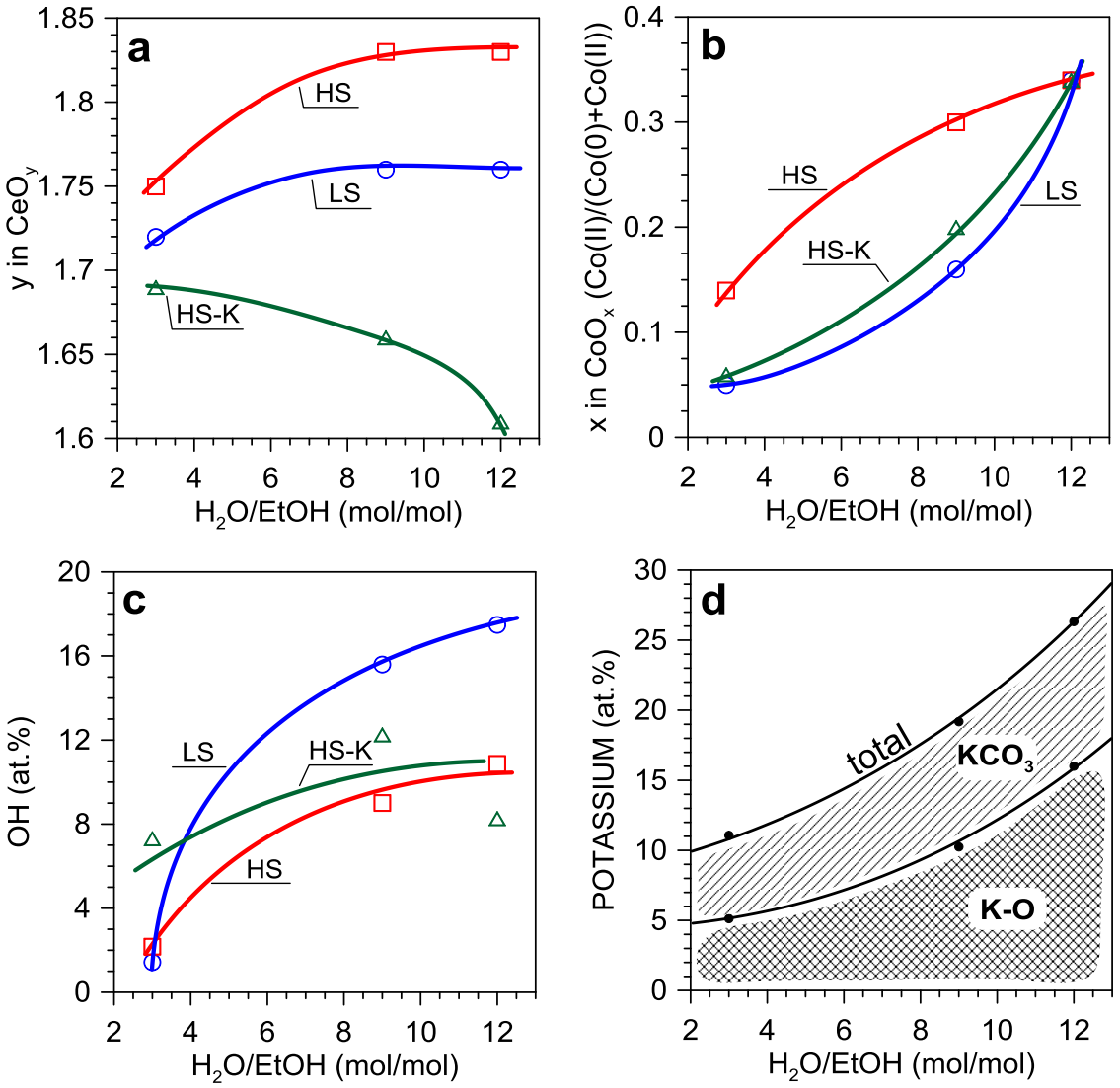

Figure 10. Dependence of (a) ceria valence state (CeO_y), (b) cobalt oxidation state (CoO_x), (c) percentage concentration of adsorbed hydroxyls, and (d) potassium distribution on the catalyst surface, with the H_2O/EtOH molar ratio for the LS-Co/CeO_2, HS-Co/CeO_2 and HS-KCo/CeO_2 catalysts under ESR at 420ºC.

The increased H_2O/EtOH molar ratio in the reaction mixture promotes the hydroxyl's species concentration (Fig. 10c) on the catalyst's surface (the hydroxyls' concentration is considered as a percentage of the overall catalytic surface, since XPS does not allow to differentiate location of hydroxyls, on cobalt or on ceria areas.

Despite the very similar, low concentration of hydroxyls under the 3/1 H_2O/EtOH molar ratio (Fig. 10), increase of the water excess induces differences in the abundance of these species on the unpromoted catalysts. Fig. 10 shows that the highest hydroxyl concentration among unpromoted catalysts is found on the LS-catalyst, which might be related to the oxidation state of both main components of the LS-catalyst – the higher share of metallic, not oxidized cobalt or/and the higher concentration of surface Ce(III) ions in the ceria support – the larger surface concentration of hydroxyls.

In contrast to the unpromoted HS-catalyst, ceria in the potassium-promoted HS-K catalyst is more reduced already under the lowest, stoichiometric reactants ratio and it shows further reduction with the increase of the water excess in the reaction mixture (Fig. 10a). At the same time, cobalt is also in lower oxidation state than it was in the case of the unpromoted HS-catalyst (Fig. 10b). The concentration of surface hydroxyls on the HS-K catalyst is much higher than this on the unpromoted HS-catalyst under the 3/1 H_2O/EtOH molar ratio, but only slightly changes at higher H_2O/EtOH molar ratios (Fig. 10c). Undoubtedly, the differences in the surface state between unpromoted HS- and promoted HS-K catalysts are related with the presence of the potassium promoter, for which the surface concentration changes with the reactants molar ratio (Fig. 10d). The progressive increase of the potassium surface concentration, measured by XPS, with the excess of water vapour in the reaction mixture results from the redispersion of potassium-containing aggregates, caused by the increased amount of chemisorbed and dissociated water vapour. As in the case of hydroxyls, the concentration of potassium-containing sites is referred to the overall catalyst's surface, without distinction between their location, on cobalt or on ceria. It was shown in ref. [40] that potassium on a very similar and free of coke catalyst is homogenously distributed over the entire catalyst's surface. The O 1s spectra show that part of potassium (both during the ESR and in pre-reduced catalyst – Fig. 2–5) is bonded to carbonate species under all H_2O/EtOH molar ratios. It is justified that carbonate species block these surface potassium sites, limiting their influence on the ESR. The concentration of the KCO_3 sites on the catalyst's surface increases with the excess of water in the reaction feed (Fig. 10d). The surface concentration of remaining potassium promoter sites ($K^{\delta+}$–$O_{surf}^{\delta-}$ species), which we denoted in short as K–O, is higher as compared to the KCO_3 amount, but it also increases with the water excess (Fig. 10d). It is reasonable that these K–O sites in the HS-K catalyst may play promoting role in the steam reforming of ethanol, providing an additional oxygen-containing species

reservoir. Similar suggestion that potassium encourages formation of active oxygen species, which are very important intermediates for soot combustion, was given by M. Sun et al. [49].

3.2. Correlation of the ESR catalytic performance with the catalysts' surface state

The correlation of the selectivity towards carbon dioxide formation with the oxidation states of cobalt and ceria is showed in Figs. 11a and 11b. In the case of unpromoted catalysts, the increase of the selectivity to CO_2 with the higher surface Co(II) contribution, shows that the latter would be an important factor influencing the ESR. However, in the presence of potassium promoter, the influence of cobalt oxidation state is limited, since; HS and HS-K catalysts with the same oxidation degree of cobalt show very different carbon dioxide production. It proves that potassium addition introduces other ESR active sites and thus the oxidation state of cobalt has minor influence in the carbon dioxide formation. The same conclusion can be drawn when considering the role of the oxidation state (a higher surface Ce(IV) ions contribution) of ceria support. Both correlation shown in Figs. 11a and 11b lead us to the assertion that in the presence of potassium the oxidation state of these main catalysts' components is not a dominant factor for the selective transformations of ethanol. The presence of oxidized cobalt and reduction-oxidation of ceria support are unavoidably influenced by the H_2O/EtOH molar ratio; however, we did not find evidences showing that they can directly influence the ESR selectivity.

An important surface feature for the selectivity of the ESR is the concentration of hydroxyl species. In Fig. 11c one can see monotonic relationship of concentration of surface adsorbed hydroxyls over LS-, HS- and HS-KCo/CeO_2 catalysts with the selectivity of carbon dioxide formation. However, the low-dispersed LS-Co/CeO_2 catalyst requires larger concentration of surface adsorbed hydroxyl species than the very well-dispersed HS-Co/CeO_2 to achieve the same selectivity, what will be discussed in the next paragraph. In the case of the unpromoted HS-catalyst and potassium-promoted HS-K catalyst the same abundance of hydroxyl species also leads to different selectivity. Similar picture is seen in relationships of the OH concentration and selectivities towards remaining ESR products, i.e., hydrogen, carbon monoxide and methane (see Fig. S2 in Supplementary Information). It suggests the existence of additional selective sites on the surface of promoted catalyst, connected with the presence of potassium promoter on the catalyst's surface, i.e., K–O sites. Taking both,

OH species and K–O sites, into consideration the ESR product selectivity over HS- and HS-K catalysts form coherent dependences, with increasing hydrogen and carbon dioxide selectivities to limit values, characteristic for the HS-K catalyst; selectivities to other products fall also to values characteristic for the HS-K catalyst (Figs. 12a-12c). Those limits are consistent with the thermodynamic limit of the hydrogen yield in the ethanol steam reforming; considering equilibrium states of side reactions the equilibrium hydrogen yield of 5.56 mole per one mole of ethanol in the feed are obtainable as against the stoichiometric value of 6.0 [42]. Also, for the same reason the thermodynamic yield of carbon dioxide is lower than the stoichiometric value of 2.0.

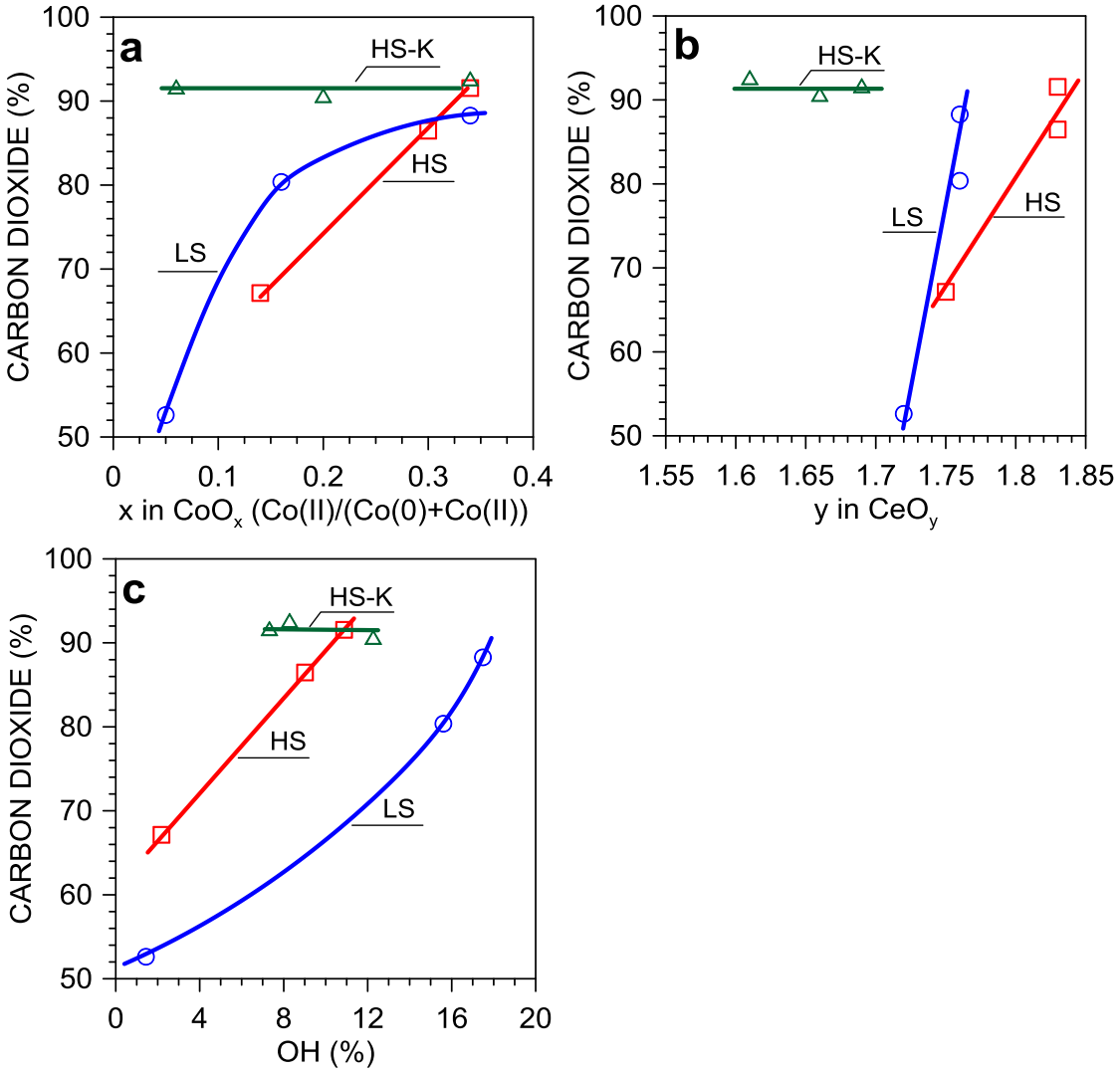

Figure 11. Correlation of CO_2 selectivity for the LS-Co/CeO_2, HS-Co/CeO_2 and HS-KCo/CeO_2 catalysts under the ESR at 420ºC with (a) cobalt oxidation state (CoO_x), (b) ceria valence state (CeO_y) and (c) percentage contribution of hydroxyls on the surface. Each point represents the different H_2O/EtOH molar ratio.

The yields of produced hydrogen and carbon dioxide in our studies reach the thermodynamic limit values (Fig. 12e). In the feed with the H_2O/EtOH molar ratio higher than stoichiometric value of 3/1 the total concentration of OH species and K–O sites on the surface of potassium-promoted catalyst is even larger than the necessary for the selective course of the ESR to gaseous products. However, a high concentration of OH species and K–O sites hampers deposition of all types of coke for all catalysts studied in this work (Fig. 12f). Small concentration of OH species and K–O sites leads to pronounced coking of the catalysts, with formation of completely (or almost completely) dehydrogenated C=C type carbonaceous deposit, in a large part as graphitic whiskers and layers (see Table S1 in Supplementary Information and Figs. 7-9). Increase of those selective surface sites first of all significantly lowers the amount of coke deposited and also changes its type from more dehydrogenated to CH_x type. For total elimination of coking phenomena, the high abundance of OH species and K–O sites, equal to or large than 25 at.% of the whole surface of catalyst is required.

Among surface oxygen-containing species molecular water is also present. However, as physically adsorbed only water molecules cannot form transition activated complexes required in a catalytic reaction on the surface of heterogeneous catalyst. Therefore, water species can be considered merely as spectators, excluded from direct participation in the ESR over catalyst's surface.

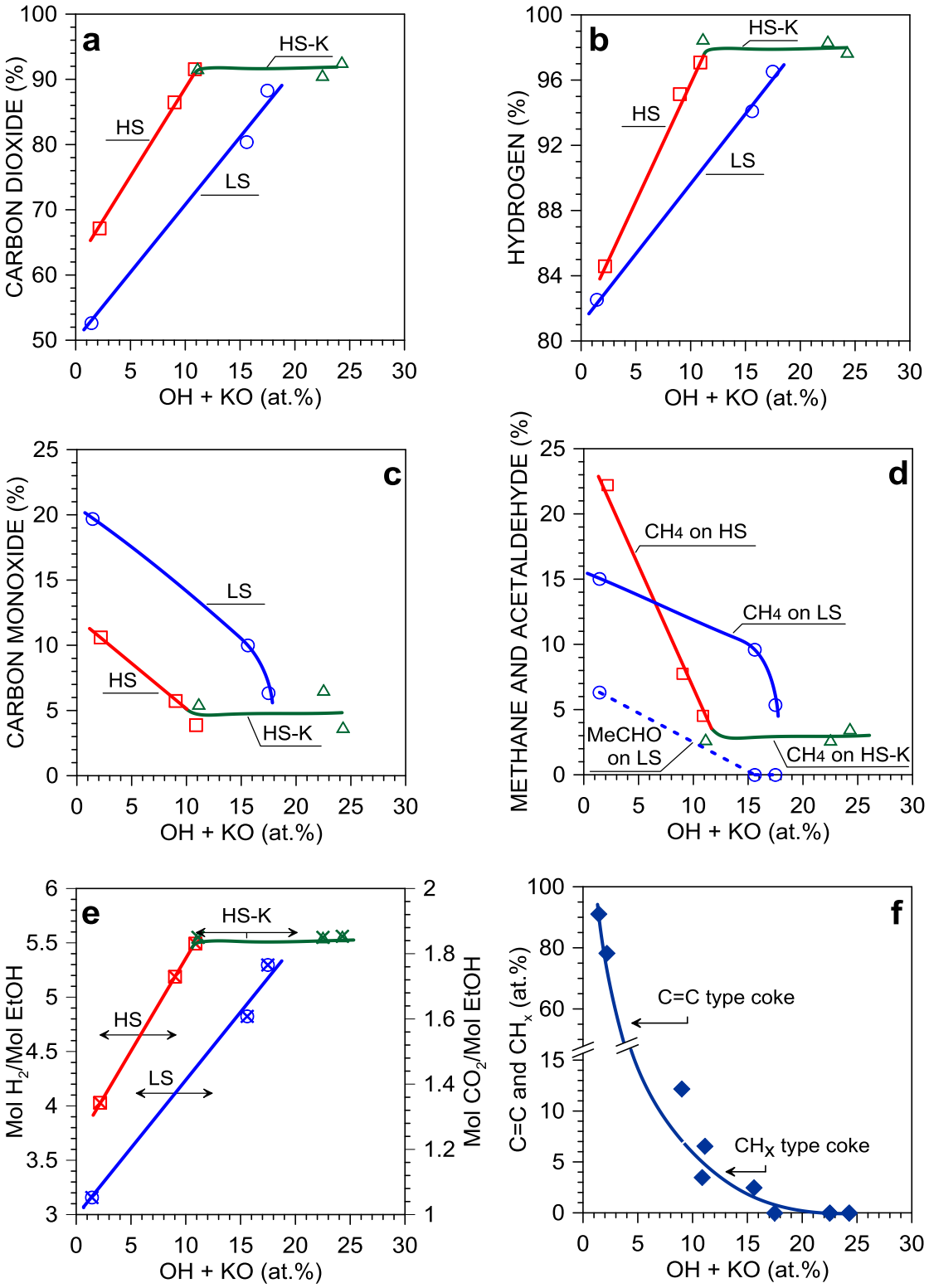

Figure 12. Correlation of (a–d) the catalysts selectivity towards H_2 and carbon-containing product, (e) H_2 and CO_2 yield, and (f) the concentration of C=C and CH_x species on the whole surface, with the concentration of oxygen-containing species on the surface of the LS-Co/CeO_2, HS-Co/CeO_2 and HS-KCo/CeO_2 catalysts under the ESR at 420ºC.

The selectivity of the steam reforming of ethanol does not depend solely on the population of OH species on the catalyst's surface since the LS-catalyst is less selective

towards all products despite the fact that it has more hydroxyls adsorbed than the HS-catalyst (Figs. 12a-12d). It suggests that the catalyst's morphology and location where oxygen-containing species are adsorbed may be equally important to their abundance. The difference in the ESR selectivity is definitely related to the dispersion of cobalt – the size of cobalt crystallites is very different, 3.8 nm in the more selective HS-catalyst and 39.3 nm in the less selective LS-Co/CeO_2 while the size of ceria support crystallites is 25.6 nm and 87.1 nm, respectively. The well dispersed, small crystallites usually have more low-coordinated sites (corners, edges and another defects on the surface of crystal lattice like steps, adatoms), which are the best and the strongest sites for chemisorption and dissociation of various chemical molecules, including water and ethanol. Reagents and their intermediates chemisorbed on cobalt and on ceria support may interact together to form desirable products of the ESR, i.e., hydrogen and carbon dioxide. On the other hand, the intimate contact of both catalyst's components – cobalt and its ceria support – and a short-enough distance from their border to the centre of the cobalt crystallites surface also may have a selective influence on the effects of the ESR [8]. The concentration of hydroxyls at the centre of crystallite surface, usually formed by flat terraces, may be insufficient for selective reaction of adsorbed ethanol and its intermediates. When the surface distance from the cobalt–ceria support border to the crystallite centre is too long (as in the case of a center of large crystallites in the LS-catalyst), nonselective ethanol transformations take place, without the possibility of its reaction with activated water. Due to an insufficient surface concentration of hydroxyl species acetaldehyde remains among final products (Fig. 12d). The comparison of the ESR effects over HS- and LS-catalysts leads us to the suggestion that the selective ceria-supported cobalt catalyst should have well dispersed cobalt particles deposited on the well dispersed support what is in agreement with previously published results [7, 8, 20].

Conclusions

The surface state and the catalytic performance of cobalt catalysts with micro- and nano-dispersed ceria supports were investigated under the steam reforming of ethanol at 420ºC for the H_2O/EtOH molar ratios equal to 3/1, 9/1 and 12/1. In the case of the nano-catalyst the effect of potassium promotion was also examined.

We found that the reduction degree of cobalt oxide and ceria during activation of catalysts with hydrogen depends on ceria support dispersion. Cobalt oxide supported

on low-dispersed ceria is more vulnerable to reduction than its counterpart with high-dispersed ceria, while potassium promoter facilitates reduction of cobalt oxide. The ceria support is reduced to some extent only in the low-dispersed catalyst, while in the unpromoted and potassium-promoted catalysts with high-dispersed ceria it remains practically fully oxidized after pre-reduction.

The catalysts surface undergoes re-organization under conditions of the steam reforming of ethanol to a degree dependent on the H_2O/EtOH molar ratio. We proved that higher dispersion (smaller crystallites) of both ceria support and cobalt in the unpromoted catalyst makes easier its oxidation under ESR conditions. The water excess in the ethanol-water vapors feed facilitates oxidation of both catalyst components. In contrast to the unpromoted high-dispersed catalyst, the ceria support in the potassium–promoted catalyst is more reduced already under the lowest, stoichiometric reactants ratio and it undergoes further reduction with the increase of the water excess in the reaction mixture. Cobalt oxidation is limited in the potassium–promoted catalyst, regardless of the feed composition. We proved that oxidation–reduction of these main catalysts components is not a general factor, crucial for the selective transformations of ethanol. The presence of oxidized cobalt and reduction–oxidation of ceria support are unavoidable effects, depended on the H_2O/EtOH molar ratio.

The concentration of potassium on the catalyst surface progressively increases simultaneously with the excess of water vapor in the reaction mixture. The part of surface potassium sites, also increasing with the water vapor excess, is bonded to carbonate species, what limit their influence on the course of the ESR. The surface concentration of remaining potassium promoter sites ($K^{\delta+}O_{surf}^{\delta-}$ sites) increases with the water excess; they may play promoting role in the steam reforming of ethanol, providing an additional oxygen–containing species reservoir.

The most crucial factor for selective conversion of ethanol over unpromoted catalysts is concentration of hydroxyl species on the catalysts surface, which increases with increased H_2O/EtOH molar ratio in the reaction mixture in the extent depending on the dispersion. In the case of promotion of the catalyst with potassium, the increasing hydroxyl concentration is supplemented by $K^{\delta+}–O_{surf}^{\delta-}$ sites. We found a coherent relation of both, OH species along with $K^{\delta+}–O_{surf}^{\delta-}$ sites, and the selectivity of the ESR to all gaseous products over unpromoted and promoted catalysts, with limits consistent with the thermodynamic limit of the hydrogen yield. Besides the surface concentration of hydroxyl species, the catalyst morphology and location where oxygen-

containing species are chemisorbed may be equally important to their abundance — the selective ceria–supported cobalt catalyst should have well dispersed cobalt particles deposited on the well dispersed support.

In addition to the role of oxygen–containing species in improving catalytic performance, the increase of both OH and $K^{\delta+}$–$O_{surf}^{\delta-}$ sites was found to lower the amount of coke deposited as well as to change its type from fully dehydrogenated C=C to CH_x type. For total elimination of coking phenomena the abundance of OH species and $K^{\delta+}$–$O_{surf}^{\delta-}$ sites on the catalyst surface should be even higher than that necessary for the selective ESR to gaseous products.

References

1 D. Zanchet, J.B.O. Santos, S. Damyanova, J.M.R. Gallo, J.M.C. Bueno *ASC Catal.* **5** (2015) 3841–3863.

2 M.N. Barroso, M.F. Gomez, L.A. Arru, M.C. Abello *Reac. Kinet. Mech. Cat.* **115** (2015) 535–546.

3 H. Song, L. Zhang, U.S. Ozkan *Top. Catal*. **55** (2012) 1324–1331.

4 Zs. Ferencz, A. Erdőhelyi, K. Baan, A. Oszkó, L. Óvári, Z. Kónya, C. Papp, H.-P. Steinrück, J. Kiss *ACS Catal.* **4** (2014) 1205–1218.

5 I.I. Soykal, B. Bayram, H. Sohn, P. Gawade, J.T. Miller, U.S. Ozkan *Appl. Catal., A* **449** (2012) 47–58.

6 H. Wang, L. Zhang, M. Li, Y. Liu, X. Bai *J. Rare Earth* **31** (2013) 565–571.

7 I.I. Soykal, H. Song, U.S. Ozkan *ACS Catal.* **2** (2012) 2335–2348.

8 A. Machocki, A. Denis, W. Grzegorczyk, W. Gac. *Appl. Surf. Sci.* **256** (2010) 5551–5558.

9 S.-W. Yu, H.-H. Huang, C.-W. Tang, C.-B Wang *Int. J. Hydrogen Energy* **39** (2014) 20700–20711.

10 H. Song, U.S. Ozkan *J. Catal.* **261** (2009) 66–74.

11 B. Bayram, I.I. Soykal, D. von Deak, J.T. Miller, U.S. Ozkan *J. Catal.* **284** (2011) 77–89.

12 A.M. Karim, Y. Su, M.H. Engelhard, D.L. King, Y. Wang *ACS Catal.* **1** (2011) 279–286.

13 A.R. Passos, L. Martins, S.H. Pulcinellin, C.V. Santilli, V. Briois *Catal. Today* **229** (2014) 88–94.

14 E. Varga, Z. Ferencz, A. Oszkó, A. Erdöhelyi, J. Kiss *J. Mol. Catal. A* **397** (2015) 127–133.

15 J. Llorca, P.R. de la Piscina, J.A. Dalmon, N. Homs *Chem. Mater.* **16** (2004) 3573–3578.

16 S. Tuti, F. Pepe *Catal. Lett.* **122** (2008) 196–203.

17 M.P. Hyman, J.M. Vohs, *Surf. Sci.* **605** (2011) 383–389.

18 M.A. Henderson, C.L. Perkins, M.H. Engelhard, S. Thevuthasan, C.H.F. Peden *Surf. Sci.* **526** (2003) 1–18.

19 N. Laosiripojana, S. Assabumrungrat *Appl. Catal., B* **66** (2006) 29–39.

20 I.I. Soykal, H. Sohn, D. Singh, J.T. Miller, U.S. Ozkan *ASC Catal.* **4** (2014) 585–592.

21 M. Greluk, P. Rybak, G. Słowik, M. Rotko, A. Machocki *Catal. Today* **242** (2015) 50–59.

22 M. Greluk, M. Rotko, A. Machocki *Catal. Lett.* **146** (2016) 163–173.

23 S. Ogo, T. Shimizu, Y. Nakazawa, K. Mukawa, D. Mukai, Y. Sekine *Appl. Catal., A* **495** (2015) 30–38.

24 S. Turczyniak, W. Luo, V. Papaefthimiou, N. S. Ramgir, M. Haevecker, A. Machocki, S. Zafeiratos *Top. Catal.* **59** (2016) 532–542.

25 V.M. Lebarbier, A.M. Karim, M.H. Engelhard, Y. Wu, B.-Q. Xu, E.J. Petersen, A.K. Datye, Y. Wang *ChemSusChem* **4** (2011) 1679–1684.

26 E. Martono, M.P. Hyman, J.M. Vohs *Phys. Chem. Chem. Phys.* **13** (2011) 9880–9886.

27 S.S.-Y. Lin, D.H. Kim, M.H. Engelhard, S.Y. Ha *J. Catal.* **273** (2010) 229–235.

28 M.P. Hyman, E. Martono, J. Vohs, *J. Phys. Chem. C* **114** (2010) 16892–16899.

29 M.S. Batista, R.K.S. Santos, E.M. Assaf, J.M. Assaf, E.A. Ticianelli. *J. Power Sources* **124** (2005) 99–103.

30 L. Qiu, F. Liu, L. Zhao, Y. Ma, J. Yao *Appl. Surf. Sci.* **252** (2006) 4931–4935.

31 A. Trovarelli *J. Am. Chem. Soc.* **124** (2002) 12923–12924.

32 S.M.F. Shahed, T. Hasegawa, Y. Sainoo, Y. Watanabe, N. Isomura, A. Beniya, H. Hirata, T. Komeda *Surf. Sci.* **628** (2014) 30–35.

33 A.M. da Silva, L.V. Mattos, J.P. de Breejen, J.H. Bitter, K.P. de Jong, F.B. Noronha *Catal. Today* **164** (2011) 234–239.

34 S.M. de Lima, A.M. da Silva, U.M. Graham, G. Jacobs, B.H. Davis, L.V. Mattos, F.B. Noronha *J. Catal.* **268** (2009) 268–281.

35 T. Mondal, K.K. Pant, A.K. Dalai *Int. J. Hydrogen Energy* **40** (2015) 2529–2544.

36 E. Martono, J.M. Vohs, *ACS Catal.* **1** (2011) 1414–1420.

37 S.M. de Lima, I.O. da Cruz, G. Jacobs, B.H. Davis, L.V. Mattos, F.B. Noronha *J. Catal.* **257** (2008) 356–368.

38 J.-W.Snoeck, G.F. Froment, M. Fowles *Ind. Eng. Chem. Res.* **41** (2002) 3548–3556.

39 B. Banach, A. Machocki *Appl. Catal., A* **505** (2015) 173–182.

40 G. Słowik, M. Greluk, A. Machocki *Mater. Chem. Phys.* **173** (2016) 219–237.

41 A.G. Gayubo, J. Vicente, J. Ereña, C. Montero, M. Olazar, J. Bilbao *J. Catal. Lett.* **144** (2014) 1134–1143.

42 K. Vasudeva, N. Mitra, P. Umasankar, S.C. Dhingra *Int. J. Hydrogen Energy* **21** (1996) 13–18.

43 V. Mas, R. Kiproes, N. Amadeo, M. Laborde *Int. J. Hydrogen Energy* **31** (2006) 21–28.

44 E.Y. García, M. Laborde *Int. J. Hydrogen Energy* **16** (1991) 307–312.

45 B.A. Sexton, A.E. Hughes, T.W. Turney *J. Catal.* **97** (1986) 390–406.

46 F. Diehl, A.Y. Khodakov *Oil Gas Sci. Technol*. **64** (2009) 11–24.

47 K. Chayakul, T. Srithanratana, S. Hengrasmee *J. Mol. Catal. A* **340** (2011) 39–47.

48 M. Haneda, Y. Kintaichi, N. Bion, H. Hamada *Appl. Catal., B* **46** (2003) 473–482.

49 M. Sun, L. Wang, B. Feng, Z. Zhang, G. Lu, Y. Guo *Catal. Today* **175** (2011) 100–105.

50 M.C. Biesinger, B.P. Payne, A.P. Grosvenor, L.W.M. Lau, A.R. Gerson, R.St.C. Smart *Appl. Surf. Sci.* **257** (2011) 2717–2730.

51 M.S. Batista, K.S. Santos, E.M. Assaf, E.A. Ticianelli *J. Power Sources* **124** (2003) 99–103.

52 L.F. Liotta, G. Di Carlo, G. Pantaleo, G. Deganello *Catal. Commun.* **6** (2005) 329–336.

53 M. Araque, J.C. Vargas, Y. Zimmermann, A.-C. Roger *Int. J. Hydrogen Energy* **36** (2011) 1491–1502.

54 G.R. Rao, B.G. Mishra *Bull. Catal. Soc. India* **2** (2003) 122–134.

55 H. Idriss *Platinum Metals Rev.* **48** (2004) 105–115.

56 X.D. Hou, Y.Z. Wang, Y.X. Zhao *Catal. Lett.* **123** (2008) 321–326.

57 Z. Liu, T. Duchoň, H. Wang, D.C. Grinter, I. Waluyo, J. Zhou, Q. Liu, B. Jeong, E.J. Crumlin, V. Matolín, D.J. Stacchiola, J.A. Rodriguez, S.D. Senanayake *Phys. Chem. Chem. Phys.* [Online early acces]. DOI: 10.1039/C6CP01212D. Published Online: March 31, 2016. http://pubs.rsc.org/en/content/articlehtml/2016/cp/c6cp01212d (accessed May 21, 2016)

58 M. Konsolakis, M. Sgourakis, S.A.C. Carabineiro *Appl. Surf. Sci.* **341** (2015) 45–54.

59 A. Pfau, K.D. Schierbaum *Surf. Sci.* **321** (1994) 71–80.

60 D.R. Mullins, M.D. Robbins, J. Zhou *Surf. Sci.* **600** (2006) 1547–1558.

61 F. Larachi, J. Pierre, A. Adnot, A. Bernis *Appl. Surf. Sci.* **195** (2002) 236–250.

62 D. Cappus, C. Xu, D. Ehrlich, B. Dillmann, C.A. Ventnce Jr., K. Al Shamery, H. Kuhlenbeck, H.-J. Freund *Chem. Phys.* **177** (1993) 533–546.

63 D.A. Creaser, P.G. Harrison *Catal. Lett.* **23** (1994) 13–24.

64 B.E. Koel, G. Praline, H.-I. Lee, J.M. White *J. Electron. Spectrosc. Relat. Phenom*. **21** (1980) 31–46.

65 J.L. Ayastuy, A. Gurbani, M.P. González-Marcos, M.A. Gutiérrez-Ortiz *Int. J. Hydrogen Energy* **37** (2012) 1993–2006.

66 T.L. Westover, A.D. Franklin, B.A. Cola, T.S. Fisher, R.G. Reifenberger *J. Vac. Sci. Techn., A* **28** (2010) 423–434.

67 Z. Hou, O. Yokota, T. Tanaka, T. Yashima *Catal. Lett.* **87** (2003) 37–42.

68 A.V. Shchukarev, D.V.; Korolkov *CEJC* **2** (2004) 347–362.

69 J. Iranmahboob, D.O. Hill, H. Toghian *Appl. Surf. Sci.* **185** (2001) 72–78.

70 B. Lamontagne, F. Semond, D. Roy *J. Electron. Spectrosc. Relat. Phenom.* **73** (1995) 81–88.

71 G. Pirug, O. Müller, H. P. Bonzel *Surf. Sci.* **73** (1993) 145–154.

72 M. Carlsson *Johnson Matthey Technol. Rev.* **59** (2015) 313–318.

73 H.P. Bonzel, H.J. Krebs *Surf. Sci.* **109** (1981) L527–L531.

74 H.P. Bonzel, G. Broden, H.J. Krebs *Appl. Surf. Sci.* **16** (1983) 373–394.

75 G. Maniak, P. Stelmachowski, A. Kotarba, Z. Sojka, V. Rico-Pérez, A. Bueno-López *Appl. Catal., B* **136–137** (2013) 302–307.

76 L. del Río, G. Marbán *Appl. Catal., B* **126** (2012) 39–46.

77 L. del Río, G. Marbán *Appl. Catal., B* **150–151** (2014) 370–379.

78 D. Teschner, A. Wootsch, O. Pozdnyakova, J. H. Sauer, A. Knop-Gericke, R. Schlögl *React. Kinet. Catal. Lett.* **87** (2006) 235–247.

79 L. Xu, Y. Ma, Y. Zhang, B. Chen, Z. Wu, J. Jiang, W. Huang *J. Phys. Chem. C* **114** (2010) 17023–17029.

80 T.-L. Chen, D.R. Mullins *J. Phys. Chem. C* **115** (2011) 3385–3392.

81 L. Óvári, S.K. Calderon, Y. Lykhach, J. Libuda, A. Erdőhelyi, C. Papp, J. Kiss, H.-P. Steinrück *J. Catal.* **307** (2013) 132–139.

82 E. de Smit, F.M.F. de Groot, R. Blume, M. Hävecker, A. Knop-Gericke, B.M. Weckhuysen *Phys. Chem. Chem. Phys*. **12** (2010) 667–680.

83 N. Hou, Y. Zhang, M. Meng *J. Phys. Chem. C* **117** (2013) 4089−4097.

84 Y. Zhang, M. Meng, F. Dai, T. Ding, R. You *J. Phys. Chem. C* **117** (2013) 23691−23700.

85 A.L.M. da Silva, J.P. den Breejen, L.V. Mattos, J.H. Bitter, K.P. de Jong, F.B. Noronha *J. Catal.* **318** (2014) 67–74.

86 S. Helveg, J. Sehested, J.R. Rostrup-Nielsen *Catal. Today* **178** (2011) 42–46.

Supporting Information

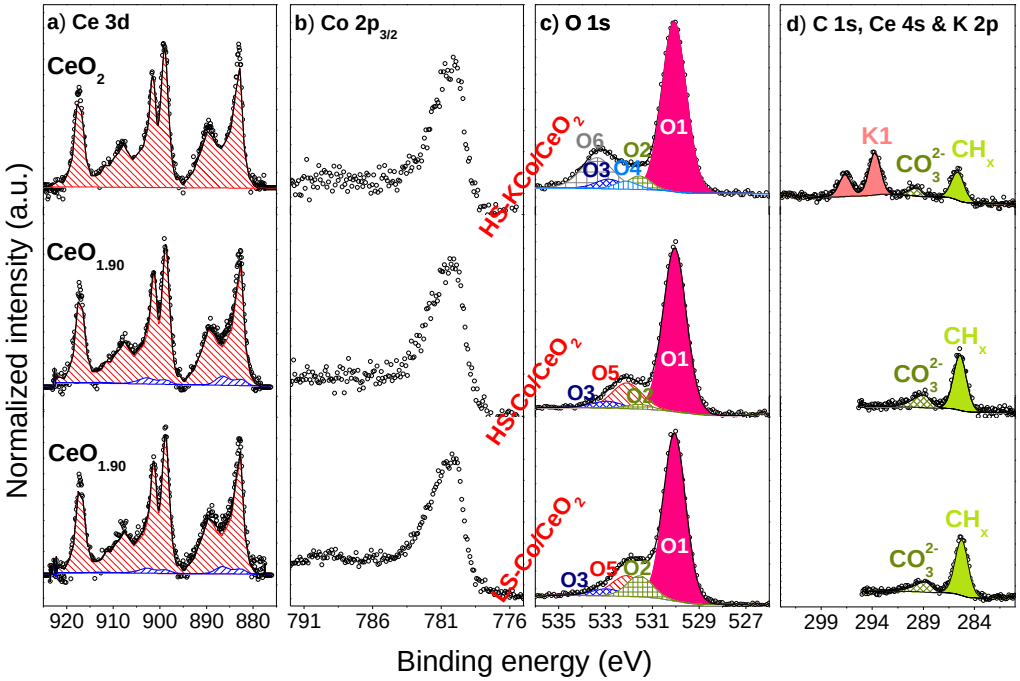

Fig. S1. The high resolution XPS spectra of (a) Ce 3d, (b) Co $2p_{3/2}$, (c) O 1s and (d) C 1s, Ce 4s & K 2p for fresh: LS-Co/CeO_2, HS-Co/CeO_2 and HS-KCo/CeO_2 catalysts; a) Ce(IV) (\\\), Ce(III) (///), b) Co(II) (\\\), Co(0) (///), c) O1 – lattice oxygen, O2 – hydroxyl and carbonate species, O5 – O^{2-} anions located near to oxygen vacancy sites (for the potassium catalyst this peak is at the same place as O4 component, therefore it can be also related to potassium carbonates), d) K1 – potassium carbonate.

Fig. S1a-d shows results of XPS characterization of as calcined samples. On the surface of all examined catalysts the Co_3O_4 spinel phase was detected [1, 2]. The oxygen components on the O 1s spectra were assigned as follows: peak O1 at 530.0 eV to oxygen in lattice of CeO_y and Co_3O_4, O2 (531.5 eV) to surface adsorbed –OH and/or CO_3^{2-} species, O3 (532.8 eV) to adsorbed H_2O, O4, (532.0 eV) to the potassium carbonate species, O5 (532.1 eV) to the O^{2-} anions located near to oxygen vacancy sites [3–5], but it seems that in this case this peak is related to the surface adsorbed carbonates, and O6 (533.4 eV) to O-C=O species. Presence of O-C=O groups on the surface of HS-KCo/CeO_2 catalyst can be a related to incomplete decomposition of citric acid during calcination. The component located at 285.4 eV on the C 1s spectra was assigned to presence of adventitious carbon impurities. The peak at 288.8 eV can be assign to the presence of CO_3^{2-} species overlapped with Ce 4s region, while the component at 290.3 eV to O−C=O species.

Table S1. The percentage contribution of different species in the Co 2p, Ce 3d, O 1s, C 1s high resolution XPS spectra of the catalyst after reduction and after the ESR.

Catalyst	H_2O/EtOH (mol/mol)	Contribution of given species in the XPS spectrum (%)									
		Co 2p	Ce 3d	O 1s				C 1s			
		Co(II)	Ce(III)	O_{latt}	OH	KCO_3, KO	H_2O	C=C	CH_X	C-O	CO_3^{2-}
LS-Co/CeO_2		0	55.3	81.6	18.4	0	0	0	55.8	0	44.2
HS-Co/CeO_2	H_2**	18.2	0	83.7	16.3	0	0	0	0	0	100
HS-KCo/CeO_2		5.0	9.95	66.1	13.0	21.0	0	0	0	0	100
LS-Co/CeO_2		4.8	55.1	57.6	31.3	0	11.1	100	0	0	0
HS-Co/CeO_2	3/1	13.9	50.6	65.9	20.4	0	13.8	100	0	0	0
HS-KCo/CeO_2		5.7	61.7	46.2	15.7	36.0	2.1	39.9	0	15.4	41.7
LS-Co/CeO_2		16.4	47.1	51.1	30.3	0	18.6	0	59.7	0.0	40.3
HS-Co/CeO_2	9/1	30.3	33.7	69.2	21.2	0	9.6	52.1	0	15.7	32.1
HS-KCo/CeO_2		20.1	68.2	30.5	23.8	42.5	3.2	0	0	14.3	85.7
LS-Co/CeO_2		34.2	47.7	59.0	34.7	0	6.3	0	0	0	100
HS-Co/CeO_2	12/1	33.8	34.7	69.1	22.6	0	8.3	0	37.9	0	62.1
HS-KCo/CeO_2		33.6	78.1	6.9	15.7	60.5	16.9	0	0	8.5	91.5

**Results obtained after the catalysts' pre-reduction (H_2/Ar) at 420ºC for 1 h.

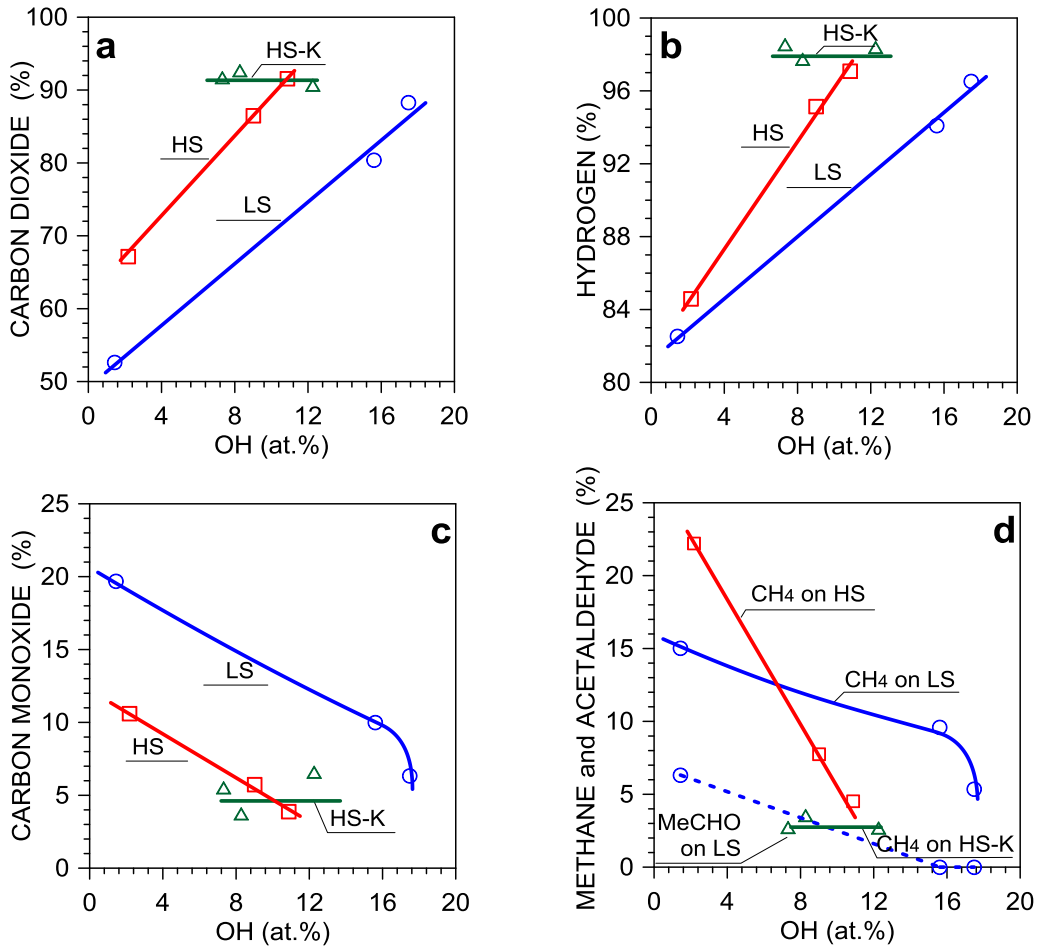

S. 2 Correlation of (a–d) the catalysts' selectivity towards H_2 and carbon-containing product with the concentration of hydroxyls on the surface of the LS-Co/CeO_2, HS-Co/CeO_2 and HS-KCo/CeO_2 catalysts under the ESR at 420ºC.

References for Supporting Information

1. M.C. Biesinger, B.P. Payne, A.P. Grosvenor, L.W.M .Lau, A.R. Gerson, R.St.C. Smart *Appl. Surf. Sci.* **257** (2011) 2717–2730.
2. S. Zhang, J. Shan, Y. Zhu, A.I. Frenkel, A. Patlolla, W. Huang, S. J. Yoon, L. Wang, H. Yoshida, S. Takeda, F. Tao, *J. Am. Chem. Soc.* **135 (**2013) 8283−8293.
3. J.P. Holgado, R. Alvarez, G Munera, *Appl. Surf. Sci.* **161 (**2000) 301–315.
4. J.P. Holgado, G. Munuera, J.P. Espinos, A.R. Gonzalez-Elipe, *Appl. Surf. Sci.* **158** (2000) 164–171.
5. M.A. Henderson, C.L. Perkins, M.H. Engelhard, S. Thevuthasan, C.H.F. Peden, *Surf. Sci.* **526** (2003) 1–18.

CHAPTER

4

Time–dependent surface state of Co/CeO_2 catalysts and their performance in the steam reforming of ethanol

OUTLINE

Abstract

Cobalt-based catalysts with ceria supports were examined in the ESR conditions ($H_2O/EtOH$ = 12/1 mol/mol, 420°C) for changes in their surface composition and catalytic performance with time-on-stream. It was found that the active phase of the unpromoted nano-catalyst was progressively oxidized, whereas in micro-ceria supported one, and potassium-promoted catalyst, cobalt, after initial oxidation, was progressively reduced with time-on-stream. For both micro- and nano-supports, the increase of Ce(III) percentage contribution on the surface was noted. The catalysts exhibited stable catalytic performance, whereas H_2 and CO_2 yield over the LS-catalyst improved with the reaction time. The surface coverage by hydroxyls and potassium bonded to oxygen species improve the catalytic properties, while diminish the amount and change the type of coke formation.

Introduction

Cobalt-based catalysts are one of the most extensively studied systems [1–18] for ethanol steam reforming (ESR), due to their low costs (comparing to noble metals) [11, 12], high activity for C–C bonds cleavage, good selectivity towards hydrogen and carbon dioxide in the low temperature range (350–450ºC) [19–21]. Among various oxides, ceria is widely suggested as a potential support for cobalt-based catalysts, designated to the ESR reaction. The excellent properties of this support have been discussed in numerous articles [1, 4, 22, 23] and reviews [24–26].

The increased attention has been paid on the role of redox properties [27–31], oxygen mobility, and oxygen storage capacity of this oxide [1] in improving catalysts' stability by inhibition of coke formation, and prevention of metal particles sintering [1, 32, 33]. Recently it was found that a support nature influences the active phase oxidation state [33–37]. Ambient Pressure X-Ray Photoelectron Spectroscopy Studies [37] showed that the cobalt oxidation state in pre-oxidized (O_2, 0.2 mbar) Co/CeO_2 (420ºC) and Co/ZnO (400ºC) catalysts differ. Cobalt supported on ceria was completely oxidized to Co_3O_4, whereas significant amounts of unreduced CoO-like oxide (probably due to formation of $Zn_{1-x}Co_xO$ solid solution) remained on the surface of Co/ZnO. The shape of spectra recorded under reducing atmosphere (H_2, 0.2 mbar) showed the ceria-supported catalyst's reduction to a extent, where metallic form was dominant, however, some unreduced cobalt oxide species also remained. Characteristic CoO-like oxide, recorded after pre-oxidation of Co/ZnO, resisted in the reducing environment. Under the ESR (H_2O/EtOH = 3/1 mol/mol, 0.2 mbar), cobalt supported on ceria was readily reduced to the metallic state, whereas particles supported on zinc oxide proved stay in the same, extremely stable [37] partly oxidized form. E. Martono and J.M. Vohs. [34] suggested that reducible supports as ZnO or CeO_2 ensure facile oxygen transport from the oxide to metal (resulting in partial oxidation of metal) [38], whereas, the oxygen exchange is limited on refractory supports as MgO or ZrO_2. In the light of aforementioned work [37], it seems that ceria's role in cobalt particles oxidation is limited. Also, P. Osorio-Vargas et al. [32] stated that the role of ceria in oxidation of metallic particles to less active oxides is rather unlikely. According to this group ceria possibly recover the metallic state of the active phase, maintaining in this way a high catalyst's selectivity to hydrogen. Note that *in situ* XRD studies [38] performed over

cobalt supported on ceria during ESR showed an increase in the reduction of cobalt oxides with time-on-stream.

Leaving aside the role of ceria in cobalt's oxidation enhancement, opinions are divided on which form of cobalt (metallic [35, 38–44], or oxidized [45–47]) is more active in the ESR. U.S. Ozkan and co-workers [38] found that regardless of the initial pre-treatment (pre-oxidation or pre-reduction), very similar Co(0)/Co(II) ratio was observed at reaction temperature of 450ºC. At this temperature also the amounts of carbon dioxide formed reached the same level. Studies of J. Llorca et al. [43] and A.R. Passos et al. [48] also suggested the existence of equilibrium between Co(0)/Co(II) under the ESR. The co-existence of both, in the reaction condition, is an undeniable fact [30, 38], therefore, there were suggestions that easy exchange between Co(0)↔Co(II) is responsible for cobalt's activity in the ESR [43, 47].

There are a few available works, that discuss the role of each form of cobalt in the ESR reaction pathways [44, 49–51], and their influence on surface's poisoning by coke formation [48, 49]. Some authors believe that divalent species of cobalt play a role in a catalyst's stabilisation over time, whereas metallic particles are responsible for coking [47–49, 52]. For example, results of time resolved *in situ* X-ray Absorption Spectroscopy combined with *on-line* mass spectrometry carried out over cobalt alumina-supported catalysts showed that the catalyst with the lowest share of CoO_x moieties suffered for marked deactivation accompanied by coke accumulation [48].

Up to now there are a few available papers devoted to studies of the ESR reaction conditions' influence on catalysts' composition. Some of them discuss the role of pre-treatment and/or initial oxidation state [38, 44, 48, 53], or reaction temperature [38, 48, 54] on catalysts' surface state. S.S.-Y. Lin et al. [21] showed that the extent of cobalt oxidation is influenced by the H_2O/EtOH molar ratio. The work of B. Bayram et al. [38] concerned the change of chemical composition of the surface and ESR selectivity as a function of time-on-stream. A pre-oxidized Co/CeO_2 catalyst's surface evolution under the ESR (H_2O/EtOH = 10/1 mol/mol) at 500ºC was investigated. It was found that the extent of reduction of cobalt oxide species with the time was progressively increasing.

Meeting the demand to understand the surface re-organisation in the course of the ESR, the XPS studies combined with time-dependent (up to 7 h) catalytic performance experiments, were performed. The aim of this work was *(i)* to present the

influence of cobalt and ceria support dispersion and potassium promotion on catalysts' reduction-oxidation behaviour in the ESR conditions ($H_2O/EtOH$ = 12/1 mol/mol, 420ºC, p_{total} = 1 atm), *(ii)* to discuss the catalytic properties of the examined catalysts, *(iii)* to correlate the surface state with catalytic performance of ceria-supported catalysts, *(iv)* to investigate the influence of oxygen-containing species on amounts of formed coke and its type.

1. Experimental

1.1. Catalysts preparation and characterization

This studies were performed on the unpromoted cobalt-based nano- (HS) and micro-ceria (LS) supported catalysts, as well as on the potassium-promoted nano-catalyst (HS-K), preparation and characterization (XRF, XRD, nitrogen adsorption, hydrogen chemisorption, H_2-TPR) of which were presented in details in the experimental section of the Chapter 3.

1.2. Combined XPS and catalytic performance experiments

The detailed description of experimental set-up and reduction procedure can be find in the experimental section of the Chapter 3.

After reduction procedure and XPS characterization, samples were transferred in UHV to the high pressure reactor. Prior to the reaction, samples were heated in the stream of Ar (50 cm^3/min, p_{total} = 1 atm) with the ramp rate 10ºC/min up to 420ºC. Water/ethanol vapours (molar ratio of 12/1, 3 cm^3/min) diluted in Ar (50 cm^3/min) were introduced to the reactor (by heated lines) at the reaction temperature (420ºC) by a Controlled Evaporation and Mixing (CEM) System (Bronkhorst). The ESR (420ºC, p_{total} = 1 atm) was carried out over 1 h (except the potassium-promoted Co/CeO_2; in this case, the ESR was carried out for 15 min due to reason described in the results part of Chapter 3). Next the flow of vapours was stopped and the samples were quenched in the stream of Ar till 80ºC, and then transferred in vacuo to the XPS analysis chamber. After the XPS characterization the ESR reaction was carried out over the samples for 2 and then 4 h (in total 7 h). After each reaction cycle, the samples were characterized by means of XPS.

In the course of the ESR reaction, carried out in the high pressure cell, the composition of gas phase products (H_2, CO_2, CO, CH_4) was monitored *on-line* by means of a micro-GC (Agilent, 490-GC).

1.3. Catalytic tests in a fixed-bed reactor

The studies of ESR catalytic behaviour (H_2O/EtOH = 12/1 mol/mol, 420ºC, p_{total} = 1 atm) were carried out also in a fixed-bed continuous-flow quartz reactor (Microactivity Reference unit, PID Eng & Tech.) under atmospheric pressure, as described in the experimental section of the Chapter 3.

The calculations of ethanol and water conversions, selectivities to hydrogen and carbon-containing products were presented in details in the experimental section of the Chapter 3, with the proviso that in the formula for H_2 selectivity, methane was the only hydrogen-containing product of the ESR among carbon-containing products.

2. Results and discussion

2.1. XPS characterization of the Co/CeO_2 catalysts during time-on-stream

This part of the work is aimed at understanding changes, on the surface of ceria-supported catalysts, occurring during the ESR (H_2O/EtOH = 12/1 mol/mol, 420ºC, p_{total} = 1 atm). In order to follow all changes, first, the influence of time-on-stream on catalyst's surface state will be discussed. In these consideration the state of the surface after catalyst's reduction was taken as the initial one (point 0 on time-on-stream axis x). After discussing the changes of elements' (cobalt, cerium, oxygen and potassium) atomic percentage contribution, the chemical state of these components isdescribed in details, basing on high-resolution XPS spectra.

Figs. 1a-d depict the surface's composition changes of main components versus reaction time. The results of changes in percentage contribution of carbon, one can find in Table S1 of Supplementary Information. Since the surface's atomic percentage contribution of carbon refers to the sum of various carbon-containing species (e.g., C=C, CH_x, C−O, CO_3^{2-}), the influence of the reaction time on carbon deposition will be discussed later.

The most prominent changes in terms of cobalt and ceria percentage contribution (Fig. 1a and b, see also Supplementary Information Table. S1), after the first ESR cycle, carried out over pre-reduced samples, occur on the surface of the HS-K

catalyst. The decrease of cobalt and ceria percentage contribution might be related to the surface's enrichment in potassium-containing species (Fig. 1d), which is probably related to potassium re-dispersion, as a result of its high affinity to water. The segregation of potassium species was previously also reported by the group of R. Espinal [46]. The extension of the reaction time to 7 h led to the conclusion that potassium-containing species re-agglomerate, as reflected in the decrease of their percentage contribution on the surface (Fig. 1d). Among examined catalysts, the potassium-promoted one, after 7 h on-the-stream, exhibited the highest percentage contribution of oxygen species (Fig. 1c). On the surface of promoted catalyst the abundance of oxygen increased from 50 to 67% with the reaction time.

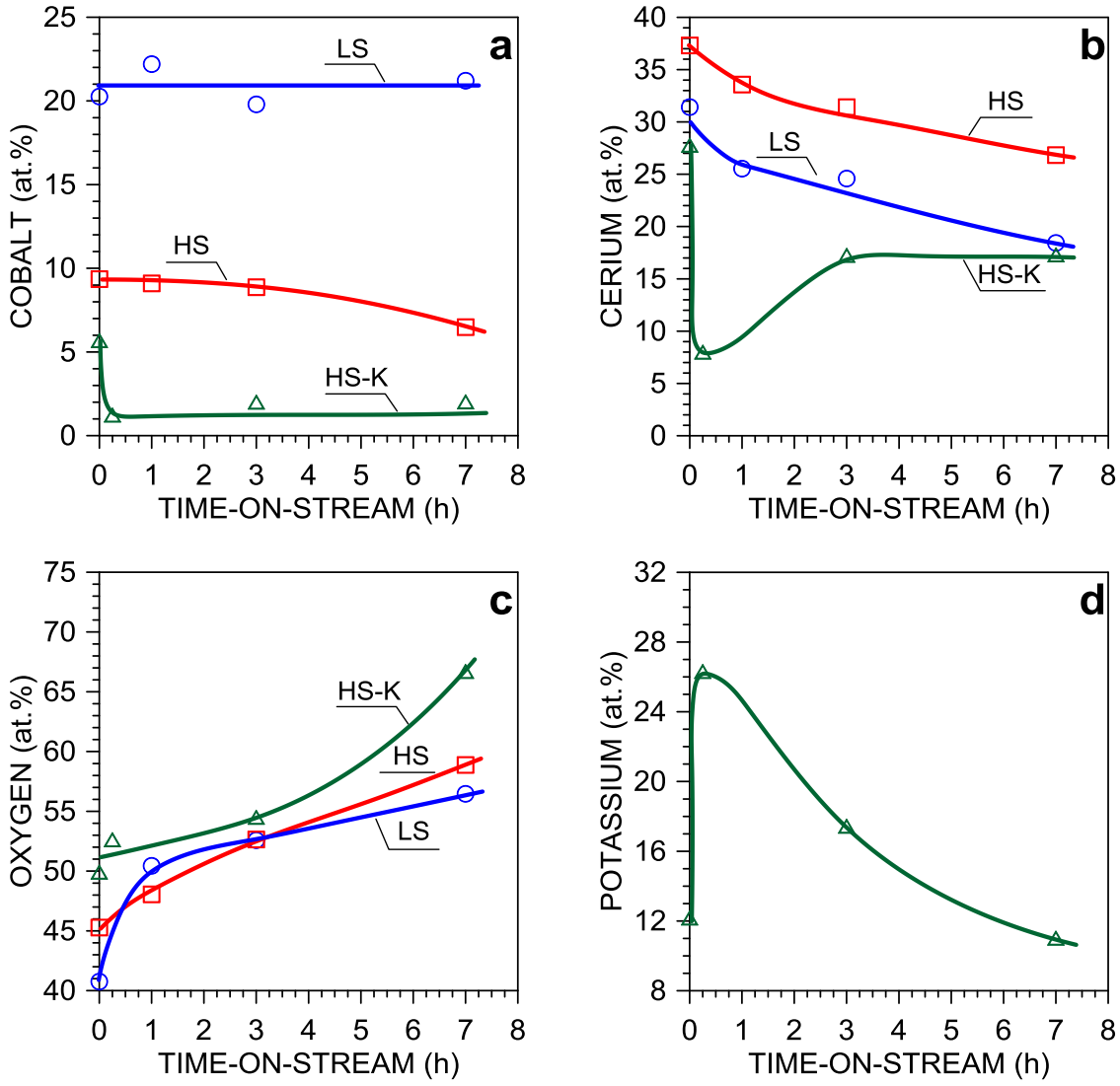

Fig. 1 The changes of the elemental surface's composition versus reaction time (H_2O/EtOH = 12/1 mol/mol, T = 420ºC, p_{total} = 1 atm). Point "0" on x-axis refers to the composition of the samples pre-reduced in hydrogen (420ºC).

Turning now to the unpromoted atomic contribution catalysts, it was found that in terms of the oxygen percentage, they exhibit the same tendency as the HS-K, meaning, the oxygen abundance is time dependent (Fig. 1c). For the HS-catalyst the difference between the percentage contribution of oxygen on the surface of the pre-reduced sample and the catalyst after the first cycle of the ESR, was less than 3%. Note that, similar result was obtained for the HS-K catalyst (Fig. 1c). On the LS-catalyst's surface (Fig. 1c), after reaction mixture introduction, the amount of oxygen species increased significantly in the first one hour of the reaction. However, after then the abundance of oxygen for both; the LS- and HS-catalysts was almost the same.

It is not clear what caused the continuous decrease of ceria percentage contribution, in the case of the unpromoted catalysts (Fig. 1b); however, it might be expected that this phenomenon is related to the increase of oxygen amounts on the surface. It can be suggested that the layer of adsorbed oxygen-containing species, formed by water dissociation, covered the support's surface and attenuate the Ce 3d signal.

Figs. 2, 4, 5 (a–d) show the high resolution XPS spectra obtained after the ESR reaction (H_2O/EtOH = 12/1 mol/mol, 420ºC) carried out over the pre-reduced (H_2/Ar, 420ºC) ceria-supported catalysts: LS (Fig. 2), HS (Fig. 4) and HS-K (Fig. 5).The Ce 3d core level spectra (Fig. 2a, 4a, 5a) were fitted with reference curves recorded over oxidized – CeO_2 (\\\) and reduced – Ce_2O_3 (///) cerium foil. The Ce $3d_{5/2}$ spectrum consist of two doublets pair. The pair located at 881.7 and 886 eV comes from Ce(III) [21, 37, 55], whereas components at 882.8 and 889.7 eV are related to the presence of Ce(IV). For the fitting procedure of Co $2p_{3/2}$ spectra, two components recorded on Co(0) and CoO reference samples were used (Fig. 2b, 4b, 5b). The Co $2p_{3/2}$ spectra were fitted with two peaks: first, with a characteristic asymmetric shape [56] (778.4 ± 0.3eV), related to the presence of metallic cobalt (///) [1, 21, 23, 35, 37, 44], and the second one (at 781.2 ± 0.3 eV) – formally ascribed to the Co(II) (\\\) species [21, 49, 57, 58].

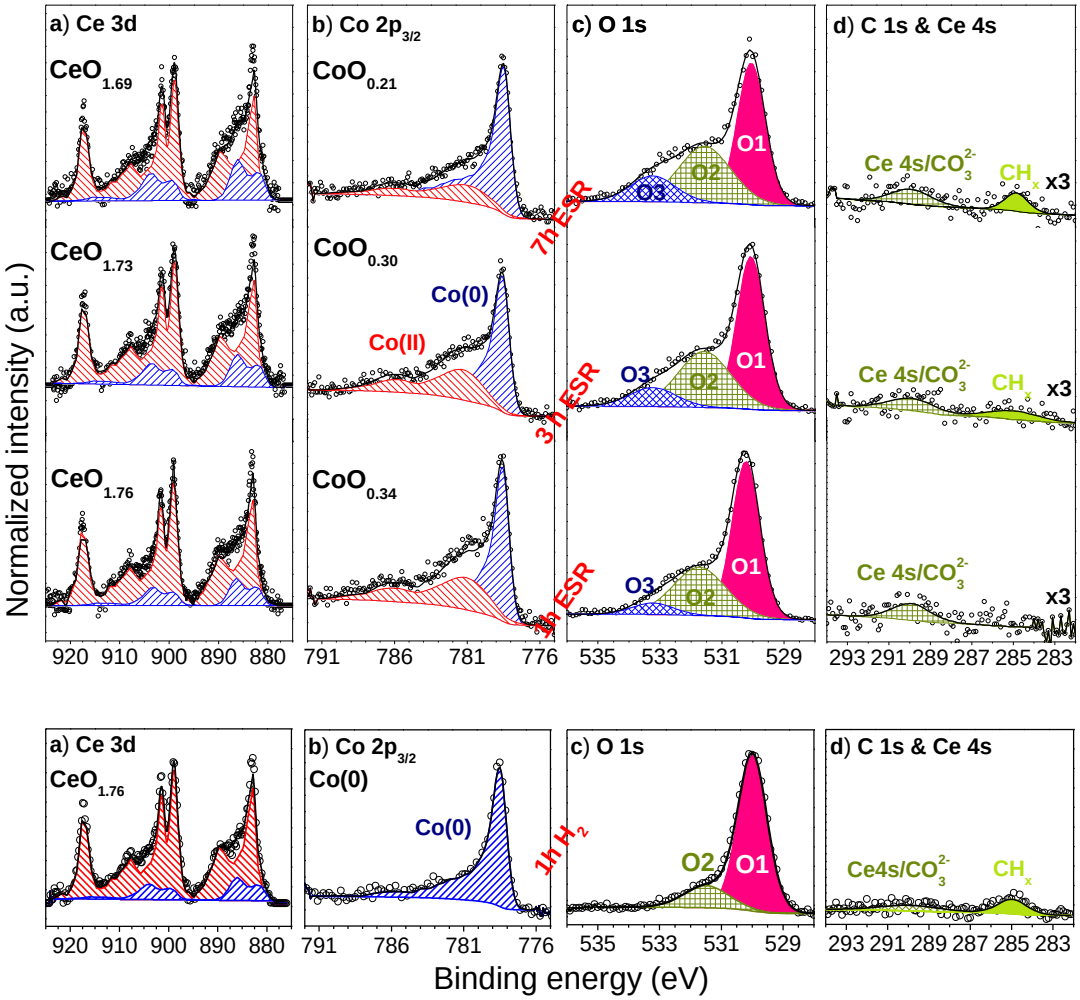

Fig. 2. The high resolution XPS spectra of (a) Ce 3d, (b) Co $2p_{3/2}$, (c) O 1s and (d) C 1s & Ce 4s collected after reduction in hydrogen (H_2/Ar, 420ºC), and after the ESR (H_2O/EtOH = 12/1 mol/mol, T = 420ºC, p_{total} = 1 atm) carried out over the pre-reduced LS-Co/CeO_2 catalyst; a) Ce(IV) (\\\), Ce(III) (///), b) Co(II) (\\\), Co(0) (///), c) O1 – lattice oxygen, O2 – hydroxyl and carbonate species, O3 – water.

After the first one hour of the ESR, the Co 2p XPS spectra recorded for the LS-catalyst revealed the presence of a cobalt oxide-like species (further abbreviated as CoO_x) (Fig. 2b), meaning that metallic cobalt, present after reduction (Fig. 2b, bottom picture), underwent oxidation. The formation of CoO_x and Co–OH on metallic cobalt, as well as on a Co/CeO_2, was previously experimentally demonstrated after successive cycles of water exposure [30, 38, 59]. The re-oxidation of metallic cobalt particles was also noted after a catalyst's exposure to the H_2O/EtOH vapours molar ratio of 4 at 450ºC [21]. After 3 h on-the-stream, some differences between the catalysts' surface state can be found. Deconvoluted spectra of the LS-catalyst suggest slight reduction of cobalt (Fig. 2b). However, one should note that after 3 h on-the-stream, the changes of the Co 2p XPS spectrum (Fig. 2b) are marginal; and within the error range of the fitting

process. Pronounced decrease of the CoO_x intensity might be noticed after extended time of the reaction (7 h ESR, Fig. 2b top picture, see also Fig. 3a).

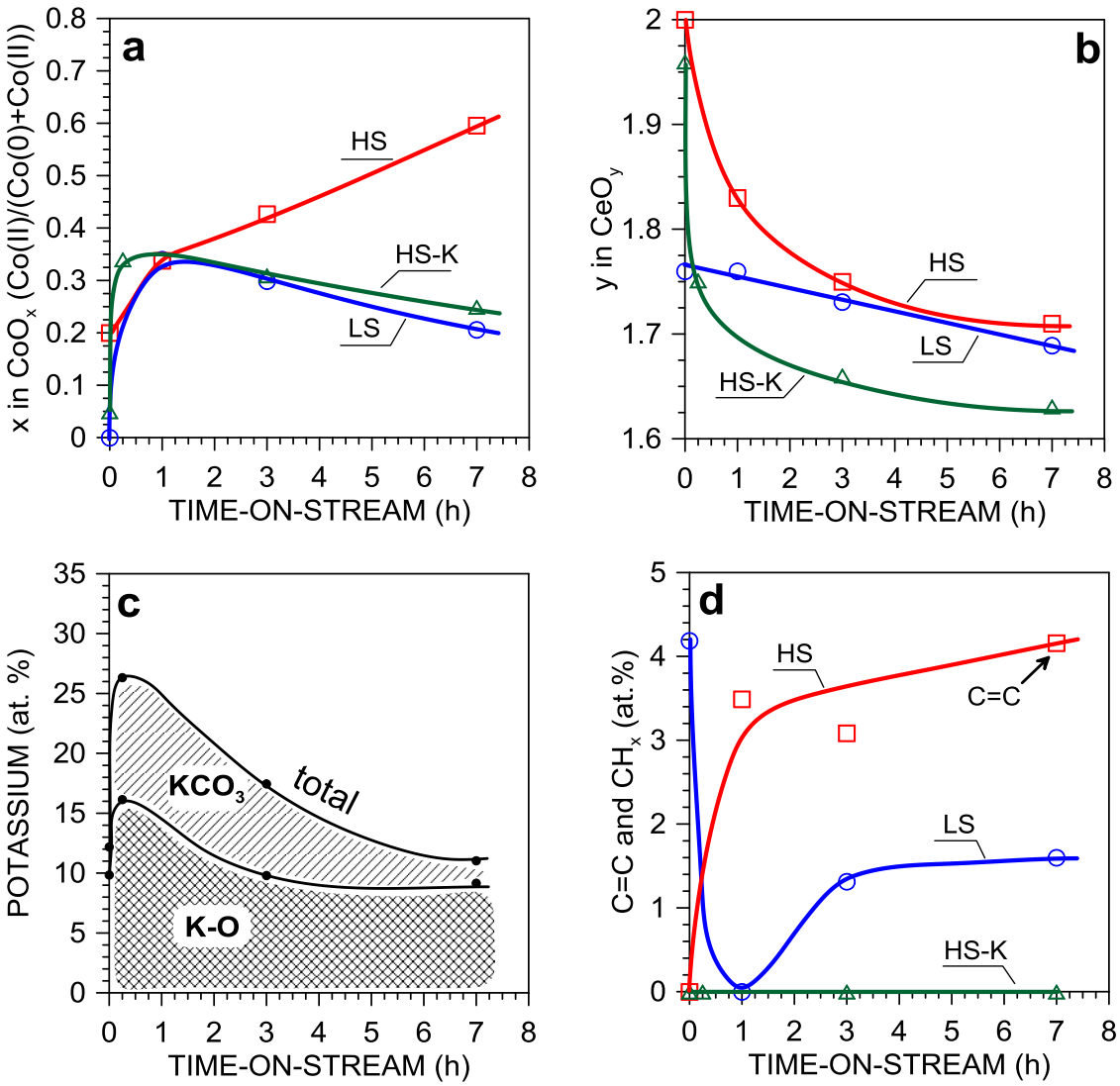

Fig. 3 The changes of (a) cobalt oxidation state (CoO_x), (b) ceria valence state (CeO_y), (c) potassium-containing species, (d) amount of C=C and CH_x species, with the reaction time (H_2O/EtOH = 12/1 mol/mol, 420ºC).

The shape of Ce 3d spectra of the pre-reduced sample and of the LS-catalyst after the first one hour of the ESR did not change significantly, which was evidenced by the same ceria valence state ($CeO_{1.76}$). The differences between ceria oxidation state are better visualized in Table S2 (Supporting Information), where it was shown that the percentage contribution of Ce(III) ions on the catalyst's surface slightly decreased after the reaction mixture introduction. This confirms that both main catalyst's component — cobalt and ceria — were re-oxidized to some extent by the reaction mixture. The changes on the Ce 3d spectrum recorded after three hours of the ESR (Fig. 2a, third picture from the bottom) are rather small, as compared to the spectra collected after 1 h.

However, more clear evidence of cerium oxide reduction might be observed in Table S2 in Supporting Information. It is evident that the percentage contribution of Ce(III) species increased from 48%, after the first hour of reaction, to 54% after three hours on-the-stream. After seven hours on-the-stream, this value increased even more – to 62% (Table S2 in Supporting Information), which was reflected in the shape of Ce 3d spectrum (Fig. 2a, top picture). The described tendency is summarized in Fig. 3b, and it clearly demonstrates linear, progressive reduction of cerium oxide with the reaction time.

In Fig. 1c it was shown that the percentage contribution of oxygen on the surface of the LS-catalyst increased rapidly after the first hour of the ESR. The high-resolution O 1s spectrum (Fig. 2c) of this catalyst allowed to clarify what caused this increase. The O 1s core level of the pre-reduced sample was fitted with two components, whereas in the case of the sample after the ESR, three components were resolved. The O1 component, located at 530.1 eV was assigned to oxygen in the lattice of ceria [60] and cobalt oxide (CoO_x), as well [49]. The peaks, at higher binding energies were attributed to the presence of oxygen-containing species, namely hydroxyls (O2; 531.6 ± 0.2 eV) [37, 56, 59], and adsorbed water (O3; 532.8 ± 0.2 eV) [59, 61]. As compared to the spectrum obtained for the pre-reduced sample, it can be concluded that the increase of oxygen percentage contribution on the catalyst's surface (Fig. 1c) is definitely related to the surface's coverage by hydroxyls and water. As for the influence of the reaction time on the shape of O 1s spectra, based on Fig. 2c and Table S2 (Supporting Information), the progressive intensity increase of both, hydroxyls and physisorbed water, can be noticed.

The high resolution spectrum of C 1s core level shows that after first one hour of the reaction the surface of the LS-catalyst was almost carbon free (Fig. 2d). Only a small peak at 290.0 ± 0.5 eV (Fig. 2d) indicates for the presence of adsorbed carbonates [62, 63]. However, one should keep in mind that this peak strongly overlaps with Ce 4s core level [63]. It is worth noticing that the reaction mixture appears to be more efficient than hydrogen in cleaning of the surface from adsorbed carbon-containing impurities (Fig. 3d). The formation of carbonaceous deposit (CH_x type) on the surface of the LS-catalyst was observed after 3 hours on-the-stream (Fig. 2d) — peak located at 284.9 eV. According to the calculations based on high resolution spectra, the percentage contribution of CH_x species slightly increased after 7 hours of the reaction (Fig. 3d). Another component on the C 1s spectrum (Fig. 2c),

at 290.0 eV increased only slightly, which was assigned to the small increase of percentage contribution of carbonates on the catalyst's surface.

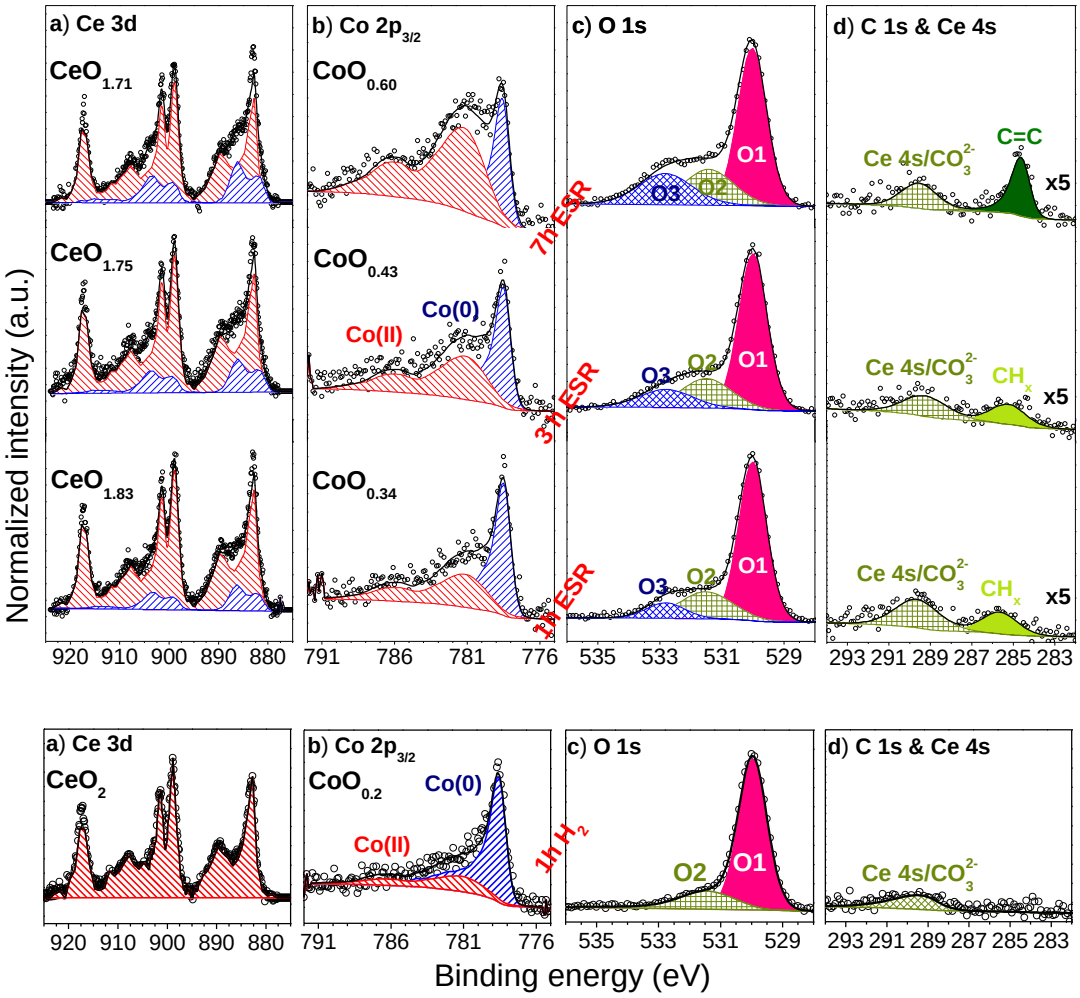

Fig. 4. The high resolution XPS spectra of (a) Ce 3d, (b) Co 2p$_{3/2}$, (c) O 1s and (d) C 1s & Ce 4s collected after reduction in hydrogen (H$_2$/Ar, 420ºC), and after the ESR (H$_2$O/EtOH = 12/1 mol/mol, T = 420ºC, p$_{total}$ = 1 atm) carried out over the pre-reduced (H$_2$/Ar, T = 420ºC) HS-Co/CeO$_2$ catalyst; a) Ce(IV) (\\\), Ce(III) (///), b) Co(II) (\\\), Co(0) (///), c) O1 – lattice oxygen, O2 – hydroxyl and carbonate species, O3 – water.

The course of changes proceeding on the surface of the HS-catalyst with the reaction time, slightly differs, as compared to the LS-catalyst. This is especially evident when comparing the spectra of cobalt for these catalysts (Fig. 2b and Fig. 4b), and analyzing the course of the curves in Fig. 2a.

Even though, cobalt oxidation state after the reduction of the HS-catalyst was different to this found for the LS-catalyst (Fig. 2a). After the first one hour on-the-stream, both catalysts exhibited the same percentage contribution of Co(II) species in the overall Co 2p core level. The spectra collected after the third hour of the ESR show evidence of different oxidation-reduction behaviour of cobalt supported on

nano-ceria. Among all examined ceria-supported catalysts, the HS was the only one, prone to oxidation of cobalt particles (Fig. 3a) with the reaction time. In Fig. 4b the continuous oxidation of cobalt is manifested by the increase of the intensity of the Co $2p_{3/2}$ component located at 781.2 eV.

The calculated cerium oxide valence state changes with the reaction time (Fig. 3b and 4a). The reaction mixture induced higher concentration of Ce(III) ions on the catalyst' surface (lowering cerium oxide valence state) than hydrogen (Fig. 3b and Table S2 in Supporting Information). It is known that presence of metal facilitates reduction shell of ceria from Ce(IV) to Ce(III), leading to the formation (by *spill-over*) of bridging surface hydroxyl groups, which are associated with Ce(III) ions [4]. The formation of these hydroxyls might be related with dissociation of water and *in statu nascendi* hydrogen. The valence state of cerium oxide in the HS-catalyst was generally higher (less reduced) than for the low-surface counterpart. According to L. Qiu et al. [64], a lower concentration of Ce(III) found for the nano-ceria-supported catalyst is related to a higher oxygen diffusion from the bulk to the subsurface and surface due to higher defects' concentration in the nano-ceria. The result obtained in this study, as well as these presented in ref. [64], are in contrast to that observed by I.I. Soykal et al. [53, 65], who reported that smaller crystallites of ceria are more readily reducible than the larger ones.

Some authors [34, 36, 52, 63, 66], suggest that in unpromoted systems, ceria influences oxidation state of cobalt. Oxygen transfer will result in the increase of cobalt oxidation state, and reduction of ceria ($2CeO_2 + Co \leftrightarrow Ce_2O_3 + CoO$). This situation might be observed only in the case of the HS-catalyst, whereas this explanation cannot be applied to the other ceria-supported catalysts (LS and HS-K) from these studies. In the Chapter 3 it was presented that average size of cobalt crystallites for the HS-catalyst is the smallest (3.8 nm), therefore, their potential oxidation (by mobile oxygen from ceria lattice, or adsorbed hydroxyls) might proceed easier, due to the high concentration of low-co-ordinated sites (corners, edges, lattice defects), and the short distance from the centre of crystallite to the cobalt–ceria boundary. The available literature data [67] may suggest that apart from crystallites size, strong metal-support interaction results in poor catalysts' reducibility. The listed factors make highly-dispersed cobalt more prone to get oxidized (by water rich mixture), as compared to the low-dispersed one. S.S.-Y. Lin et al. [21, 67] studies of the Co/CeO_2-ZrO_2 (Ce/Zr = 3) with small cobalt crystallites size (6.4 nm) [67] showed that

after the H_2O/EtOH (4/1 molar ratio, 450ºC, 2.5 h) vapours introduction, followed by water exposure (450ºC, 4 h) [21], the catalyst's surface was even more oxidized. According to studies of A.M. da Silva et al. [68], small cobalt particles (<4 nm) is easy to deactivate due to their oxidation. Similar behaviour of the HS-catalyst might be observed in these studies after extension of the reaction time to 7 h, further, distinct oxidation of cobalt ($CoO_{0.60}$) confirmed susceptibility of small cobalt crystallites to oxidation in water-reach conditions. In this light the conclusion that in the case of highly-dispersed cobalt particles water form strong bonds with metallic cobalt sites, resulting in their marked oxidation [21], is strongly supported.

The number of components fitted to the O 1s spectra of the HS-catalyst, and their assignments are the same, as those for the low-surface area catalyst. One may note that the intensity of O2 component (Fig. 4c) is very similar after each XPS measurement, whereas the intensity of the component assigned to physisorbed water (O3) is increasing.

Interestingly, in opposite to the LS-catalyst, the surface of the HS was carbon free after reduction (Fig. 3d and Fig. 4d), whereas after first one hour of the ESR, the appearance of CH_x species (284.9 eV) in the C 1s spectrum, can be noticed. The lack of carbon deposit on the LS-catalyst's surface after the first hour can be related to the existence of "induction period", as mentioned in M. Greluk et al. [14]. This period is needed for the formation of stable nucleus of carbon. It might suggest that the mechanism of coke formation on the HS-catalyst's surface is different, but this would required further insight research. After the seventh hour of the reaction, the formation of carbon (284.6 eV) on the HS-catalyst surface is noticed (Fig. 4c).

The Co 2p XPS spectra recorded for the HS-K catalysts (Fig. 5b) showed that introduction of the reaction mixture (for 15 min) over the pre-reduced sample, caused rapid re-oxidation of metallic cobalt particles. After 3 h reaction time there are not significant changes of the Co 2p peak shape; however, the decrease of the Co(II) component's intensity (Fig. 5b) after 7 h on-the-stream, confirmed undoubtedly the progressive reduction of cobalt oxide-like phase. The comparison of the Co 2p spectra of the catalysts with high-dispersed ceria (Fig. 4b and 5b) clearly shows that potassium generally stabilizes metallic cobalt particles against oxidation (see also Fig. 3a), even though the oxidation state of cobalt after 15 min of the ESR was the same, as recorded for the unpromoted samples after 1 h. Studies of Z. He et al. [69] suggested that the stabilization of ceria supported metal particles against oxidation upon potassium

loading can be caused by a weaker metal-support interaction. On the other hand, N. Nejar et al. [70] stated that the reduction of transition metals' oxides is facilitated in the presence of potassium. The same conclusion was drawn in the Chapter 3. Moreover, it was reported that potassium species lower a catalyst' work function, thus redox processes occur more readily [71], which affect also catalytic properties of a material.

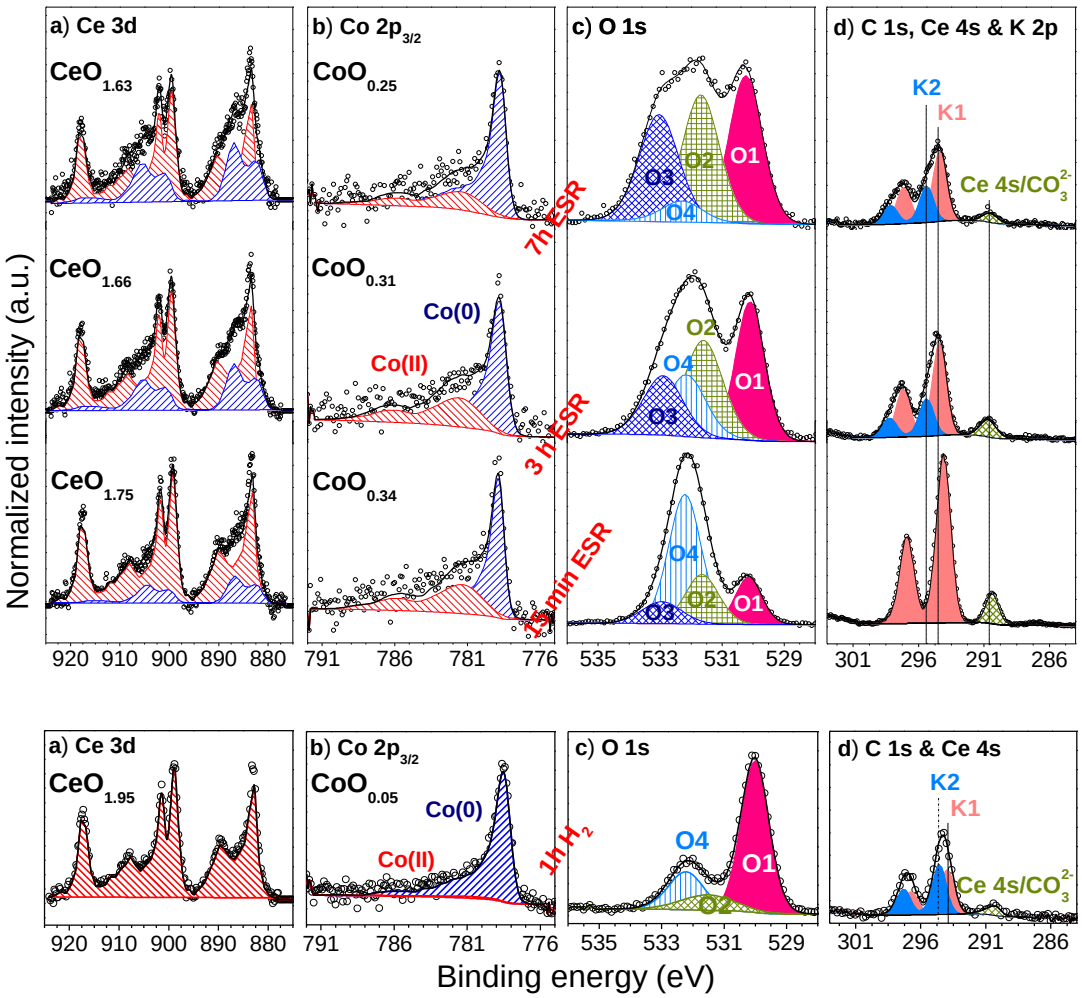

Fig. 5 The high resolution XPS spectra of (a) Ce 3d, (b) Co 2p$_{3/2}$, (c) O 1s and (d) C 1s & Ce 4s collected after reduction in hydrogen (H_2/Ar, 420ºC), and after the ESR (H_2O/EtOH = 12/1 mol/mol, T = 420ºC, p_{total} = 1 atm) carried out over the pre-reduced (H_2/Ar, T = 420ºC) HS-KCo/CeO$_2$ catalyst; a) Ce(IV) (\\\), Ce(III) (///), b) Co(II) (\\\), Co(0) (///), c) O1 – lattice oxygen, O2 – hydroxyl and carbonate species, O3 – water, O4 – carbonate species bonded to potassium, d) probable assignments of K1 and K2 species can be found in the text.

The initial state (after reduction) of cerium oxide in the HS-K differs slightly, as compared to the HS-catalyst (Fig. 3b). Small concentration of Ce(III) ions on the pre-reduced surface can be find, in opposite to that observed for the pre-reduced HS (Table S2 in Supporting Information). In the reaction mixture, the calculated valence state of cerium oxide decreased even more (Fig. 5a), and this tendency continued with

the extension of the reaction time (Fig. 3b). The lower valence state of ceria found in the potassium-promoted catalyst may be related to the increase of defect sites concentration in the surface of ceria [23, 72], as well as, enhanced formation [73] of oxygen-containing species [74], origination of which will be presented in the paragraph concerning the changes in the O 1s spectra.It is worth noting, that the addition of potassium influenced cerium valence state, generally lowering it, as compared to the unpromoted counterpart (Fig. 3b).

The O 1s spectra of the HS-K catalyst (Fig. 5c) are different than those previously presented in Figs. 2c and 4c. The difference is caused by the appearance, after pre-reduction, of a new component, named O4 (532.1 ± 0.2 eV), which is most likely related to a defective layer of potassium carbonates [75, 76] (further abbreviated KCO_3), as suggested in the Chapter 3. Note that, from Fig. 5c and 5d, it is evident that the increase of the intensity of the O4 component occurs simultaneously with the increase of K 2p and CO_3^{2-} components' intensity.

The calculations, presented in the Chapter 3, led to the conclusion that beside KCO_3 species, potassium might exist in another potassium to oxygen bonded form. This would not be surprising since in literature it was previously suggested that potassium may participate in redox cycles between K_xO_y and K_xO_{y+1} [77]. On the other hand, according to so far presented research [71], potassium species like, K_2CO_3, KOH, KNO_3, CH_3COOH cannot be distinguished in the K 2p spectrum. Therefore, the other form of potassium was simply named as K–O, and based on cited research [71], it would appear at the same binding energy as KCO_3 species. Since some K 2p spectra (compare spectrum after 15 min and 7 h of the ESR, Fig. 5d) exhibited small asymmetry towards higher binding energies, it was suggested that potassium species might have changed their electronic environment, which was manifested as an appearance of a new feature. The K 2p spectrum, therefore, was resolved into two potassium components, namely K1 and K2, where probably both are related to the KCO_3 and K–O sites, however, the K2 component may result from the change in local environment of potassium to oxygen bonded species (K1).

Returning to the discussion of the O 1s spectra, the percentage contribution of O4 component in the overall spectrum significantly increased after the reaction mixture introduction (Fig. 5c and Table S2 in Supplementary Information). The increase of O4 component's intensity was in line with the increase of the K 2p intensity (Fig. 5d). The results showed that after 15 min ESR the atomic percentage contribution of

potassium species increased slightly than twice, as compared to the pre-reduced sample (Fig. 3c). It should be highlighted that due to the surface's enrichment in potassium-containing species, which suggest their high dispersion and migration over the catalyst's surface, cobalt and ceria were barely seen in the XPS spectra. After 3 h, on-the-stream, the intensity of the O4 component decreased (Fig. 5c) which was followed by the increase of the percentage contribution of hydroxyls (O2), and water (O3) on the surface. The decrease of the intensity was also observed for the K 2p component, and for the peak formally ascribed mainly to the presence of carbonate (Fig. 5d). After 7 h of the reaction the further decrease of above mentioned components intensity, was noted. The intensity decrease of peaks, assigned to the presence of potassium-containing species, may be related to their agglomeration, or to their penetration into pores of the catalyst. Studies of N. Nejar et al. [70] showed that at 450ºC the loss of potassium in the gas stream does not occur.

It is important to mention that, the potassium promotion significantly hindered coke formation (Fig. 3d), probably caused by a presence of K–O sites (Fig. 3c). Potassium species neutralize acidic sites on catalysts' surface [46], and in addition, they reduce the contribution of disproportionation of carbon monoxide, which is regarded as one of a coke precursor [13, 14]. On the surface of this catalyst, the main carbon-containing species, were carbonates; negligible amounts of C–O species (Table S2 in Supporting Information), not marked in Fig. 5d, were also found after 15 min of the reaction.

2.2. The ESR catalytic performance of the catalysts

All catalysts within entire measurements exhibited 100% conversion of ethanol. Fig. 6 presents the results of catalysts' selectivity in the ESR at 420ºC. In graphs, presented in this section, zero on the time-on-stream scale is related to the time, when mixture vapours were introduced to the reactor, over the pre-reduced catalyst. In Fig. 6 it can be seen that generally the biggest changes in catalysts' selectivity were observed at the early stage of the ESR. As it is evidenced in Fig. 6a and b, after the first one hour of the ESR the catalysts showed high selectivity to hydrogen (96-98%) and carbon dioxide (90–93%), except for the LS-catalyst. Over this catalyst the selectivities to hydrogen and carbon dioxide were lower in the first three hours of the ESR reaction, and they were progressively increasing with the time-on-stream. A lower selectivity of this catalyst to the most desirable products, is related to a lower conversion of water

(18%), as compared to the other catalysts. In three hours in the reaction, the catalyst exhibited higher water conversion and better selectivity. Due to the excess of water in relation to the stoichiometry of the ESR, its maximum conversion is 25% only.

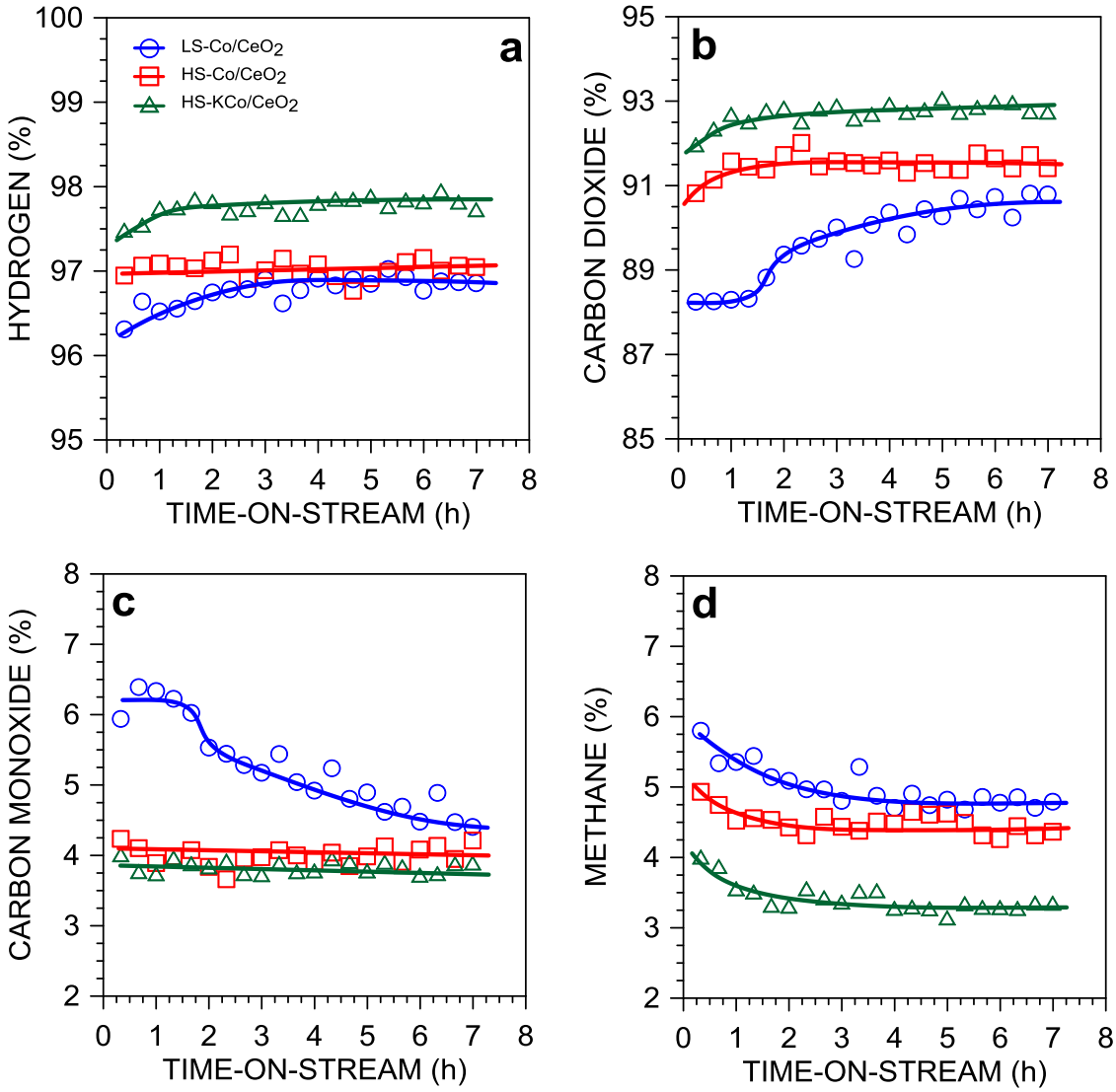

Fig. 6. The effect of time-on-stream on ceria-supported catalysts' selectivity towards hydrogen, carbon dioxide, carbon monoxide and methane (H_2O/EtOH = 12/1 mol/mol, 420ºC, p_{total} = 1 atm).

As it is shown in Fig. 7, both hydrogen and carbon dioxide yields were between 5.3–5.6 and 1.76–1.86 mol/mol_{EtOH}, which is in agreement with thermodynamics [78]. The highest yield of hydrogen was recorded over the HS-K catalyst.

The selectivities to undesirable by-products, as carbon monoxide and methane, were generally lower than 6.5%. It is worth noting that the tendencies observed in Fig. 6d, concerning the catalysts' selectivity to methane, are very similar for all catalysts. Whereas carbon monoxide selectivity curve obtained for the LS-catalyst differs significantly from the others. This chapter is not aimed to explain the reaction

pathway, it can be seen that there is a close link between the LS-catalyst's selectivity towards carbon monoxide (Fig. 6c) and carbon dioxide (Fig. 6b). However, it is unclear if the increase of the catalyst's selectivity towards carbon dioxide with simultaneous decrease of carbon monoxide formation is related to WGS reaction, or another pathway of ethanol transformation.

In general, among the examined catalysts, the LS exhibited the worst catalytic performance, which may result from low cobalt and ceria dispersion. In the case of catalysts with highly-dispersed ceria, it can be concluded that potassium doping resulted in the decrease of the catalyst's selectivity towards methane (Fig. 6d), which influenced formation of higher amounts of hydrogen (Fig. 6a) and carbon dioxide (Fig. 6b), being in line with previously reported results [15, 17].

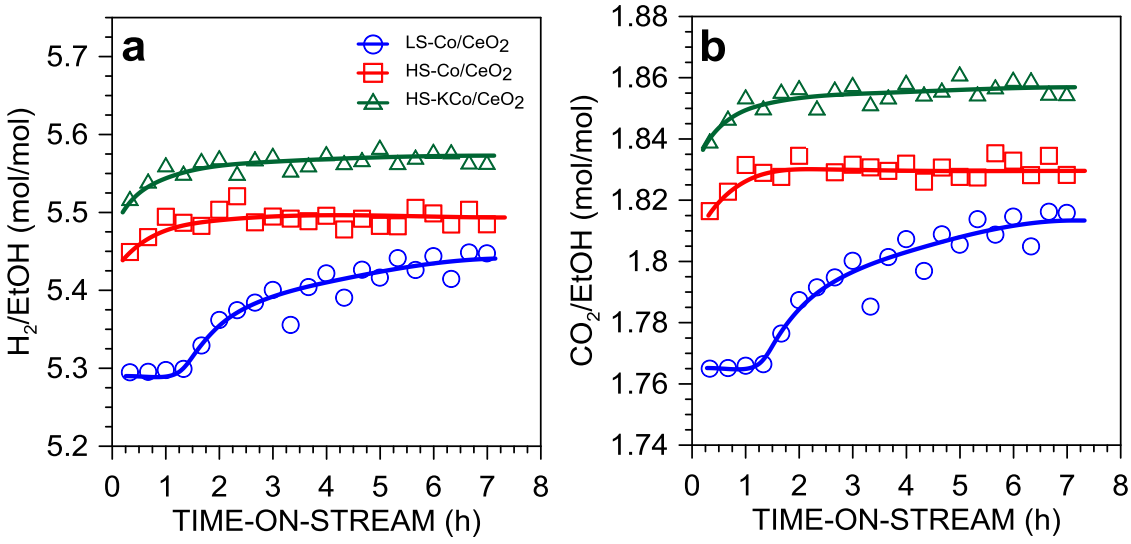

Fig. 7. The effect of time-on-stream on hydrogen (a) and carbon dioxide (b) yield for ceria-supported catalysts (H_2O/EtOH = 12/1 mol/mol, 420°C, p_{total} = 1 atm).

2.3. The influence of the surface state on ESR catalytic performance

The reaction time undoubtedly influences catalysts' composition (Fig. 1) and oxidation state of main components (Fig. 3a and 3b). However, the results showed no major impact of the main components oxidation state to the selectivity. The comparison of Figs. 3a and 6b, led to the conclusion that influence of CoO_x on catalysts' selectivity to carbon dioxide is rather limited. First of all, the same percentage contribution of CoO_x species result in different catalysts' selectivity. Moreover, the HS-catalyst's vulnerability to oxidation has no clear impact on catalytic properties of this sample. Very similar situation might be observed when considering the influence of cerium oxidation state on catalysts' selectivity to carbon monoxide. Comparing Fig. 3b and 6b

one may see that the biggest changes at the early stage of the ESR were observed for HS- and HS-K catalysts, whereas in terms of their selectivity to carbon dioxide (as well as to the other products), these changes were not so strongly marked. Additionally, after 2 h on-the-stream the selectivities of these catalysts towards carbon dioxide change very slightly, in contrast to the observation of cerium oxidation state. Therefore, similar to cobalt oxidation state, this factor might be not a dominant one for the selective transformations of ethanol.

The factor influencing unpromoted catalysts' selectivity is most probably the concentration of surface adsorbed hydroxyl species. However, the catalysts' selectivity does not depend only on hydroxyls abundance, as depicted in Fig. 8a. Similar to what was found in the Chapter 3, in the case of the LS-catalyst the surface coverage of OH species was the highest even though it exhibited the lowest ESR performance. It was suggested that apart from hydroxyls' concentration, the catalyst's morphology and hydroxyls species location, are also important factors controlling the selectivity. The active phase dispersion, therefore, the number of surface low-coordinated sites and the distance from the centre of cobalt crystallite to the cobalt–ceria surface border, should not be omitted, as discussed in details in the Chapter 3.

Turning now to the HS-K catalyst, changes in hydroxyls' concentration, with the time (Fig. 8a), are opposite than the selectivity to carbon dioxide which increases rather slightly. It suggested that apart from hydroxyls, another selective sites, probably related to the presence of potassium promoter on the catalyst's surface (i.e., K–O sites), are also involved. As depicted in Fig. 8b, the concentration of hydroxyls and K–O sites depends on the reaction time. The increase of hydroxyls abundance on the surface proceeds simultaneously with a decrease of K–O sites concentration. Very slow increase of the sum of these species (Fig. 8c) might be responsible for a slight improvement of the catalyst's selectivity towards carbon dioxide (Fig 6b).

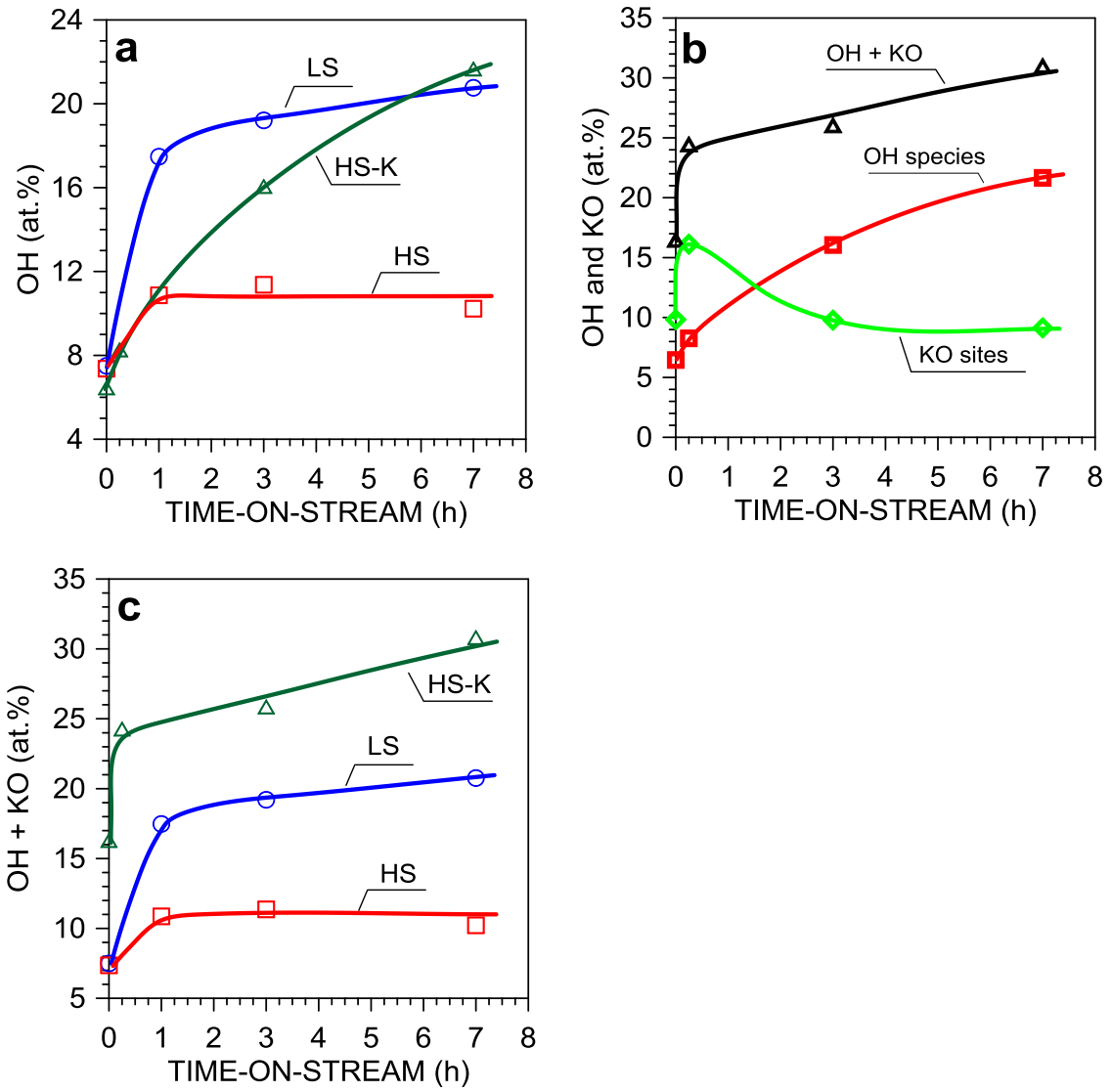

Fig. 8 The changes of hydroxyls and K–O sites with time-on-stream (H_2O/EtOH = 12/1 mol/mol, 420ºC) for ceria-supported cobalt catalysts.

The increase of surface adsorbed hydroxyls concentration was found to hinder the transformation of CH_x species into the fully dehydrogenated carbonaceous forms (Fig. 9a). In the case of potassium-promoted catalyst, the concentration of hydroxyls is not the only factor, that hinders formation of coke. This is based on the fact, that the similar concentration of hydroxyls does not necessarily result in the catalyst's coking (see Fig. 9a). If the influence of K–O sites is considered in addition to the hydroxyl groups, a linear correlation can be found (Fig. 9b). Based on the obtained results it can be suggested that in order to maintain the surface carbon free, it should be covered by easy accessible (not too strongly bonded, see the Chapter 1) oxygen-containing species, as hydroxyls and K–O sites.

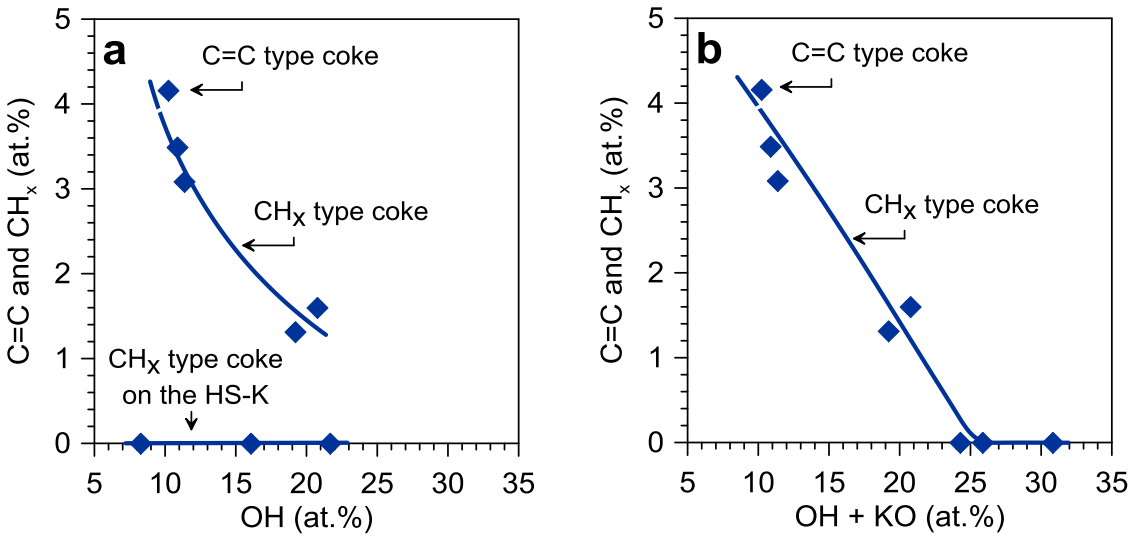

Fig. 9 Correlation of atomic percentage contribution of C=C and CH_x species with (a) hydroxyls concentration, and (b) sum of hydroxyls and K–O sites on the catalysts' surface.

Conclusions

This studies presented the influence of time-on-stream on surfaces' state, and ESR catalytic performance of cobalt-based catalysts with nano- and micro-ceria supports, as well as, potassium-promoted nano-ceria counterpart. It was found that cobalt particles supported on nano-ceria were prone to oxidation with the reaction time, whereas the other catalysts, even if were initially oxidized, were progressively reduced with time-on-stream. The reaction time influenced also cerium oxidation state. The percentage contribution of Ce(III) was found to increase on the surface of all catalysts. The catalysts' selectivity was not found to be influenced by oxidation-reduction behaviour of cobalt and ceria. In the case of unpromoted catalysts, the promoting role in the ESR was assigned to hydroxyls, the concentration of which depends on catalysts' dispersion and the reaction time. Since the LS-catalyst exhibited worse catalytic performance than the HS, even though the concentration of hydroxyls on its surface was higher, beside the abundance of hydroxyls, the catalyst's morphology and location where these species are chemisorbed, might be important as well.

Potassium addition introduced another type of selective sites, influencing the ESR selectivity. Apart of potassium was found to be bonded to carbonate species, whereas the remained amount of potassium probably exists on the surface as K–O sites, which are expected to play an important role in the ESR. The concentration of hydroxyls and K–O sites changed with the time-on-stream. The slight increase of the catalyst's selectivity to hydrogen and carbon dioxide was related to the sum of OH and

K–O sites. A decrease of K–O sites percentage contribution and simultaneous increase of hydroxyls concentration, with the reaction time. Moreover, the presence of both oxygen-containing species reduces coke formation, and hinders the transformation of CH_x species into fully dehydrogenated carbonaceous form.

References

1 H. Song, U.S. Ozkan *J. Catal.* **261** (2009) 66–74.

2 H. Song, L. Zhang, R.B. Watson, D. Braden, U.S. Ozkan *Catal. Today* **129** (2007) 346–354.

3 H. Song, B. Mirkelamoglu, U.S. Ozkan *Appl. Catal., A* **382** (2010) 58–64.

4 S.M. de Lima, A.M. da Silva, U.M. Graham, G. Jacobs, B.H. Davis, L.V. Mattos, F.B. Noronha *J. Catal.* **268** (2009) 268–281.

5 S.-W. Yu, H.-H. Huang, C.-W. Tang, C.-B. Wang Int. *J. Hydrogen Energy* **39** (2014) 20700–20711.

6 H. Wang, J.L. Ye, Y. Liu, Y.D. Li, Y.N. Qin *Catal. Today* **129** (2007) 305–312.

7 H. Song, U.S. Ozkan *J. Mol. Catal. A* **318** (2010) 21–29.

8 H. Wang, Y. Liu, L. Wang, Y.N. Qin *Chem. Eng. J.* **145** (2008) 25–31.

9 S.S.-Y. Lin, D.H. Kim, S.Y. Ha *Catal. Lett.* **122** (2008) 295–301.

10 S.S.-Y. Lin, D.H. Kim, S.Y. Ha *Appl. Catal., A* **355** (2009) 69–77.

11 P. Rybak, B. Tomaszewska, A. Machocki, W. Grzegorczyk, A. Denis, *Catal. Today* **176** (2011) 14–20.

12 A. Machocki, A. Denis, W. Grzegorczyk, W. Gac *Appl. Surf. Sci.* **256** (2010) 5551–5558.

13 G. Słowik, M. Greluk, A. Machocki *Mater. Chem. Phys.* **173** (2016) 219–237.

14 M. Greluk, P. Rybak, G. Słowik, M. Rotko, A. Machocki *Catal. Today* **242** (2015) 50–59.

15 M. Greluk, M. Rotko, A. Machocki *Catal. Lett.* **146** (2016) 163–173.

16 B. Banach, A. Machocki, P. Rybak, A. Denis, W. Grzegorczyk, W. Gac *Catal. Today* **176** (2011) 28–35.

17 B. Banach, A. Machocki, *Appl. Catal., A* **505** (2015) 173–182.

18 A. Machocki, T. Ioannides, E. Papadopoulou, B. Banach *Fuel Processing Technol.* **148** (2016) 341–349.

19 J. Llorca, P.R. de la Piscina, J.A. Dalmon, J. Sales, N. Homs *Appl. Catal., B* **43** (2003) 355–369.

20 J. Llorca, N. Homs, J. Sales, P.R. de la Piscina *J. Catal.* **209** (2002) 306–317.

21 S.S.-Y. Lin, D.H. Kim, M.H. Engelhard, S.Y. Ha *J. Catal.* **273** (2010) 229–235.

22 S.M. de Lima, A.M. Silva, I.O. da Cruz, G. Jacobs, B.H. Davis, L.V. Mattos, F.B. Noronha *Catal. Today* **138** (2008) 162–168.

23 Zs. Ferencz, A. Erdöhelyi, K. Baan, A. Oszkó, L. Óvári, Z. Kónya, C. Papp, H.-P. Steinrück, J. Kiss *ACS Catal*. **4** (2014) 1205–1218.

24 D. Zanchet, J.B.O. Santos, S. Damyanova, J.M.R. Gallo, J.M.C. Bueno *ASC Catal.* **5** (2015) 3841–3863.

25 J.L. Contreras, J. Salmones, J.A. Colín-Luna, L. Nuño, B. Quintana, I. Córdova, B Zeifert, C. Tapia, G.A. Fuentes *Int. J. Hydrogen Energy* **39** (2014) 18835–18853.

26 L.V. Mattos, G. Jackobs, H.D. Burtron, F.B. Noronha *Chem. Rev.* **112** (2012) 4094–4123.

27 M.G. Cutrufello, I. Ferino, V. Solinas, A. Primavera, A. Trovarelli, A. Auroux, C. Picciau *Phys. Chem. Chem. Phys*. **1** (1999) 3369–3375.

28 A. Birot, F. Epron, C. Descorme, D. Duprez *Appl. Catal., B* **79** (2008) 17–25.

29 H. Song, L. Zhang, U.S. Ozkan *Top. Catal.* **55** (2012) 1324–1331.

30 I.I. Soykal, H. Song, J.T. Miller, U.S. Ozkan *Top Catal.* **57** (2014) 785–795.

31 A. Trovarelli *Cat. Rev. Sci. Eng.* **38** (1996) 439–520.

32 P. Osorio-Vargasa, C.H. Camposb, R.M. Navarroc, J.L.G. Fierroc, P. Reyesa *Appl. Catal., A* **505** (2015) 159–172.

33 M. Konsolakis, Z. Ioakimidis, T. Kraia, G.E. Marnellos *Catalysts* **6** (2016) DOI:10.3390/catal6030039.

34 E. Martono, J.M. Vohs, *ACS Catal.* **1** (2011) 1414–1420.

35 V.M. Lebarbier, A.M. Karim, M.H. Engelhard, Y. Wu, B.-Q. Xu, E.J. Petersen, A.K. Datye, Y. Wang, *ChemSusChem* **4** (2011) 1679–1684.

36 S. Davidson, J. Sun, Y. Wang *Top Catal.* **56** (2013) 1651–1659.

37 S. Turczyniak, W. Luo, V. Papaefthimiou, N. S. Ramgir, M. Haevecker, A. Machocki, S. Zafeiratos *Top. Catal.* **59** (2016) 532–542.

38 B. Bayram, I.I. Soykal, D. von Deak, J.T. Miller, U.S. Ozkan *J. Catal.* **284** (2011) 77–89.

39 M.S. Batista, K.S. Santos, E.M. Assaf, E.A. Ticianelli *J. Power Sources* **124** (2003) 99–103.

40 H. Song, L. Zhang, U. S. Ozkan *Green Chem.* **9** (2007) 686–694.

41 M. Domínguez, E. Taboada, H. Idriss, E. Molins, J. Llorca *J. Mater. Chem.* **20** (2010) 4875–4883.

42 V.A. de la Peña O'Shea, N. Homs, E.B. Pereira, R. Nafria, P.R. de la Piscina *Catal. Today* **126** (2007) 148–152.

43 J. Llorca, J.A. Dalmon, P.R. de la Piscina, N. Homs *Appl. Catal., A* **243** (2003) 261–269.

44 A.M. Karim, Y. Su, M.H. Engelhard, D.L. King, Y. Wang *ACS Catal.* **1** (2011) 279–286.

45 L. del Río, G. Marbán *Appl. Catal., B* **150–151** (2014) 370–379.

46 R. Espinal, E. Taboada, E. Molins, R.J. Chimentao, F. Medina, J. Llorca *Appl. Catal., B* **127** (2012) 59–67.

47 S. Ogo, T. Shimizu, Y. Nakazawa, K. Mukawa, D. Mukai, Y. Sekine *Appl. Catal., A* **495** (2015) 30–38.

48 A.R. Passos, L. Martins, S.H. Pulcinellin, C.V. Santilli, V. Briois *Catal. Today* **229** (2014) 88–94.

49 M.P. Hyman, J.M. Vohs, *Surf. Sci.* **605** (2011) 383–389.

50 M.P. Hyman, E. Martono, J. Vohs, *J. Phys. Chem. C* **114** (2010) 16892–16899.

51 E. Martono *Mechanistic Studies of Alcohol Steam Reforming Catalysts*. 2013, University of Pennsylvania: Pennsylvania.

52 E. Martono, J.M. Vohs *J. Catal.* **291** (2012) 79–86.

53 I.I. Soykal, H .Sohn, U.S. Ozkan *ACS Catal.* **2** (2012) 2335–2348.

54 E. Varga, Z. Ferencz, A. Oszkó, A. Erdöhelyi, J. Kiss, *J. Mol. Catal. A* **397** (2015) 127–133.

55 B.E. Koel, G. Praline, H.-I. Lee, J.M. White *J. Electron. Spectrosc. Relat. Phenom.* **21** (1980) 31–46.

56 M.C. Biesinger, B.P. Payne, A.P. Grosvenor, L.W.M. Lau, A.R. Gerson, R.St.C. Smart *Appl. Surf. Sci.* **257** (2011) 2717–2730.

57 S. Zafeiratos, F. Paloukis, G. Papakonstantinou, D. Teschner, M. Hävecker, E. Vass, P. Schnörch, A. Knop-Gericke, R. Schlögl, B. Moreno, E. Chinarro, J.R. Jurado, S.G. Neophytides *Catal. Today* **157** (2010) 250–256.

58 S. Zafeiratos, T. Dintzer, D. Teschner, R. Blume, M. Hävecker, A. Knop-Gericke, R. Schlögl *J. Catal.* **269** (2010) 309–317.

59 L. Xu, Y. Ma, Y. Zhang, B. Chen, Z. Wu, J. Jiang, W. Huang *J. Phys. Chem. C* **114** (2010) 17023–17029.

60 A. Pfau, K.D. Schierbaum *Surf. Sci.* **321** (1994) 71–80.

61 A. Galtayries, J. Grimblot *J. Electr. Spectrosc. Rel. Phen.* **98–99** (1999) 267–275.

62 C. Padeste, N.W. Cant, D.L. Trimm *Catal Lett.* **28** (1994) 301–311.

63 L. Óvári, S.K. Calderon, Y. Lykhach, J. Libuda, A. Erdőhelyi, C. Papp, J. Kiss, H.-P. Steinrück *J. Catal.* **307** (2013) 132–139.

64 L. Qiu, F. Liu, L. Zhao, Y. Ma, J. Yao *Appl. Surf. Sci.* **252** (2006) 4931–4935.

65 I.I. Soykal, H. Sohn, D. Singh, J.T. Miller, U.S. Ozkan *ASC Catal.* **4** (2014) 585–592.

66 D.R. Mullins *Surf. Sci. Rep.* **70** (2015) 42–85.

67 S.S.-Y. Lin, H. Daimon, S.Y. Ha *Appl. Catal., A* **366** (2009) 252–261.

68 A.M. da Silva, L.V. Mattos, J.P. de Breejen, J.H. Bitter, K.P. de Jong, F.B. Noronha *Catal. Today* **164** (2011) 234–239.

69 Z. He, X. Wang, Y. Pu, Z. Qian *Int. J. Hydrogen Energy* **37** (2012) 11132–11140.

70 N. Nejar, M.J. Illán-Gómez *Appl. Catal., B* **70** (2007) 261–268.

71 G. Maniak, P. Stelmachowski, A. Kotarba, Z. Sojka, V. Rico-Pérez, A. Bueno-López *Appl. Catal., B* **136–137** (2013) 302–307.

72 K. Chayakul, T. Srithanratana, S. Hengrasmee *J. Mol. Catal. A* **340** (2011) 39–47.

73 M. Sun, L. Wang, B. Feng, Z. Zhang, G. Lu, Y. Guo *Catal. Today* **175** (2011) 100–105.

74 F.L.S. Carvalho, Y.J.O. Asencios, A.M.B. Rego, E.M. Assaf *Appl. Catal., A* **483** (2014) 52–62.

75 A.V. Shchukarev, D.V.; Korolkov *CEJC* **2** (2004) 347–362.

76 H.P. Bonzel, G. Broden, H.J. Krebs *Appl. Surf. Sci.* **16** (1983) 373–394.

77 Q. Li, X. Wang, Y. Xin, Z. Zhang, Y. Zhang, C. Hao, M. Meng, L. Zheng, L. Zheng *Sci. Rep* **4** (2014) 4725.

78 K. Vasudeva, N. Mitra, P. Umasankar, S.C. Dhingra *Int. J. Hydrogen Energy* **21** (1996) 13–18.

Supporting Information

Table S1. The percentage contribution (at.%) of elements on the surface of Co/CeO_2 catalysts under the ESR (H_2O/EtOH) = 12/1 mol/mol) calculated on the base of high resolution XPS spectra after taking into account the RSF for each element.

Catalyst	Time-on-stream (h)	Contribution of an element (at. %)*				
		Co	Ce	O	C	K
LS-Co/CeO_2	**H_2****	**20.3**	**31.4**	**40.8**	**7.5**	**-**
	1.00	22.2	25.6	50.5	1.8	-
	3.00	19.8	24.6	52.6	3.0	-
	7.00	21.2	18.5	55.5	3.8	-
HS-Co/CeO_2	**H_2****	**9.4**	**37.3**	**45.3**	**8.0**	**-**
	1.00	9.1	33.6	48.1	9.2	-
	3.00	8.9	31.4	52.7	7.0	-
	7.00	6.5	26.8	58.9	7.8	-
HS-KCo/CeO_2	**H_2****	**5.6**	**27.8**	**50.0**	**4.4**	**12.2**
	0.25	1.2	8.0	52.6	11.8	26.3
	3.00	2.0	17.3	54.5	8.7	17.5
	7.00	2.0	17.3	66.7	2.9	11.0

*Calculated as: $n_i = n_i/\sum n_{i-j} \cdot 100\%$, where n_i = {Co, Ce, O, C, K}c and n_{i-j} = Co+Ce+O+C+K.
**Results obtained after catalysts pre-reduction (H_2/Ar) at 420ºC for 1 h.

Table S2. The percentage contribution of different species in the Co 2p, Ce 3d, O 1s, C 1s high resolution XPS spectra of the catalyst after reduction and after the ESR.

Catalyst	Time-on-stream	Contribution of given species in the XPS spectrum (%)									
	(h)	Co 2p	Ce 3d	O 1s				C 1s			
		Co(II)	Ce(III)	O_{latt}	OH	KCO_3, KO	H_2O	C=C	CH_X	C-O	CO_3^{2-}
LS-Co/CeO_2	H_2**	0	55.3	81.6	18.4	0	0	0	55.8	0	44.2
	1	34.2	47.7	59	34.7	0	6.3	0	0	0	100
	3	29.9	53.9	52.5	36.5	0	10.9	0	44.1	0	55.9
	7	20.6	62.2	48.9	36.8	0	14.3	0	41.6	0	58.4
HS-Co/CeO_2	H_2**	18.2	0	83.7	16.3	0	0	0	0	0	100
	1	33.8	34.7	69.1	22.6	0	8.3	0	37.9	0	62.1
	3	42.7	49.6	64.5	21.6	0	13.9	0	43.9	0	56.1
	7	59.6	57.2	59	17.4	0	23.6	53.6	0	0	46.4
HS-KCo/CeO_2	H_2**	5	10	66.1	13	21	0	0	0	0	100
	0.25	33.6	49.8	6.9	15.7	60.5	16.9	0	0	8.5	91.5
	3	30.9	67.9	31.7	29.5	20.7	18.1	0	0	0	100
	7	24.9	73.8	33.5	32.5	5.3	28.8	0	0	0	100

**Results obtained after catalysts' pre-reduction (H_2/Ar) at 420ºC for 1 h.

CHAPTER

5

Zirconia-supported cobalt catalysts' surface state under steam reforming of ethanol with various H_2O/EtOH molar ratios

OUTLINE

Abstract

The surface state of cobalt-based catalysts supported on a micro- and nano-zirconia, promoted also with potassium, were investigated under the ESR (420°C) with various H_2O/EtOH molar ratios. The surface state of catalysts was correlated with the ESR selectivity. It was found that unpromoted catalysts suffer from intensive coking under ESR, while promoted catalyst is free of coke under all H_2O/EtOH molar ratios. Both Co(0) and Co(II) are present on the surface, but Co(0) dominates. It was proved that oxidation state of cobalt is not directly related to the selectivity of the ESR, whereas OH species along with $K^{\delta+}$–$O_{surf}{}^{\delta-}$ sites (in promoted catalyst) play an important role. Their abundance enhance selectivity of the ESR, and totally restrain coke deposition. In spite of generally low dispersion of zirconia-supported catalysts, the morphology and size of crystallites and a location of oxygen-containing species seems to be equally important with their abundance.

Introduction

Catalysts for ethanol steam reforming (ESR) attract interest of research groups all over the world, as evidenced by the number of available publications [1–18]. The current knowledge about the process and catalysts for the ESR has been summarized in a few extensive reviews [1–9]. In general, most of research groups have suggested that very promising candidates for the ESR are low-cost cobalt-based catalysts which exhibit high selectivity towards hydrogen and carbon dioxide [10–18]. Many authors underline the influence of the support acid-base properties on catalysts' performance [1, 3, 9, 19, 20]. It was concluded that ideal support should not favour dehydration reactions producing ethylene as a by-product, and thereby causing severe carbon deposition and a catalyst deactivation. Such ethanol transformations might be observed in the case of acidic supports, e.g., alumina [12, 19, 21–23]. From the other side, metal oxides with sites of strong basicity facilitate ethanol condensation to higher oxygenates [24]. Oxides with redox properties (e.g., CeO_2), able to release and restore oxygen, may contribute to the direct formation and release of CO_2 (e.g., $CO + O_{latt} \leftrightarrow CO_2$) [25], as well as, gasification of deposited carbon [14]. The oxygen exchange capacity of ceria can be easily enhanced by addition of dopants like calcium [26], lantana [27], or zirconia [14] into ceria structure, improving its properties towards hindering of coke formation.

Even though zirconia has a low oxygen mobility, shows no reducibility [14], and its surface acidity is higher as compared to ceria [19], its good thermal stability [28] made it a potential candidate for catalyst's support. The zirconia-supported systems have been found to be active in partial oxidation of methane [29], low-temperature oxidation of carbon monoxide [30], water gas shift reaction [31], catalytic decomposition of alcohols [32] and other reactions including steam reforming [33–40] and oxidative steam reforming [41]. Additionally, PdO/*m*-ZrO_2 recently has been found to be active in selective oxidation of ethanol to acetic acid [42]. Large variety of zirconia applications in catalysis encourages for further research over these systems.

Nowadays it seems that one of the most important issues for developing rational improvement strategies is to understand the influence of the surface state on catalysts' performance under the ESR. The determination of the pathways for the reaction of ethanol on metallic and partially oxidized cobalt foil was the main concern of M.P. Hyman and J.M. Vohs studies [43]. The results have revealed that the primary

reaction pathway on metallic cobalt sites is ethanol decarbonylation to carbon monoxide, hydrogen, and carbon, while on Co(II) sites ethanol undergoes dehydrogenation leading for formation of acetaldehyde. Under experimental conditions behaviour of an unsupported cobalt oxide differs from that of the supported, in terms of its reducibility and activity; however, the presence of Co(0)/Co(II) pair under the ESR was observed also on ZnO, MgO, Al_2O_3, CeO_2, ZrO_2 supported catalysts [23, 33, 44–46]. The authors agreed that metallic form of cobalt is more active for C–C bonds cleavage [11, 17, 21, 33, 46–49] and water gas shift reaction [46–48] than Co(II).

Studies of A. Karim et al. [46] over Co/MgO catalysts have shown that methane selectivity strongly depends on the Co(0)/Co(II) content on the surface. The authors found that Co(0) plays an important role in the increase of carbon dioxide selectivity, whereas Co(II) species exhibit higher activity, than Co(0), for ethanol dehydrogenation and a higher selectivity towards methane. Higher methane selectivity in the ESR, was assigned to the methanation of carbon monoxide and carbon dioxide [46]. Therefore, it was suggested that crucial role for obtaining high selectivity towards desirable products, such as hydrogen and carbon dioxide, could be achieved by stabilization of metallic cobalt particles and preventing of their oxidation under the ESR conditions [46, 50].

Quite recently it was found that the Co(0)/Co(II) ratio is associated with the support chemistry [18, 51] and promoters addition [21, 49, 50, 52–54]. E. Martono and J.M. Vohs [18] suggested that transfer of oxygen from the support to cobalt particles is more facile on reducible supports (e.g., CeO_2), as compared to more refractory ones (e.g., ZrO_2).

S. Davidson et al. [53] have found that the addition of zinc oxide facilitated the oxidation of metallic cobalt probably enhancing oxygen mobility of ceria support, while in the case of zirconia-supported catalyst after zinc oxide promotion [50] the oxidation of Co(0) particles was inhibited. Further research of S. Davidson et al. [55] have suggested that the addition of zinc oxide inhibited ability of Co/ZrO_2 for water dissociation, therefore, resulting in a higher Co(0)/Co(II) ratio. Furthermore studies of K.-S. Kim et al. [54] demonstrated that sodium promoter enhanced the reducibility of cobalt phase in Co/ZnO catalysts, improving selectivity to hydrogen and lowering methane formation. J. Llorca et al. [56] concluded that sodium plays a role in CH_x species evolution under the ESR, promoting methane steam reforming. Apart from the

the ability of the support for water dissociation and –OH species formation, which are the additional source of the readily available oxygen is another important issue.

In view of progressive increase of interest in determination of the oxidation state of cobalt and a support under the ESR [49], the XPS studies combined with gas chromatography analysis were conducted. The aim of these studies was better understanding the influence of the catalyst's surface state on catalytic performance under the ESR carried out over zirconia-supported cobalt catalysts. The studies include the role of the zirconia support dispersion, potassium promotion and the different H_2O/EtOH molar ratios in enhancement of catalysts' selectivity towards hydrogen and carbon-containing products.

1. Experimental

1.1. Catalysts' preparation

The Co/ZrO_2 catalysts were prepared by impregnation of a commercial nano- (high surface – HS) and micro- (low surface – LS) dispersed zirconia support (<100 nm and <5 μm, S_{total} = 47.7 and 5.4 m^2/g, respectively, Aldrich). Prior to the impregnation, the supports were dried at 120ºC for 3 h. The solution of cobalt nitrate and citric acid CA (the relative molar concentration of cobalt and CA was 1/1) was used for impregnation. After impregnation, the catalysts precursor were dried at 120ºC for 12 h, then calcined at 400ºC with a heating rate of 2ºC/min up to the calcination set point and maintained for 1 h at this temperature. The catalysts were denoted as LS- and HS-Co/ZrO_2. Next, the obtained HS-catalyst precursor was impregnated with potassium nitrate solution in order to introduce 2 wt.% of potassium promoter to the catalyst (further abbreviated as HS-K) and again the catalyst was dried at 110ºC for 12 h, then calcined at 400ºC with a heating rate of 2ºC/min up to the calcination set point and maintained for 1 h at this temperature.

1.2. Catalysts' characterization

Details of methods that were employed for catalyst's characterization (XRF, XRD, nitrogen adsorption, hydrogen chemisorption, H_2-TPR) were presented in details in the experimental section of the Chapter 3.

1.3. Combined XPS and catalytic performance experiments

The detailed description of experimental set-up and measurements procedure can be find in the experimental section of the Chapter 3.

The surface experienced variable degree of charging, which were neutralized by means of flood gun source. The obtained high-resolution XPS spectra were calibrated for O 1s core lever (530.0 eV). In this studies high resolution spectra were collected for Co 2p, Zr 3d, O 1s, C 1s & K 2p regions (with the same settings as described in the Chapter 3), and processed according to the procedure presented in the Chapter 3.

1.4. Catalytic tests in a fixed-bed reactor

The studies of ESR catalytic behaviour (H_2O/EtOH molar rations 3/1, 9/1 and 12/1, 420ºC, p_{total} = 1 atm) were carried out in a fixed-bed continuous-flow quartz reactor (Microactivity Reference unit, PID Eng & Tech.) under atmospheric pressure, as shown in the Chapter 3.

1.5. Post reaction TEM catalysts' characterization

The procedure of spent catalysts characterization (H_2O/EtOH = 3/1 mol/mol, 420ºC, p_{total} = 1 atm) was described in details in the Chapter 3.

2. Results

2.1. Reduction of the catalysts in hydrogen

Table 1 shows the characterization of the cobalt-based zirconia-supported catalysts. Cobalt contents for all catalysts was comparable, and it was close to 9 wt.%. The surface area of the HS-catalyst was 22.0 m^2/g, while the LS-catalyst exhibited the lowest surface area (8.9 m^2/g). It is worth to mention that the LS-catalysts' surface area is higher than the surface area of bare support (5.4 m^2/g), proving that deposition of cobalt on its surface increased the porosity of the final catalyst.

The potassium promotion had a negative effect on the catalyst's surface area (14.6 m^2/g). It can be noticed that the average cobalt crystallites size of potassium-promoted catalyst (43.5 nm) were similar to these found for the unpromoted micro-dispersed catalyst (42.3 nm), whereas the high-dispersed catalyst's cobalt crystallites size were only two times smaller (22.5 nm).

Table 1. Results of the Co/ZrO_2 catalysts characterization.

Catalyst	**BET surface area**[a]	**Volumes of pores**[a]	**Pore diameter**[a]	**Cobalt content**[b]	**Average crystallite size**[c]		**Average cobalt crystallite size**[d]	**Cobalt dispersion**[d]	**Cobalt surface area**[d]
	m^2/g	cm^2/g	**nm**	**wt.%**	**nm**		**nm**	**%**	$m^2/g_{cat.}$
					Co_3O_4	ZrO_2			
LS-Co/ZrO_2	8.9	0.05	21.9	8.84±0.35	21.4	86.9	42.3	2.4	1.4
HS-Co/ZrO_2	22.0	0.15	27.0	9.54±0.29	16.8	25.7	22.5	4.4	2.9
HS-KCo/ZrO_2	14.6	0.12	29.7	8.92±0.27	20.9	25.1	43.5	2.3	1.4

[a] Determined by the low-temperature N_2 adsorption.
[b] Determined by XRF.
[c] Determined by XRD.
[d] Determined by the hydrogen chemisorption measurements.

Fig. 1 depicts the Zr 3d, Co $2p_{3/2}$, O 1s and C 1s & K 2p spectra of the LS-, HS-, and HS-K catalysts recorded after reduction in hydrogen. The XPS spectra of fresh (after calcination) samples, can be found in the Supporting Information (Fig. S.1). Regardless of the support dispersion (low- or high-dispersed zirconia) the Zr 3d spectra show a spin-orbit splitting of ~2.38 eV with a Zr $3d_{5/2}$ peak located at 182.2 eV. In literature the Zr $3d_{5/2}$ line, characteristic of ZrO_2 is reported between 182.2–182.9 eV [57–62]. The absence of significant changes on the Zr 3d spectra after the catalysts' reduction is not surprising, since it was found that the reduction of the bare zirconium oxide does not proceed at 420ºC (Fig. 2).

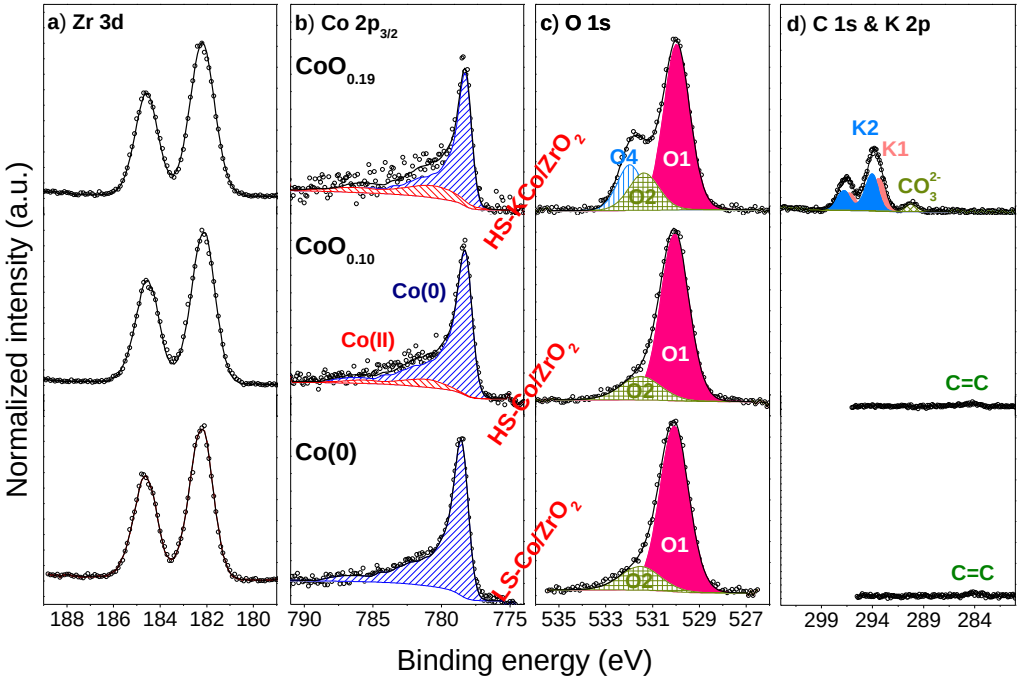

Fig. 1. The high resolution XPS spectra of (a) Zr 3d, (b) Co $2p_{3/2}$, (c) O 1s and (d) C 1s & K 2p collected after reduction (H_2/Ar = 50/50 cm^3, 420ºC, 1 h) of LS-Co/ZrO_2, HS-Co/ZrO_2 and HS-KCo/ZrO_2 catalysts; b) Co(II) (\\\), Co(0) (///), c) O1 – lattice oxygen, O2 – hydroxyl and carbonate species, O4 – carbonate species bonded to potassium, d) probable assignments of K1 and K2 species can be found in the text.

On the surface of calcined samples, Co_3O_4 [50, 63, 64] was the main phase (Fig. S1b, Supporting Information), whereas after catalysts' reduction the most dominant form of cobalt on the surface was Co(0) (///) (Fig. 1a). The binding energy (BE) of this component (778.4 ± 0.2 eV) is close to this reported in literature [50, 65], as well as, to those recorded for ceria-supported catalysts, as described in previous chapters (Chapter 2 and Chapter 3). A small contribution of the component assigned to the presence of Co(II) (\\\) (781.2 ± 0.2 eV) [10, 43, 63, 66, 67] can be found for the HS-catalyst and its potassium-promoted counterpart. The comparison of the XPS spectra recorded for the HS- and HS-K catalysts revealed that the lower reduction degree of cobalt's surface can be observed for the potassium-promoted catalyst.

In the O 1s spectra (Fig. 1c) for all catalysts, peaks located at 530.0 (O1) and 531.5 eV (O2) can be resolved. The first peak is assigned to the lattice oxygen, mostly in zirconia [68, 69], however, the oxygen from CoO_x lattice should also appear close to this binging energy [64]. In literature the peak located at 1.5 ± 0.2 eV higher binding energy, in relation to the main oxygen component, is usually ascribed to the presence of –OH [61, 62, 64, 69, 70] or carbonates [71]. Even though XPS technique does not allow

to differentiate where hydroxides are located, according to the literature they are most probably distributed on both: cobalt (as Co–OH [72]) and zirconia (as Zr–OH [73]). Therefore, oxygen-containing species would be considered as adsorbed on the surface of catalysts', without distinction to their location. The O 1s spectrum of the HS-K catalyst exhibits also an additional component named O4 (532.0 ± 0.2 eV). The oxygen component at this BE for potassium-containing compounds has been found on the O 1s XPS spectra recorded for KO_x [74, 75], K_xO_y [76–79], K_2CO_3 [80] or even KOH [81–83]. The normalized intensity ratio of components located at 532.0 eV (O 1s) and 290.0 eV (C 1s) (assigned further to CO_3^{2-} species) was equal 3, therefore, suggesting that the O4 component is most likely related to the presence of carbonates. Taking into account that this peak was observed only for the potassium-promoted sample it is probably related to the presence of KCO_3 species.

In the C 1s region two small peaks at 284.4 eV for the unpromoted catalysts, and 290.2 eV for the potassium-promoted sample can be found. The low binding energy peak is attributed to carbon impurities, whereas the high binding energy peak is related to the presence of HCO_3^- or CO_3^{2-} [84].

The higher binding energy peaks on the spectrum for the HS-K catalyst (293.2 and 296.0 eV) are related to the K 2p region. The position of the peaks indicates for the presence of potassium in a cationic chemical environment [85]. Analysis of the peaks position and full width at half maximum (FWHM) may suggest existence of two different types of bonds between potassium and the surface. The maxima of the peaks at K $2p_{3/2}$ high resolution spectrum were found at 293.4 ± 0.2 eV (K1) and 294.1 ± 0.2 eV (K2), and their position does not correspond to the so far published data for potassium compounds like KNO_3 (292.9 eV) [81], $KHCO_3$ (292.9 ± 0.2 eV) [80] or K_2CO_3 (292.2 ± 0.2 eV) [80, 86] or K_2O (292.4 eV) [87, 88]. However, peaks, characteristics of K $2p_{3/2}$, close to the BE obtained in this studies has been reported [78, 85, 89–94], and generally they have been assigned to the oxidic forms of potassium. A. Caballero et al. [78] have assigned the peaks at 293.4 and 531.8 eV to the formation of $O_2^{\delta-}$ species associated to oxidized potassium atoms, being very close to the stoichiometry of K_2O_2. H.H. Huang et al. [91] have studied the adsorption of potassium on the MgO (100) and they have observed the K $2p_{3/2}$ feature at 293.5 eV at a low potassium coverage of 0.2 ML. This was assigned to the presence of potassium-atoms initially bonded with the surface oxygen of MgO (100). The same authors [92] have explained the origin of the peak at 532.1 eV as chemisorbed oxygen species observed in

the oxidation of potassium multilayer. The small amount of potassium (2 wt.%), as well as, its high dispersion did not allowed to determine the exact state of potassium based on the XRD results. Like it was mentioned before, the position of the K 2p peaks does not correspond to earlier reported potassium species, however, the BE provides the evidence for potassium oxidic nature. The presence of both: carbonates and adsorbed oxygen species may also indicate for the existence of fairly stable carbonates coordinated to K^+ sites, however, potassium can be also weakly bonded with zirconia surface as Zr–O–K, after substitution of proton in hydroxyl species by the potassium ions. The existence of Zr–O–K species is probable, since one role of the potassium is to bind with the support, in order to neutralize its acidity [95]. In addition, the Co–O–K cannot be excluded. It is very likely that potassium ions chemisorbed on weakly bonded carbonates, as well as, on the top of surface oxygen will give signals on the XPS spectrum at the same or very close BE. This will result in appearance of potassium component at lower BE (293.4 eV).

Therefore, summarizing the current available publications and results from previous chapters (Chapter 3 and Chapter 4) of this thesis, it is suggested that K1 component is related to $K^{\delta+}$–$O_{surf}^{\delta-}$ sites (abbreviated as K–O) and in the presence of carbonates (290.0 eV) also to KCO_3 sites. This can be supported by the work of G. Maniak et al. [93] which has shown that regardless of the potassium compound (KOH, K_2CO_3, KNO_3, CH_3COOK) used to promote Co_3O_4, the same BE of the K 2p components was obtained (294.0 eV and 296.8 eV).

The origin of the high binding energy peak at 294.1 eV (K2), therefore, may be a result of the decrease of electron density of potassium sites. Also it cannot be excluded that oxygen transfer (from the surface of the support and/or cobalt active phase) allowed for formation of different weakly bonded to the surface defective KO_x species. However, in order to understand the origin of K2 component, more studies by means of different techniques are required.

After reduction in hydrogen, the potassium segregation, or dispersion, on the surface was observed. The potassium percentage contribution on the surface of the fresh oxide catalyst was 3% while after reduction it increased up to 16%. The phenomenon of potassium segregation on reduced surfaces has been previously reported by the group of K. Engvall [96].

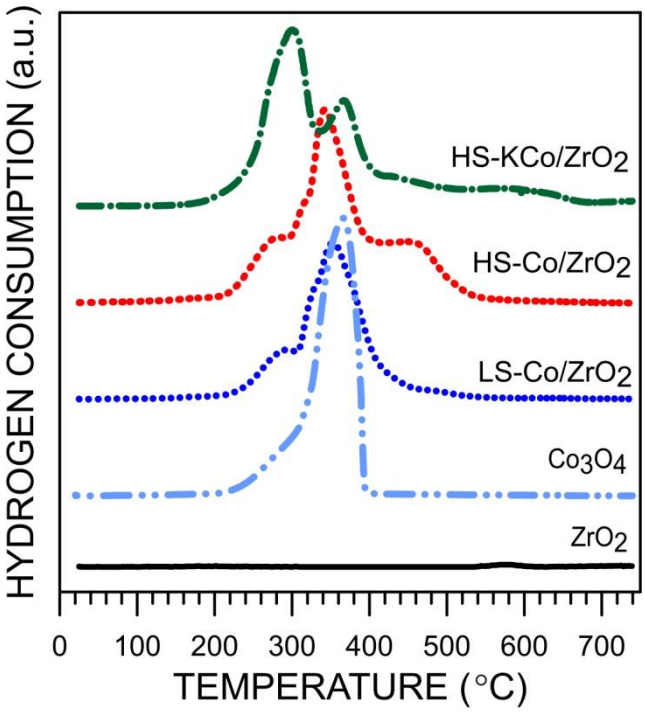

Fig. 2. H_2-TPR profiles of zirconia support, bare cobalt oxide and cobalt-based catalysts.

For better insight into the catalysts' reduction behaviour, the H_2-TPR profiles are given. The Fig. 2 shows that the best reducibility – just in the moderate temperature range – of cobalt species (zirconia reduction at examined conditions does not occur) exhibited the LS-catalyst. Two pronounced peaks around 300 and 365ºC can be easily resolved. The obtained profile is similar to this, characteristic for pure Co_3O_4 (Fig. 2) [98, 98] and it can be assigned to the two step reduction of Co_3O_4. The very small peak appearing around 500ºC might be attributed to the reduction of Co(II) species interacting with the support [97]. The H_2-TPR profiles obtained for HS- and HS-K catalysts are rather complicated, and they clearly indicate for the existence of cobalt–zirconia interaction. The existence of cobalt species strongly interacting with the support was previously reported by B. Jongsomjit et al. [99] for Co/Al_2O_3 catalysts. A comparison of the HS- and HS-K catalysts TPR profiles showed that the peak at 300ºC was more pronounced for the potassium-promoted catalyst, however, generally for this catalyst the reduction profile was extended notably to the higher temperatures upon doping. The extension of TPR profile may suggest the existence of the charge transfer from cobalt to adjacent ions of K^+ and formation of Co–O–K bonds stabilizing cobalt in higher oxidation state. The result indicates that potassium introduction is responsible for deterioration of the catalyst's reducibility, what can be related to the enhancement of the zirconia-supported catalyst's performance.

2.2. XPS characterization of catalysts after the ESR with a stoichiometric H_2O/EtOH molar ratio

The XPS spectra obtained for the pre-reduced catalysts after reaction (420ºC, p_{total} = 1 atm, t = 1 h) in the H_2O/EtOH molar ratio equal 3/1 mol/mol were presented in Fig. 3. The samples exposition to the H_2O/EtOH vapours caused the evident surface's oxidation in each catalyst. The percentage contribution of Co(II) after the ESR reaction increased significantly (compare Fig. 1b and Fig. 3b, see also Supporting Information Table S1). The amount of cobalt(II) oxide species can be expressed as $CoO_{0.18}$, $CoO_{0.25}$, and $CoO_{0.32}$ for the LS-, HS- and potassium-promoted Co/ZrO_2 catalysts. The obtained values suggest that the high-surface area catalyst was more vulnerable to oxidation, and that cobalt particles in the case of potassium-promoted catalyst were even less resistant to oxidation.

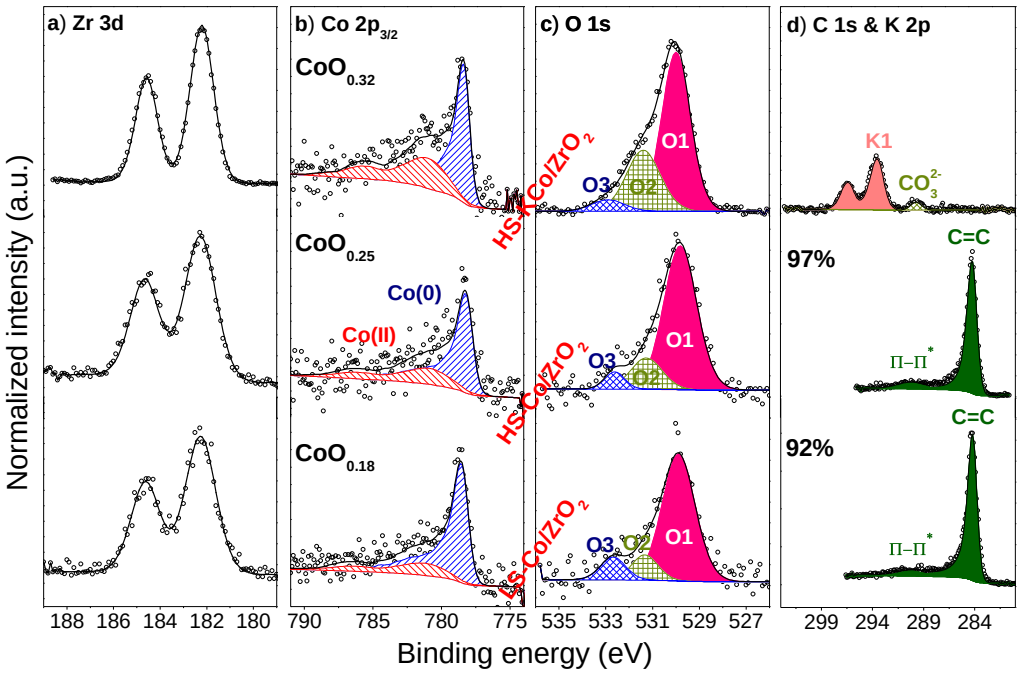

Fig. 3. The high resolution XPS spectra of (a) Zr 3d, (b) Co $2p_{3/2}$, (c) O 1s and (d) C 1s & K 2p collected after the ESR (H_2O/EtOH = 3/1 mol/mol, 420ºC, p_{total} = 1 atm, 1 h) carried out over the pre-reduced (H_2/Ar, 420ºC) LS-Co/ZrO_2, HS-Co/ZrO_2 and HS-KCo/ZrO_2 catalysts. The percentages given in the graph d) reflect the percentage atomic coverage of carbon on the surface; b) Co(II) (\\\), Co(0) (///), c) O1 – lattice oxygen, O2 – hydroxyl and carbonate species, O3 – adsorbed water, d) K1 refers to KCO_3 and K–O species.

These results are in agreement with the temperature-programmed oxidation experiment carried out by M. Greluk et al. [100] on similar KCo/ZrO_2 catalyst's (with a little smaller average size of cobalt crystallites, 31.0 nm). The authors [100] have found that

the major consumption of oxygen by the KCo/ZrO_2 catalyst occurs around 255ºC. The small oxygen-consumption peak was also found around 105ºC. The obtained profile was ascribed to the gradual oxidation via CoO to Co_3O_4.

The best fitting of the O 1s spectra for all catalysts can be obtained when a new component (O3) at 532.9 ± 0.2 eV is considered. The detected oxygen component in literature is usually assigned to the presence of water adsorbed on the surface [101]. The presence of hydroxyl species, as well as, water seems to be the main reason of cobalt oxidation [10]. One may note the absence of the component previously denoted as O4, even though the presence of carbonates was confirmed by the C 1s spectrum. It can be explained by the fact that the concentration of potassium carbonates species was very small (as seen in Fig. 3d), therefore, the component O4 strongly overlaps with the component O2. In order to exclude the contribution of KCO_3 species from O2 component in the O 1s spectrum, the atomic concentration of these species was calculated based on the peak located at 290.0 eV.

On the surface of the unpromoted catalysts significant coking was observed. The HS-catalyst exhibited slightly higher percentage atomic contribution of carbon on the surface (97%) than its LS-counterpart (92%) (Table 2). In both cases the asymmetric shape and the position (284.2 eV) of the main component indicates for the presence of graphitic carbon [102]. The broad peak at 290 eV can be a result of π-π^* satellite or metal carbonate [103]. Potassium promotion hindered coke formation as shown in Fig. 3d. Literature data clearly show that the presence of potassium as an independent phase or the active catalyst's component (for instance as K_2O, KOH, K_2CO_3) enhances the oxidation activity of catalysts towards soot oxidation [86].

After the ESR, the K 2p peak's shifts back towards lower BE (293.6 eV), and only one potassium component could be resolved (K1). Quite interesting is that the percentage coverage of the surface by potassium for the reduced sample was 16% while for the sample after the ESR (H_2O/EtOH = 3/1 mol/mol) was 10% (Table 2). Basing on this data it can be expected that potassium could be washed out from the surface, it could penetrate the support becoming inaccessible during reaction [104], or even re-organize to form bigger agglomerates.

Table 2. The percentage contribution (at.%) of elements on the surface of catalysts under the ESR calculated on the basis of high resolution XPS spectra after taking into account the atomic sensitivity factor of each element

Catalyst	H_2O/EtOH (mol/mol)	Contribution of an element (at.%)*				
		Co	Zr	O	C	K
LS-Co/ZrO_2		22.1	22.4	50.0	3.6	-
HS-Co/ZrO_2	H_2**	11.3	26.4	58.8	3.5	-
HS-KCo/ZrO_2		3.2	20.3	56.1	4.3	16.1
LS-Co/ZrO_2		1.9	1.8	4.7	91.5	-
HS-Co/ZrO_2	3/1	0.4	1.0	2.0	96.7	-
HS-KCo/ZrO_2		3.0	22.6	61.4	2.9	10.1
LS-Co/ZrO_2		15.9	16.2	46.4	21.4	-
HS-Co/ZrO_2	9/1	7.4	11.2	28.8	52.6	-
HS-KCo/ZrO_2		2.8	17.4	57.9	8.6	13.2
LS-Co/ZrO_2		17.6	19.1	53.1	10.2	-
HS-Co/ZrO_2	12/1	8.3	24.4	57.5	9.8	-
HS-KCo/ZrO_2		1.7	16.0	56.2	8.7	17.4

*Calculated as: $n_i = n_i/\sum n_{i-j} \cdot 100\%$, where n_i = {Co, Zr, O, C, K} and n_{i-j} = Co+Zr+O+C+K.
**Results obtained after the catalysts pre-reduction (H_2/Ar) at 420ºC for 1 h.

2.3. XPS characterization of catalysts after the ESR at high H_2O/EtOH molar ratio

As demonstrated in the Fig. 4b the peak at 781.2 eV is indicative of CoO_x species [10]. The increase of water contribution in the ESR reaction mixture undoubtedly favours surface's oxidation. The observed trend was similar to that described above. The Co(II) percentage contribution for the HS-catalyst was slightly higher ($CoO_{0.35}$) than for the LS-counterpart ($CoO_{0.27}$). The previous observation that potassium promotion of the zirconia-supported catalyst facilitated cobalt active phase oxidation has been confirmed also in this case ($CoO_{0.38}$).

The O 1s spectra of the all catalysts, obtained after the ESR (H_2O/EtOH = 9/1 mol/mol), suggest the existence of three oxygen containing components on the surface, with two ascribed to the presence of surface adsorbed species. The comparison of the Figs. 3 and 4 clearly shows the increase of the percentage contribution of the O2 component, assigned to the presence of both carbonates and hydroxide species (see also Table S1 in Supporting Information). The XPS spectrum of the O 1s obtained for the HS-K exhibits the pronounced shoulder indicating that on the surface of potassium-promoted catalyst the concentration of both CO_3^{2-} and –OH is the highest (see also Table S1 in Supporting Information).

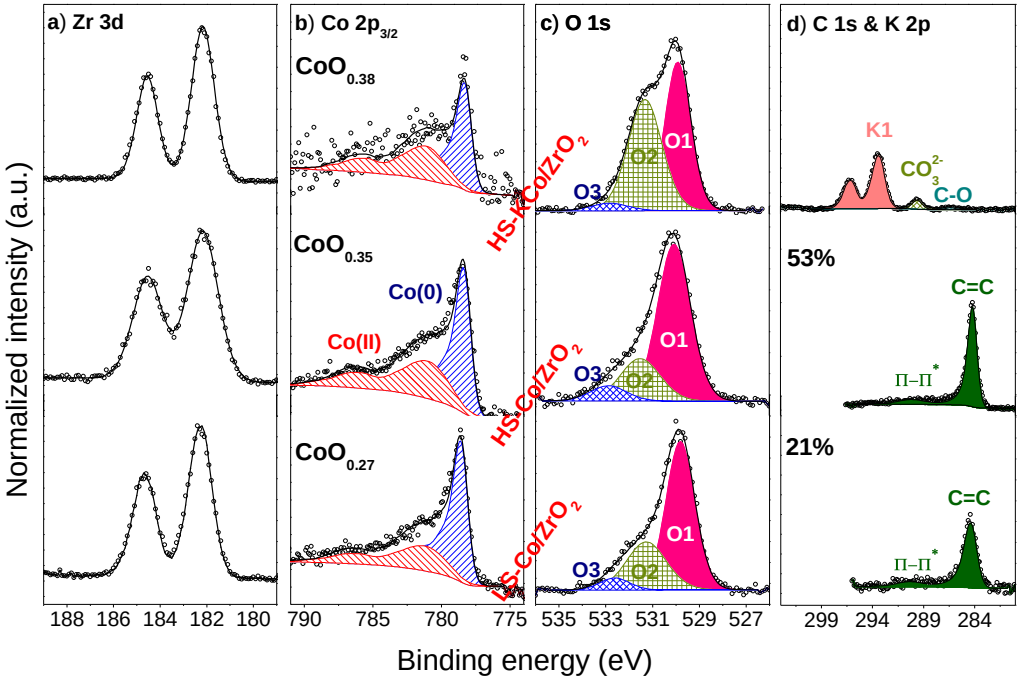

Fig. 4. The high resolution XPS spectra of (a) Zr 3d, (b) Co $2p_{3/2}$, (c) O 1s and (d) C 1s & K 2p collected after the ESR (H_2O/EtOH = 9/1 mol/mol, 420ºC, p_{total} = 1 atm, 1 h) carried out over the pre-reduced (H_2/Ar, 420ºC) LS-Co/ZrO_2, HS-Co/ZrO_2 and HS-KCo/ZrO_2 catalysts. The percentages given in the graph d) reflect the percentage atomic coverage of carbon on the surface; b) Co(II) (\\\), Co(0) (///), c) O1 – lattice oxygen, O2 – hydroxyl and carbonate species, O3 – adsorbed water, d) K1 refers to KCO_3 and K–O species.

The increase of water excess in the feed slowed down the rate of coke deposition, reflected in the lower carbon coverage. In the case of the HS-catalyst the percentage coverage of the surface by carbon was equal to 53% while for the LS-counterpart – 21% (Table 2). On the surface of potassium-promoted catalyst only the higher contribution of carbonates was noted. Also, the position of the K 2p component did not changed significantly (293.5 eV) as compared to those, recorded for the samples after the ESR, carried out with lower H_2O/EtOH molar ratios. Moreover, the surface's coverage by the potassium was only a little higher (13%) than the previously reported value (10%) obtained after treatment under stoichiometric H_2O/EtOH molar ratio (Table 2).

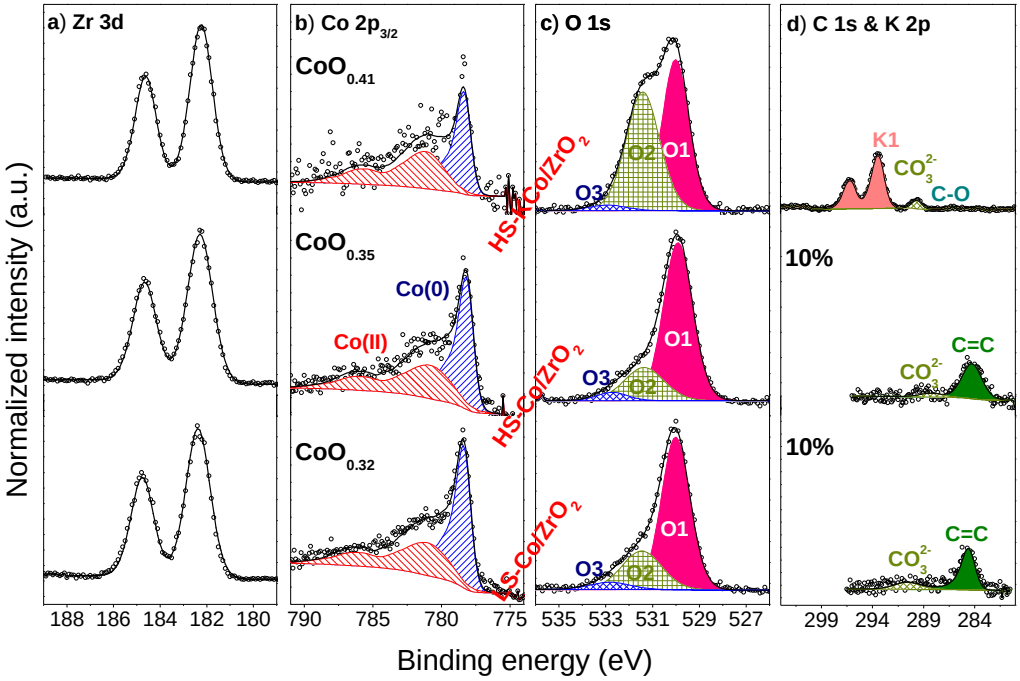

Fig. 5. The high resolution XPS spectra of (a) Zr 3d, (b) Co $2p_{3/2}$, (c) O 1s and (d) C 1s & K 2p collected after the ESR (H_2O/EtOH = 12/1 mol/mol, 420ºC, p_{total} = 1 atm, 1 h) carried out over the pre-reduced (H_2/Ar, 420ºC) LS-Co/ZrO_2, HS-Co/ZrO_2 and HS-KCo/ZrO_2 catalysts. The percentages given in the graph d) reflect the percentage atomic coverage of carbon on the surface; b) Co(II) (\\\), Co(0) (///), c) O1 – lattice oxygen, O2 – hydroxyl and carbonate species, O3 – adsorbed water, d) K1 refers to KCO_3 and K–O species.

The XPS spectra obtained when the ESR is carried out with higher H_2O/EtOH molar ratio, i.e., 12/1, did not exhibit significant changes (Fig. 5). The Co(II) contribution in the Co $2p_{3/2}$ spectra remained almost the same. The CoO_x values for the LS-, HS- and potassium-promoted catalysts were equal $CoO_{0.32}$, $CoO_{0.35}$ and $CoO_{0.41}$, indicating that the increase of the H_2O/EtOH molar ratio did not caused any significant, additional oxidation of the surface. This proved that regardless of the H_2O/EtOH molar ratio, a mixed metal-ionic form of cobalt is always present under reaction conditions. It is worth noting that CoO_x values found for the unpromoted zirconia-supported catalysts are similar to those recorded for ceria-supported catalysts (Chapter 3). For other components, like Zr 3d and O 1s there were only minor changes. However, it was noted that after the increase of water contribution, the carbon coverage significantly decreased and was equal 10 at.% for the LS- and HS-catalyst (Table 2), accompanied with an increase of potassium percentage coverage (17%).

2.4. The ESR catalytic performance of the catalysts

Table 3 presents the catalytic performance of cobalt-based zirconia-supported catalysts catalytic performance under the H_2O/EtOH equal 3/1, 9/1 and 12/1 molar ratios. Except for the HS-catalyst at 3/1 molar ratio, surface of which was almost totally covered by carbon (97%), all examined systems exhibited 100% conversion of ethanol. For the molar ratio of 3 the degree of water conversion was significantly lower than it should result from the stoichiometry of the ESR reaction (only 29–39%) indicating non-selective ethanol transformations reaction paths. The higher water conversion, was achieved with the increase of water excess in the feed, and is followed by improved selectivity towards the most desirable products, hydrogen and carbon dioxide.

The HS-K catalyst exhibited the highest selectivities to hydrogen and carbon dioxide, for all the H_2O/EtOH molar ratios.

Table 3. Activity and selectivity of catalysts after 1 h in the ESR at 420ºC.

Catalyst	H_2O/EtOH (mol/mol)	Conv. (%)	Selectivity (%)					H_2/EtOH (mol/mol)	CO_2/EtOH (mol/mol)
		EtOH	H_2	CO_2	CO	CH_4	MeCHO		
LS-Co/ZrO_2	3/1	100	94.8	66.0	18.0	5.0	10.9	3.96	1.32
HS-Co/ZrO_2		89.9	85.2	70.5	11.6	14.1	3.9	4.23	1.41
HS-KCo/ZrO_2		100	97.5	87.2	10.0	2.8	0.0	5.23	1.74
LS-Co/ZrO_2	9/1	100	90.4	75.0	10.8	14.2	0.0	4.50	1.50
HS-Co/ZrO_2		100	94.5	83.8	7.5	8.7	0.0	5.03	1.68
HS-KCo/ZrO_2		100	98.6	91.5	6.3	2.2	0.0	5.49	1.83
LS-Co/ZrO_2	12/1	100	92.2	78.6	9.4	12.0	0.0	4.72	1.57
HS-Co/ZrO_2		100	95.7	87.4	5.8	6.8	0.0	5.24	1.75
HS-KCo/ZrO_2		100	98.6	93.6	4.2	2.2	0.0	5.60	1.87

The selectivity of the ESR towards hydrogen over the catalysts varied between 85% (4.2 $\mathrm{mol_{H_2}/mol_{EtOH}}$) and 99% (5.6 $\mathrm{mol_{H_2}/mol_{EtOH}}$) for the reactants molar ratio of 3/1 and 12/1. The hydrogen yield obtained for the HS-K catalyst was close to the thermodynamic predicted [105].

For the stoichiometric reactants mixture some amounts of acetaldehyde were recorded over both, LS- and HS-catalysts. The LS-catalyst exhibited higher formation of acetaldehyde (10.9%) comparing to the HS-counterpart (3.9%). This by-product was absent when the reaction mixtures with the excess of water were used. The methane selectivity for the LS-catalyst increased, whereas for the HS-counterpart decreased with the excess of water. The increase of the water amount in the feed caused increase of the selectivity towards carbon dioxide from 66–71% for the H_2O/EtOH molar ratio of 3/1

to 75–84% for 9/1 mol/mol and to 77–87% for 12/1 mol/mol. At the same time, in the case of both catalysts the selectivities to methane and carbon monoxide decreased. The zirconia-supported catalysts' selectivity to methane and carbon dioxide is relativity higher, as compared to better performing catalysts, for example these presented in the Chapter 3. The decrease of the amounts of methane formed could be achieved also after potassium promotion, which is in agreement with results noted for potassium-promoted ceria-supported catalyst (Chapter 3). It is worth nothing that regardless of the H_2O/EtOH molar ratio the selectivities of potassium-promoted catalyst towards hydrogen and carbon dioxide are the highest and very low sensitive to the feed composition.

2.5. The influence of the ESR conditions on the catalysts' coking

The nature and the morphology of the carbonaceous deposit was determined by the TEM studies of the spent catalysts after the H_2O/EtOH =3/1 mol/mol (Fig. 6-8). It was found that in the case of the LS-catalyst carbon occurs on the surface mainly in the form of nanofilaments, while in the case of the HS-counterpart nanofilaments, carbon nanospheres and encapsulating carbon have been found. The nanofibers observed for the unpromoted catalysts definitely differ in the length. Those observed for the LS-catalyst are significantly longer. In Fig. 6 darker spots represents cobalt particles which are encapsulated in carbon fibers. The main form of carbon detected on the LS- and HS-catalysts was graphitic carbon located between cobalt and zirconia particles (Fig. 6 and 7). The results of TEM studies for the HS-K catalyst confirmed results of the XPS studies. The surface of this catalyst (Fig. 8) remained carbon free, indicating that potassium promoter significantly inhibits coke deposition.

Big cobalt particles favour formation of carbon nanofibers, that destroys the sample, which consequently causes the reactor blockage and increase of the pressure drop in the catalyst bed [106]. In the case of smaller cobalt particles in catalysts carbon is deposited only on the outer layers of the catalyst.

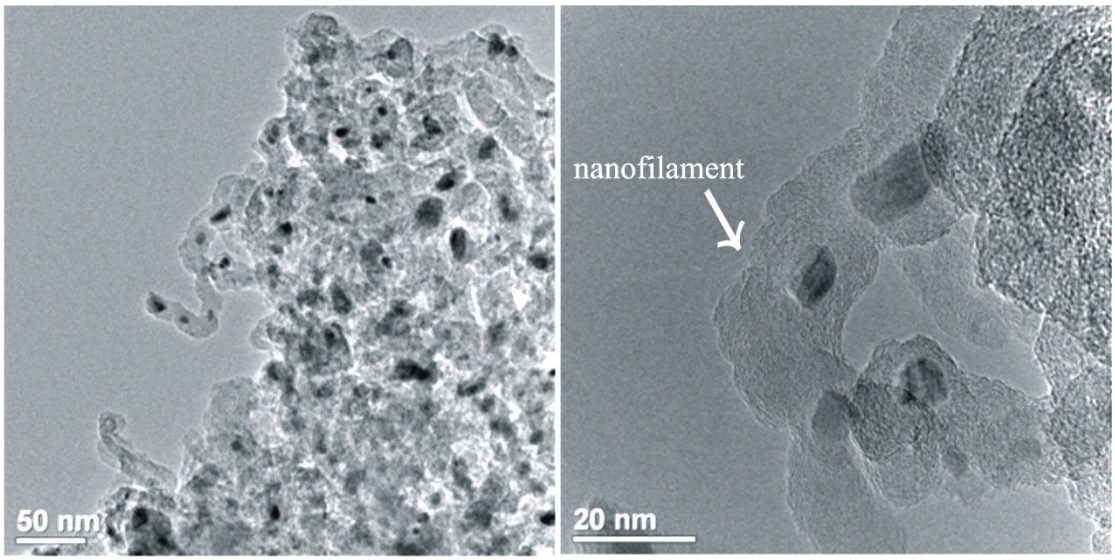

Fig. 6. TEM images of the LS-Co/ZrO_2 catalyst after 1 h ESR (H_2O/EtOH =3/1 mol/mol, 420ºC).

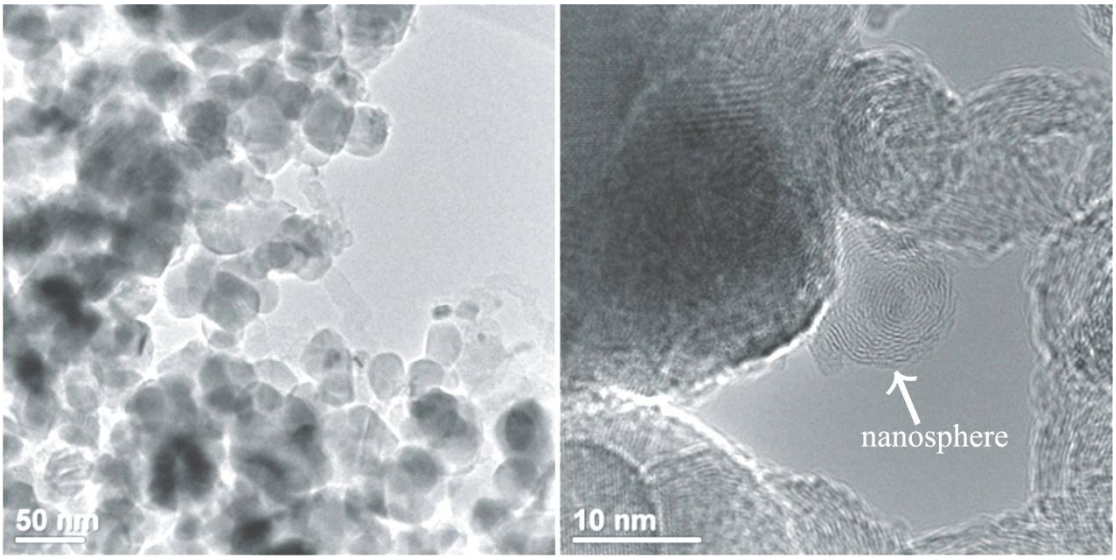

Fig. 7. TEM images of the HS-Co/ZrO_2 catalyst after 1 h ESR (H_2O/EtOH =3/1 mol/mol, 420ºC).

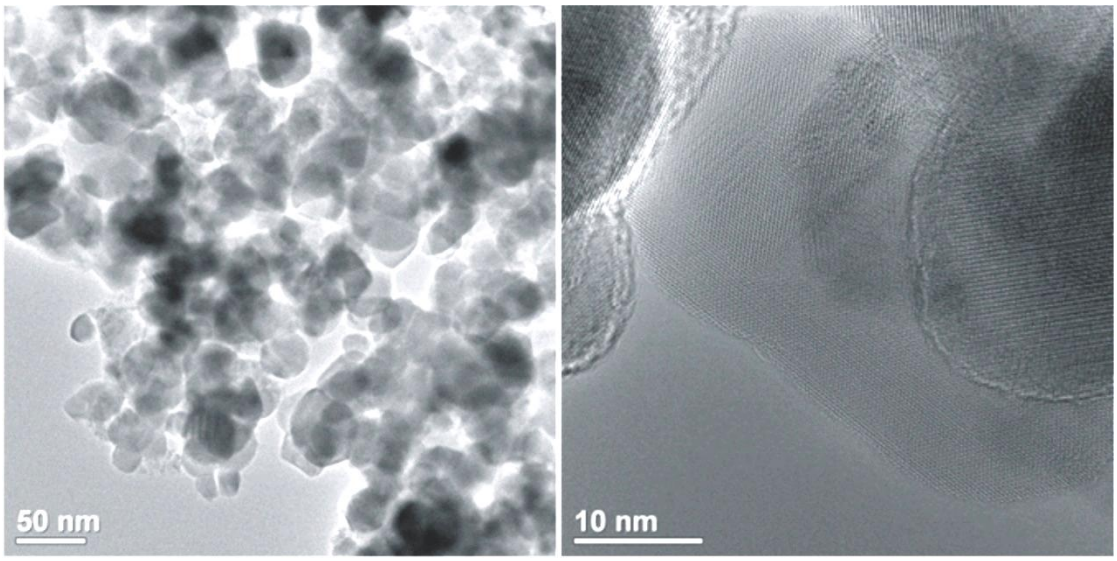

Fig. 8. TEM images of the HS-KCo/ZrO_2 catalyst after 1 h ESR (H_2O/EtOH =3/1 mol/mol, 420ºC).

3. Discussion

Generally, all zirconia-supported catalysts used in this part of the thesis were low-dispersed ones – a nature of these supports does not allow preparing a highly-dispersed cobalt active phase (Table 1). Regardless of the dispersion of zirconium oxide used as the support of cobalt active phase, the mean size of cobalt crystallites was large – in the best case (HS-catalyst) larger than 20 nm, whilst in the LS- and HS-K catalysts larger than 40 nm. The concentration of highly-coordinated sites, on smooth planes and terraces, of the crystallites surface dominates that with low-coordination numbers as at corners, edges, ad-atoms and other lattice defects. Chemisorptive properties of these surface sites are different. The distance of the centres of smooth planes from the rich in low-coordinated cobalt–support borders is rather long. These features of the catalysts studied may be reflected in the observed surface state and in effects of the ESR.

3.1. The influence of the H_2O/EtOH molar ratio on the catalysts' surface

The unpromoted zirconia-supported catalysts suffered from intensive coking. The amount of carbon formed on the surface could be lowered by the increase of H_2O/EtOH molar ratio while the reactants composition did not affect on type of deposited carbon. The surface of catalysts was covered by fully dehydrogenated carbon species, even if the ESR reaction was carried out with high excess of water (12/1

mol/mol) (Fig. 9). In contrast to the unpromoted catalysts, the surface of the HS-K catalyst was free of coke under all H_2O/EtOH molar ratios.

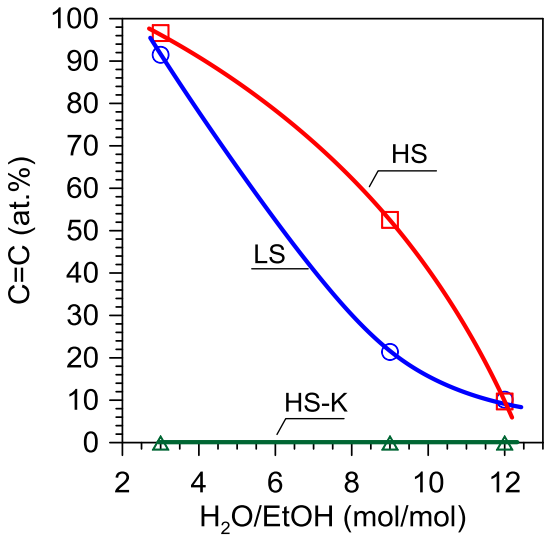

Fig. 9. Dependence of percentage contribution of C=C species on the catalysts' surface, on the H_2O/EtOH molar ratio for the LS-Co/ZrO_2, HS-Co/ZrO_2 and HS-KCo/ZrO_2 catalysts under ESR at 420ºC.

Due to high carbon coverage, the analysis of the unpromoted catalysts surface's state concerns only that area of the catalysts' surface which was visible and measurable by the XPS technique. Therefore, the surface contribution of all elements of the catalysts in the whole samples under stoichiometric and 9/1 H_2O/EtOH molar ratios is very small. It is also worth noticing that in the potassium-promoted catalyst the surface concentration of cobalt is much lower than that in the bulk and it falls with water excess in the reaction feed. In that case the percentage contribution of carbon (in carbonate species mainly, without any C=C type coke) is not high. From Table 2 it can be concluded that the decrease of the cobalt (and zirconium also) surface concentration is coupled with the rise of potassium contribution with surplus of water.

The influence of reactants molar ratio on the surface's state of zirconia supported catalysts is presented on Fig. 10. It can be seen that higher excess of water causes the progressive oxidation of cobalt active phase (Fig. 10a).

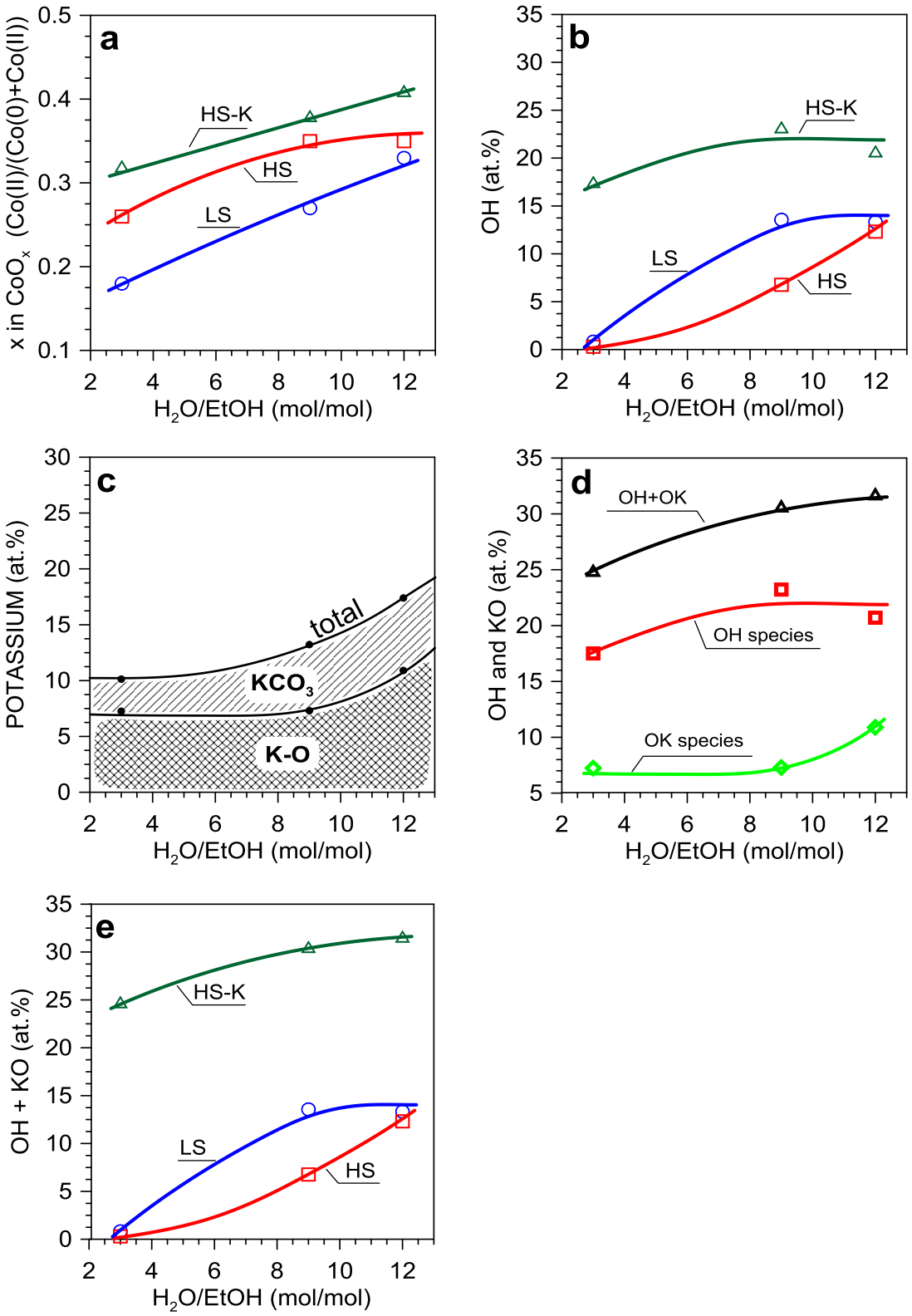

Fig. 10. Dependence of (a) cobalt oxidation state (CoO_x), (b) percentage concentration of adsorbed hydroxyls, (c) potassium distribution on the catalyst's surface, (d) concentration of OH and K–O sites on HS-K, and (e) concentration of OH + KO sites on the H_2O/EtOH molar ratio for the LS-Co/ZrO_2, HS-Co/ZrO_2 and HS-KCo/ZrO_2 catalysts under ESR at 420ºC.

The results showed (Fig. 10a) that the HS-catalyst (with smaller cobalt crystallites) was more prone to get oxidized than the LS-counerpart (with lager cobalt crystallites).

It suggests that cobalt crystallites size (Table 1) is an important factor influencing catalysts' oxidation under the reaction conditions in the unpromoted catalysts. However, even though the potassium-promoted catalyst exhibited bigger cobalt crystallites size than those in the HS-catalyst (44 nm vs. 22 nm, respectively, Table 1), and moreover they were comparable to cobalt crystallites of the LS one (42 nm); the HS-K was more oxidable under the reaction condition. The HS-K was also more resistant to reduction, as shown in Figs. 1 and 2. Thus, in the case of potassium-promoted catalyst another factor than cobalt active phase crystallites size may additionally promote surface's oxidation. The potassium promoter (beside other aspects of promotion) may create new crystalline defects on the initially flat surface of large cobalt crystallites. It may be also suggested that the highly-dispersed zirconia support make cobalt oxidation easier – the both HS- and HS-K catalysts with better-dispersed (HS, d_{ZrO_2} = 25–26 nm) supports were more prone to oxidation than the low-dispersed (LS, d_{ZrO_2} = 87 nm).

A significant increase of hydroxyl's concentration is seen when reaction mixtures with the H_2O/EtOH molar ratios, higher than the stoichiometric, were used (Fig. 10b). The both unpromoted catalysts exhibited very similar and very low concentration of hydroxyls under the stoichiometric reactants mixture. However, also the large amounts of coke should be taken into consideration in that case. After the increase of water excess, the higher abundance of hydroxyls was found on the surface of unpromoted catalysts. This might be assigned to the higher share of oxidized cobalt in the active phase. Note that for very similar share of CoO_x species on the surface of the unpromoted catalysts under the H_2O/EtOH molar ratio of 12/1 (Fig. 10a), almost identical concentration of hydroxyls was found (Fig. 10b). It may be considered as a circumstance that oxidation of cobalt active phase is coupled with hydroxyl species formation. However, –OH species may be also formed on the surface of the zirconia support [73].

The concentration of hydroxyls on the surface of the HS-K catalyst is much higher than on the unpromoted LS- and HS-catalysts, already at the stoichiometric reactants molar ratio, and it also increases with the H_2O/EtOH molar ratio (Fig. 10b). The question is whether this effect is directly related to the presence of potassium-containing species on the catalyst's surface.

Fig. 10c shows that with the increase of the H_2O/EtOH molar ratio the total concentration of potassium and the share of KCO_3 species on the catalyst's surface increases. The concentration of remaining K–O sites between the 3/1–9/1 H_2O/EtOH molar ratios change very little and at higher water excess (12/1 molar ratio) the increase of the share of K–O sites on the catalyst's surface is more pronounced. It is justified that those surface potassium sites bonded to carbonate species have limited influence on the course of the ESR sites. Therefore, only K–O sites are those potassium ones potentially employed to the course of the ESR. When comparing the surface concentration of hydroxyl species (Fig. 10b) with that of K–O sites (Fig. 10c) one can notice that the former is much higher than the latter. It enables us to propose that the K–O sites create places, additional to hydroxyl species, on the catalyst's surface providing a supplementary reservoir of oxygen-containing species that aid keeping the surface in a clean, uncoked state under ESR conditions. The abundance of K–O sites on the surface of the potassium-promoted zirconia supported cobalt catalyst is lower than amount of hydroxyl species (Fig. 10d). However, considering the concentration of both OH and K–O sites together it can be seen (Fig. 10e) that it is much higher than the concentration of hydroxyls on the unpromoted catalysts, and it increases slightly with increasing reactants molar ratio.

3.2. Correlation of the ESR catalytic performance with the catalysts' surface

The analysis of the influence of the cobalt oxidation state and the amount of surface adsorbed –OH species on the selectivity of the ESR to carbon dioxide over each catalyst (Fig. 11) shown that both factors could be important for good catalyst's selectivity in the ESR. In Fig. 11a the linear relationships between cobalt oxidation state and catalysts' selectivity, nevertheless, for each catalyst, are shown. It suggests that an importance of the cobalt oxidation state in the case of higly-dispersed zirconia supported catalysts should not be neglected. Because the surface's concentration of cobalt active phase (Table 2) and extent of its oxidation (Table S1 in Supporting Information) are very different in all catalysts and under various H_2O/EtOH molar ratios, the possible influence of the surface concentration of oxidized cobalt species (proportional also to the Co(II)–Co(0) pair amounts) on the ESR selectivity was considered in Fig. 11b. Clearly separated relationships of carbon dioxide selectivity and Co(II) amounts for each catalyst were found. At the same concentration of cobalt ions very different selectivities of the ESR are obtainable. It proves that other surface

species are responsible for more or less selective course of the ESR. The both surface hydroxyls, or hydroxyls and K–O sites together can be considered.

Two relationships of surface hydroxyls' concentration with the selectivity of carbon dioxide formation are shown in Fig. 11c. The first is the relationship for the HS- and HS-K catalysts with better dispersed zirconium oxide support, in spite of different cobalt crystallites size and presence or not of potassium promoter in both catalysts. It increases to a certain limit value of the ESR selectivity to carbon dioxide. The second relationship concerns the LS-catalyst with the lowdispersed support and large cobalt crystallites. The ESR selectivity over the LS-catalyst is lower than that in the presence of HS-catalysts – at the same concentration of –OH species on the surface of unpromoted catalysts, different selectivity to carbon dioxide is achievable. Therefore, it might be concluded that another important factor influencing the unpromoted catalysts' selectivity is the dispersion of both – the active phase and the zirconia support. Similar two dependences are also seen in relationship to the –OH concentration and selectivities towards remaining ESR products, i.e., hydrogen, carbon monoxide and methane (see Fig. S2 in Supplementary Information).

The correlation in Fig. 11c shows that –OH species and the dispersion of the catalyst components are directly related to the ESR product selectivity. However, in previous section, as well as, in previous Chapters it was shown that potassium promoter undoubtedly introduces its own sites on the catalyst surface providing supplementary reservoir of oxygen-containing species additionally improving the catalyst properties. Considering both, –OH species together with K–O sites, as those directly influenced the ESR selectivity over HS-K catalyst, the relationships similar to those presented in Fig. 11c are obtained. The selectivities towards two main products of the ESR, i.e. to carbon dioxide (Fig. 12a) and hydrogen (Fig. 12b) over HS- and HS–K catalysts go to limit values, characteristic for the latter catalyst. Those the highest selectivities result from the thermodynamic equilibrium of side reactions enabling hydrogen to reach the yield of 5.56 mole per one mole of ethanol in the feed as against the stoichiometric value of 6.0 [105]. Also, for the same reason the yield of carbon dioxide is lower than the stoichiometric value of 2.0. In our studies the yields of hydrogen and carbon dioxide reach the thermodynamic limit values (Fig. 12e). The ESR selectivities towards other products also fall to values characteristic for the potassium-promoted catalyst (Figs. 12c and 12d). In Figs. 12b and 12d changes in hydrogen and hydrogen containing methane formed over LS–catalyst in relation to

hydroxyl species surface concentration have the opposite direction to those observed for HS- and HS–K catalyst. They may indicate for significant participation of a non-selective side path of the ESR process, i.e., methanation of the surface carbonaceous deposit or of carbon oxides, over that catalyst with very low-dispersed cobalt active phase and zirconia support. However, stating why on this specific catalyst and why the share of this path is higher than on both HS–catalysts is out of the scope of the thesis.

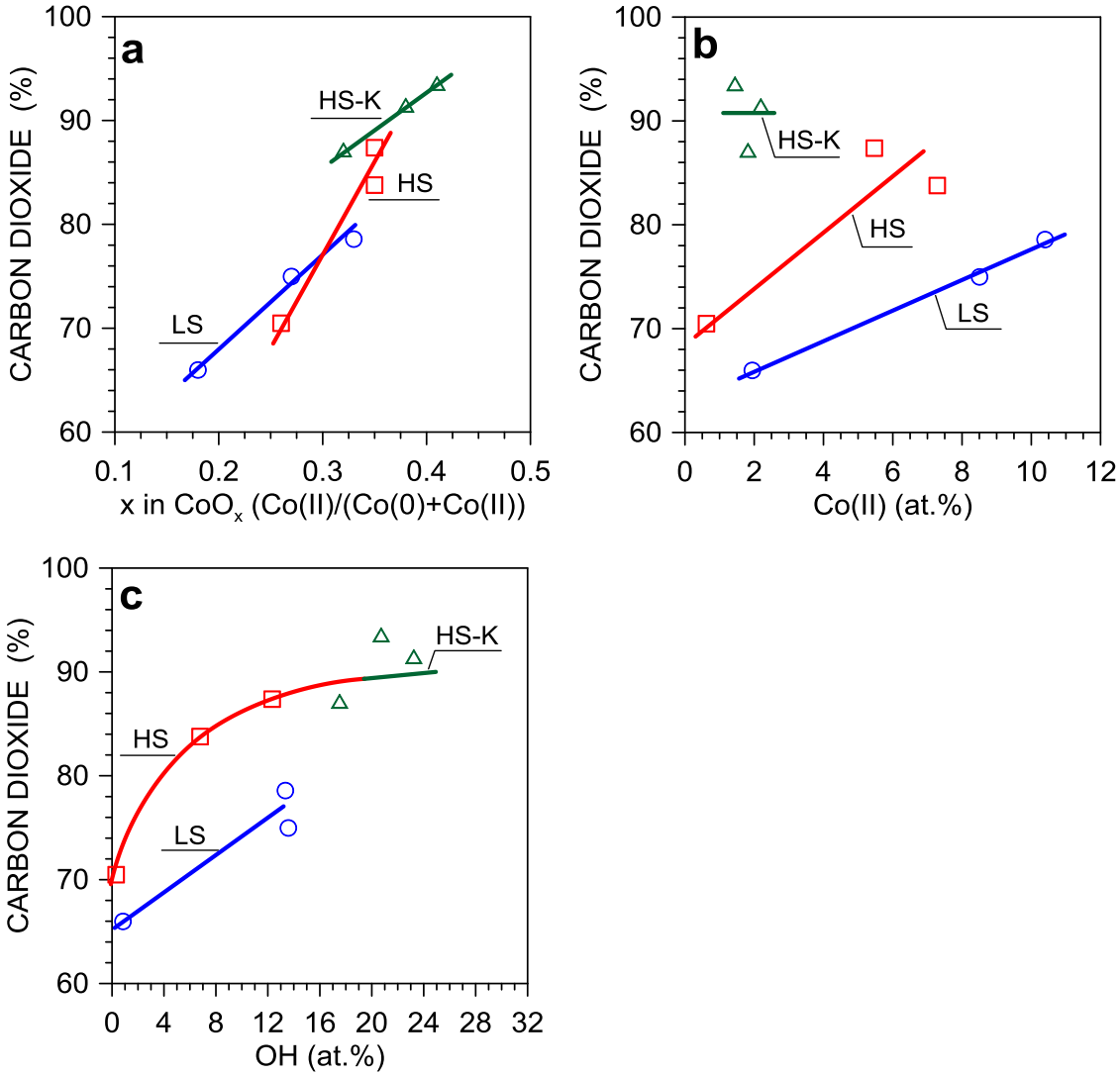

Fig. 11. Correlation of CO_2 selectivity for the LS-, HS- and HS-K catalysts under the ESR at 420ºC with (a) cobalt oxidation state (CoO_x), (b) cobalt ions Co(II) surface atomic concentration, and (c) percentage contribution of hydroxyls on the surface.

The analysis of results shown in Figs. 12a–12e, obtained for the HS- and LS-catalysts, allow for the conclusion that, in spite of generally low dispersion of zirconia-supported catalysts, the morphology of crystallites of cobalt and its support, their size and the location of oxygen-containing species are as important as their abundance. This problem was discussed in details in Chapter 3.

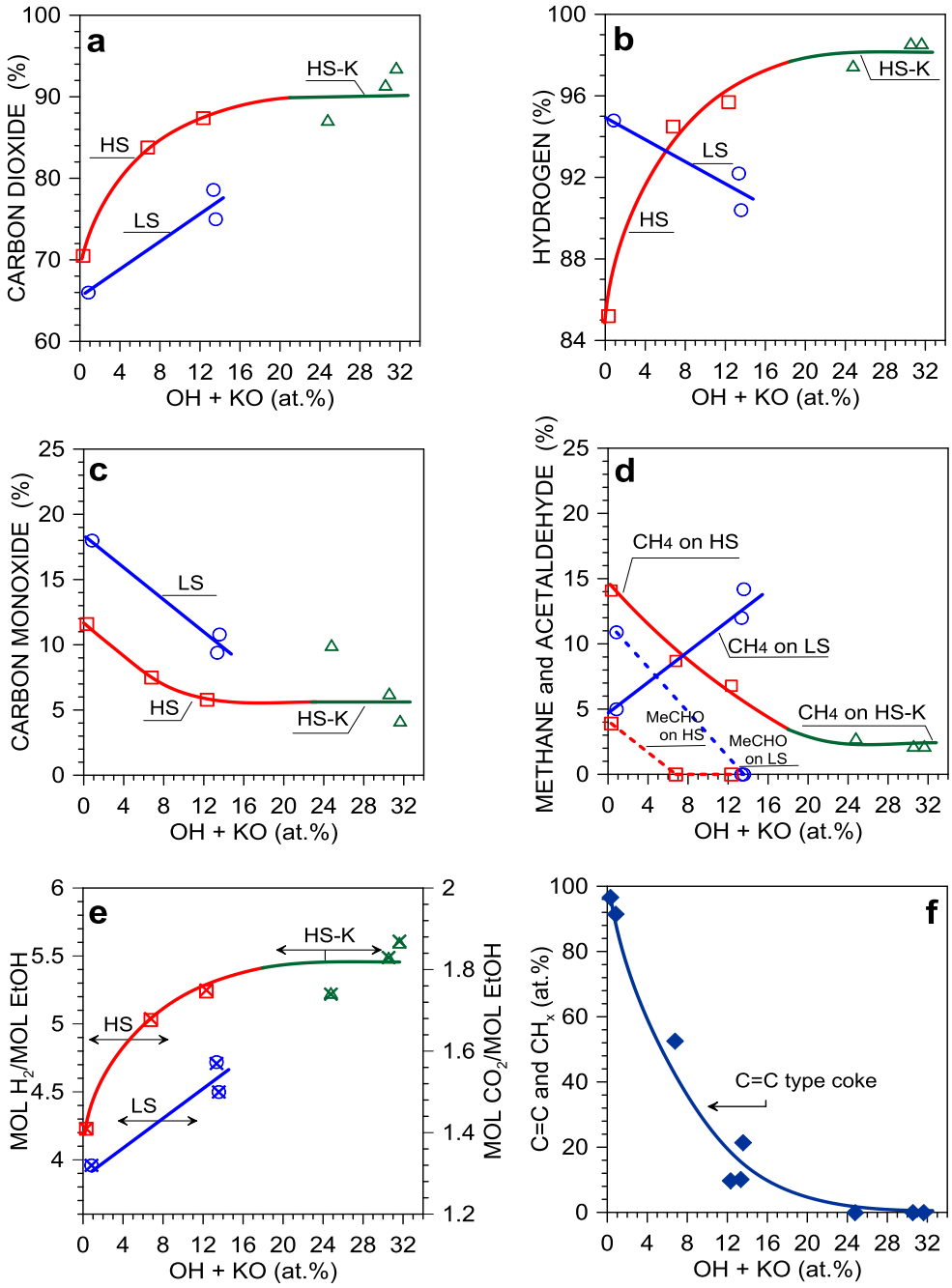

Fig. 12. Correlation of (a–d) the catalysts' selectivity towards H_2 and carbon-containing products, (e) H_2 and CO_2 yield (the red, blue and green ×symbols refer to the CO_2 yield for the HS-, LS- and HS-K, respectively), and (f) the concentration of C=C species on the whole surface, with the concentration of hydroxyl species and K–O sites on the surface of the LS-Co/ZrO_2, HS-Co/ZrO_2 and HS-KCo/ZrO_2 catalysts under the ESR at 420ºC. Each point represents a different H_2O/EtOH molar ratio.

The influence of oxygen-containing species concentration on the amount of coke formed is undeniable (Fig. 12f). Very small abundance of these species led to dramatic catalyst's coking by completely (or almost completely) dehydrogenated C=C type (Table S1 in Supplementary Information) carbonaceous deposit, mainly as graphitic nanofibers (Figs. 6 and 7). The increase of the concentration of oxygen-

containing species significantly reduces the catalysts' coking, however, without changing its type to more hydrogenated. The total elimination of coking phenomena can be reach when c.a. 25 at.% (or more) coverage of the whole surface of the catalyst is achieved.

Conslusions

In this part of the thesis there were presented results of XPS studies of Co/ZrO_2 catalysts with micro- and nano-dispersed supports under the steam reforming of ethanol with various (3/1, 9/1 and 12/1) H_2O/EtOH molar ratios at 420ºC. The effect of potassium promotion was also examined. Generally, all used zirconia-supported catalysts were low-dispersed ones – a nature of this support does not allow preparing a highly-dispersed cobalt active phase.

The reducibility of cobalt oxide (zirconium oxide support is unreducible in hydrogen atmosphere at 420^{o}C) in catalysts pre-activation step depends on catalyst's dispersion. Cobalt oxide in poorly dispersed catalyst is easier to reduce by hydrogen than its counterpart; whereas potassium promoter facilitates reduction of cobalt oxides in zirconia-supported catalysts.

The unpromoted zirconia-supported cobalt catalysts suffer from intensive coking under the steam reforming of ethanol that could be lowered by the increase of water excess in the feed. The surface of catalysts is covered by fully dehydrogenated carbonaceous deposit, mainly in the form of graphitic nanofibers, even if the ESR reaction is carried out with as high excess of water vapour as 12/1 mol/mol. Contrary to the unpromoted catalysts the surface of the potassium-promoted catalyst is free of coke under all (beginning from the stoichiometric) H_2O/EtOH molar ratios.

The XPS results showed that under the examined ESR conditions both forms of cobalt (metallic and cobalt(II) ions) are present on the catalysts' surface; however, the metallic form is the most dominant one. The share of CoO_x species depends on the H_2O/EtOH molar ratio and it increases with increasing water excess. The oxidation extent depends also on the support dispersion, as well as, on potassium promotion. The catalyst with a low-surface area is less prone to oxidation of cobalt than the high-surface area counterpart under each ESR conditions. The potassium promotion facilitates oxidation of cobalt particles supported on zirconium oxide. However, it was proved that oxidation state of cobalt is not directly responsible for the selectivity of the steam reforming of ethanol.

The surface species directly involved in determining the ESR selectivity are hydroxyl species. The higher concentration of hydroxyls improves the ESR selectivity. Potassium promotion introduces other selective sites, which together with hydroxyls play a promoting role in the ESR. The concentration of –OH species and $K^{\delta+}$–$O_{surf}^{\delta-}$ sites on the catalysts surface raise with the H_2O/EtOH molar ratio, what enhance the selectivity of the ESR towards all gaseous products to values achievable over potassium-promoted catalyst, limited by the thermodynamics. In addition to the role of oxygen-containing species in improving the ESR selectivity, the increase of both –OH species and $K^{\delta+}$–$O_{surf}^{\delta-}$ sites was found to lower the amount of coke deposited.

In spite of the low dispersion of zirconia-supported catalysts, the morphology and the size of cobalt and support crystallites, and the adsorption site of oxygen-containing species are as important as their abundance.

References

1. D. Zanchet, J.B.O. Santos, S. Damyanova, J.M.R. Gallo, J.M.C. Bueno *ASC Catal.* **5** (2015) 3841–3863.
2. J.L. Contreras, J. Salmones, J.A. Colín-Luna, L. Nuño, B. Quintana, I. Córdova, B Zeifert, C. Tapia, G.A. Fuentes *Int. J. Hydrogen Energy* **39** (2014) 18835–18853.
3. L.V. Mattos, G. Jackobs, H.D. Burtron, F.B. Noronha *Chem. Rev.* **112** (2012) 4094–4123.
4. P.R. de la Piscina, N. Homs *Chem. Soc. Rev.* **37** (2008) 2459–2467.
5. M. Ni, D.Y.C. Leung, M.K.H. Leung *Int. J. Hydrogen Energy* **32** (2007) 3238–3247.
6. V. Subramani, C. Song *Catalysis* **20** (2007) 65–106.
7. F. Frusteri, S. Freni *J. Power Sources* **173** (2007) 200–209.
8. V.D. Parkash, A.E. Rodrigues *Chem. Eng. J.* **117** (2006) 39–49.
9. S. Turczynak, A. Machocki *Przem. Chem.* **93** (2014) 1850–1854.
10. S.S.-Y. Lin, D.H. Kim, M.H. Engelhard, S.Y. Ha *J. Catal.* **273** (2010) 229–235.
11. A.R. Passos, L. Martins, S.H. Pulcinellin, C.V. Santilli, V. Briois *Catal. Today* **229** (2014) 88–94.
12. J. Llorca, N. Homs, J. Sales, P.R. de la Piscina *J. Catal.* **209** (2002) 306–317.
13. F. Haga, T. Nakajima, H. Miya, S. Mishima *Catal Lett.* **48** (1997) 223–227.
14. H. Song, U.S. Ozkan *J. Catal.* **261** (2009) 66–74.

15. H. Song, B. Mirkelamoglu, U.S. Ozkan *Appl. Catal., A* **382** (2010) 58–64.
16. B. Bayram, I.I. Soykal, D. von Deak, J.T. Miller, U.S. Ozkan *J. Catal.* **284** (2011) 77–89.
17. E. Martono, M.P. Hyman, J.M. Vohs *Phys. Chem. Chem. Phys.* **13** (2011) 9880–9886.
18. E. Martono, J.M. Vohs *ACS Catal.* **1** (2011) 1414–1420.
19. H. Song, L. Zhang, U.S. Ozkan *Top. Catal.* **55** (2012) 1324–1331.
20. A. Machocki *Przem. Chem.* **85** (2006) 1045–1048.
21. Zs. Ferencz, A. Erdöhelyi, K. Baan, A. Oszkó, L. Óvári, Z. Kónya, C. Papp, H.-P. Steinrück, J. Kiss *ACS Catal*. **4** (2014) 1205–1218.
22. P. Bichon, G. Haugom, H.J. Venvik, A. Holmen, E.A. Blekkan *Top Catal.* **49** (2008) 38–45.
23. J. Llorca, J.A. Dalmon, P.R. de la Piscina, N. Homs *Appl. Catal., A* **243** (2003) 261–269.
24. T. Nishiguchi, T. Matsumoto, H. Kanai, K. Utani, Y. Matsumura, W.-J. Shen, S. Imamura *Appl. Catal. A* **279** (2005) 273–277.
25. G.R. Rao, B.G. Mishra *Bull. Catal. Soc. India* **2** (2003) 122–134.
26. H. Song, U.S. Ozkan *J. Phys. Chem. A* **114** (2010) 3796–3801.
27. F.L.S. Carvalho, Y.J.O. Asencios, A.M.B. Rego, E.M. Assaf *Appl. Catal., A* **483** (2014) 52–62.
28. P.D.L. Mercera, J.G. van Ommen, E.B.M. Doesburg, A.J. Burggraaf, J.R.H. Ross *Appl. Catal.* **71** (1991) 363–391.
29. A. Scarabello, D.D. Nogare, P. Canu, R. Lanza *Appl. Catal., B* **174–175** (2015) 308–322.
30. M.M. Yung, E.M. Holmgreen, U.S. Ozkan *Catal Lett.* **118** (2007) 180–186.
31. G. Águila, S. Guerrero, P. Araya *Catal. Commun.* **9** (2008) 2550–2554.
32. S. Mostafa, Jason R. Croy, H. Heinrich, B. Roldan Cueny *Appl. Catal., A* **366** (2009) 353–362.
33. J. Sun, A.M. Karim, D. Mei, M. Engelhard, X. Bao, Y. Wang *Appl. Catal., B* **162** (2015) 141–148.
34. A.G. Sato, D.P. Volanti, D.M. Meira, S. Damyanova, E. Longo, J.M.C. Bueno *J. Catal.* **307** (2013) 1–17.
35. P. Rybak, B. Tomaszewska, A. Machocki, W. Grzegorczyk, A. Denis, *Catal. Today* **176** (2011) 14–20.

36. A. Machocki, A. Denis, W. Grzegorczyk, W. Gac *Appl. Surf. Sci.* **256** (2010) 5551–5558.
37. T. Yamazaki, N. Kikuchi, M. Katoh, T. Hirose, H. Saito, T. Yoshikawa, M. Wada *Appl. Catal., B* **99** (2010) 81–88.
38. R. Padilla, M. Benito, L. Rodríguez, A. Serrano, G. Muñoz, L. Daza *Int. J. Hydrogen Energy* **35** (2010) 8921–8928.
39. M.H. Youn, J.G. Seo, S. Park, J.C. Jung, D.R. Park, I.K. Song *Int. J. Hydrogen Energy* **33** (2008) 7475–7463.
40. S.M. de Lima, A.M. Silva, I.O. da Cruz, G. Jacobs, B.H. Davis, L.V. Mattos, F.B. Noronha *Catal. Today* **138** (2008) 162–168.
41. J.-L. Bi, Y.-Y. Hong, C.-C. Lee, C.-T. Yeh, C.-B. Wang *Catal. Today* **129** (2007) 322–329.
42. S. Letichevsky, P.C. Zonetti, P.P.P. Reis, J. Celnik, C.R.K. Rabello, A.B. Gaspar, L.G. Appel *J. Mol. Catal. A* **410** (2015) 177–183.
43. M.P. Hyman, J.M. Vohs *Surf. Sci.* **605** (2011) 383–389.
44. S.-W. Yu, H.-H. Huang, C.-W. Tang, C.-B. Wang Int. *J. Hydrogen Energy* **39** (2014) 20700–20711.
45. L. Óvári, S.K. Calderon, Y. Lykhach, J. Libuda, A. Erdőhelyi, C. Papp, J. Kiss, H.-P. Steinrück *J. Catal.* **307** (2013) 132–139.
46. A.M. Karim, Y. Su, M.H. Engelhard, D.L. King, Y. Wang *ACS Catal.* **1** (2011) 279–286.
47. L.P.R. Profeti, E.A. Ticianelli, E.M. Assaf *Appl. Catal., A* **360** (2009) 17–25.
48. S. Tuti, F. Pepe *Catal. Lett.* **122** (2008) 196–203.
49. E. Varga, Z. Ferencz, A. Oszkó, A. Erdöhelyi, J. Kiss *J. Mol. Catal. A* **397** (2015) 127–133.
50. V.M. Lebarbier, A.M. Karim, M.H. Engelhard, Y. Wu, B.-Q. Xu, E.J. Petersen, A.K. Datye, Y. Wang, *ChemSusChem* **4** (2011) 1679–1684.
51. E. Martono, J.M. Vohs *J. Catal.* **291** (2012) 79–86.
52. S. Ogo, T. Shimizu, Y. Nakazawa, K. Mukawa, D. Mukai, Y. Sekine *Appl. Catal., A* **495** (2015) 30–38.
53. S. Davidson, J. Sun, Y. Wang *Top Catal.* **56** (2013) 1651–1659.
54. K.-S. Kim, H.-R. Seo, S.Y. Lee, J.-G. Ahn, W.Ch. Shin, Y.-K. Lee *Top Catal.* **53** (2010) 615–620.
55. S.D. Davidson, J. Sun, Y. Wang *Top Catal.* **269** (2015) 140–147.

56. J. Llorca, N. Homs, J. Sales, J.-L.G. Fierro, P.R. de la Piscina *J. Catal.* **222** (2004) 470–480.
57. Y. Pan, Y. Gao, D. Kong, G. Wang, J. Hou, S. Hu, H. Pan, J. Zhu *Langmuir* **28** (2012) 6045–6051.
58. S. Tsunekawa, A. Asami, S. Ito, M. Yashima, T. Sugimoto *Appl. Surf. Sci.* **252** (2005) 1651–1656.
59. W. Wang, H.T. Guo, J.P. Gao, X.H. Dong, Q.H. Qin *J. Mater. Sci.* **35** (2000) 1495–1499.
60. R. Brenier, J. Mugnier, E. Mirica *Appl. Surf. Sci.* **143** (1999) 85–91.
61. Y.S. Li, P.C. Wong, K.A.R. Mitchell *Appl. Surf. Sci.* **89** (1995) 263–269.
62. P.C. Wong, Y.S. Li, M.Y. Zhou, K.A.R. Mitchell *Appl. Surf. Sci.* **89** (1995) 255–261.
63. S. Zafeiratos, T. Dintzer, D. Teschner, R. Blume, M. Hävecker, A. Knop-Gericke, R. Schlögl *J. Catal.* **269** (2010) 309–317.
64. M.C. Biesinger, B.P. Payne, A.P. Grosvenor, L.W.M. Lau, A.R. Gerson, R.St.C. Smart *Appl. Surf. Sci.* **257** (2011) 2717–2730.
65. Y.T. Law, T. Dintzer, S. Zafeiratos *Appl. Surf. Sci.* **258** (2011) 1480–1487.
66. S. Zafeiratos, F. Paloukis, G. Papakonstantinou, D. Teschner, M. Hävecker, E. Vass, P. Schnörch, A. Knop-Gericke, R. Schlögl, B. Moreno, E. Chinarro, J.R. Jurado, S.G. Neophytides *Catal. Today* **157** (2010) 250–256.
67. J.E. Kim, J. Lim, G.Y. Lee, S.H.Choi, U.N. Maiti, W.J. Lee, Ho.J. Lee, S.O. Kim *ACS Appl. Mater. Interfaces* **8** (2016) 1571–1577.
68. Z.-Y. Lim, C. Wu, W.G. Wang, K.-L. Choy, H. Yin *J. Mater. Chem. A*, **4** (2016) 153–159.
69. A. Galtayries, J. Grimblot *J. Electr. Spectrosc. Rel. Phen.* **98–99** (1999) 267–275.
70. A. Roustila, J. Chêne, C. Séverac *J. Alloys Compd.* **356–357** (2003) 330–335.
71. Y. Liu, B. Liu, Q. Wang, C. Li, W. Hu, Y. Liu, P. Jing, W. Zhao, J. Zhang *J. Catal.* **296** (2012) 65–76.
72. L. Xu, Y. Ma, Y. Zhang, B. Chen, Z. Wu, J. Jiang, W. Huang *J. Phys. Chem. C* **114** (2010) 17023–17029.
73. E.I. Kauppi, K. Honkala, A.O.I. Krause, J.M. Kanervo, L. Lefferts *Top. Catal.* **59** (2016) 823–832.

74. B. Lamontagne, F. Semond, D. Roy *J. Electron. Spectrosc. Relat. Phenom.* **73** (1995) 81–88.
75. G. Pirug, O. Müller, H. P. Bonzel *Surf. Sci.* **73** (1993) 145–154.
76. D. Krix, H. Nienhaus *Appl. Surf. Sci.* **270** (2013) 231–237.
77. C.-K. Choo, D. Suzawa, K. Tanaka *Surf. Sci.* **600** (2006) 1518–1525.
78. A. Caballero, J.P. Espinós, A. Fernández, L. Soriano, A.R. González-Elipe *Surf. Sci.* **364** (1996) 253–265.
79. A.P. Baddorf *Surf. Sci.* **264** (1992) 73–80.
80. A.V. Shchukarev, D.V. Korolkov *CEJC* **2** (2004) 347–362.
81. H.-J. Won, B. Baigalmaa, J.-Kwon Moon, C.-H. Jung, K.-W. Lee, J.-H. Hyun *J. Radioanal Nucl. Chem.* **287** (2011) 525–531.
82. Y. Joseph, G. Ketteler, C. Kuhrs, W. Ranke, W. Weiss, R. Schlögl *Phys. Chem. Chem. Phys.* **3** (2001) 4141–4153.
83. K. Kishi, S. Ikeda *Bull. Chem. Soc. Jpn.* **46** (1973) 341–345.
84. Y. Kebukawa, M.E. Zolensky, A.L.D. Kilcoyne, Z. Rahman, P. Jenniskens, G.D. Cody *Meteorit. Planet. Sci.* **49** (2014) 2095–2103.
85. D. Salinas, G. Pecchi, V. Rodríguez, J.L.G. Fierro *Mod. Res. Catal.* **4** (2015) 68–77.
86. Q. Li, X. Wang, Y. Xin, Z. Zhang, Y. Zhang, C. Hao, M. Meng, L. Zheng, L. Zheng *Sci. Rep* **4** (2014) 4725.
87. D. Salinas, G. Pecchi, V. Rodríguez, J.L.G. Fierro *J. Phys. D: Appl. Phys.* **38** (2005) 41–50.
88. A. Burri, N. Jiang, S.-E. Park *Catal. Sci. Technol.* **2** (2012) 514–520.
89. D. Courcot, C. Pruvost, E. A. Zhilinskaya, A. Aboukaïs *Kinet. Catal.* **45** (2004) 614–621.
90. P. Finetti, M.J. Scantlebury, R. McGrath, F. Borgatti, M. Sambi, L. Zaratin, G. Granozzi *Surf. Sci.* **461** (2000) 240–254.
91. H.H. Huang, X Jiang, Z Zou, W.S Chin, G.Q Xu, W.L Dai, K.N Fan, J.F Deng, *Surf. Sci.* **412/413** (1998) 555–561.
92. H.H. Huang, X. Jiang, Z. Zou, G.Q. Xu, W.L. Dai, K.N. Fan, J.F. Deng *Surf. Sci.* **398** (1998) 203–210.
93. G. Maniak, P. Stelmachowski, A. Kotarba, Z. Sojka, V. Rico-Pérez, A. Bueno-López *Appl. Catal., B* **136–137** (2013) 302–307.
94. J. Iranmahboob, D.O. Hill, H. Toghian *Appl. Surf. Sci.* **185** (2001) 72–78.

95. D.A. King, D.P. Woodruff *The Chemical Physics of Solid Surfaces*. Vol. 6. 1993, Elsevier Science Publishers B.V.: Amsterdam, 225–251.
96. K. Engvall, L. Holmlid, A. Kotarba, J.B.C. Pettersson, P.G. Menon, P. Skaugset *Appl. Catal., A* **134** (1996) 239–246.
97. R. Wang, C. Chen, S. Deng, P. Shen, L. Gong, N. Zhang *J. Chil. Chem. Soc.* **59** (2014) 2710–2716.
98. F.B. Noronha, C.A. Perez, M. Schmal, R. Fréty *Phys. Chem. Chem. Phys.* **1** (1999) 2861–2867.
99. B. Jongsomjit, J. Panpranot, J.G. Goodwin Jr. *J.Catal.* **204** (2001) 98–109.
100. M. Greluk, P. Rybak, G. Słowik, M. Rotko, A. Machocki *Catal. Today* **242** (2015) 50–59.
101. A. Galtayries, J. Grimblot *J. Electr. Spectrosc. Rel. Phen.* **98–99** (1999) 267–275.
102. S. Turczyniak, W. Luo, V. Papaefthimiou, N. S. Ramgir, M. Haevecker, A. Machocki, S. Zafeiratos *Top. Catal.* **59** (2016) 532–542.
103. J. Światowska, V. Lair, C. Pereira-Nabais, G. Cote, P. Marcus, A. Chagnes *Appl. Surf. Sci.* **257** (2011) 9110–9119.
104. T.Y. Kim, J. Baek, C. Song, Y.S. Yun, D.S. Park, W. Kim, J.W. Han, J. Yi *J. Catal.* **323** (2015) 85–99.
105. K. Vasudeva, N. Mitra, P. Umasankar, S.C. Dhingra *Int. J. Hydrogen Energy* **21** (1996) 13–18.
106. G. Słowik, M. Greluk, A. Machocki *Mater. Chem. Phys.* **173** (2016) 219–237.

Supporting Information

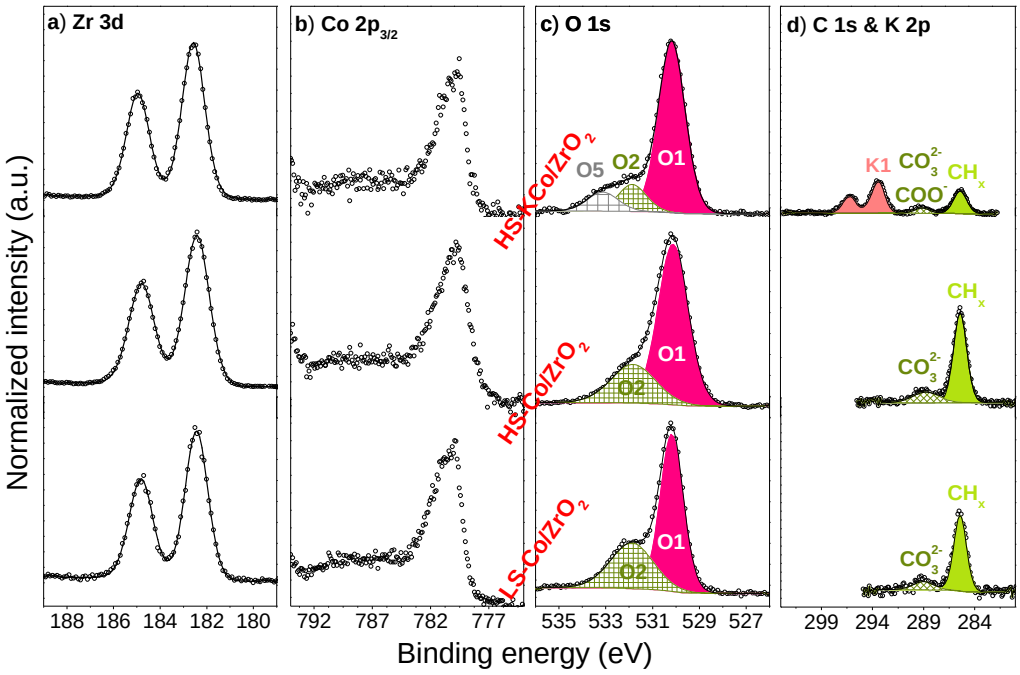

Fig. S1. The high resolution XPS spectra of (a) Zr 3d, (b) Co $2p_{3/2}$, (c) O 1s and (d) C 1s, Ce 4s & K 2p for fresh (in the oxide form): LS-Co/ZrO_2, HS-Co/ZrO_2 and HS-KCo/ZrO_2 catalysts; c) O1 – lattice oxygen, O2 – hydroxyl and carbonate species, O5 – COO^- species d) K1 – $KCO_3^{2-}$and K–O sites.

Table S1. The percentage contribution of different species in the Co 2p, O 1s, C 1s high resolution XPS spectra of the catalyst after reduction and after the ESR.

		Contribution of given species in the XPS spectrum (%)							
	H_2O/EtOH (mol/mol)	Co 2p	O 1s				C 1s		
Catalyst		Co(II)	O_{latt}	OH	KCO_3, KO	H_2O	C=C	C-O	CO_3^{2-}
LS-Co/ZrO_2		0.0	83.5	16.5	0.0	0.0	100.0	0.0	0.0
HS-Co/ZrO_2	H_2 **	10.2	83.2	16.8	0.0	0.0	100.0	0.0	0.0
HS-KCo/ZrO_2		18.8	65.6	20.1	14.3	0.0	0.0	0.0	100.0
LS-Co/ZrO_2		17.5	74.2	17.9	0.0	7.9	100.0	0.0	0.0
HS-Co/ZrO_2	3/1	25.5	78.4	16.1	0.0	5.5	100.0	0.0	0.0
HS-KCo/ZrO_2		31.9	63.1	33.2	0.0	3.7	0.0	0.0	100.0
LS-Co/ZrO_2		27.0	65.2	29.3	0.0	5.5	100.0	0.0	0.0
HS-Co/ZrO_2	9/1	34.6	70.6	23.5	0.0	5.9	100.0	0.0	0.0
HS-KCo/ZrO_2		37.6	47.4	50.3	0.0	2.3	0.0	31.4	68.6
LS-Co/ZrO_2		32.5	71.1	25.1	0.0	3.7	100.0	0.0	0.0
HS-Co/ZrO_2	12/1	34.6	74.4	21.5	0.0	4.1	100.0	0.0	0.0
HS-KCo/ZrO_2		41.0	49.3	48.4	0.0	2.3	0.0	25.5	74.5

**Results obtained after the catalysts' pre-reduction (H_2/Ar) at 420ºC for 1 h.

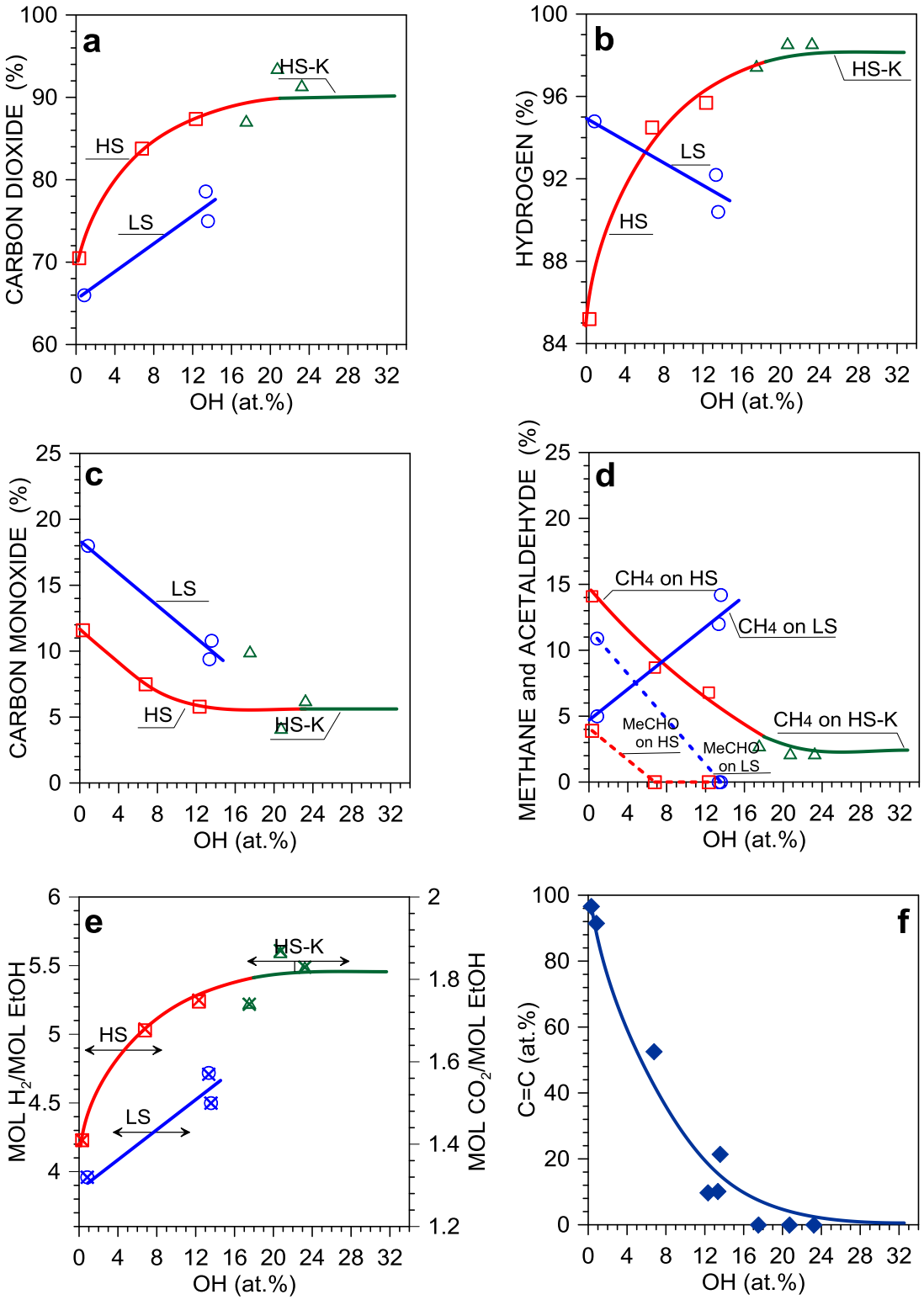

Fig. S.2 Correlation of (a–d) the catalysts' selectivity towards H_2 and carbon-containing product, (e) H_2 and CO_2 yield (the red, blue and green ×symbols refer to the CO_2 yield for the HS, LS and HS-K, respectively), and (f) the concentration of C=C species on the whole surface, with the concentration of hydroxyls on the surface of the LS-Co/ZrO_2, HS-Co/ZrO_2 and HS-KCo/ZrO_2 catalysts under the ESR at 420ºC. Each point represents a different H_2O/EtOH molar ratio.

CHAPTER

6

Time-dependent analysis of the surface state and the ESR catalytic performance of Co/ZrO_2 catalysts

OUTLINE

Abstract

Zirconia-supported cobalt catalysts were examined in the ESR condition ($H_2O/EtOH$ = 12/1 mol/mol, 420℃) for changes of their surfaces' composition and catalytic performance with time-on-stream. It was found that, with the reaction time, the active phase (cobalt) of all catalysts underwent progressive oxidation, which is promoted by the potassium addition. The catalysts supported on nano-zirconia exhibited stable catalytic performance, whereas H_2 and CO_2 yield over the LS-catalyst rapidly decreased with the reaction time. The unpromoted catalysts experienced severe coke formation, which hampered the determination of the sites that might promote the ESR reaction. The coking phenomenon was suppressed after the catalyst's promotion with potassium. It was found that both hydroxyls and potassium containing species (K–O) hinder coke formation and might play a promoting role in the course of the ESR

Introduction

Cobalt-based zirconia-supported catalysts has been less studied for the ESR reaction as compared to ceria-supported ones, apparently due to their rather poor catalytic performance at relatively low temperatures (<420ºC) [1, 2]. Most of the so far published works, devoted to studies of the ESR over zirconia-supported cobalt catalysts, concern their basic characterization and/or catalytic behaviour [1–9]. However, there are also studies in which authors made an attempt to understand the influence on the catalytic performance of factors such as: the support dispersion [2], the synthesis parameters [9], the metal loading [10], the addition of a promoter [11], and the active phase oxidation state [10, 11].

A. Machocki et al. [2] showed that support morphology and cobalt dispersion influences the activity and selectivity of pre-reduced zirconia-supported cobalt catalysts (H_2O/EtOH= 21/1 mol/mol, T = 420ºC). Whereas the ethanol conversion achieved was 100% regardless of the support nature, the catalyst with a low-dispersed zirconia support exhibited lower water conversion than its high-dispersed counterpart. This influenced the catalysts' performance with the low-dispersed catalysts to show worse selectivity towards hydrogen and carbon dioxide.

Very similar high-dispersed zirconia-supported cobalt catalyst was examined in terms of its ESR catalytic performance (H_2O/EtOH= 21/1 mol/mol, T = 420ºC) omitting the reduction step [1]. In this case, the initial ethanol conversion was significantly lower (44%) as compared to previous studies [2], while water conversion was very similar. The selectivity to such products as hydrogen and carbon dioxide was very low, whereas the increase of the contribution of acetaldehyde and acetone in the by-products was observed. The authors [2] found that the catalyst was deactivated very fast, which was assigned to the intensive coking and/or sintering of the catalyst.

In studies of J. Sun et al. [10] it was suggested that over zirconia-supported cobalt catalyst ethanol is first transformed into acetaldehyde, which then is converted to acetone via condensation/ketonization process. Further steam reforming of acetone results in formation of hydrogen, carbon oxides, and small amounts of methane. According to the authors, close interaction of Co(II) with zirconia was responsible for such reaction pathway. They suggested that this interaction probably results in passivation of acidic sites on the catalyst's surface, enhancing dehydrogenation activity. It was also suggested that balanced acid-base properties promote

condensation/ketonization of acetaldehyde, whereas steam reforming of acetone proceeds on metallic cobalt particles sitting at the tip of carbon nanofibers, formed in the course of the ESR.

So far, there were no studies concerning the influence of the reaction time on the surface state and the ESR catalytic performance of unpromoted and potassium-promoted zirconia-supported catalysts. The aim of this study was to gain knowledge regarding the surface state of zirconia-supported cobalt catalysts during the ESR, and try to correlate it with the catalysts' selectivity.

1. Experimental

1.1. Catalysts preparation and characterization

This studies were performed on the unpromoted cobalt-based nano- (HS) and micro-zirconia (LS) supported catalysts, as well as, on the potassium-promoted nano-catalyst (HS-K), preparation and characterization (XRF, XRD, nitrogen adsorption, hydrogen chemisorption, H_2-TPR) of the catalysts were presented in details in the experimental section of the Chapter 5.

1.2. Combined XPS and catalytic performance experiments

The detailed description of experimental set-up and catalysts pre-reduction procedure can be find in the experimental section of the Chapter 3 and Chapter 5.

The samples experienced variable degrees of charging. To minimize this effect a flood gun source was used. The XPS spectra were calibrated for the main peak in O 1s (530 eV).

After reduction procedure and XPS characterization, samples were transferred in UHV to the high pressure reactor. Prior to the reaction, samples were heated in the stream of Ar (50 cm^3/min, p_{total} = 1 atm) with the ramp rate 10ºC/min up to 420ºC. Water/ethanol vapours (molar ratio of 12/1, 3 cm^3/min) diluted in Ar (50 cm^3/min) were introduced to the reactor (by heated lines) at the reaction temperature (420ºC) by a Controlled Evaporation and Mixing (CEM) System (Bronkhorst). The ESR (420ºC, p_{total} = 1 atm) was carried out over 1 h. Next, the flow of vapours was stopped and the samples were quenched in the stream of Ar till 80ºC, and then transferred in the UHV to the XPS analysis chamber. After the XPS characterization, the ESR reaction was carried out over the unpromoted samples for 2 h (in total 3 h) and for

potassium-promoted catalyst for 2 h and additionally 4 h (in total 7 h). After each reaction cycle, the samples were characterized by means of XPS.

In the course of the ESR reaction, carried out in the high pressure cell, the composition of gas phase products (H_2, CO_2, CO, CH_4) was monitored *on-line* by means of a micro-GC (Agilent, 490-GC).

1.3. Catalytic tests in a fixed-bed reactor

The studies of ESR catalytic behaviour (H_2O/EtOH = 12/1 mol/mol, 420ºC, p_{total} = 1 atm) were carried out also in a fixed-bed continuous-flow quartz reactor (Microactivity Reference unit, PID Eng & Tech.) under atmospheric pressure, as described in the experimental section of the Chapter 3.

The calculations of ethanol and water conversions, selectivities to hydrogen and carbon-containing products were presented in details in the experimental section of the Chapter 3, with the proviso that in the formula for H_2 selectivity, methane was the only hydrogen-containing product of the ESR found among carbon-containing products.

2. Results and discussion

2.1. XPS characterization of the Co/ZrO_2 catalysts during time-on-stream

The unpromoted zirconia-supported catalysts suffered for severe coke formation (Fig. 1), which hindered XPS analysis after only 3 h on-the-stream. Due to this inconvenience, only a small surface area of the unpromoted samples was measurable for XPS. The results of relative surfaces' composition, omitting the carbon influence can be found in Fig. S1 in the Supporting Information, enclosed to this chapter.

In the case of the unpromoted catalysts the initial coverage of carbonaceous deposit was comparable for both, while this was also the case after the first hour of the ESR (Fig. 1). Furthermore, after 3 h the atomic concentration of carbon increased significantly, and was more pronounced for the HS-catalyst as compared to LS (Fig. 1). It should be mentioned that on the surface of both unpromoted samples carbon deposit was visible even with naked eye. However, the surface of the HS-catalyst was homogeneously covered with a porous carbon layers, whereas the surface of the LS-counterpart was destroyed by carbon growing out from inner layers of the sample, exposing parts of a clean (free of carbon)

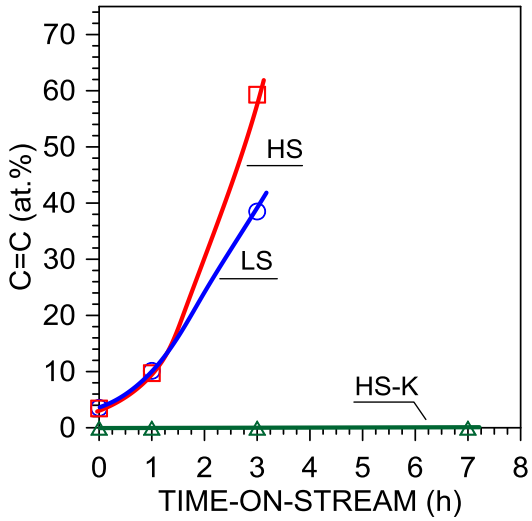

Fig. 1 The changes of C=C species atomic concentration on the surface of cobalt-based zirconia-supported catalysts versus reaction time of the ESR (H_2O/EtOH = 12/1 mol/mol, 420ºC, p_{total} = 1 atm).

Characterization of the HS-K surface allowed to conclude, that this catalyst did not suffer from coking even after 7 h on-the-stream (Fig. 1). It confirms the very important role of potassium species in suppression of coke formation.

Keeping in mind all of the above considerations on the catalysts surfaces' coverage with carbon, the change of surface composition during time-on-stream can be discussed.

The results that present the influence of the ESR reaction time on catalysts' surface state are depicted in Fig. 2a-d (see also Fig. S1 in Supplementary Information). As it is shown (Fig. 1a), only the potassium-promoted catalyst's surface did not exhibit the changes of cobalt relative concentration on the surface. The amount of cobalt remained stable within the entire measurement time, whereas in the case of unpromoted samples, the increasing amount of coke (Fig. 1) caused severe decrease of the XPS signal and thus the percentage contribution, of the other elements (cobalt, zirconium, and oxygen, Fig. 2a-c). When omitting carbon in the calculation of the elemental composition of the samples, one may see that the amount of cobalt for the all unsupported catalysts was still decreasing (Fig. S1a, Supporting Information). The concentration of zirconium on the surface of unpromoted catalysts decrease severely with the time (Fig. 2b). Taking into account only the carbon-free part of the catalyst the percentage contribution of zirconium is slowly decreasing on the surface of the HS-catalyst, whereas in the case of the LS-catalyst is increased between the first and the third hour on-the-stream (Fig. S1b, Supporting Information). As of oxygen percentage contribution on the whole catalyst's basis it was found that it decreases with

the time-on-stream (Fig. 2c). However, when omitting carbon in calculations, the percentage contribution of oxygen is slowly but progressively increasing with the reaction time (Fig. S1c in Supporting Information).

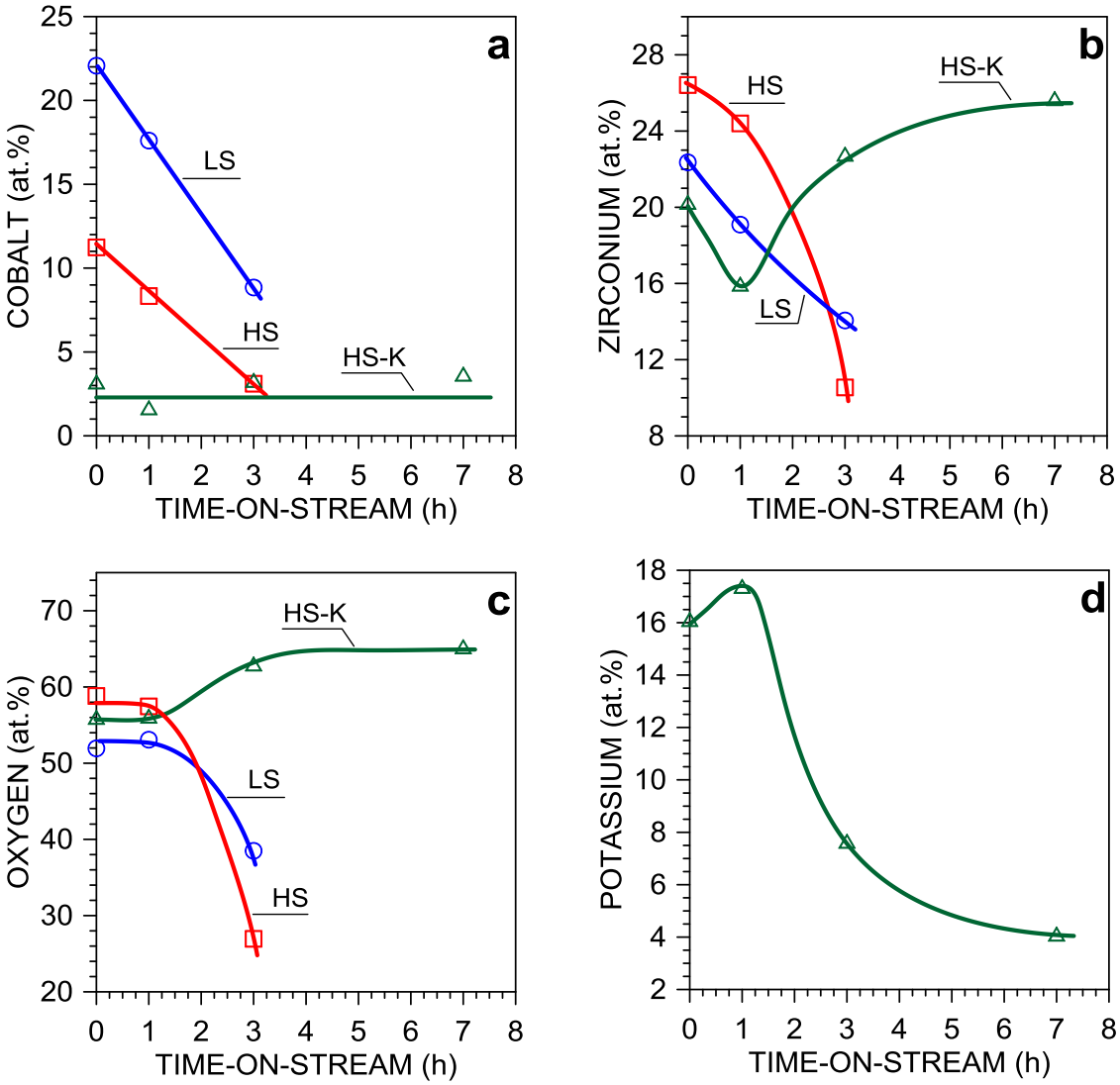

Fig. 2 The changes of elemental surface's composition of cobalt-based zirconia-supported catalysts with the ESR reaction time (H_2O/EtOH = 12/1 mol/mol, 420ºC, p_{total} = 1 atm).

Zirconium concentration (Fig. 2b) for potassium-promoted catalyst, after an initial decrease in the first one hour of the reaction, increased with the reaction time, which can be probably connected with a decrease of the amounts of potassium species on the catalyst's surface (Fig. 2d). Moreover, the surface of this catalyst was progressively oxidized, as evidenced by Fig. 2c.

Figs. 3, 5, 6 show the high resolution XPS spectra obtained after the ESR reaction (H_2O/EtOH = 12/1 mol/mol, 420ºC) carried out over the pre-reduced (H_2/Ar, 420ºC) zirconia-supported catalysts.

The Zr 3d spectra recorded for the LS-catalyst (Fig. 3a), as well as, for other catalysts (Fig. 5a and 6a), did not exhibit changes with the ESR reaction time. The peaks, characteristic of zirconium oxide [12–18], were located at 182.2 and 184.6 eV.

The evolution of Co $2p_{3/2}$ spectra of the LS-catalyst were presented in Fig. 3b. The Co $2p_{3/2}$ spectrum of the pre-reduced sample (Fig. 3b, bottom picture) was fitted with one peak (778.4 ± 0.3eV), of a characteristic asymmetric shape [19, 20] (with a weak satellite structure [21]), which in literature is assigned to the presence of metallic form of cobalt (///) [11, 21–27]. One hour after the introduction of the ESR reaction mixture (Fig. 3b, middle picture), the appearance of another feature at higher binding energy (781.2 ± 0.3 eV) can be seen. The presence of this component is a result of oxidation of cobalt particles and it was assigned to the cobalt(II) oxide-like species (\\\) [10, 11, 21, 22, 24, 25, 27–29], further abbreviated as CoO_x. The oxidation of metallic cobalt particles by the ESR reaction mixture was proved by many research teams [22, 23, 30–34]. After 3 h on-the-stream, the contribution of CoO_x species in the overall Co $2p_{3/2}$ spectrum of the LS-catalyst, slightly increased from 33 to 36% (Fig. 4a), indicating progresive oxidation of the sample with the time.

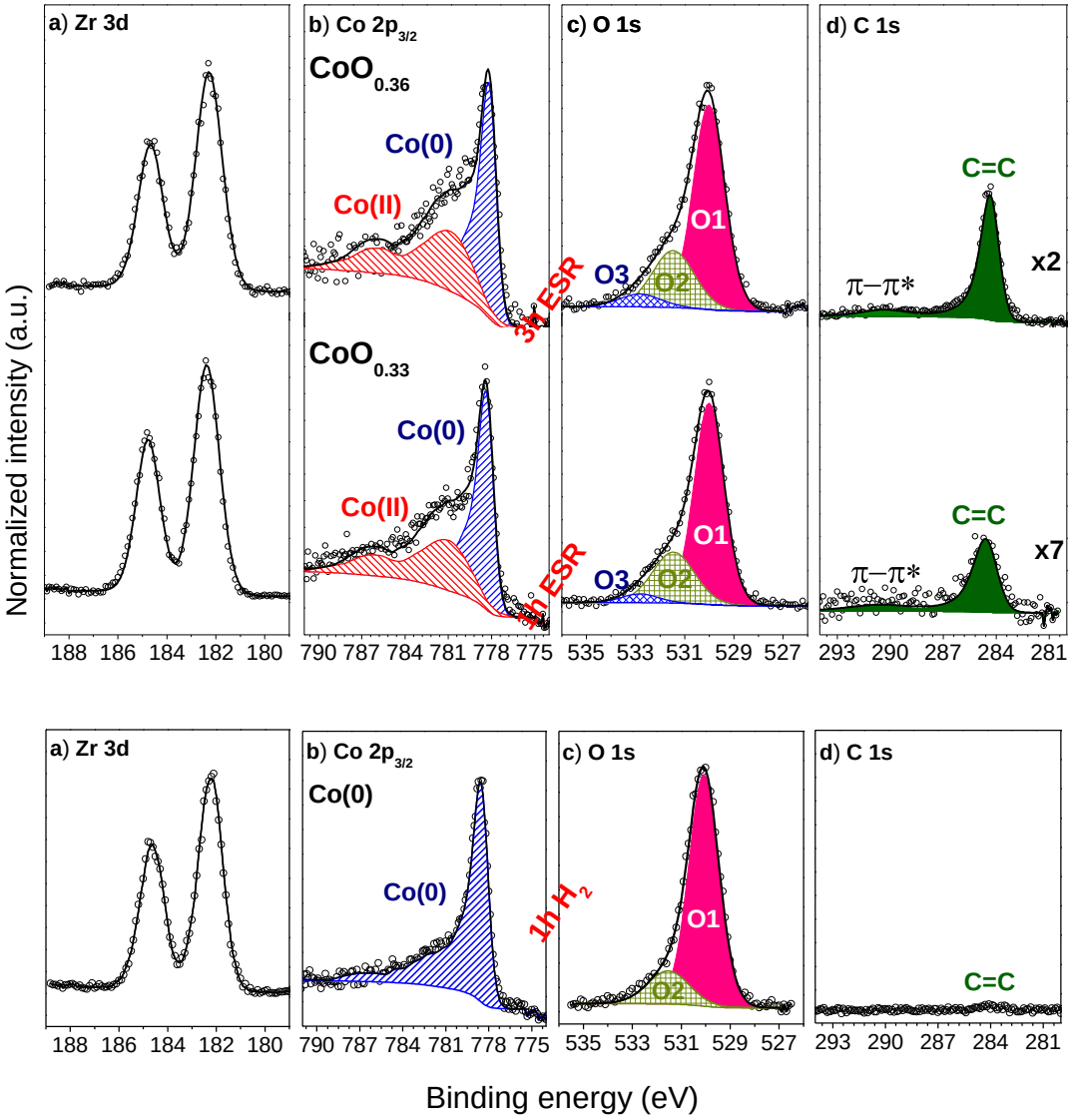

Fig. 3. The high resolution XPS spectra of (a) Zr 3d, (b) Co $2p_{3/2}$, (c) O 1s and (d) C 1s collected after reduction in hydrogen (H_2/Ar, 420ºC), and after the ESR (H_2O/EtOH = 12/1 mol/mol, T = 420ºC, p_{total} = 1 atm) carried out over the pre-reduced LS-Co/ZrO_2 catalyst; b) Co(II) (\\\), Co(0) (///), c) O1 – lattice oxygen, O2 – hydroxyl and carbonate species, O3 – water.

On the surface of the pre-reduced LS-catalyst two types of oxygen were found (Fig. 3c). The first one, at 530.0 eV (O1) is characteristic for metal oxides [35] and it was assigned to the oxygen in the lattice of zirconium oxide [18, 35, 36] in the case of just pre-reduced LS-catalyst. However, the main peak for the Co–O bond in CoO_x could also appear close to this binding energy [19–21, 24, 27, 28, 37]. The peak at 531.5 eV (O2) in literature is usually attributed to O^- and OH^- species [18, 19, 24, 35, 38–40]. Therefore even though the Zr 3d spectrum did not allow to separate the Zr–OH bonds (Fig. 3a), which were expected [16, 41, 42], the O 1s spectrum provided information about the presence of this type of bonds. The exposition of the sample to the H_2O/EtOH

reaction mixture resulted in appearance on the spectrum of the third component (O3), which in the absence of organic compounds on the catalyst surface is most probably rated to the presence of adsorbed water [19].

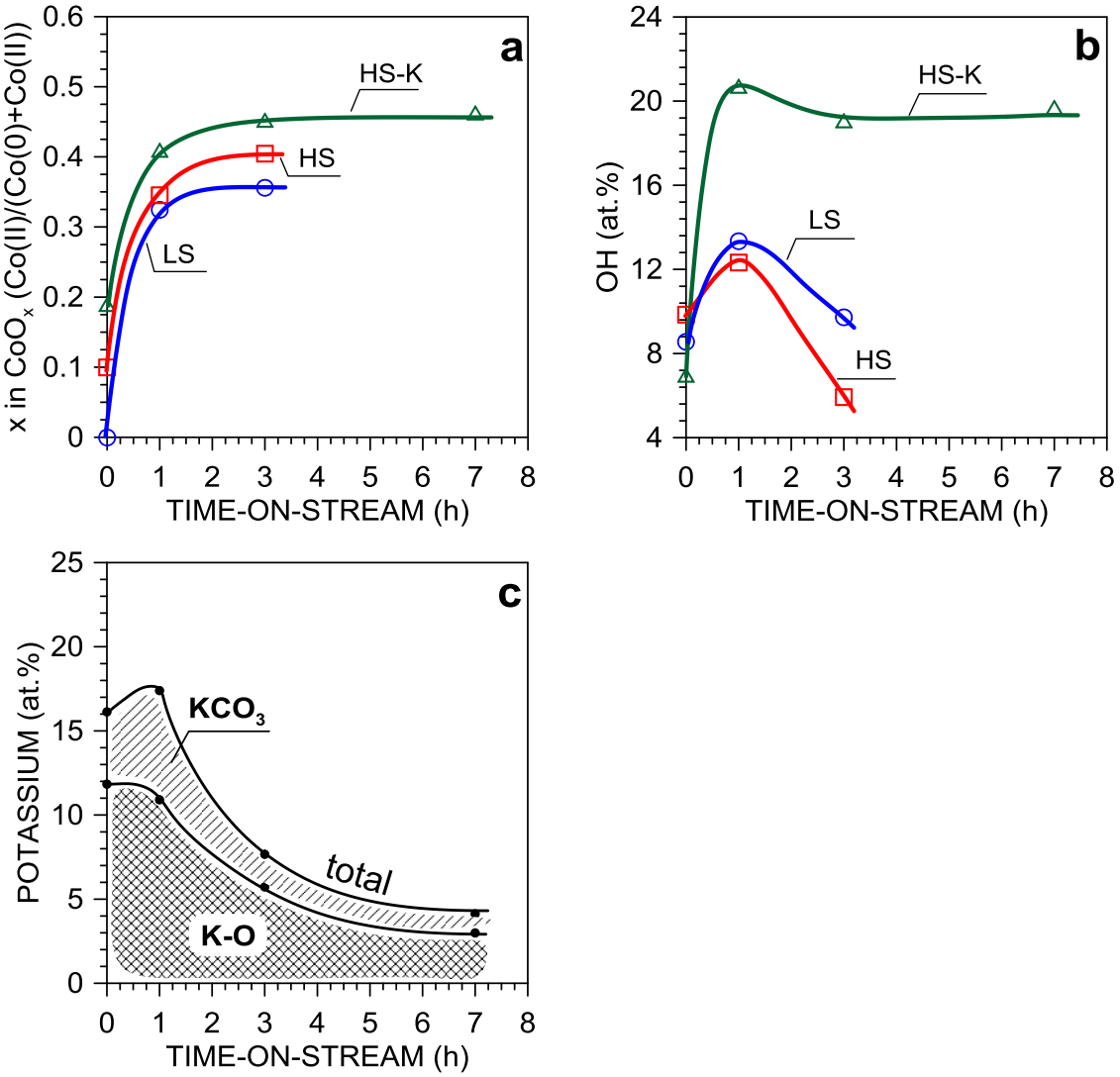

Fig. 4 The changes of (a) cobalt oxidation state (CoO_x), (b) hydroxyls concentration, (c) potassium containing species, with the time of the ESR (H_2O/EtOH = 12/1 mol/mol, 420°C).

The contribution of hydroxyls on the LS-catalyst's surface increased after the first hour of the ESR, as compared to the pre-reduced surface (Fig. 4b Table S2 in Supplementary Information). After 3 hours of the ESR, the percentage contribution of this component in the overall O 1s spectrum did not change (Table S2), whereas the significant decrease of its percentage contribution on the whole catalyst's basis was noted (Fig. 4b), which was attributed to the formation of coke, covering the surface.

As mentioned, the surface of the LS-catalyst was very vulnerable to coking. The amount of carbon on the surface after 3 h on-the-stream increased 10 times, as compared to the state of the sample after reduction (Fig. 1). Since the problem of severe

coking was raised at the beginning of the discussion in this chapter, here it would be only mentioned, that the previous statement about the nature of carbon formed (C=C type) was based on the shape and position of the main C 1s peak; 284.4 eV (Fig. 3d) [24, 43].

The surface of the HS-catalyst underwent similar changes to those observed for the LS-catalyst, even if on the pre-reduced HS-catalyst, some amounts of unreduced CoO_x species were observed ($CoO_{0.10}$ Fig. 5b). However, after 1 h of the ESR the concentration of these species, in the overall Co $2p_{3/2}$ spectrum, was only slightly higher ($CoO_{0.35}$) as compared to the LS ($CoO_{0.33}$). The facility of the HS-catalyst to get oxidized under the ESR reaction conditions was confirmed after 3 h of the reaction (Fig. 5b). The concentration of oxidized cobalt species was equal $CoO_{0.41}$ against $CoO_{0.36}$ found for the LS (see Fig. 4a).

On the surface of the pre-reduced HS-catalyst, two types of oxygen species were also detected (Fig. 5c), and as previously they were assigned to the lattice oxygen (O1) and OH species (O2). The percentage contribution of hydroxyls in the overall O 1s core level was similar to that recorded for the LS (Table S2, Supporting Information). After the first one hour in the ESR the concentration of OH species increased and it was slightly lower as compared to the LS. The same tendency is observed when the concentration of hydroxyls is considered on the whole catalyst's surface basis (Fig. 4b). After 3 hours on-the-stream, the concentration of hydroxyls on the catalyst's surface was significantly decreased (Fig. 4b). This is probably an effect of the catalyst's coking (Fig. 1), since on the free of coke parts of catalysts the OH concentration increased (Fig. S2 in Supplementary Information). Similar to the LS-catalyst, the surface of the HS after reduction was coated by dehydrogenated carbon deposit (Fig. 5d), the amount of which was progressively increasing with the reaction time (Fig. 1).

Fig. 6 depicts results of XPS studies carried out over the HS-K catalyst. As one can see, the shape and the position of Zr 3d core level (Fig. 6a) is similar to those recorded for LS- and HS-catalysts (Figs. 3a and 5a). The reduction of the fresh sample was not complete (Fig. 6b, Table. S1, Supplementary Information). On the surface of the pre-reduced HS-K catalyst both forms of cobalt: Co(0) and Co(II) were observed (Fig. 6b), with predominance of the metallic one. The percentage contribution of CoO_x species in the overall $Co2p_{3/2}$ spectrum was the highest among all zirconia-supported catalysts measured here (Fig. 4a).

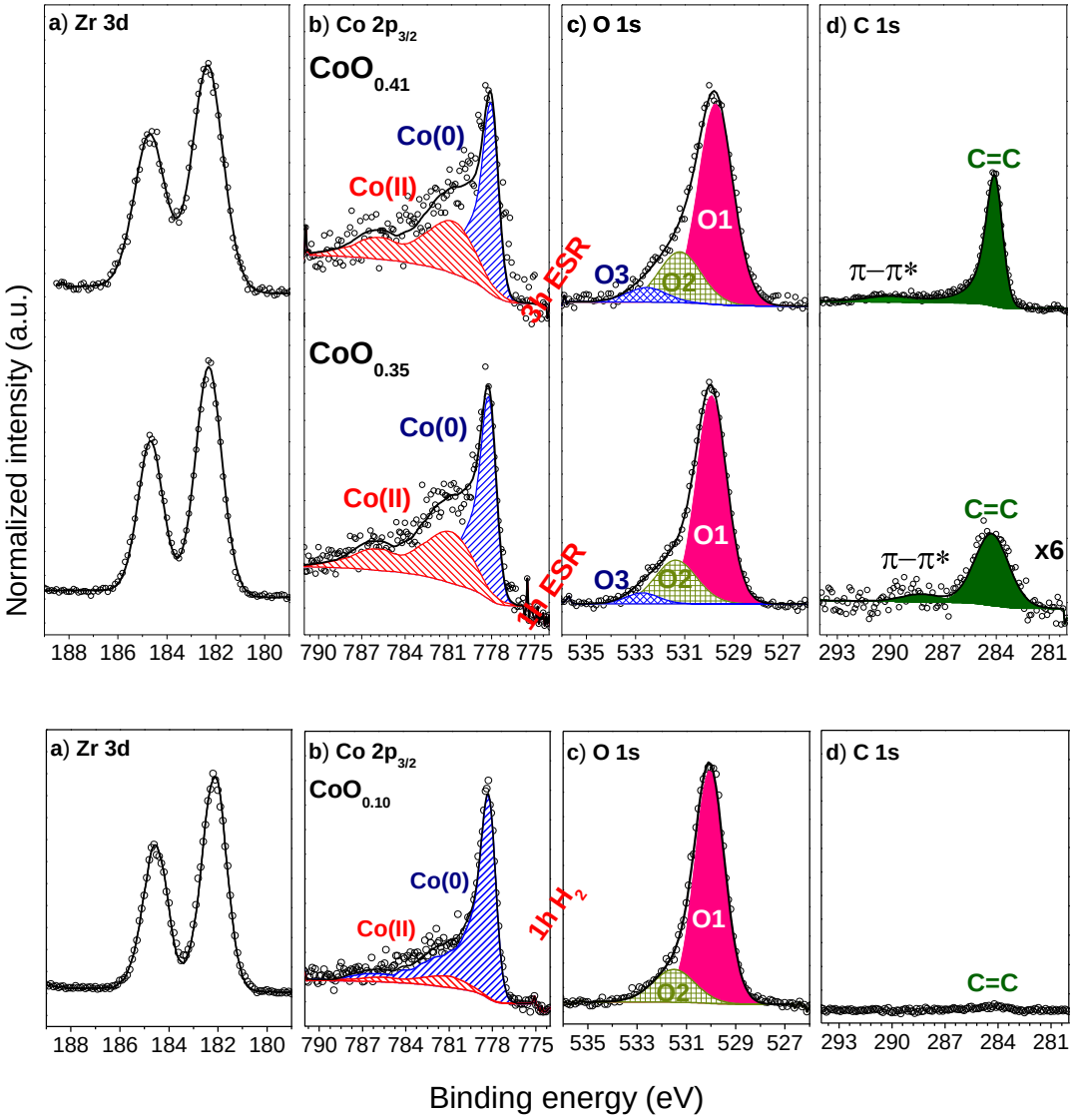

Fig. 5. The high resolution XPS spectra of (a) Zr 3d, (b) Co $2p_{3/2}$, (c) O 1s and (d) C 1s collected after reduction in hydrogen (H_2/Ar, 420ºC), and after the ESR (H_2O/EtOH = 12/1 mol/mol, T = 420ºC, p_{total} = 1 atm)carried out over the pre-reduced (H_2/Ar, T = 420ºC) HS-Co/ZrO_2 catalyst, b) Co(II) (\\\), Co(0) (///), c) O1 – lattice oxygen, O2 – hydroxyl and carbonate species, O3 – water.

Comparison of the Co 2p spectra of the pre-reduced HS- and HS-K catalysts suggests that potassium promoter hinders the reduction of cobalt oxide species. Previous temperature-programmed reduction (TPR) studies [1, 4], as well as, the results presented in the Chapter 5, showed that potassium promotion hindered the HS-Co/ZrO_2 catalyst's reducibility, which might be explained by a stronger interaction of the active phase with the support [4, 44]. In literature it was suggested [44, 45], that a stronger metal-support interaction result in a more active and selective catalyst. Moreover, even though the XPS results presented in ref. [11] showed that promotion of the Co/ZrO_2 with zinc oxide improves reducibility of cobalt oxide species, the TPR profiles of the

catalysts presented in the same paper [11] suggest that addition of a promoter should extend the reduction profile of the promoted catalyst towards higher temperatures. Meaning that more unreduced cobalt species should be expected in the case of the promoted catalyst, which perfectly matches the results obtained in this study.

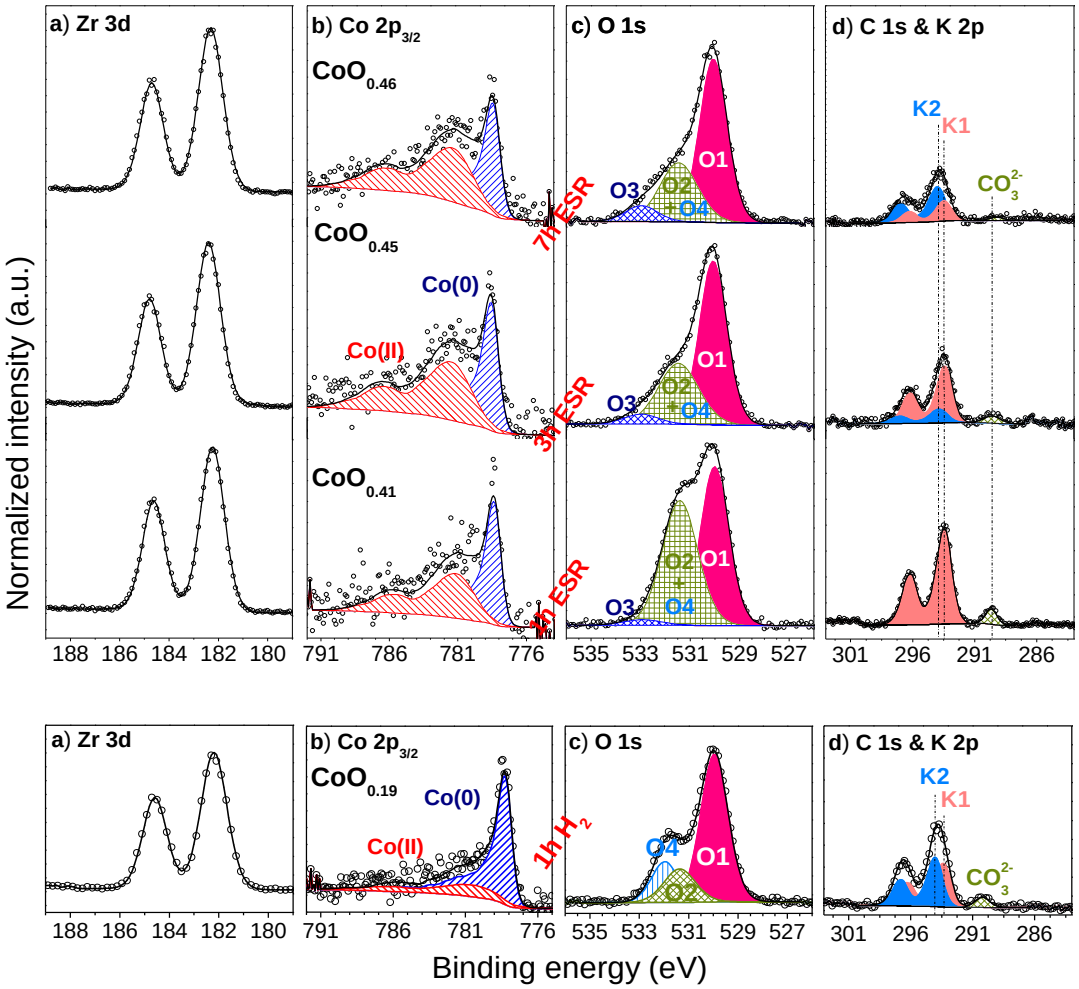

Fig. 6 The high resolution XPS spectra of (a) Zr 3d, (b) Co $2p_{3/2}$, (c) O 1s and (d) C 1s & K2p collected after reduction in hydrogen (H_2/Ar, 420ºC), and under the ESR (H_2O/EtOH = 12/1 mol/mol, T = 420ºC, p_{total} = 1 atm) carried out over the pre-reduced (H_2/Ar, T = 420ºC) HS-KCo/ZrO_2 catalyst; b) Co(II) (\\\), Co(0) (///), c) O1 – lattice oxygen, O2 – hydroxyl and carbonate species, O3 – water, O4 – carbonate species bonded to potassium, d) probable assignments of K1 and K2 species can be found in the text.

The influence of the addition of potassium promoter on the surface's oxidation state is more prominent under the ESR reaction mixture than after the pre-reduction. In Fig. 6b it was presented that cobalt active phase was slightly oxidized with the time-on-stream, and that the extent of cobalt oxidation under each conditions was higher as compared to the other catalysts (Fig. 4a).

Potassium promotion also caused some changes of the O 1s XPS spectra (Fig. 6c). Apart from the previously observed components (Fig. 3c and 5c)

an additional one, at a higher binding energy (532.0 eV), can be resolved. This component (O4) in the presence of potassium (K 2p component at 293.8 and 296.6 eV), is most probably related to the potassium carbonate species (further abbreviated as KCO_3), as suggested in ref. [46, 47]. The presence of the component at 290 eV [48–51] may suggest the existence of carbonates (i.a., potassium carbonates) on the surface, albeit its intensity indicates for a low concentration of these kind of species on the catalyst's surface. Moreover, the normalized intensity ratio of $O4/CO_3^{2-}$components, correspond to the stoichiometry of carbonates (O/C = 3). During the course of the ESR, the O4 components disappears (Fig. 6c, second picture from the bottom). This is related to a low concentration of potassium carbonates, as compared to the concentration of hydroxyls, which significantly increased after the first one hour of the ESR (see Fig. 6c and Table S2 in Supporting Information). It is supposed that the component O4 may strongly overlap with the component O2, making their separation almost impossible.

As the ESR reaction time is progressing, the intensity of the component O2 – therefore, mostly a concentration of hydroxyls – was continuously decreasing (Fig. 4b). In this point it should be highlighted that in the XPS O 1s spectra (Fig. 6c) the O4 and O2 components were not separated, whereas in the case of figures, where the concentration of hydroxyls for the HS-K catalyst were depicted (i.e., Fig.4b), the presented values correspond to the concentration of hydroxyls only (without contribution of carbonates – the method of calculations was presented in the Chapter 3).

We turn now our attention to the potassium species. After the first hour of the ESR the concentration of potassium-containing species on the surface slightly increased, as compared to the surface's state after the reduction (Fig. 4c and Table S1, Supporting Information). The surface's enrichment in these species might be probably related to their re-dispersion resulting from potassium affinity to water. However, after the extension of the reaction time, the progressive significant decrease of the K 2p core level intensity was observed. This was simultaneous with the decrease of the C 1s component (carbonates species) located at 290 eV (Fig. 6d), suggesting possible agglomeration of potassium-containing species. In the previous paragraph it was mentioned that potassium occurs on the surface in the form of KCO_3. The comparison of the normalized intensity of $K\ 2p/CO_3^{2-}$components, with the assumption of 1/1 stoichiometry of K/CO_3, suggests the existence of another type of potassium sites, $K^{\delta+}–O_{surf}^{\delta-}$ which were shortly denoted as K–O (Fig. 4c). Some authors suggest [52–55] that K–O sites might by generated from the reaction of surface's hydroxyls with

potassium carbonates (substitution of hydrogen in OH species by potassium ion), or even by a decomposition of potassium carbonates at high temperature (above 750ºC), i.e., much higher than the temperature of this studies, therefore the latter case is not applied here. The XPS does not allow to distinct where K–O sites are located; they might be distributed over particles of the active phase [56] (Co–O–K), as well as, on the surface of zirconia (Zr–O–K) [52].

The currently available literature suggest [47, 57] that both types of potassium bond to oxygen sites (KCO_3 and K–O) cannot be distinguished in the K 2p peak. From the other side, one may observe that after, 3 h and 7 h time-on-stream, the high-resolution XPS spectra of the K 2p was slightly shifted, broadened, and exhibited a small asymmetry towards higher binding energies (Fig. 6d). Those modifications allowed to pick fit the K 2p spectra with two components, namely K1 and K2. Since the origin of K2 component cannot be explained with the current state of knowledge, it was suggested that it arises from differences in the local chemical environment of the surface [47]. This means that both K1 and K2 components are likely related to the presence of potassium to oxygen bonded species (KCO_3 and K–O). This can be supported by the fact that some shifts on the binding energy scale of the K 2p spectrum were observed after a sample heating in a vacuum, and reduction in hydrogen [47].

The XPS data confirmed that potassium-catalyst was far more resistant to coke formation (Fig. 6d and Fig. 1) than unpromoted ones. Literature data suggests that potassium promotion may reduce the contribution of disproportionation of carbon monoxide, which leads to coke formation [4, 58]. R. Espinal et al. [59] stated that the addition of potassium to a catalyst might reduce the number and strength of acid sites (which are commonly known as those on which coke precursors are chemisorbed [60]), and in turn hinder coke formation. This is very suggestive conclusion since zirconia, as compared to ceria, is more acidic support [60], and the influence of potassium addition to zirconia-supported catalysts was more pronounced in the XPS spectra than in the case of the catalyst with ceria-support (Chapter 4).

2.2. The ESR catalytic performance of the catalysts

Zirconia-supported cobalt catalysts were examined for their ESR catalytic performance (H_2O/EtOH = 12/1 mol/mol, 420ºC, p_{total} = 1 atm). Fig. 7 depicts the changes in catalyst's selectivity during the long-term studies. In presented figures, zero

on the time-on-stream scale is related to the time, when mixture vapours were introduced to the reactor, over the just pre-reduced catalysts.

As follows from Fig. 7 the catalytic performance of zirconia-supported catalyst differs, even though all catalysts exhibited 100% of ethanol conversion. The catalysts showed different behaviour towards products' formation at the early stage of the ESR (Fig. 7a-d). This is in agreement with studies of J. Sun et al. [10], which suggest that zirconia-supported catalysts show an induction period (1–2 h) in which their selectivity experience rapid changes. The initial selectivity to hydrogen recorded over the samples with high-dispersed supports was between 99-96%, whereas for carbon dioxide it was equal 93-87%. The LS-catalyst exhibited the lowest selectivity towards these products, which can be related to a lower water conversion, than it results from the reaction stoichiometry (~20% against 25%).

The selectivities to hydrogen are consistent with the thermodynamic limit of 5.6 $\mathrm{mol_{H_2}/mol_{EtOH}}$ [61] (Fig. 8a) against the stoichiometric prediction of 6.0. The carbon dioxide yield for all catalysts was in the range of 1.5–1.86 $\mathrm{mol_{CO_2}/mol_{EtOH}}$ (Fig. 8b) against the stoichiometric value of 2.0.

It is worth to note that after the first one hour on-the-stream, the selectivity to hydrogen over the LS and HS-K decreased (Fig. 7a), and while for the HS-K it achieved stable value after 2 h, in the case of the LS it was progressively decreasing. The reason of this behaviour for these catalysts is probably different. The decrease of the LS-catalyst selectivity towards hydrogen and carbon dioxide was followed by coke formation and a decrease in the water conversion. However, the amount of coke formed on the surface of high-dispersed catalyst was higher, but this catalyst exhibited stable water conversion and products selectivity. It might suggest that the type of coke deposited on the surface of the HS-catalyst differs from this deposited on the LS-catalyst.

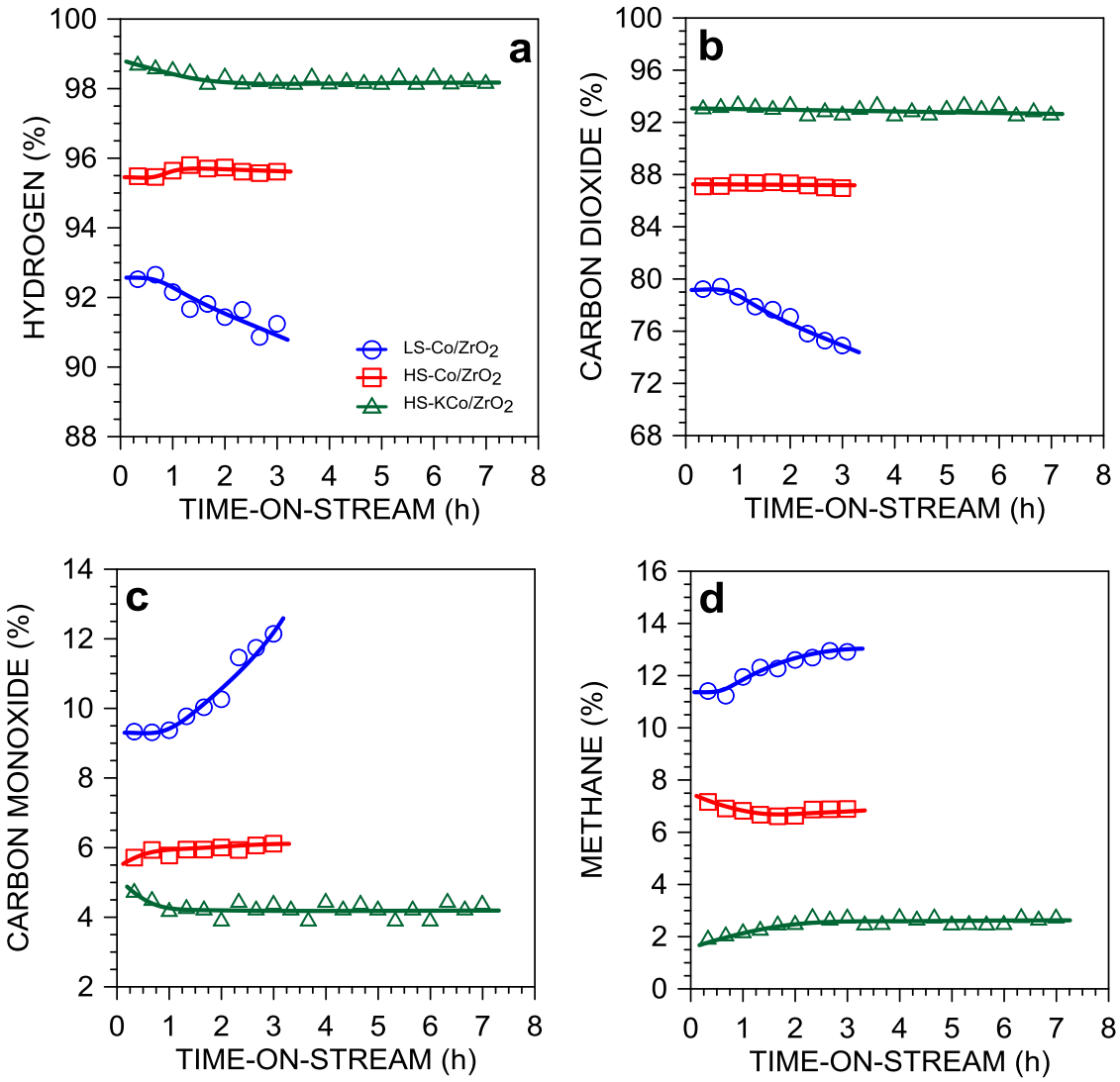

Fig. 7. The effect of time-on-stream on zirconia-supported catalysts' selectivity towards hydrogen, carbon dioxide, carbon monoxide and methane (H_2O/EtOH = 12/1 mol/mol, 420ºC, p_{total} = 1 atm).

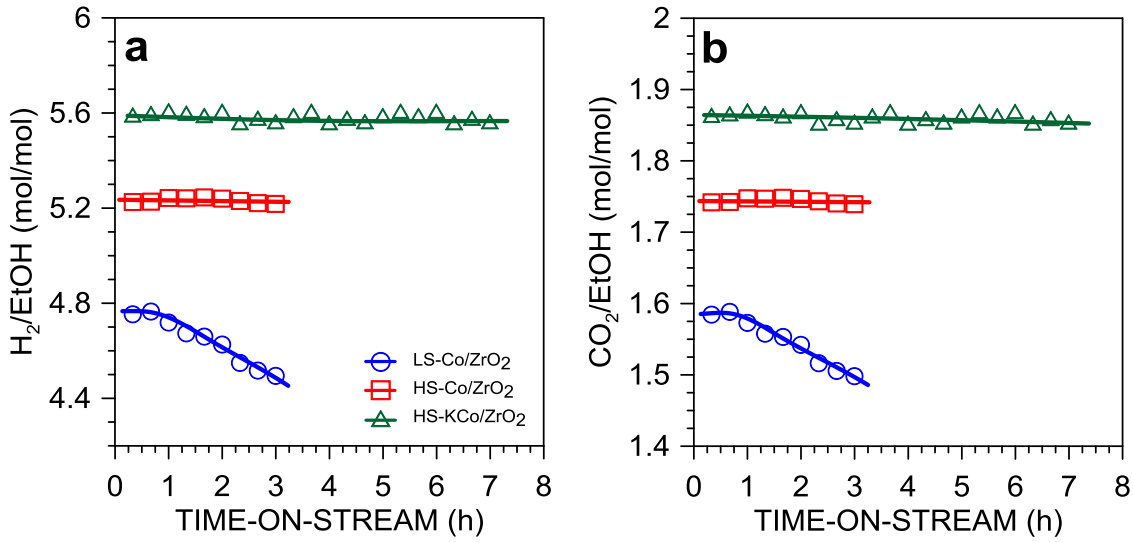

Fig. 8. The effect of time-on-stream on (a) hydrogen and (b) carbon dioxide yield obtained over zirconia-supported catalysts (H_2O/EtOH = 12/1 mol/mol, 420ºC, p_{total} = 1 atm).

As for the selectivity of catalysts to by-products, during the entire measurement only carbon monoxide and methane were formed (Fig. 7c and 7d). The selectivity to those products did not exceed 13%, which was two times higher, as compared to the ceria-supported catalysts (Chapter 4). Fig. 7c shows that over the unpromoted samples, the selectivity to carbon monoxide increases with the reaction time, which was strongly pronounced in the case of the LS-catalyst. Over this catalyst also the significant increase in methane formation with the reaction time was observed (Fig. 7d).

Evidently, the HS-K catalyst exhibited the best catalytic performance. The alkali promotion improved selectivity to hydrogen and carbon dioxide (Fig. 7a and 7b) and significantly decreased the selectivity towards methane (Fig. 7d) and carbon monoxide (Fig. 7c) which is agreement with the so far published results [62–65].

2.3. The influence of the surface state on ESR catalytic performance

The active phase (cobalt) of all zirconia-supported catalysts was progressively oxidized with time-on-stream (Fig. 4a), whereas at the same time the catalytic behaviour of these catalyst was completely different (Figs. 7 and 8). Therefore, it suggested that the oxidation state of the active phase might be not the main factor influencing catalyst's selectivity. The presence of CoO_x species results probably from the presence of high water excess in the feed, which oxidises the active phase [10, 11, 31].

According to the results presented in this study, the OH species along with K–O sites might play an important role in in the enhancement of catalyst's ESR activity and selectivity. Some researchers believe that the activity of catalysts and selectivity of catalytic reactions can be improved by the presence oxygen-containing species, generated due to a close contact of the active phase with the alkali (Na, Li, K) [56, 66–68], stabilising a metal of the active phase in higher oxidation state [56, 66].

When the concentration of OH and K–O sites decreased (Fig. 9a) a small decrease of the HS-K catalyst selectivity towards hydrogen and carbon dioxide was also noted (Figs. 8a and 8b). Fig. 9b shows that a decrease of the sum of OH and K–O sites was mainly caused by the decrease of the concentration of the K–O sites on the surface, whereas the amounts of hydroxyls was almost stable during the ESR reaction.

In the case of the unpromoted catalysts, is difficult to determine the influence of hydroxyls' concentration (Fig. 9a) on the catalytic performance (Fig. 7). While considering the concentration of OH species on the overall catalysts' basis (Fig. 9a)

it can be seen that in both cases their amounts decrease after 3 h in the stream, whereas only in the case of LS-catalyst significant decrease of the catalyst's selectivity was noted (Fig. 7). The surface coverage by OH species was slightly higher for the LS- than HS-catalyst (Fig. S2, Supporting information) during the ESR. Additionally, the concentration of OH species only slightly increased between the first and the third hour of the ESR. Nevertheless, the LS-catalyst exhibited worse ESR performance, which clearly worsened with the time-on-stream (Fig. 7). In this view, not only hydroxyls' concentration but also its location, are important factors in the course of the ESR.

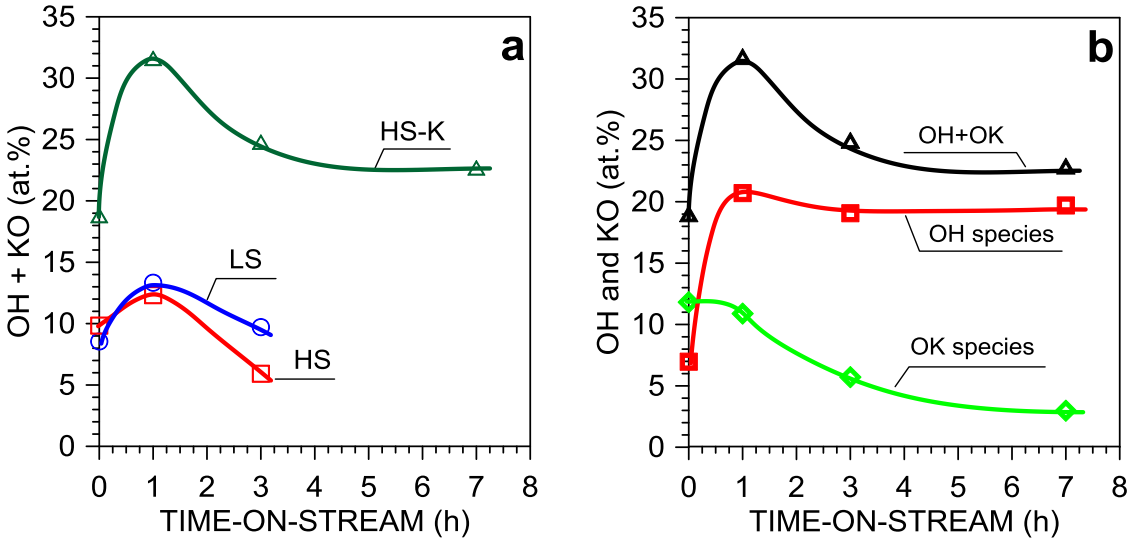

Fig. 9 The changes of hydroxyls and K–O sites with time-on-stream (H_2O/EtOH = 12/1 mol/mol, 420ºC) for (a) zirconia-supported cobalt catalysts and (b) HS-K catalyst.

The dispersion of the active phase is undoubtedly very important, however, the average cobalt crystallite size for the LS and HS-K were comparable (42 and 44 nm, respectively, see Chapter 5). Another factor that may explain the pronounced differences in catalysts' selectivity, with the concentration of OH species and cobalt dispersion being rather similar, is the catalyst's morphology. I.I. Soykal et al. [69] suggested that supports with different morphology, therefore, with different crystal planes, may result in different orientation of cobalt species affecting products distribution.

The only indisputable conclusion that arises from this part of the thesis is that the presence of potassium introduces some new selective sites, that hinder coke formation and result in a good catalyst, regardless of the particles size of cobalt.

Another important fact is the presence of coke. Even though, XPS measurements confirmed that the amount of coke on the catalyst's surface of the

HS-catalyst increased faster between first and third hour of the reaction (as compared to the LS) (Fig. 1), the product selectivity to products over this catalyst were higher and they were stable over the entire measurement period. In the Chapter 3 and 5 it was presented that the nature of carbon formed depends on the support dispersion. TEM analysis showed that the low-surface area supports favour formation of fibrous deposit, whereas the high-surface counterparts – graphitic layers are located between the crystallites. The first type of carbon forms a thick porous cover capping the catalyst's surface that becomes invisible in the XPS measurements. However, the gaseous reactants and products can diffuse into this carbon layer and react on the catalyst's surface. The fibrous deposit causes the fragmentation of the catalyst, plugging in its pores and further coking [58, 70, 71]. This might result to catalyst's deactivation, if particles of the active metal are encapsulated in it, and are not available for the reactants [58, 70, 72–74]. G. Słowik et al. [58] suggested that cobalt particles located over carbon whiskers may result in different catalyst's selectivity due to a change of cobalt active phase–support boundary to Co/C, which acts as a new catalyst. J. Sun et al. [10] suggested that metallic cobalt nanoparticles attached to tips of formed carbon nanotubes are responsible for the acetone steam reforming reaction.

It might be supposed that differences in the LS- and HS-catalysts' selectivity during the course of the ESR could be related to the nature of the carbon formed. Therefore, further microscopic studies are required in order to specify the nature of formed deposit, as well as, its location.

Whether significant changes in catalysts' ESR selectivity with time-on-stream over the LS-catalyst result from non-measurable changes in the state of the original zirconia-supported cobalt catalyst's surface hidden under porous carbon cover, or they result from the change of the support (carbon instead of zirconia) of some amounts of cobalt crystallites, it is obvious that considering the previously proposed ESR reaction paths (Chapter 2, Fig. 6) the ratio between acetate and ethoxy species on the whole catalyst's surface changes toward the latter ones. The lower amounts of acetate species lead to the decrease in carbon dioxide formation. The increase in ethoxy species amounts raises the carbon monoxide and methane selectivities. All these changes give lower concentration of hydrogen among the other ESR products.

It is quite important that in the presence of high concentration of both OH and K–O sites the formation of carbon could be lowered (Fig. 10). However, in the case of zirconia-supported cobalt catalysts the high abundance of these species does not

influence the type of carbon formed. The only type of carbon, that was detected on the surface of the unpromoted catalyst was fully dehydrogenated, of the C=C type.

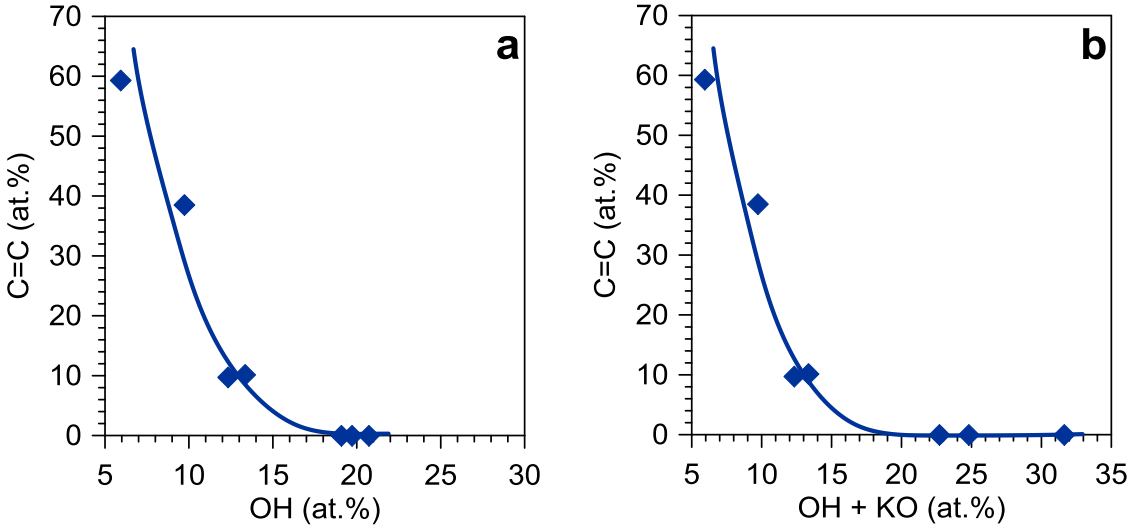

Fig. 10 Correlation of atomic percentage contribution of C=C species with (a) hydroxyls' concentration, and (b) sum of hydroxyls and K–O sites on the catalysts' surface.

In the case of zirconia-supported catalysts it is not clear if the hydroxyls' concentration around 20 at.%, in the absence of potassium, would be sufficient to keep surface carbon free (Fig. 10a). Due to the lack of sufficient information it is suggested that both OH and K–O sites (Fig. 10b) are required in order to slow down and finally to prevent the coking phenomenon.

Conclusions

In this studies the pre-reduced (H_2/Ar, 420ºC) zirconia-supported cobalt catalysts were examined for their surface state and catalytic performance in the ESR (H_2O/EtOH = 12/1 mol/mol, 420ºC). The unpromoted catalysts were found to experience progressive cobalt oxidation with the time-on-stream also in dependence with the catalyst's dispersion. Cobalt particles supported on nano-zirconia were more prone to oxidation than in the case of those supported on micro-zirconia. The potassium promotion enhanced oxidation of cobalt particles supported on nano-zirconia.

Hydrogen and carbon dioxide selectivity was not influenced by the oxidation state of cobalt. In the case of potassium-promoted catalyst, the promoting role in the ESR could be assigned to the presence of hydroxyls and K–O sites. The slight decrease in the concentration of these species was followed by a small decrease in the catalytic selectivity. For the unpromoted catalyst the role of OH species in improvement of

catalytic properties was undetermined. This might be related to the intensive coke deposition (C=C type) on the surface of the unpromoted catalysts, which disturbed XPS analysis. The surface of the HS-catalyst experienced severe coking, however, the selectivities over this catalyst remained stable during the entire measurement. In the case of the LS-catalyst, the amount of carbon formed, was a little lower that on the HS, whereas rapid decrease of the catalyst's selectivity with the reaction time was noted. The possible reasons of this difference were discussed. It was shown that the addition of potassium improves significantly the catalyst's resistance to coking, that was attributed to the high concentration of hydroxyls and K–O sites on the catalyst's surface.

References

1. P. Rybak, B. Tomaszewska, A. Machocki, W. Grzegorczyk, A. Denis *Catal. Today*, **176** (2011) 14–20.
2. A. Machocki, A. Denis, W. Grzegorczyk, W. Gac *Appl. Surf. Sci.* **256** (2010) 5551–5558.
3. R. Padilla, M. Benito, L. Rodríguez, A. Serrano, G. Muñoz, L. Daza *Int. J. Hydrogen Energy* **35** (2010) 8921–8928.
4. M. Greluk, P. Rybak, G. Słowik, M. Rotko, A. Machocki *Catal. Today* **242** (2015) 50–59.
5. H. Song, L. Zhang, R.B. Watson, D. Braden, U.S. Ozkan *Catal. Today* **129** (2007) 346–354.
6. T.A. Maia, H.M. Assaf, E.M. Assaf *Mater. Chem. Phys.* **132** (2012) 1029–1034.
7. W. Gac *Catal. Today* **176** (2011) 131–133.
8. S.D. Davidson, J. Sun, Y. Wang *Top Catal.* **269** (2015) 140–147.
9. H. Song, L. Zhang, U.S. Ozkan *Green Chem.* **9** (2007) 686–694.
10. J. Sun, A.M. Karim, D. Mei, M. Engelhard, X. Bao, Y. Wang *Appl. Catal., B* **162** (2015) 141–148.
11. V.M. Lebarbier, A.M. Karim, M.H. Engelhard, Y. Wu, B.-Q. Xu, E.J. Petersen, A.K. Datye, Y. Wang, *ChemSusChem* **4** (2011) 1679–1684.
12. Y. Pan, Y. Gao, D. Kong, G. Wang, J. Hou, S. Hu, H. Pan, J. Zhu *Langmuir* **28** (2012) 6045–6051.

13. S. Tsunekawa, A. Asami, S. Ito, M. Yashima, T. Sugimoto *Appl. Surf. Sci.* **252** (2005) 1651–1656.
14. W. Wang, H.T. Guo, J.P. Gao, X.H. Dong, Q.H. Qin *J. Mater. Sci.* **35** (2000) 1495–1499.
15. R. Brenier, J. Mugnier, E. Mirica *Appl. Surf. Sci.* **143** (1999) 85–91.
16. Y.S. Li, P.C. Wong, K.A.R. Mitchell *Appl. Surf. Sci.* **89** (1995) 263–269.
17. P.C. Wong, Y.S. Li, M.Y. Zhou, K.A.R. Mitchell *Appl. Surf. Sci.* **89** (1995) 255–261.
18. A. Galtayries, R.Sporken, J. Riga, G. Blanchard, R. Caudano *J. Electr. Spectrosc. Rel. Phen.* **88–91** (1998) 951–956.
19. M.C. Biesinger, B.P. Payne, A.P. Grosvenor, L.W.M. Lau, A.R. Gerson, R.St.C. Smart *Appl. Surf. Sci.* **257** (2011) 2717–2730.
20. A. Galtayries, J. Grimblot *J. Electr. Spectrosc. Rel. Phen.* **98–99** (1999) 267–275.
21. S. Zafeiratos, F. Paloukis, G. Papakonstantinou, D. Teschner, M. Hävecker, E. Vass, P. Schnörch, A. Knop-Gericke, R. Schlögl, B. Moreno, E. Chinarro, J.R. Jurado, S.G. Neophytides *Catal. Today* **157** (2010) 250–256.
22. S.S.-Y. Lin, D.H. Kim, M.H. Engelhard, S.Y. Ha *J. Catal.* **273** (2010) 229–235.
23. Zs. Ferencz, A. Erdöhelyi, K. Baan, A. Oszkó, L. Óvári, Z. Kónya, C. Papp, H.-P. Steinrück, J. Kiss *ACS Catal*. **4** (2014) 1205–1218.
24. S. Turczyniak, W. Luo, V. Papaefthimiou, N. S. Ramgir, M. Haevecker, A. Machocki, S. Zafeiratos *Top. Catal.* **59** (2016) 532–542.
25. A.M. Karim, Y. Su, M.H. Engelhard, D.L. King, Y. Wang *ACS Catal.* **1** (2011) 279–286.
26. H. Song, U.S. Ozkan *J. Catal*. **261** (2009) 66–74.
27. S. Zafeiratos, T. Dintzer, D. Teschner, R. Blume, M. Hävecker, A. Knop-Gericke, R. Schlögl *J. Catal.* **269** (2010) 309–317.
28. M.P. Hyman, J.M. Vohs *Surf. Sci. Lett.* **605** (2011) 383–389.
29. V. Papaefthimiou, T. Dintzer, V. Dupuis, A. Tamion, F. Tournus, A. Hillion, D. Teschner, M. Hävecker, A. Knop-Gericke, R. Schlögl, S. Zafeiratos *ACS Nano* **5** (2011) 2182–2190.
30. I.I. Soykal, H. Song, J.T. Miller, U.S. Ozkan *Top Catal.* **57** (2014) 785–795.

31. B. Bayram, I.I. Soykal, D. von Deak, J.T. Miller, U.S. Ozkan *J. Catal.* **284** (2011) 77–89.
32. A.R. Passos, L. Martins, S.H. Pulcinellin, C.V. Santilli, V. Briois *Catal. Today* **229** (2014) 88–94.
33. J. Llorca, J.A. Dalmon, P.R. de la Piscina, N. Homs *Appl. Catal., A* **243** (2003) 261–269.
34. E. Varga, Z. Ferencz, A. Oszkó, A. Erdöhelyi, J. Kiss *J. Mol. Catal. A* **397** (2015) 127–133.
35. M.M. Yung, E.M. Holmgreen, U.S. Ozkan *Catal Lett.* **118** (2007) 180–186.
36. Z.-Y. Lim, C. Wu, W.G. Wang, K.-L. Choy, H. Yin *J. Mater. Chem. A,* **4** (2016) 153–159.
37. N. Weidler, S. Paulus, J. Schuch, J. Klett, S. Hoch, P. Stenner, A. Maljusch, J. Brötz, C. Wittich, B. Kaiser, W. *Jaegermann Phys. Chem. Chem. Phys.* **18** (2016) 10708–10718.
38. J.-C. Dupin, D. Gonbeau, P. Vinatier, A. Levasseur *Phys. Chem. Chem. Phys.* **2** (2000) 1319–1324.
39. J.E. Kim, J. Lim, G.Y. Lee, S.H.Choi, U.N. Maiti, W.J. Lee, Ho.J. Lee, S.O. Kim *ACS Appl. Mater. Interfaces* **8** (2016) 1571–1577.
40. L. Xu, Y. Ma, Y. Zhang, B. Chen, Z. Wu, J. Jiang, W. Huang *J. Phys. Chem. C* **114** (2010) 17023–17029.
41. E.I. Kauppi, K. Honkala, A.O.I. Krause, J.M. Kanervo, L. Lefferts *Top. Catal.* **59** (2016) 823–832.
42. A. Roustila, J. Chêne, C. Séverac *J. Alloys Compd.* **356–357** (2003) 330–335.
43. N.M. Rodriguez, P.E. Anderson, A. Wootsch, U.vWild, R. Schlogl, Z. Paal *J. Catal*. **197** (2001) 365–377.
44. P. Kumar, Y. Sun, R.O. Idem *Energy & Fuels* **21** (2007) 3113–3123.
45. J.A. Lercher, J.H. Bitter, W. Hally, W. Niessen, K. Seshan *Stud. Surf. Sci. Catal.* **101** (1996) 463–472.
46. A.V. Shchukarev, D.V. Korolkov *CEJC* **2** (2004) 347–362.
47. H.P. Bonzel, G. Broden, H.J. Krebs *Appl. Surf. Sci.* **16** (1983) 373–394.
48. J. Światowska, V. Lair, C. Pereira-Nabais, G. Cote, P. Marcus, A. Chagnes *Appl. Surf. Sci.* **257** (2011) 9110–9119.

49. G. Tyuliev, D. Panayotov, I. Avramova, D. Stoichev, Ts. Marinov *Mater. Sci. Eng., C* **23** (2003) 117–121.
50. M.E. Gálvez, S. Ascaso, P. Stelmachowski, P. Legutko, A. Kotarba, R. Moliner, M.J. Lázaro *Appl. Catal., B* **152–153** (2014) 88–98.
51. A. Miyakoshi, A. Uenob, M. Ichikawa *Appl. Catal., A* **219** (2001) 249–258.
52. N. Hou, Y. Zhang, M. Meng *J. Phys. Chem. C* **117** (2013) 4089−4097.
53. Z.-Q. Zou, M. Meng, J.-J. He *Mater. Chem. Phys.* **124** (2010) 987–993.
54. Y. Liu, M. Meng, Z.-Q. Zou, X.-G. Li, Y.-Q. Zha *Catal. Commun.* **10** (2008) 173–177.
55. A. lordan, M. Zaki, C. Kappenstein *J. Chem. Soc. Faraday. Trans.* **89** (1993) 2527–2536.
56. B. Liu, T. Huang, Z. Zhang, Z. Wang, Y. Zhang, J. Li *Catal. Sci. Technol.* **4** (2014) 1286–1292.
57. G. Maniak, P. Stelmachowski, A. Kotarba, Z. Sojka, V. Rico-Pérez, A. Bueno-López *Appl. Catal., B* **136–137** (2013) 302–307.
58. G. Słowik, M. Greluk, A. Machocki *Mater. Chem. Phys.* **173** (2016) 219–237.
59. R. Espinal, E. Taboada, E. Molins, R.J. Chimentao, F. Medina, J. Llorca *Appl. Catal., B* **127** (2012) 59–67.
60. H. Song, L. Zhang, U.S. Ozkan *Top. Catal*. **55** (2012) 1324–1331.
61. K. Vasudeva, N. Mitra, P. Umasankar, S.C. Dhingra *Int. J. Hydrogen Energy* **21** (1996) 13–18.
62. B. Banach, A. Machocki, *Appl. Catal., A* **505** (2015) 173–182.
63. K.-S. Kim, H.-R. Seo, S.Y. Lee, J.-G. Ahn, W.Ch. Shin, Y.-K. Lee *Top Catal.* **53** (2010) 615–620.
64. J. Llorca, N. Homs, J. Sales, J.-L.G. Fierro, P.R. de la Piscina *J. Catal.* **222** (2004) 470–480.
65. M. Greluk, M. Rotko, A. Machocki *Catal. Lett.* **146** (2016) 163–173.
66. P. Panagiotopoulou, D.I. Kondarides *J. Catal.* **267** (2009) 57–66.
67. H.N. Evin, G. Jacobs, J. Ruiz-Martinez, G.A. Thomas, B.H. Davis *Catal Lett.* **120** (2007) 166–178.
68. Y.P. Zhai, D. Pierre, R. Si, W.L. Deng, P. Ferrin, A.U. Nilekar, G.W. Peng, J.A. Herron, D.C. Bell, H. Saltsburg, M. Mavrikakis, M. Flytzani-Stephanopoulos *Science and Engineering* **329** (2010) 1633–1636.

69. I.I. Soykal, B. Bayram, H. Sohn, P. Gawade, J.T. Miller, U.S. Ozkan, *Appl. Catal., A* **449** (2012) 47–58.

70. D.L. Trimm *Catal. Today* **37** (1997) 233–238.

71. D.L. Trimm *Catal. Today* **49** (1999) 3–10.

72. J. Vicente, C. Montero, J. Ereña, M.J. Azkoiti, J. Bilbao, A.G. Gayubo *Int. J. Hydrogen Energ*. **39** (2014) 12586–12596.

73. H. Wang, Y. Liu, L. Wang, Y.N. Qin *Chem. Eng. J.* **145** (2008) 25–31.

74. P. Bichon, G. Haugom, H.J. Venvik, A. Holmen, E.A. Blekkan *Top Catal.* **49** (2008) 38–45.

Supporting Information

Table S1. The percentage contribution (at.%) of elements on the surface of Co/ZrO_2 catalysts under the ESR (H_2O/EtOH) = 12/1 mol/mol) calculated on the base of high resolution XPS spectra after taking into account the RSF for each element.

Catalyst	Time on stream (h)	Contribution of an element (at. %)*				
		Co	Zr	O	C	K
LS-Co/ZrO_2	H_2**	**22.1**	**22.4**	**52.0**	**3.6**	**-**
	1.00	17.6	19.1	53.1	10.2	-
	3.00	8.9	14.1	38.5	38.5	-
HS-Co/ZrO_2	H_2**	**11.3**	**26.4**	**58.8**	**3.5**	**-**
	1.00	8.3	24.4	57.5	9.8	-
	3.00	3.1	10.6	27.0	59.5	-
HS-KCo/ZrO_2	H_2**	**3.2**	**20.3**	**56.1**	**4.3**	**16.1**
	0.25	1.7	16.0	56.2	8.7	17.4
	3.00	3.3	22.8	63.1	3.1	7.7
	7.00	3.7	25.7	65.3	1.1	4.1

*Calculated as: $n_i = n_i/\sum n_{i-j}\cdot 100\%$, where n_i = {Co, Zr, O, C, K} and n_{i-j} = Co+Z+O+C+K.
**Results obtained after the catalysts pre-reduction (H_2/Ar) at 420ºC for 1h.

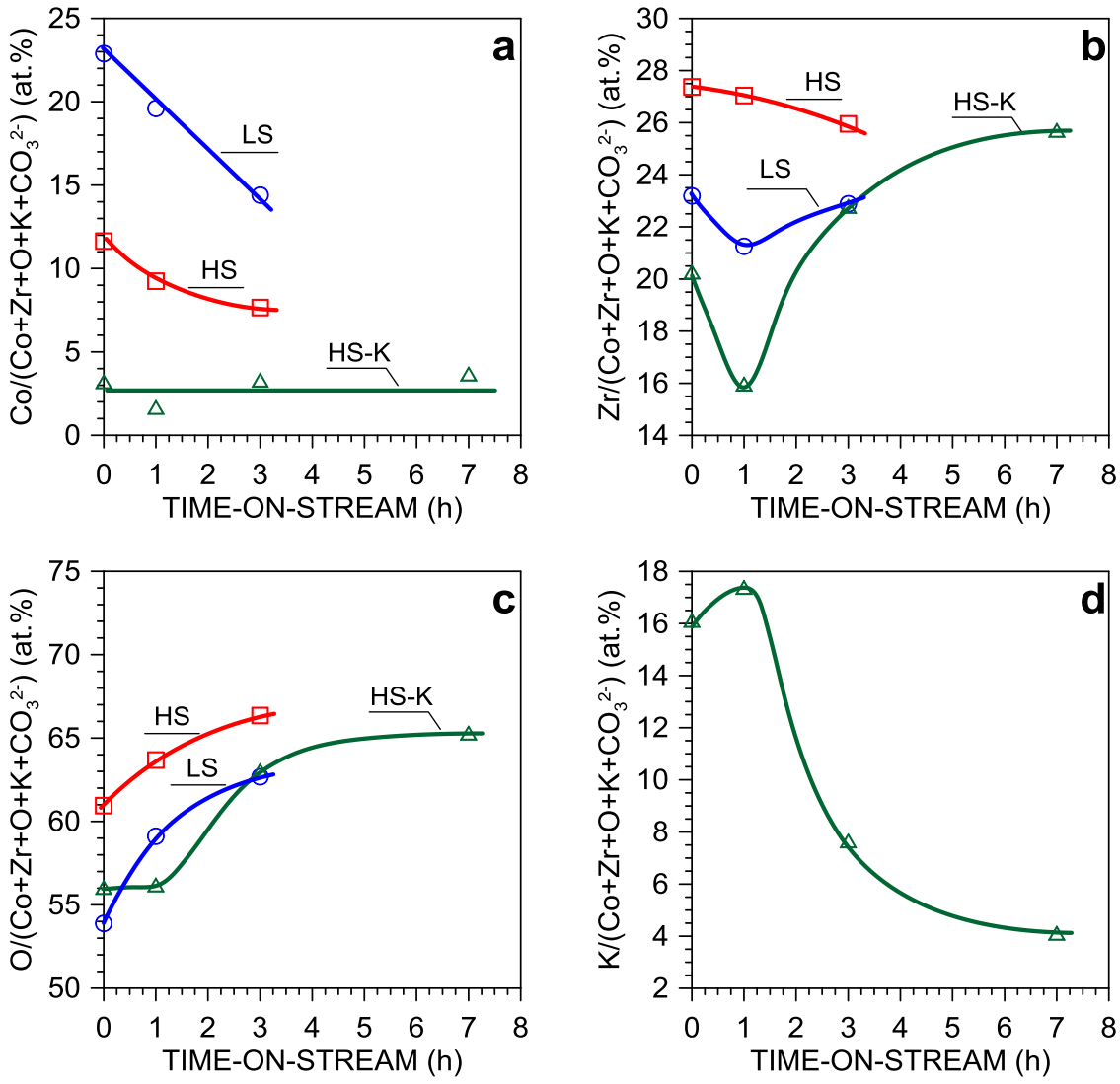

Fig. S1 The changes of the relative elemental surface's composition versus reaction time.

Table S2. The percentage contribution of different species in the Co 2p, O 1s, C 1s high resolution XPS spectra of the catalyst after reduction and after the ESR.

Catalyst	Time-on-stream (h)	Contribution of given species in the XPS spectrum (%)								
		Co 2p	O 1s				C 1s			
		Co(II)	O_{latt}	OH	KCO_3, KO	H_2O	C=C	CH_X	C-O	CO_3^{2-}
LS-Co/ZrO_2	H_2**	0	83.5	16.5	0.0	0.0	100.0	0.0	0.0	0.0
	1	32.5	71.1	25.1	0.0	3.7	100.0	0.0	0.0	0.0
	3	35.6	69.0	25.3	0.0	5.8	100.0	0.0	0.0	0.0
HS-Co/ZrO_2	H_2**	10.2	83.2	16.8	0.0	0.0	100.0	0.0	0.0	0.0
	1	34.6	74.4	21.5	0.0	4.1	100.0	0.0	0.0	0.0
	3	40.5	72.0	22.0	0.0	6.0	100.0	0.0	0.0	0.0
HS-KCo/ZrO_2	H_2**	18.8	65.6	20.1	14.3	0.0	0.0	0.0	0.0	100.0
	1	41.0	49.3	48.4	n.a.	2.3	0.0	0.0	25.5	74.5
	3	45.3	62.0	33.3	n.a.	4.7	0.0	0.0	38.1	61.9
	7	46.3	61.8	31.9	n.a.	6.3	0.0	0.0	0.0	100.0

**Results obtained after catalysts' pre-reduction (H_2/Ar) at 420ºC for 1 h.
n.a. - not analysed

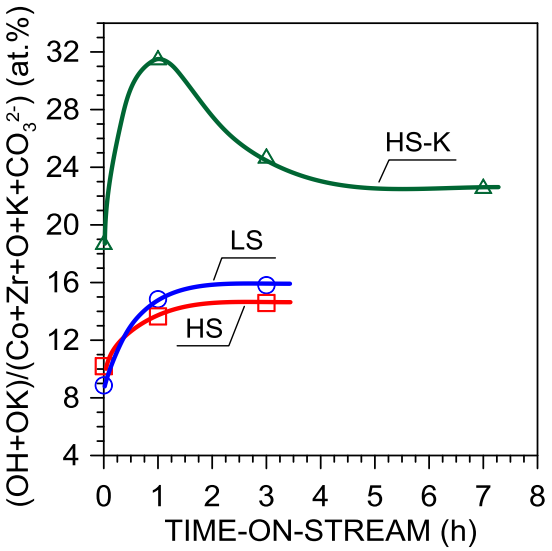

Fig. S2 The changes of the relative surface's concentration of hydroxyls and K–O sites versus reaction time.

CONCLUSIONS

Summary and general conclusions

OUTLINE

Abstract

This chapter is aimed to summarize the main results of the work presented in this thesis, to highlight similarities and differences in the surface state and the catalytic performance of unpromoted and potassium-promoted ceria- and zirconia-supported cobalt catalysts.

In this study nano- and micro-cerium(IV) (25 nm and <5 μm) and zirconium(IV) (100 nm and <5 μm) oxides were used as supports of unpromoted and potassium-promoted (2 wt.%) cobalt-based (8–9 wt.%) catalysts for the ethanol steam reforming (ESR) reaction. It was found that the dispersion and the morphology of the support, as well as, the oxide type, influence cobalt particles size. Using the same catalysts' preparation method, it was shown that cobalt crystallites are in general bigger over zirconia-supported catalysts (23–44 nm) as compared to the ceria-supported ones (4–40 nm).

The X-ray photoelectron spectroscopy (XPS) studies showed that pre-reduction of the catalysts' in hydrogen resulted in different concentration of cobalt(II) oxide-like species (CoO_x) on the surface, which is in accordance with the temperature programmed reduction (TPR) profiles. It was found that the reducibility of cobalt oxides is strongly related to cobalt crystallites size, the type of the support, and as well as, to the presence of a promoter. Cobalt crystallites supported on low-dispersed oxides were reduced to nearly completely metallic form – Co(0), whereas small, variable amounts of CoO_x were observed on the surface of pre-reduced unpromoted and potassium-promoted nano-catalysts ($CoO_{0.05–0.19}$). The addition of potassium influenced the reduction behaviour of catalysts, but is influence depends on the type of the support.

In potassium-promoted catalysts, cobalt particles supported on ceria were more prone to reduction ($CoO_{0.05}$) than those supported on zirconia ($CoO_{0.19}$). Based on the so far published studies it might be suggested that the differences in the catalyst's reducibility may result from differences in the cobalt–support interaction, and/or even penetration of Co^{2+} ions into the support structure [2–4]. Addition of a potassium promoter might both weaken or reinforce the cobalt–oxygen bond strength [5, 6], depending on the support type [7, 8].

The pre-reduced ceria- and zirconia-supported cobalt catalysts were examined, focusing on their surface state and its effect on the catalytic performance in the ESR. The results of the studies carried out in H_2O/EtOH = 3/1 mol/mol (420ºC) over the unpromoted nano-ceria cobalt catalyst under various pressure (0.2–20 mbar), showed that the pressure increase influences the catalyst's oxidation state, affecting in parallel the carbon-containing products distribution. Very low pressure conditions (0.2 mbar in the *in-situ* synchrotron studies) induced strong reduction of the surface (both, cobalt and ceria), followed by increase of CO selectivity. It is accepted that the presence of oxygen-adsorbed species might influence ethanol transformation [9–14], however, even though under 0.2 mbar total pressure the surface was covered by adsorbed hydroxyl species, carbon monoxide was the main carbon-containing product after the ESR. Therefore, it was suggested that at very low pressure, chemisorption of hydroxyls, alcohol, and products occur preferentially on the strong chemisorption centres, that restrain reactants mobility over the surface. Low reactants mobility might hinder the possibility of their reaction with other species, and inhibit further dissociation of water and ethanol due to the occupancy of adsorption sites. Higher pressure of the ESR reaction (2–20 mbar) resulted in formation of CoO_x sites and increasing Ce(IV) ions concentration. Additionally, the increase of the pressure also might cause the involvement of weak chemisorption centres, thus an active participation of adsorbed hydroxyls in ethanol transformation. Therefore, basing on this part of research, it was concluded that higher carbon dioxide yield can be assigned both to the presence of CoO_x species [15] and to more reactive/mobile –OH groups, that might be adsorbed in the support and cobalt as well [16–18].

The effect of the pressure of the reactants vapours on the ESR carbon-containing products is graphically summarized in Fig. 1.

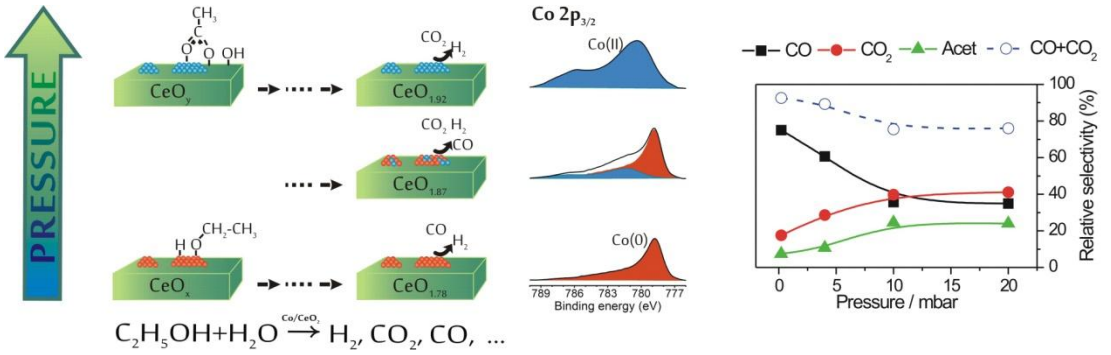

Fig. 1 The influence of the pressure (0.2–20 mbar) on catalyst's surface state and carbon-containing products distribution (HS-Co/CeO_2, H_2O/EtOH=3/1 mol/mol, 420ºC).

The studies in the low-pressure regime were also performed on zirconia-supported catalysts. Due to similar conclusions, these studies have not been presented in this thesis.

The studies of the ESR that were performed over all ceria- and zirconia-supported catalysts with various reactants molar ratios (H_2O/EtOH equal 3/1, 9/1, and 12/1 mol/mol) at 420ºC under total pressure of 1 atm, showed that the catalysts undergo progressive oxidation to an extent related to the dispersion and the feed's composition. The concentration of CoO_x species increased with the water excess, and it was generally higher for zirconia-supported catalysts. It is worth to note that the abundance of CoO_x species on the surface of the unpromoted ceria- and zirconia-suppoted catalysts for the H_2O/EtOH molar ratio of 12/1 was very similar, i.e., $CoO_{0.33–0.35}$. Under the H_2O/EtOH = 12/1 mol/mol the influence of the support type on cobalt oxidation state was more pronounced in the case of potassium-promoted catalysts. Cobalt particles in the potassium-promoted ceria-supported catalyst were less susceptible to oxidation than in the zirconia-supported counterpart ($CoO_{0.38}$ vs. $CoO_{0.41}$). Oxidation of cobalt active phase seemed to be the sole factor determining the ESR selectivity, when the changes on the surface were considered only in terms of one catalyst. However, when both groups (ceria- and zirconia-supported catalysts), were considered together, it appeared that other surface species govern the ESR selectivity.

Based on TPR experiments, zirconium oxide is resistant to reduction at 420ºC. This is confirmed by the XPS spectra of Zr 3d which did not show any significant changes during the pre-reduction and the ESR reaction with all applied H_2O/EtOH molar ratios. Therefore, the presence of bonds than other Zr–O–Zr, e.g., Zr–OH [19], was concluded from the O 1s spectra. In the case of ceria-supported catalysts, both Ce 3d and O 1s spectra evidenced the increase of concentration of Ce(IV) ions on the

surface of the unpromoted catalysts with the increasing excess of water in the feed. In the case of potassium-promoted catalyst, the opposite tendency was observed —ceria support undergoes reduction under higher H_2O/EtOH molar ratios.

It was found that a common feature of ceria- and zirconia-supported catalysts, regardless of the oxidation state of cobalt and supporting it oxides, was the increasing concentration of hydroxyls on the catalyst's surface, with the increase of the H_2O/EtOH molar ratio. The high concentration of surface adsorbed hydroxyls, and most probably their location on the catalyst's surface, improve the selectivity and the yield of hydrogen and carbon dioxide formed, as well as, the catalyst's resistance to coke formation (Fig. 2).

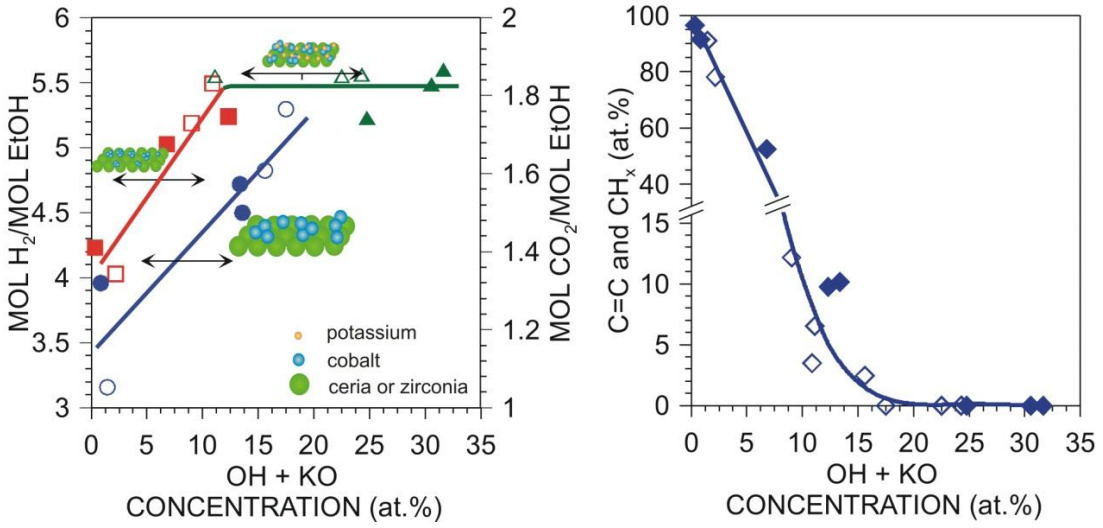

Fig. 2 Correlation of H_2 and CO_2 yields, and the concentration of C=C and CH_x species on the whole catalyst's surface with the concentration of surface oxygen-containing species on the surface of catalysts under the ESR at 420ºC. Each point refers to different H_2O/EtOH molar ratio. Open symbols: ○, □, △ refer to LS-, HS- and HS-K ceria-supported catalysts, whereas filled ones ●, ■, ▲ LS-, HS- and HS-K to zirconia-supported catalysts, respectively. In right figure, open symbols ◇ are related to all ceria-supported catalysts, whereas filled ◆ to zirconia-supported ones.

Under the stoichiometric ratio of reactants, the concentration of surface hydroxyls is low for both unpromoted ceria- and zirconia-supported catalysts; nevertheless, the amount of these species was lower in the case of the latter ones. Under the H_2O/EtOH = 3/1 mol/mol, all unpromoted catalysts suffered for severe coking. The coking phenomenon could be reduced with the increase in OH species concentration, thus with a higher of water excess in the feed. However, the zirconia-supported catalysts experienced very intensive coking even at as high excess of water as 12/1 mol/mol. The nature of the carbon formed depends on both cobalt and support dispersion. In the case of the low-surface area (low-dispersed) catalysts, carbon

probably diffused inside cobalt crystallites destroying the sample from the inner layers and it grew up on the surface mainly in the form of graphitic whiskers. In the case of high-surface area (high-disperded) catalysts, carbon was deposited only in the outer layers of catalysts, without destroying the surface of the catalyst. The differences in formation of carbonaceous deposit on the surface of high- and low-dispersed catalysts were clearly seen after the increase of the water excess in the feed. The amount of formed deposit decreased, nevertheless, the way of its accretion could be observed also without any additional equipment. Fig 3 shows photos of spent ceria-supported samples. The surface of high-dispersed catalyst was "homogenously" covered by carbon deposit.

Fig. 3 The coke formation on the surface of unpromoted high-dispersed ceria-supported catalysts after the ESR (H_2O/EtOH = 9/1 mol/mol, 420ºC, t = 1 h).

In the case of the ceria-supported catalysts it was found that the increase of water excess, accompanied by an increase of hydroxyls concentration, also influences the type of carbon formed, preventing from the formation of completely dehydrogenated carbon (C=C type) with the change its type to CH_x species. On the surface of unpromoted zirconia-supported catalysts, regardless of the water excess, the completely dehydrogenated carbonaceous deposit was the only type of carbon.

Potassium promotion of the catalysts introduces another type of selective sites ($K^{\delta+}$–$O_{surf}^{\delta-}$) that provide an additional source of oxygen-containing species, which along with hydroxyls play an important role in improving catalyst's performance and hindering coke formation (Fig. 2). The selectivities towards hydrogen and carbon dioxide were higher than over the unpromoted catalysts, while the surface of ceria- and zirconia-supported catalysts was free of coke (except for the potassium-promoted ceria-supported catalyst after the ESR carried out with stoichiometric reactants mixture). The concentration of $K^{\delta+}$–$O_{surf}^{\delta-}$ sites on the surface of potassium-promoted catalysts increases with the increasing extent of water, which was directly related to the increasing percentage contribution of potassium on the catalyst's surface in the case of both, ceria- and zirconia-supported catalysts. The phenomenon of surface's enrichment in potassium species (segregation of potassium) during the catalyst's reduction was previously presented in literature [20], and it was explained by re-dispersion of potassium over the surface. In the case when this phenomenon is observed under the

ESR conditions it might be related to a strong affinity of potassium to water. The very important feature, that differentiate potassium-promoted ceria-supported catalyst from its zirconia-supported counterpart is the change of the atomic contributions of potassium on the surface with the increase of the H_2O/EtOH molar ratio. It was found that when the water excess is increased, potassium species were more strongly re-dispersed over the surface of ceria-supported catalysts (11–26 at.% under different H_2O/EtOH molar ratios) than over the zirconia-supported one (10–17 at.% under different H_2O/EtOH molar ratios). This result underline a fundamental difference in the behaviour of potassium species on the surface of ceria- and zirconia-supported cobalt catalysts.

The presence of potassium was found to influenced not only the amount of the produced hydrogen, carbon dioxide and coke, but also the formation of methane and carbon monoxide, which is significantly lowered, as compared to those formed over the unpromoted catalysts. This observation was in line with previously reported results [21, 22]. According to literature results, potassium doping hinders coke formation by: *(i)* neutralization of acidic sites on catalysts' surface [20], *(ii)* decrease of disproportionation of carbon monoxide, which is regarded as one of a coke precursor [23, 24], and *(iii)* promotion of the steam reforming [25] of CH_x species, which are also well known coke precursor [9–12].

The differences between ceria- and zirconia-supported catalysts become even more prominent when surfaces' evolution and the ESR catalytic performance (H_2O/EtOH = 12/1 mol/mol, 420ºC, p_{total} = 1 atm) are examined with respect to the reaction time.

The results described in this thesis, show that among ceria-supported catalysts, only the unpromoted nano-dispersed one was prone to oxidation, whereas the other ceria-supported catalysts (potassium-promoted nano-catalyst and low-dispersed catalyst) undergo progressive reduction with time-on-stream. Regarding the Ce(IV) ions concentration, it was found that it was decreasing for all catalysts. Different oxidation-reduction behaviour of the unpromoted nano-ceria-supported catalysts was assigned to its very small cobalt crystallites size (3.8 nm) [26], as compared to the other catalysts, and according to literature data, to a strong metal-support interaction [27]. Contrary, all zirconia-supported catalysts experienced continuous oxidation of cobalt active phase in the course of the ESR. The studies confirmed the previously observed

tendency that cobalt supported on low-dispersed supports undergoes lower extent of oxidation, as compared to the high-dispersed oxide supports.

The XPS spectra proved that potassium promoter improves reducibility of cobalt active phase in the case of ceria-supported catalyst, in opposite to what was observed for the zirconia-supported catalyst. Moreover, our studies showed that the time of the ESR reaction influences potassium abundance on the catalysts surface. The amount of potassium species (KCO_3 and $K^{\delta+}–O_{surf}^{\delta-}$ sites) progressively decrease with the time-on-stream. Unfortunately we were not able to provide a firm explenation of the reason(s) of progressive decrease of potassium species on the surface, but according to the literature, is expected that potassium-containing species could re-agglomerate [28], since even at 450ºC the loose of potassium to the gas phase does not occur [29]. However, this phenomenon requires more extensive studies in order to solve what is the reason of observed changes in potassium concentration on the catalyst's surface. It was found that the decrease of the $K^{\delta+}–O_{surf}^{\delta-}$ sites concentration on the promoted catalysts' surface, proceed simultaneously with the increase of hydroxyls concentration with the ESR reaction time. These changes are directly related to the catalytic behaviour of the potassium-promoted catalysts.

The catalysts' selectivity was not found to be influenced by the oxidation-reduction behaviour of cobalt and the oxide supports. In the case of unpromoted ceria-supported catalysts, the promoting role in the ESR was assigned to hydroxyls, concentration of which depends on catalysts' dispersion, morphology and probably on their location on the surface, as well as, the ESR reaction time. In the case of the unpromoted zirconia-supported catalysts, the role of adsorbed hydroxyls in the ESR selectivity changes with time-on-stream remained uncertain, since the catalysts suffered from intensive coking. Both unpromoted micro-ceria and micro-zirconia supported catalysts exhibited worse catalytic performance than their high-dispersed counterparts. However, whereas the selectivity to hydrogen and carbon dioxide over the micro-ceria-supported catalyst was getting better with time-on-stream, the same selectivities over the micro-zirconia-supported catalyst were rapidly decreasing. It was suggested that the differences in the catalysts' selectivity result from their different tendency for coking. In addition, severe coking results in formation (especially in the carbonaceous deposit consisted of fibrous filaments with particles of cobalt on their tops) of a new boundary Co/C (apart from cobalt–support), which acts as a new catalyst [24], influencing the catalyst's selectivity. The apparent differences between ceria- and

zirconia-supported catalysts in terms of coking are related to a lower concentration of hydroxyls on the surface of the latter ones, and as suggested in literature, to the poor oxygen mobility and oxygen storage capacity of zirconia [30], as well as to more acidic nature of its surface [30].

It was generally found that the formation of carbon monoxide and methane is double in the case of the zirconia-supported catalysts, as compared to the ceria-supported one, but it could be significantly lowered by potassium addition. It might be expected that those by-products are responsible for severe coking of zirconia-supported catalysts.

The catalytic behaviour of potassium-promoted and unpromoted nano-ceria-supported catalysts does not significantly change with time-on-stream under the ESR condition. The most prominent changes were observed in the initial stage of the ESR, after which the catalysts' selectivity stabilizes. The potassium-promoted catalysts exhibits the best catalytic performance, which was related to the higher concentration of surface hydroxyls and $K^{\delta+}$–$O_{surf}^{\delta-}$ sites, as compared to the unpromoted catalysts. It is very important to note that the beneficial influence of potassium addition was more prominent in the case of zirconia-supported catalysts. The differences between the surface state (e.g., the rate and amount of coke formation) and catalytic performance of potassium-promoted and unpromoted catalysts are much more pronounced for zirconia-supported catalysts.

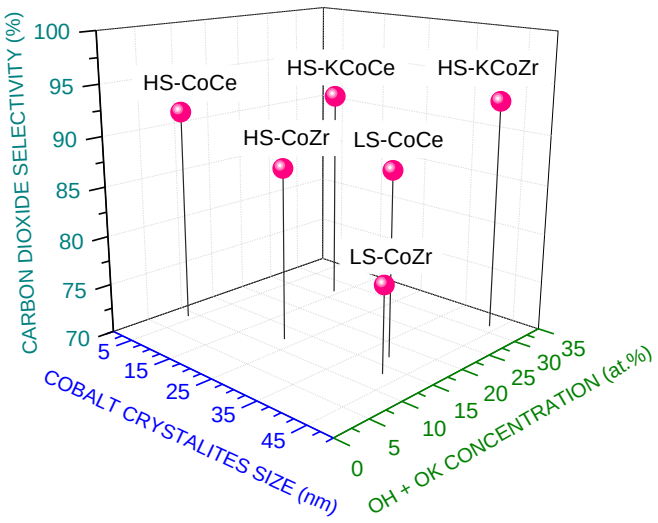

Fig. 4 The influence of cobalt crystallites size and the surface oxygen-containing species atomic concentration on the ceria- and zirconia-supported catalysts' selectivity towards carbon dioxide (H_2O/EtOH = 12/1 mol/mol, 420ºC, t = 1 h).

Apart from the surface concentration of hydroxyls and $K^{\delta+}$–$O_{surf}^{\delta-}$, the size of cobalt crystallites also influences the ESR. Fig. 4 depicts that the potassium promoter enables selective ESR, even if the cobalt crystallites are very large. This is the most pronounced in the case of potassium-promoted zirconia-supported catalyst.

References

1. R. Wang, C. Chen, S. Deng, P. Shen, L. Gong, N. Zhang *J. Chil. Chem. Soc.* **59** (2014) 2710–2716.
2. M.S. Batista, K.S. Santos, E.M. Assaf, E.A. Ticianelli *J. Power Sources* **124** (2003) 99–103.
3. L.F. Liotta, G. Di Carlo, G. Pantaleo, G. Deganello *Catal. Commun.* **6** (2005) 329–336.
4. M. Araque, J. C. Vargas, Y. Zimmermann, A.-C. Roger *Int. J. Hydrogen Energy* **36** (2011) 1491–1502.
5. M. Haneda, Y. Kintaichi, N. Bion, H. Hamada *Appl. Catal., B* **46** (2003) 473–482.
6. M. Sun, L. Wang, B. Feng, Z. Zhang, G. Lu, Y. Guo *Catal. Today* **175** (2011) 100–105.
7. S. Davidson, J. Sun, Y. Wang *Top Catal.* **56** (2013) 1651–1659.
8. V.M. Lebarbier, A.M. Karim, M.H. Engelhard, Y. Wu, B.-Q. Xu, E.J. Petersen, A.K. Datye, Y. Wang, *ChemSusChem* **4** (2011) 1679–1684.
9. S.M. de Lima, I.O. da Cruz, G. Jacobs, B.H. Davis, L.V. Mattos, F.B. Noronha *J. Catal.* **257** (2008) 356–368.
10. S.M. de Lima, A.M. Silva, I.O. da Cruz, G. Jacobs, B.H. Davis, L.V. Mattos, F.B. Noronha, *Catal. Today* **138** (2008) 162–168.
11. S.M. de Lima, A.M. da Silva, U.M. Graham, G. Jacobs, B.H. Davis, L.V. Mattos, F.B. Noronha *J. Catal.* **268** (2009) 268–281.
12. S.M. de Lima, A.M. Silva, U. M. Graham, G. Jacobs, B. H. Davis, L.V. Mattos, F.B. Noronha *Appl. Catal., A* **352** (2009) 95–113.
13. A.M. da Silva, L.V. Mattos, J.P. de Breejen, J.H. Bitter, K.P. de Jong, F.B. Noronha *Catal. Today* **164** (2011) 234–239.
14. D. Zanchet, J.B.O. Santos, S. Damyanova, J.M.R. Gallo, J.M.C. Bueno, *ASC Catal.* **5** (2015) 3841–3863.
15. L. del Río, G. Marbán *Appl. Catal., B* **150–151** (2014) 370–379.

16. L. Xu, Y. Ma, Y. Zhang, B. Chen, Z. Wu, J. Jiang, W. Huang *J. Phys. Chem. C* **114** (2010) 17023–17029.
17. I.I. Soykal, H. Song, J.T. Miller, U.S. Ozkan *Top Catal.* **57** (2014) 785–795.
18. B. Bayram, I.I. Soykal, D. von Deak, J.T. Miller, U.S. Ozkan *J. Catal.* (2011) 77–89.
19. E.I. Kauppi, K. Honkala, A.O.I. Krause, J.M. Kanervo, L. Lefferts *Top. Catal.* **59** (2016) 823–832.
20. R. Espinal, E. Taboada, E. Molins, R.J. Chimentao, F. Medina, J. Llorca *Appl. Catal., B* **127** (2012) 59–67.
21. B. Banach, A. Machocki, *Appl. Catal., A* **505** (2015) 173–182.
22. M. Greluk, M. Rotko, A. Machocki *Catal. Lett.* **146** (2016) 163–173.
23. M. Greluk, P. Rybak, G. Słowik, M. Rotko, A. Machocki *Catal. Today* **242** (2015) 50–59.
24. G. Słowik, M. Greluk, A. Machocki *Mater. Chem. Phys.* **173** (2016) 219–237.
25. J. Llorca, N. Homs., J. Sales, J.-L.G. Fierro, P.R. de la Piscina *J. Catal.* **222** (2004) 470–480.
26. A.L.M. da Silva, L.V. Mattos, J.P. den Breejen, J.H. Bitter, K.P. de Jong, F.B. Noronha *Catal. Today* **164** (2011) 262–267.
27. S.S.-Y. Lin, H. Daimon, S.Y. Ha *Appl. Catal., A* **366** (2009) 252–261.
28. A. Caballero, J.P. Espinós, A. Fernández, L. Soriano, A.R. González-Elipe *Surf. Sci.* **364** (1996) 253–265.
29. N. Nejar, M.J. Illán-Gómez *Appl. Catal., B* **70** (2007) 261–268.
30. H. Song, U.S. Ozkan *J. Catal.* **261** (2009) 66–74.

List of publications

A. PUBLISHED

[1] **S. Turczyniak** *„Rentgenowska spektroskopia fotoelektronów”* in *“Adsorbenty i katalizatory. Wybrane technologie a środowisko”* edit. J. Ryczkowski, Rzeszów 2012, 205–218.

[2] **S. Turczyniak**, Y.T. Law, A. Machocki, S. Zafeiratos *Spektroskopia fotoelektronów badaniach katalizatorów reformingu parowego etanolu (X-Ray Photoelectron Spectroscopy in study of catalysts for the ethanol steam reforming),* in *“Nauka i przemysł – metody spektroskopowe w praktyce, nowe wyzwania i możliwości”* edit. Z. Hubicki, Lublin 2013, 617–624.

[3] **S. Turczyniak**, A. Machocki, *Katalizatory do otrzymywania wodoru w reformingu parowym bioetanolu (Catalysts for hydrogen production by steam reforming of bio-ethanol), Przem. Chem.* **931** (2014) 1850–1854.

[4] S. Turczyniak, W. Luo, V. Papaefthimiou, N.Ramgir, M. Haevecker, A. Machocki, **S. Zafeiratos,** *A comparative Ambient Pressure X-ray Photoelectron and Absorption Spectroscopy Study of Various Cobalt-based Catalysts in Reactive Atmospheres, Top. Catal.* **59** (2016) 532–542.

[5] S. Turczyniak, D. Teschner, A. Machocki, **S. Zafeiratos**, *Effect of surface state on the catalytic performance of Co/CeO_2 ethanol steam reforming catalyst, J. Catal* **340** (2016) 321–330.

B. ORAL PRESENTATIONS

[1] **S. Turczyniak**, P. Rybak, Y.T. Law, D. Teschner, M. Hävecker, A. Knop-Gericke, A. Machocki, S. Zafeiratos, *In situ investigation of ceria supported cobalt catalysts for the steam reforming of bio-ethanol*, The 45th Polish Annual Conference on Catalysis, Cracow 13–15.03.2013, Book of Abstracts, ISBN: 978-83-60514-18-4, 30.

[2] **S. Turczyniak**, Y.T. Law, D. Teschner, A. Machocki, S. Zafeiratos, *Spektroskopia fotoelektronów w badaniach katalizatorów reformingu parowego etanolu* (*X-Ray Photoelectron Spectroscopy in study of catalysts for the ethanol steam reforming*),

in *„Nauka i Przemysł. Metody spektroskopowe w praktyce, nowe wyzwania i możliwości”,* edit. Z. Hubicki, Lublin 2013, 617-627.

[4] S. Turczyniak, P. Rybak, Y.T. Law, D. Teschner, M. Hävecker, A. Knop-Gericke, A. Machocki, **S. Zafeiratos**, *In situ study of the active surface state of Co/CeO_2 catalyst during ethanol steam reforming*, 11th European Congress on Catalysis EUROPACAT-XI, 1–6.09 2013, Lyon, France, Book of Abstracts Discussion Symposium 7: New features in steam and oxy-steam reforming of oxygenates, S3-T2-DS7-2-10, 82

[5] **S. Turczyniak**, M. Greluk, G. Słowik, M. Rawski, W. Gac, S. Zafeiratos, A. Machocki, *Surface state and catalytic performance of promoted and unpromoted cobalt based catalysts under steam reforming of ethanol*, The 48th Polish Annual Conference on Catalysis, Cracow 2016, Book of Abstracts, 34–35.

C. POSTERS

[1] **S. Turczyniak**, Y.T. Law, D. Teschner, A. Machocki, S. Zafeiratos, *Katalizatory do reformingu parowego etanolu (Catalysts for the etanol steam reforming)*, Forum innowacyjne nanomateriały, Lublin 18–19.06.2013, Book of Abstracts, ISBN: 978-83-63503-12-3, 101–102.

[2] **S. Turczyniak**, P. Rybak, Y.T. Law, D. Teschner, M. Hävecker, A. Knop-Gericke, A. Machocki, S. Zafeiratos, *In situ study of the active surface state of Co/CeO_2 catalyst during ethanol steam reforming*, 11th European Congress on Catalysis EUROPACAT-XI, 1–6.09 2013, Lyon, France, Book of Abstracts Discussion Symposium 7: New features in steam and oxy-steam reforming of oxygenates, Poster 3-T2-112, 82

[3] **W. Gac**, S. Turczyniak, P. Rybak, A. Machocki, D. Teschner, M. Hävecker A. Knop-Gericke, S. Zafeiratos, *Insight into properties of Co/CeO_2 catalysts in ethanol steam reforming reaction conditions*, GDRI 6th International Annual Meeting, Wierzba 9–13.2013, Book of Abstracts, 113–116.

[4] S. Turczyniak, **M. Rotko**, A. Machocki, S. Zafeiratos, *XPS studies of model cobalt/cerium-foil catalysts*, The 46th Polish Annual Conference on Catalysis, 19–21.03.2014 Cracow, ISBN 978-83-60514-19-1, P-79, 182.

[5] **S. Turczyniak**, P. Rybak, Y.T. Law, D. Teschner, M. Hävecker, A. Knop-Gericke, A. Machocki, S. Zafeiratos, *In situ study of the active surface state of Co/CeO_2 catalyst*

during ethanol steam reforming, Workshop du GdR C(RS)2, Synchrotron SOLEIL – L'Orme des Merisiers Saint-Aubin, France, 14–17.10.2014.

[6] S. Turczyniak, **G. Słowik**, A. Machocki, S. Zafeiratos, *Quasi in–situ XPS studies of Co–based catalysts under steam reforming of ethanol*, The 47th Polish Annual Conference on Catalysis, 16–18.03.2015 Cracow.

[7] S. Turczyniak, **G. Słowik**, A. Machocki and S. Zafeiratos, *Changes of the Co/CeO_2 catalyst surface during steam reforming of ethanol studied under various pressure regimes*, The 47th Polish Annual Conference on Catalysis, 16–18.03.2015 Cracow.

D. OBTAINED PROJECTS

[1] **2013–2015** The grant (a part of the special-purpose subsidies of Ministry of Science and Higher Education) for young scientists and doctoral students: *"Badania zmian właściwości powierzchni katalizatorów kobaltowych z nośnikami mikro- i nanozdyspergowanymi". (Studies of changes of the surface state of micro- and nano-supported cobalt-based catalysts).*

[2] **2014–2016** The grant (a part of the special-purpose subsidies of Ministry of Science and Higher Education) for young scientists and doctoral students: *"Wpływ zmian stanu powierzchni katalizatorów kobaltowych w warunkach reformingu parowego etanolu na ich właściwości katalityczne" (The influence of the changes of the surface state of cobalt-based catalysts under steam reforming of ethanol on their catalytic properties).*

[3] **2016–2017** The grant (a part of the special-purpose subsidies of Ministry of Science and Higher Education) for young scientists and doctoral students: *"Wpływ stanu chemicznego powierzchni katalizatorów na ich delektywność do tworzenia wodoru podczas "pracy" w warunkach reforming parowego bio-etanolu. Badania quasi in situ spektroskopią fotonów wzbudzanych promieniowaniem rentgenowskim" (The influence of chemical state of the surface of catalysts on their selectivity towards hydrogen under steam reforming of bio-ethanol conditions. Quasi in situ X-ray Photoelectron Spectroscopy studies).*

E. WORK IN RESEARCH PROJECTS

[1] **01.01.2012-31.12.2013** University of Maria Curie-Sklodowska (Poland) and Institute of Chemistry and Processes for Energy, Environment and Health (ICPEES) – joint research unit with a partnership between the French National Research Council (CNRS) and the University of Strasbourg (France), "*Understanding reaction pathways of ethanol reforming overZnO supported Co and Ni model catalysts*"

[2] **01.05.2013-30.04.2016** Collaborative Project No 325358, *Development of a Portable Internal Reforming Methanol High Temperature PEM Fuel Cell System - IRMFC*, under the Seventh Framework Programme of the European Communities - Energy, Fuel Cells and Hydrogen Joint Undertaking.

Sylwia TURCZYNIAK

Surface composition of cobalt catalysts for steam reforming of ethanol

Résumé

L'objectif de cette thèse de doctorat a consisté à déterminer l'influence des conditions réactionnelles du vaporeformage de l'éthanol (ESR), de la dispersion du catalyseur et de la promotion par le potassium sur l'état de la surface. Ce travail a aussi aidé à comprendre l'influence de ces facteurs sur les propriétés catalytiques. Nous avons utilisé les catalyseurs à base de cobalt (promus et non promus par le potassium) supportés à l'oxyde de cérium et à l'oxyde de zirconium à faible et à forte dispersion. Les changements de l'état de la surface des catalyseurs pendant la réaction d'ERS ont été étudiés à travers la spectrométrie photoélectronique X (XPS), alors que les changements des produits ont été analisés en utilisant la spectrométrie de masse et la chromatographie en phase gazeuse. Le catalyseur supporté sur oxyde de cérium à forte dispersion a été caractérisé sous une basse pression (0.2-20 mbar) avec le rapport molaire eau/éthanol de 3/1 (420ºC). Les autres tests ont été faits sur tous les catalyseurs sous une pression totale de 1 atm avec les rapports molaires de 3/1, 9/1, 12/1 (420ºC). Nous avons utilisé un mélange eau/éthanol dans un rapport molaire de 12/1 pour étudier les changements de l'état de la surface de tous les catalyseurs dans le temps. Il a été démontré que la sélectivité d'ESR des catalyseurs pour produire des gaz et pour déposer le carbone est réglée par la concentration des groupes hydroxyles sur la surface. Quant aux catalyseurs promus, elle dépend aussi de la concentration $K^{\delta+}–O_{surf}^{\delta-}$.

Mots-clés: catalyseurs à base de cobalt, oxyde de cérium, oxyde de zirconium, promoteur de potassium, vaporeformage de l'éthanol, XPS

Résumé en anglais

The aim of the thesis was determination the influence of the ethanol steam reforming (ESR) reaction conditions, catalyst's dispersion and potassium promotion on a surface's composition and understanding the influence of these changes on catalysts' performance. Cobalt-based catalysts (unpromoted and promoted with potassium) with low- and high-dispersed ceria and zirconia supports were used. The changes of the surface state of catalysts during the ESR were studied by means of X-ray photoelectron spectroscopy, whereas the reaction products evolution was followed by mass spectrometer or gas chromatograph. Highly-dispersed ceria-supported catalyst was characterized under low pressure conditions (0.2–20 mbar) with the water/ethanol molar ratio equal to 3/1 (at 420ºC). The other tests were carried out over all catalysts under total pressure of 1 atm with 3/1, 9/1 and 12/1 molar ratios (at 420ºC). The water/ethanol ratio of 12/1 was chosen for studies of the surface state of all catalysts with time-on-stream. It was found that the ESR selectivity to gaseous products and carbon deposition is governed mainly by surface hydroxyl species concentration; in the promoted catalysts together with $K^{\delta+}–O_{surf}^{\delta-}$ surface sites.

Keywords: cobalt catalysts, ceria, zirconia, potassium promoter, ethanol steam reforming, XPS